Experimental and Numerical Modeling of Heat Transfer in Wall Assemblies

A Thesis Submitted to the College of

Graduate Studies and Research

in Partial Fulfillment of the Requirements

for the Degree of Master of Science in the

Department of Mechanical Engineering at the

University of Saskatchewan

Saskatoon

By

Charles Tunde Aire

PERMISSION TO USE

In presenting this thesis in partial fulfillment of the requirements for a Postgraduate degree from the University of Saskatchewan, I agree that the Libraries of this University may make it freely available for inspection. I further agree that permission for copying of this thesis in any manner, in whole or in part, for scholarly purposes may be granted by the professor or professors who supervised my thesis work or, in their absence, by the Head of the Department or the Dean of the College in which my thesis work was done.

It is understood that any copying or publication or use of this thesis or parts thereof for financial gain shall not be allowed without my written permission. It is also understood that due recognition shall be given to me and to the University of Saskatchewan in any scholarly use which may be made of any material in my thesis. Requests for permission to copy or to make other use of material in this thesis in whole or part should be addressed to:

The Head of Department

Department of Mechanical Engineering

57 Campus Drive

University of Saskatchewan

Saskatoon

S7N 5A9

DISCLAIMER

The names of certain commercial products were exclusively used to meet the dissertation and/or exhibition requirements for the degree of Master of Science at the University of Saskatchewan. Reference in this dissertation to any specific commercial products, process, or service by trade name, trademark, manufacturer, or otherwise, does not constitute or imply its endorsement, recommendation, or favoring by the University of Saskatchewan. The views and opinions of the author expressed herein do not state or reflect those of the University of Saskatchewan, and shall not be used for advertising or product endorsement purposes.

ABSTRACT

It is critical for the construction industry to ensure that new building designs and materials, including wall and floor assemblies, provide an acceptable level of fire safety. A key fire safety requirement that is specified in building codes is the minimum fire resistance rating. A manufacturer of building materials (e.g., insulation or drywall) is currently required to perform full-scale fire furnace tests in order to determine the fire resistance ratings of assemblies that use their products. Due to the cost of these tests, and the limited number of test facilities, it can be difficult to properly assess the impact of changes to individual components on the overall fire performance of an assembly during the design process. It would be advantageous to be able to use small-scale fire tests for this purpose, as these tests are relatively inexpensive to perform. One challenge in using results of small-scale fire tests to predict full-scale fire performance is the difficulty in truly representing a larger product or assembly using a small-scale test specimen. Another challenge is the lack of established methods of scaling fire test results.

Cone calorimeter tests were used to measure heat transfer through small-scale specimens that are representative of generic wall assemblies for which fire resistance ratings are given in the National Building Code of Canada. Test specimens had a surface area of 111.1 mm (4.375 in.) by 111.1 mm (4.375 in.), and consisted of single or double layers of gypsum board, stone wool insulation and spruce-pine-fir (SPR) studs. As the specimens were designed to represent a one-quarter scale model of a common wall design, with studs spaced at a centre-to-centre distance of 406.4 mm (16 in.), the wood studs were made by cutting nominal 2x4 studs (38 mm by 89 mm) into 9.25 mm by 89 mm (0.375 in. by 3.5 in.) pieces. The scaled studs were then spaced at a centre-to-centre distance of 101.6 mm (4 in.). Three types of gypsum board were tested: 12.7 mm (0.5 in.) regular and lightweight gypsum board, and 15.9 mm (0.625 in.) type X

gypsum board. Temperature measurements were made at various points within the specimens during 70 min exposures to an incident heat flux of 35, 50 and 75 kW/m^2 using 24 AWG Type K thermocouples and an infrared thermometer. Temperature measurements made during cone calorimeter tests were compared with temperature measurements made during fire resistance tests of the same generic assemblies and the result show a very good agreement for the first 25 min of testing at the unexposed side.

A one-dimensional conduction heat transfer model was developed using the finite difference method in order to predict temperatures within the small-scale wall assemblies during the cone calorimeter tests. Constant and temperature-dependent thermal properties were used in the model, in order to study the effects of changes to materials and thermal properties on fire performance. A comparison of predicted and measured temperatures during the cone calorimeter tests of the generic wall assemblies is presented in this thesis. The model had varying degrees of success in predicting temperature profiles obtained in the cone calorimeter tests. Predicted and measured times for temperatures to reach 100°C and 250°C on the unexposed side of the gypsum board layer closest to the cone heater were generally within 10%. There was less agreement between predicted and measured times to reach 600°C at this location, and the temperature increase on the unexposed side of the test specimen. The model did not do a good job in predicting temperatures in the insulated double layer walls. Sensitivity studies show that the thermal conductivity of the gypsum board has the most significant impact on the predicted temperature.

ACKNOWLEDGEMENTS

The author would like to thank the giver of life, 'the lifter of my head', 'my help in ages past and my hope for years to come', the Lord God Almighty for the strength, health and wisdom in starting and completing this research. The author would also like to take this opportunity to thank the following people and organization for their support, involvement, and financial assistance through which this research was made possible.

- Professor D.A. Torvi for his supervision of this research and almost fatherly guidance throughout the study especially in times of "non-academic" troubles. Thank you and God bless you Sir.
- Professor C.J. Simonson, Professor A. Odeshi for their direction as part of the author's supervisory committee.
- Professor E.J. Weckman of the Mechanical and Mechatronics Department, University of Waterloo, for her guidance throughout this study.
- Mr. Rick Retzlaff and Mr. Dave Deutscher of the Mechanical Engineering Department for technical assistance in experiments.
- The Department of Mechanical Engineering and the Natural Sciences and Engineering Research Council of Canada for their funding of this research.
- Mrs. Odeshi for her intercession during difficult times.
- My parents, for their inspiration, love, and intercession during my entire life and education. My brothers and sisters for their encouragement. My Cousin and wife, Osobase and Janet Aire, for their love and support.
- My fiancée, Mosunmola Majekodunmi, for her patience, encouragement and unconditional love throughout this study. God bless you all.

TABLE OF CONTENTS

LIST OF TABLES

LIST OF FIGURES

NOMENCLATURE

Notation

a = the distance from centerline.

c_p = the specific heat [J/kg·K]

F = view factor

Fo = Fourier number

g = acceleration due to gravity [m/s^2]

G = thermal energy generation rate per unit volume [W/m^3]

Gr_L = grashof number

h = convective heat transfer coefficient [W/m^2· K]

k = thermal conductivity [W/m· K]

L = thickness [m]

$\overline{Nu_L}$ = Nusselt number

Pr = Prandtl's number

q''_{conv} = Convective heat loses [W/m^2]

q''_{in} = Incident heat flux from cone heater [W/m^2]

q''_{net} = heat flux conducted into the surface of the wall assembly [W/m^2]

q''_{rad} = Radiative heat flux loses [W/m^2]

Ra_L = Raleigh number

T = temperature [°C]

t = time [s]

x = depth in wall assembly from exposed surface [m]

Greek Symbols

α = thermal diffusivity [m^2/s]

β = expansion coefficient of air [K^{-1}]

Δ = change in

ε = emissivity σ = Stephan Boltzmann's constant [$W/m^2 \cdot K^4$]

ρ = density [kg/m^3]

ν = kinematic viscosity of air [m^2/s]

Subscripts

a = ambient

d,1-2 = elemental area dA1 and surface 2,

d,1-3 = elemental area dA1 and surface 3,

d,1-4 = elemental area dA1 and surface 4

f = film

i = initial

max = maximum

sur = surrounding

vap = vapour

CHAPTER ONE: INTRODUCTION

One of the most critical issues for the construction industry is to ensure that building designs address fire safety issues. These fire safety issues include: fire resistance (the ability of a material, product or assembly to withstand fire or give protection from it for a period of time), surface flame spread (propagation of flame away from the source of ignition across a surface) and non-combustibility (inability of a material to undergo combustion under specified fire exposure conditions). Fire performance of materials is usually determined through full-scale fire tests such as the Steiner tunnel test or the CAN/ULC-S101 [1] furnace test. The manufacturer of a building material (e.g. insulation, drywall and studs) is required to perform full-scale tests such as the CAN/ULC-S101 [1] furnace test for wall and floor assemblies in order to determine the fire resistance and flame spread ratings of assemblies that use their product. These tests facilities are very limited and the tests are very expensive to perform (e.g., ~$25,000/wall test). Therefore it has become very difficult to properly assess the impact of changes to individual components on the overall fire performance of an assembly during the design process.

It would be advantageous to be able to use small-scale fire tests to evaluate fire performance, as these tests are relatively inexpensive to perform. One challenge to using results of small-scale fire tests to predict full-scale fire performance is the difficulty in truly representing a larger product or assembly using a small-scale test specimen. Another challenge is the lack of established methods of scaling fire test results. This thesis research was aimed at evaluating the ability of one small-scale fire test, the cone calorimeter, to predict the full-scale fire performance of wall assemblies. The cone calorimeter is relatively inexpensive to operate and uses small test specimens (e.g., 100 mm by 100 mm). In this project cone calorimeter tests were used to

measure heat transfer through small-scale specimens that are representative of generic wall assemblies for which fire resistance ratings are given in the National Building Code of Canada.

This thesis presents temperature measurements made within small scale wall assembly specimens during cone calorimeter tests and a one dimensional conduction heat transfer model developed using the finite difference method in order to predict temperatures within the small-scale wall assemblies during the cone calorimeter tests. It compares temperatures predicted using the numerical model and temperatures measured during the cone calorimeter tests of the generic wall assemblies. It presents the effects of changes to thermal properties and materials on fire performance of the small-scale assemblies. This research will be useful in assisting manufacturers of building products during the design process to better understand how potential changes to their products will affect fire resistance test results, thus reducing the need for full-scale fire testing.

1.1 WALL ASSEMBLY

The term wall assembly will be used here to refer to a curtain wall or load bearing wall that may or may not be used to provide a fire separation in a building. An example of a wall assembly is shown in Figure 1.1. Most building walls in Canada are made using steel or wood studs with insulation covered with gypsum boards. This type of construction is economical, flexible, can be constructed very quickly.

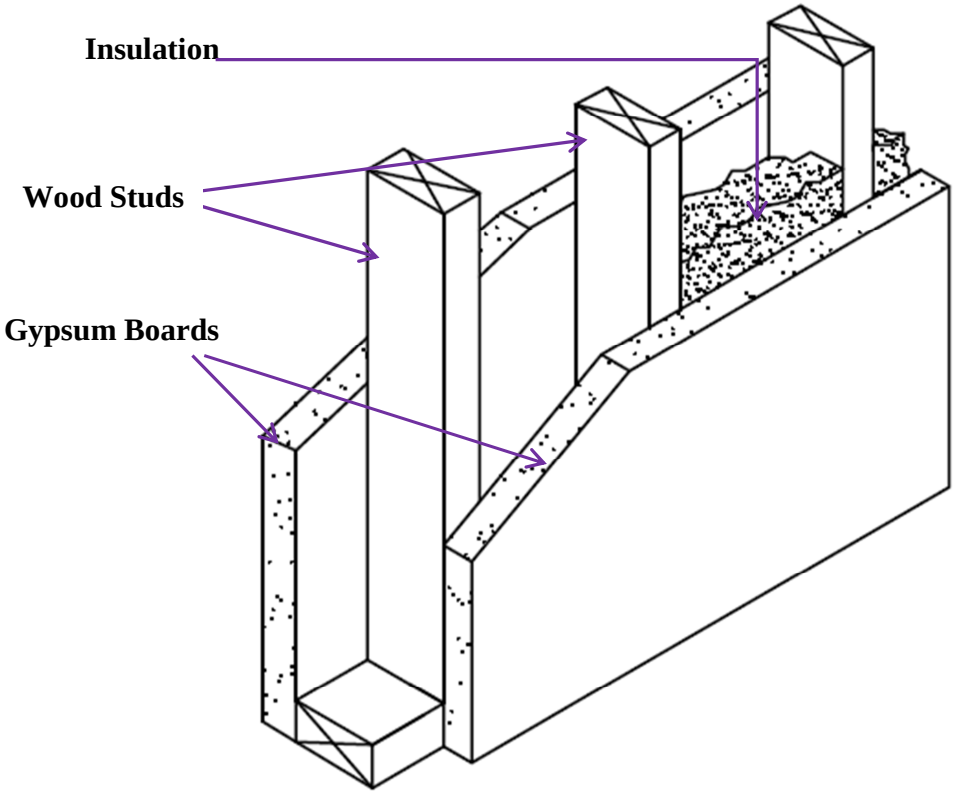

Figure 1.1: A Typical Wall Assembly.

1.2 FIRE RESISTANCE

Fire resistance is defined as “the ability of a material, product, or assembly to withstand fire or give protection from it for a period of time” [2]. Fire resistance is usually quantified using a fire resistant rating, which is the time (in hours or minutes) for which the element can meet certain criteria when exposed to a standard fire resistant test. Fire resistance is assessed by conducting a full scale fire resistant test on building element or assembly. The fire resistance of typical assemblies can also be assessed from the generic ratings, proprietary ratings or calculation methods. A generic rating here refers to listings of fire resistance of typical materials without reference to individual manufacturers or detailed specifications while proprietary ratings refers to

listings of proprietary products with reference to specific manufacturers and are based on full-scale tests results that are commissioned by the manufacturers of the products.

1.2.1 Fire Resistance Tests

Standard fire resistance tests are performed on representative specimens of actual building elements by subjecting them to a standard temperature-time exposure in a furnace in order to evaluate their fire resistance. Standard temperature-time curves do not really simulate real fires but rather provide a standard method of comparison between the fire performances of assemblies. Many countries have building codes that specify fire resistance ratings of building materials and assemblies for particular occupancies. Examples of the standard fire resistance tests include: CAN/ULC-S101 [1], ASTM E 119 [3] and ISO [4]. These tests are controlled to follow a temperature-time curve (e.g. ASTM E 119 or ISO 834, shown in Figure 1.2).

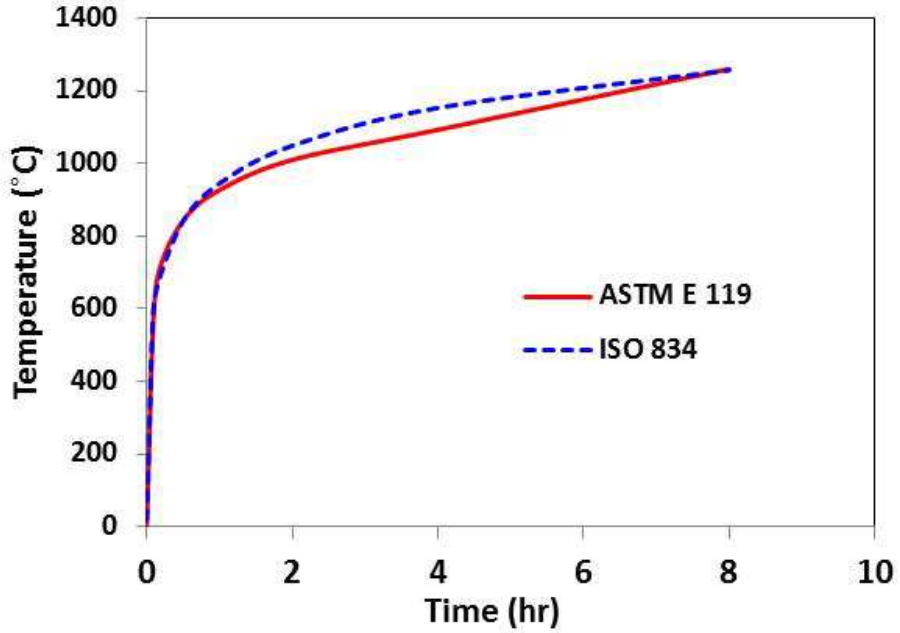

Figure 1.2: ASTM E 119 [3] and ISO 834 [4] Temperature-Time Curves

1.2.2 Full Scale Fire Resistance Furnace

An example of a full-scale fire test furnace includes a large steel box lined with materials (e.g. fire bricks), an exhaust chimney, and a small window for observation. The full-scale fire test furnace is also equipped with a number of oil or gas fuelled burners and several thermocouples or other devices for measuring the furnace temperatures. A full-scale wall or floor specimen has a minimum size of 3.0 x 3.0 m^2 [5] and is built in a frame away from the furnace before bringing this frame into the furnace for testing. At the start of the test, loads may also be applied. The burners are ignited and controlled to follow a temperature-time curve in the fire resistance test standard. The loading frame of a full scale furnace is connected to the test frame which allows the design load to be evenly distributed over the surface with the help of a series of hydraulic pistons. An example of a full scale test furnace is the National Research Council of Canada NRCC test furnace shown in Figure 1.3 [6]. Walls are tested in the vertical orientation whereas floors or roofs are tested in the horizontal orientation.

Figure 1.3: Full-Scale Test Furnace (NRCC) [5] (reprinted with permission).

1.2.3 Intermediate Scale Furnace

As a result of the increasing demand for fire rated wall and floor assemblies that are made from new materials, it has become very important to determine the fire resistance performance of these assemblies. Owing to the time and high cost involved in full scale testing, the need for an alternative solution that is less expensive and less time consuming has been on-going. Part of the solution to this problem has been the construction of an intermediate scale furnace which produces heat exposures that follow the standard temperature-time curve in a similar fashion to the full scale furnace. The NRCC has developed and conducted tests using intermediate scale furnaces [6]. Figure 1.4 [6] shows an intermediate scale furnace (1.2 m wide, 1.8 m long and 0.5 m deep) developed at the NRCC. The furnace can be used in conducting tests for loaded and unloaded wall and floor assemblies. Sultan et al [6] mentioned that the heat flux exposure in the intermediate scale furnace is 15% higher than that in a full scale furnace for a floor furnace.

Figure 1.4: Intermediate Scale Furnace (NRCC) [6] (reprinted with permission).

1.3 FAILURE CRITERIA

Three failure criteria stipulated in CAN/ULC S101 [1] and ASTM E 119 [3] are used to determine the end of the test, which gives the fire resistance rating. The failure criteria are:

1. Stability or structural failure which occurs when the test specimen can no longer support the applied load;
2. Integrity failure, which occurs when there is a crack that allows a passage of hot gases or flame hot enough to ignite a cotton pad; and
3. Insulation failure, which occurs when the average temperature on the unexposed side rises by 139˚C above its initial temperature, or when the temperature reading from a single thermocouple on the unexposed side rises above 180˚C.

Failure is said to have occurred if any of the three criteria is met. The fire resistant rating is determined as the time from the start of the test to this failure point.

1.4 WALL ASSEMBLY MATERIALS

1.4.1 Gypsum Board

A key contributor to the fire performance of a building element is gypsum board. Gypsum board is the general name for a body of panel products comprising a non-combustible core which is made of gypsum and a paper surface on each face. Gypsum board is often called drywall, wallboard or plasterboard. The non-combustible property of gypsum cores and paper laminated surfaces make them different from other panel type building boards such as plywood, fibre board and hard board. Gypsum board is often used as an interior finish as it is relatively easy to work with, can be easily painted and has good fire performance.

As gypsum board is heated, a number of phenomena occur. The core of this product is gypsum, a crystalline mineral called calcium sulphate dehydrate ($CaSO_4.2H_2O$) found in sedimentary rock formations, which is non-combustible and contains chemically bound water, which is slowly released as steam at around 100°C under normal atmospheric pressure [7]. As a considerable fraction of the mass of the gypsum is water (approximately 21%), a significant amount of energy is required, which impacts the heat transfer through the board.

Calcination (release of water) is a two stage process. The first stage involves the conversion of calcium sulphate dihydrate (gypsum) to calcium sulphate hemihydrate

$$CaSO_4\ 2H_2O + \ heat \rightarrow \ CaSO_4\ \frac{1}{2}H_2O + \frac{3}{2}H_2O \qquad (1.1)$$

The second stage involves the conversion of calcium sulphate hemihydrate to calcium sulphate anhydrate

$$CaSO_4\ \frac{1}{2}H_2O + \ heat \rightarrow \ CaSO_4\ + \frac{1}{2}H_2O \qquad (1.2)$$

Both reactions are endothermic and liquid water is released, which then requires an additional amount of energy to evaporate [7]. Thermal Gravimetric Analysis (TGA)and Differential Scanning Calorimeter (DSC) tests of gypsum board [8,9] also reveal that another reaction occurs at a temperature above 600°C where a significant mass loss in the gypsum board occurs, due to the decarbonation of calcium carbonate to produce calcium oxide (quicklime) and carbon dioxide

$$CaCO_3\ + heat \rightarrow \ CaO\ + CO_2 \qquad (1.3)$$

Sultan [10] reported that gypsum boards used in wall assemblies fall-off on the exposed side when the temperature of the mid-thickness or unexposed side exceeds 600˚C. The fall-off occurs

as a result of crack formations and decarbonation of calcium carbonate to calcium oxide at this temperature causing the gypsum board to lose its structural strength.

Gypsum wall boards are easy to install in buildings because they typically come in 48 in. (1.2 m) or 54 in. (1.4 m) widths and 8-12 ft. (2.4 - 3.7 m) lengths (or longer) which enables them to quickly cover a large wall area. They can be very easily cut by using a utility knife or different varieties of saws, and can be easily fastened to the walls using screws or nails.

Three types of gypsum board that are commonly used are: regular, lightweight and type X (a gypsum board with special core additive to increase the natural fire resistance of regular gypsum board). Regular gypsum board is used in many locations within buildings, while type X is used when a higher fire resistance rating is needed. Type X boards are reinforced with some glass fibre and may contain other additives to improve their fire performance. Lightweight gypsum board is a relatively new product, which is increasingly being used in place of the traditional regular gypsum board, because of its reduced weight.

1.4.2. Insulation

Walls and floor assemblies are insulated due to acoustics and also to decrease heat flow during the cooling and heating seasons. Building insulation is rated using thermal resistance to heat flow values called R_{value} [11]

$$R_{value} = \frac{t}{k} \tag{1.4}$$

where t is the thickness in m and k is the thermal conductivity in W/m·K.

The type of insulation material, its thickness and its density affect the R-value of the thermal insulation. There are basically five types of insulation used in different parts of a building: batts, spray, loose-fill, rolls and rigid foam boards. Batts are commonly made of fiberglass, or mineral or stone wool and mostly fitted between the studs in the walls and also joists of ceilings and floors.

1.5 FIRE TESTING OF WALL AND FLOOR ASSEMBLIES

Many studies have been performed on temperature measurements in gypsum board wall assemblies. The focus of this review will be full-scale tests conducted at the National Research Council of Canada's Institute for Research in Construction (NRCC), as these full-scale fire tests have been used to provide data on generic wall and floor assemblies for the appendices in the National Building Code of Canada (NBCC). Selected tests performed at other laboratories and by other researchers are referenced in Table 1.1.

Various research projects have been conducted to measure temperatures in full and small scale fire resistance tests of gypsum board wall assemblies at the NRCC. Sultan et al [12] carried out seven full-scale (4 m by 5 m) fire resistant tests on non-insulated, loaded and non-loaded, regular gypsum board protected wall assemblies to determine the temperature profiles and fire resistance ratings and of the assemblies. The assemblies were made up of single layer and double layers of regular gypsum boards on the exposed and unexposed sides, with wood studs for the single layer assemblies, and wood and steel studs for the double layer assemblies. The results revealed that in the non-loaded double layer wall assemblies, the type of stud has a negligible effect on the fire resistance rating. Kodur et al [13] carried out ten full-scale fire resistant tests on load-bearing gypsum board, wood studded shear wall assemblies with and without resilient channels (strips of

metal with an offset that space the drywall a half inch away from the framing to improve sound transmission loss in a building) on the fire exposed side. Wall assemblies with a single layer 12.7 mm type X gypsum board on both the exposed and unexposed sides, and wall assemblies with a single board on the exposed side and double boards on the unexposed side were tested. The effects of the placement of the shear membrane on the exposed/unexposed face, type of shear membrane, insulation type, load intensity and resilient channel on the fire resistance of wall assemblies were determined. Sultan et al [14] carried out temperature measurements during fire resistance tests on insulated and non-insulated intermediate scale wall assemblies (914 by 914 mm) protected by 12.7 mm and 15.9 mm type X gypsum boards on steel studs and 12.7 mm gypsum boards on wood studs. The tests were conducted using walls with three different gypsum board arrangements: a single layer gypsum board on both the exposed and unexposed side, double layers of gypsum board on both the exposed and unexposed side and single layer gypsum board on the exposed side along with a double layer gypsum board on the unexposed side. The effects of glass, mineral and cellulose fiber insulation thickness on the fire performance of intermediate scale tests were studied. Sultan et al [15] conducted temperature measurements on insulated and non-insulated intermediate scale regular gypsum board protected (914 by 914 mm) assemblies. The assemblies tested used double gypsum board layers on both the exposed and unexposed sides, wood and lightweight steel studs with mineral wool, glass and cellulose fiber insulation. The average temperatures on the exposed and unexposed boards, and within the insulation were presented. The impact of the use of different insulation and stud types, and mass per unit area were investigated, along with the presence of glass fibre in the gypsum board core.

Table 1.1: Selected Research Work on Fire Resistance Tests of Wall Assemblies

Authors	Wall Assemblies	Gypsum Board Type	Insulation Type	Size of Wall (mm)	Measurements
Park et al [16]	Steel Studs Double Layer Gypsum Boards	15.9 mm Type X	Non-insulated	3048 x 3048	Temperature
Kontogeotgos et al [17]	Steel Studs Double Layer Gypsum Boards	12.5 mm Regular	Non-insulated	1250 x 1050	Temperature
Urbas & Shaw [18]	Steel/Wood Studs Double Layer Gypsum Boards	16 mm Type X & 13 mm Regular	92 mm Expanded Polystyrene	1000 x 1000	Temperature
Jones [19]	Wood/Steel Studs Single Layer Gypsum Board Wall	Regular	Non-insulated	1010 x 2010	Temperature

1.6 FIRE MODELS

The introduction of performance-based building codes and performance-based fire safety design has made it necessary to develop and validate fire resistance models for assessing building assemblies. While the predictions of models in the literature show good agreement with experimental results, there is still some room for improvements, as it has been very difficult to completely capture all of the underlying physics in the fire models. A few examples of fire test models found in the literature for wall assemblies made of gypsum board and wood or steel studs, and the agreement between numerical and experimental results are presented below.

1.6.1 Thomas

Thomas [20] used a finite element program called TASEF to model heat transfer in walls exposed to the standard fire resistance temperature-time curve. The convective heat transfer coefficients were adjusted so as to have a good correlation with experimental results, and all other properties used in the simulation were determined from the literature. The author neglected mass transfer of moisture, and claimed that at a temperature above 120^{o}C the net effect of moisture movement is insignificant. Figure 1.5 shows the locations of thermocouples and predicted temperatures for the wall assembly. Figure 1.6 shows the comparison of predicted and measured temperatures for the wall assembly. The predictions of the wall model are in good agreement with experimental results at point 4 (the ambient side of the wall), and in poorer agreement at points 2,3 and 5, with the model predictions being much higher than the experimental results.

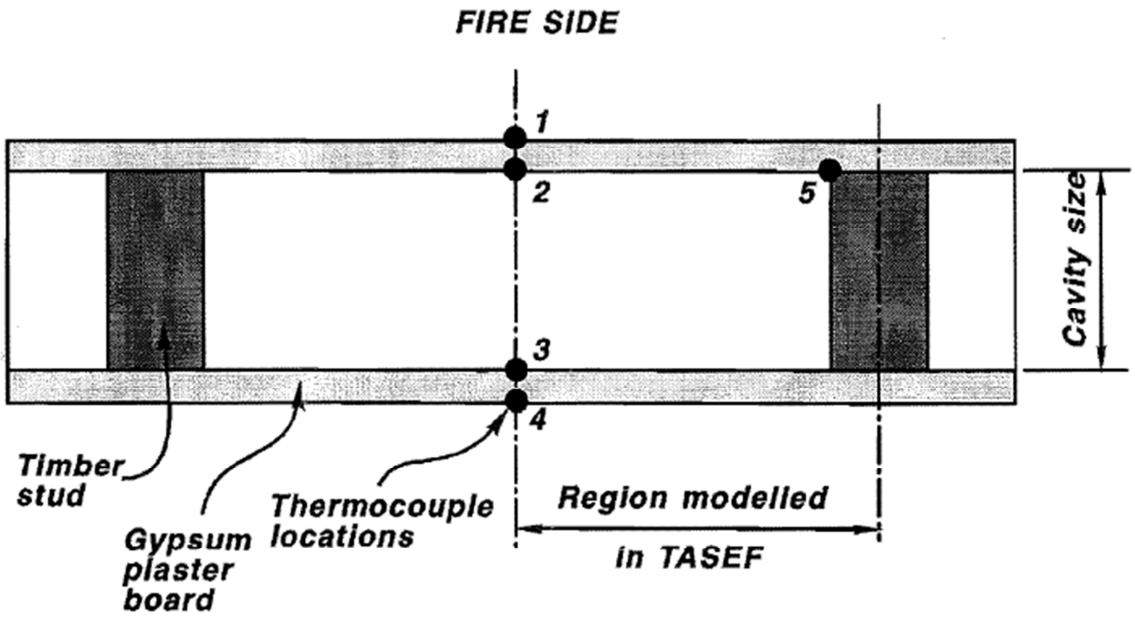

Figure 1.5: Thermocouple Locations Used By Thomas [20] (reprinted with permission)

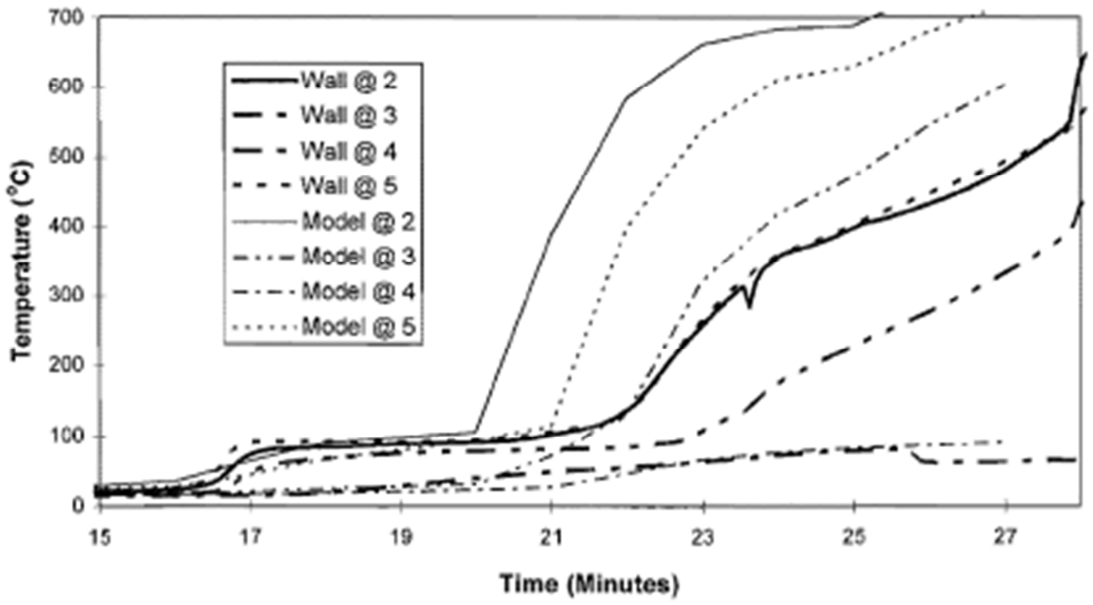

Figure 1.6: Comparison of Temperatures Predicted and Measured By Thomas [20] (reprinted with permission).

1.6.2 Takeda and Mehaffey

Takeda and Mehaffey [21] and Takeda [22] described two dimensional models, WALL2D [21] and WALL2DN [22], which were developed at the NRCC to predict the heat transfer through non-insulated and insulated wood-stud walls protected by gypsum board. The models use explicit finite difference techniques to solve the governing equations with material property data derived from tests on gypsum boards and wood at NRCC. WALL2DN was used to model wall assemblies with four different types of insulation and also to simulate the opening of joints between boards by modelling the shrinkage of gypsum boards. Figure 1.7 shows the thermocouple locations for the non-insulated wall assembly. Figure 1.8 compares the numerical and experimental results for a non-insulated wood studded gypsum board wall assembly. The model predictions and the experimental results show a reasonable agreement. The time to

insulation failure predicted by the model is 57 min 30 s which is very close to the experimental value of 51 min 8 s.

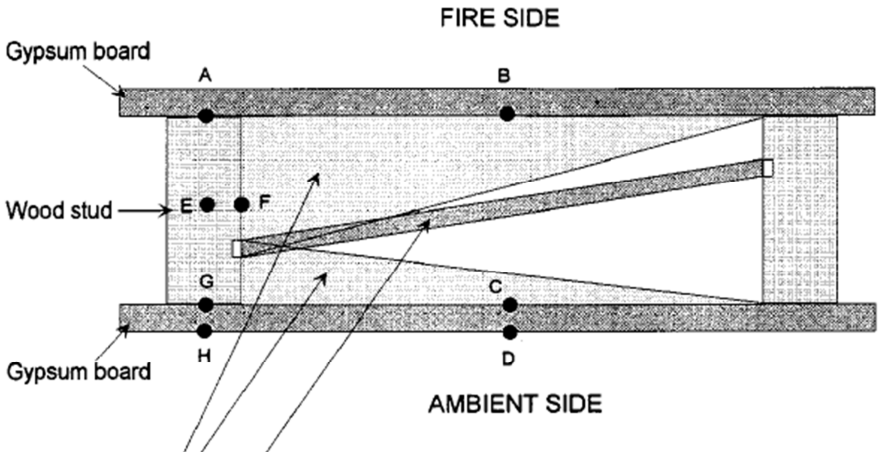

Figure 1.7: Thermocouple Locations Used By Takeda and Mehaffey [21] (reprinted with permission)

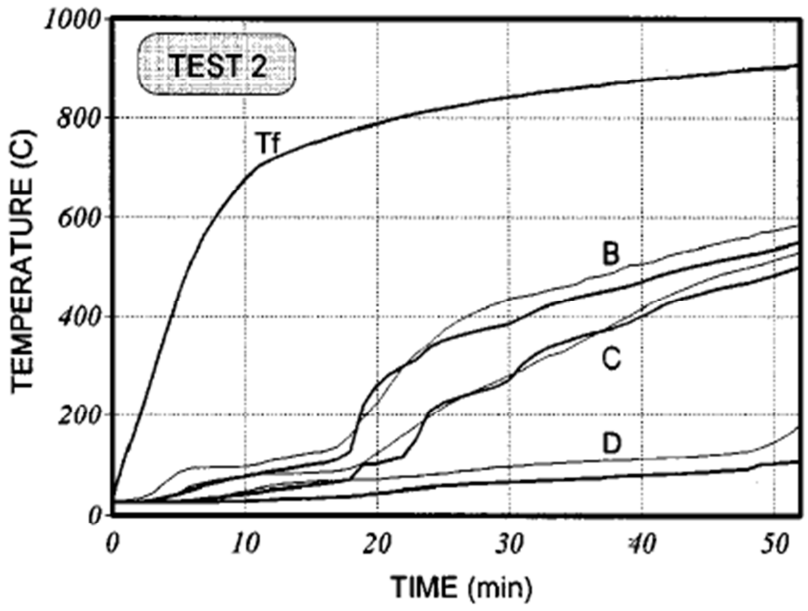

Figure 1.8: Comparison of Temperatures Predicted and Measured By Takeda and Mehaffey [21] (reprinted with permission). (T_f is fire temperature, refer to Figure 1.7 for Locations B, C and D).

1.6.3 Clancy

Clancy [23-25] developed a two-dimensional numerical algorithm based on an alternating direction implicit finite difference method called ADIDRAS for modeling heat transfer in walls. The model was used to predict radiative heat transfer in the assemblies as well as accounting for the shrinkage gaps that develop between the dried wood and gypsum. The author accounted for moisture movement by considering increased thermal conductivity and shrinkage gaps between the stud and gypsum. The observation made was that heat transfer was significantly increased by moisture transfer for areas within a solid where the temperature is less than 100°C. Heat transfer was reduced by moisture transfer in areas with temperature between 100°C and 150°C, whereas heat transfer was not affected by moisture transfer in areas above 150°C. Figure 1.9 shows the thermocouple locations and Figure 1.10 shows the comparison between results of the ADIDRAS model and the wall experiment. From Figure 1.9, B is the thermocouple location at the back of the exposed board, C is the thermocouple location at the face of the unexposed gypsum board and D is the thermocouple location at the unexposed side. In general, the experimental and numerical results were in good agreement.

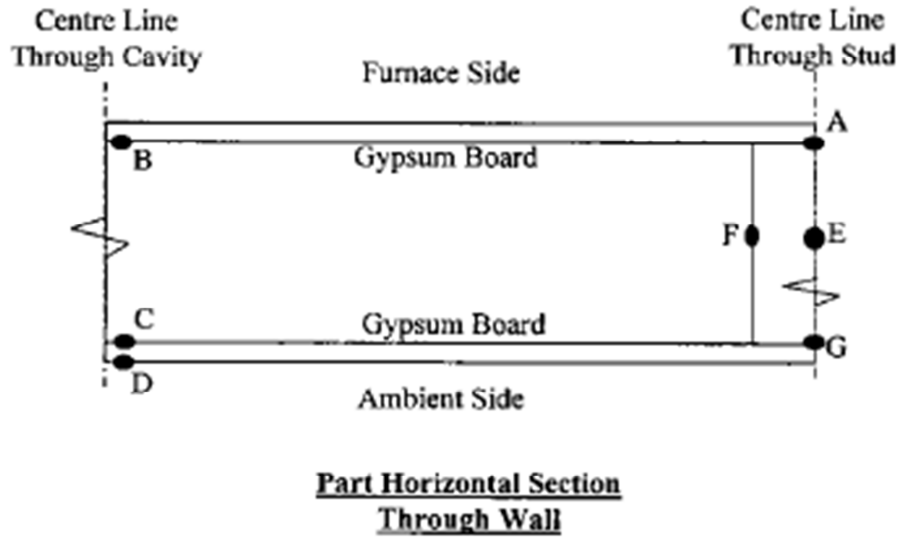

Figure 1.9 Thermocouple Locations Used By Clancy [23] (reprinted with permission)

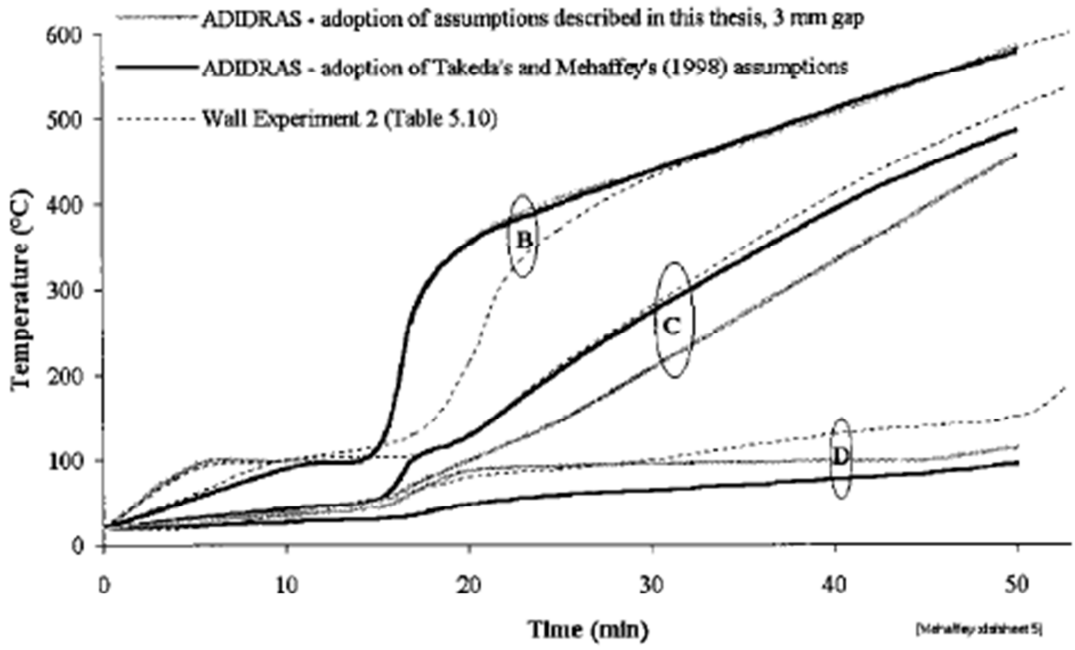

Figure 1.10: Comparison of Temperatures Predicted and Measured By Clancy [23] (see Figure 1.9 for thermocouple locations) (reprinted with permission).

1.6.4 Collier

Collier [26] developed a one-dimensional finite difference model that predicts temperature increase across the section of a structural wall exposed to standard (standard temperature-time curve) and non-standard (realistic) fires. Four intermediate-scale (2.10 m x 1.0 m) fire tests were used for the verification of the model. The model predictions for the beginning of the char of the gypsum board paper and time to failure are conservative compared to the experimental results. Figure 1.11 shows the comparison between one test [26] and the predictions from the model.

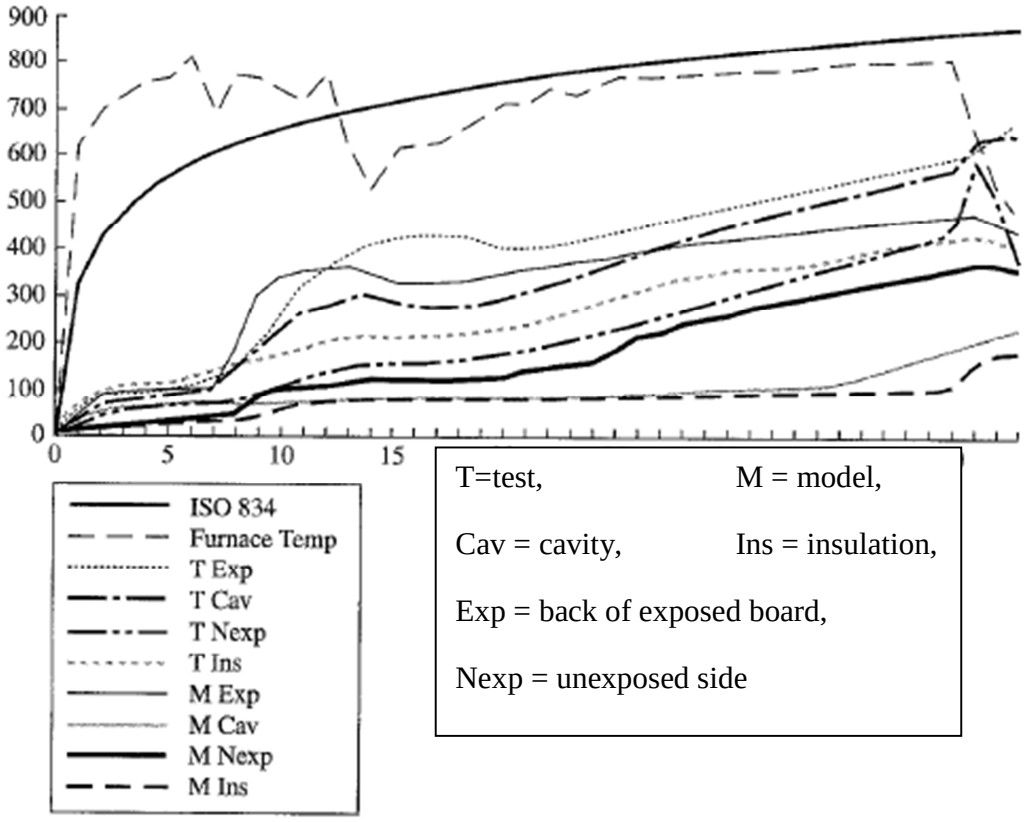

Figure 1.11: Comparison of Temperatures Predicted and Measured By Collier [26].
(reprinted with permission)

1.6.5 Alfawakhiri

Alfawakhiri [27] used a one-dimensional finite difference computer model called TRACE to predict heat transfer through insulated steel stud wall assemblies. The modes of heat transfer considered in the assembly include: convection and radiation to the exposed gypsum board surface, conduction through the exposed gypsum board, insulation and unexposed gypsum board and radiation and convection from the unexposed surface of the assembly to the surroundings. Gypsum board shrinkage, heat transfer through metal studs and moisture movement within the gypsum board were neglected. Predicted and experimental results were in good agreement. Figure 1.12 shows a comparison between results from a test and the model for one of the wall assemblies [27].

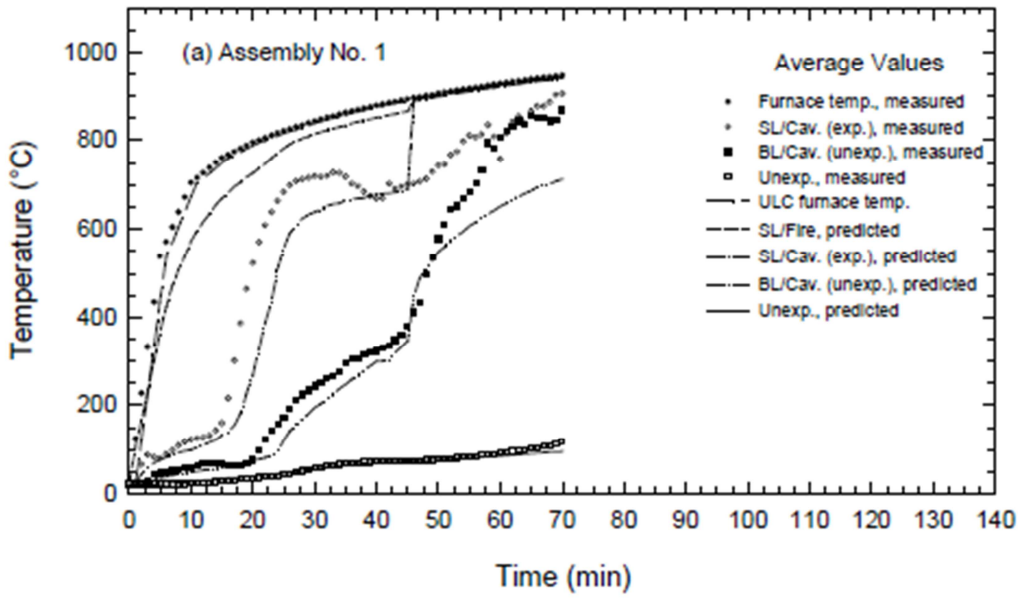

Legend: SL - Gypsum Board Single Layer, BL – Gypsum Board Base layer, FL – Gypsum Board Face Layer, Std.- Stud, Cav. Cavity, Exp. – Exposed Side, Unexp. - Unexposed Side.

Figure 1.12: Comparison of Temperatures Predicted and Measured By Alfawakhiri [27] (reprinted with permission)

1.6.6. Sultan

Sultan [10] developed a one-dimensional model to predict heat transfer through steel-stud, non-insulated and non-load bearing gypsum board wall assemblies. The model was validated with two non-insulated and non-load bearing full-scale fire resistance tests. The model gave a conservative prediction of the fire resistance with predicted temperature and failure times being approximately 3% lower than the experimental results as shown in Figure 1.13.

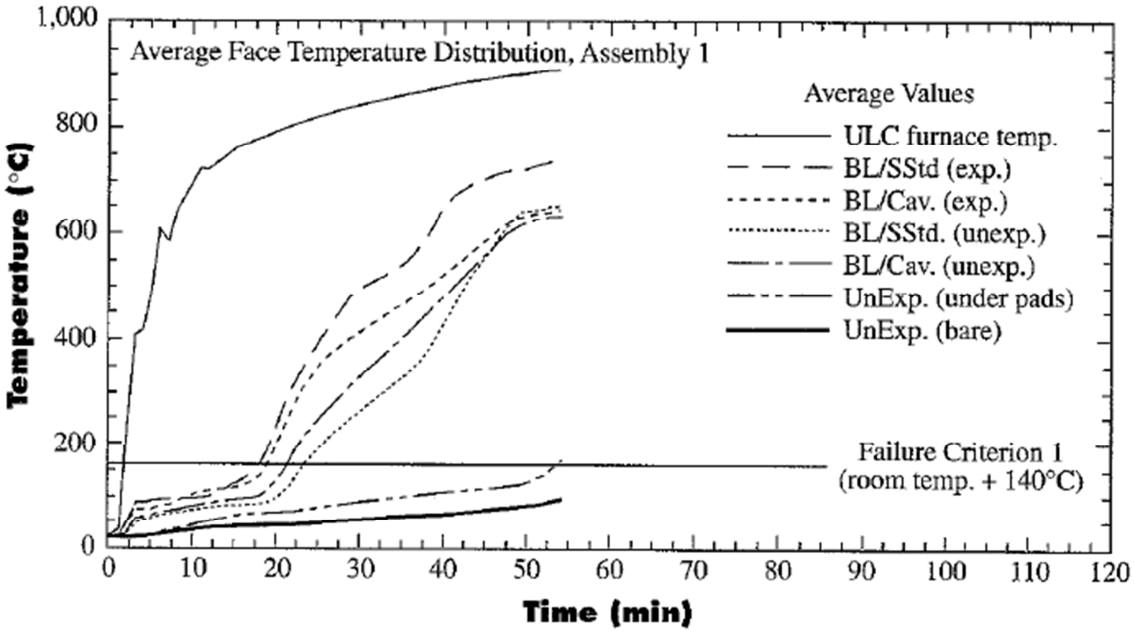

Legend: SL - Gypsum Board Single Layer, BL – Gypsum Board Base layer, FL – Gypsum Board Face Layer, Std.- Stud, Cav. Cavity, Exp. – Exposed Side, Unexp. - Unexposed Side.

Figure 1.13: Comparison of Temperatures Predicted and Measured By Sultan [10] (reprinted with permission).

1.6.7 Shahbazian et al

Shahbazian et al [28] proposed a method of calculating temperature distributions in axially loaded cold-formed thin walled steel studs in wall assemblies exposed to fire from one side. The method is based on a heat balance analysis for nodes representing the main components of the panel. The proposed model was validated by comparing experimental results with the proposed one dimensional model and a 2-D ABAQUS finite element model. Figure 1.14 shows the predicted and measured temperatures for the exposed and unexposed side of the wall. A very good agreement between predicted and measured results was obtained at the earlier stages of the testing, but the agreement was not as good at the later stages of the testing.

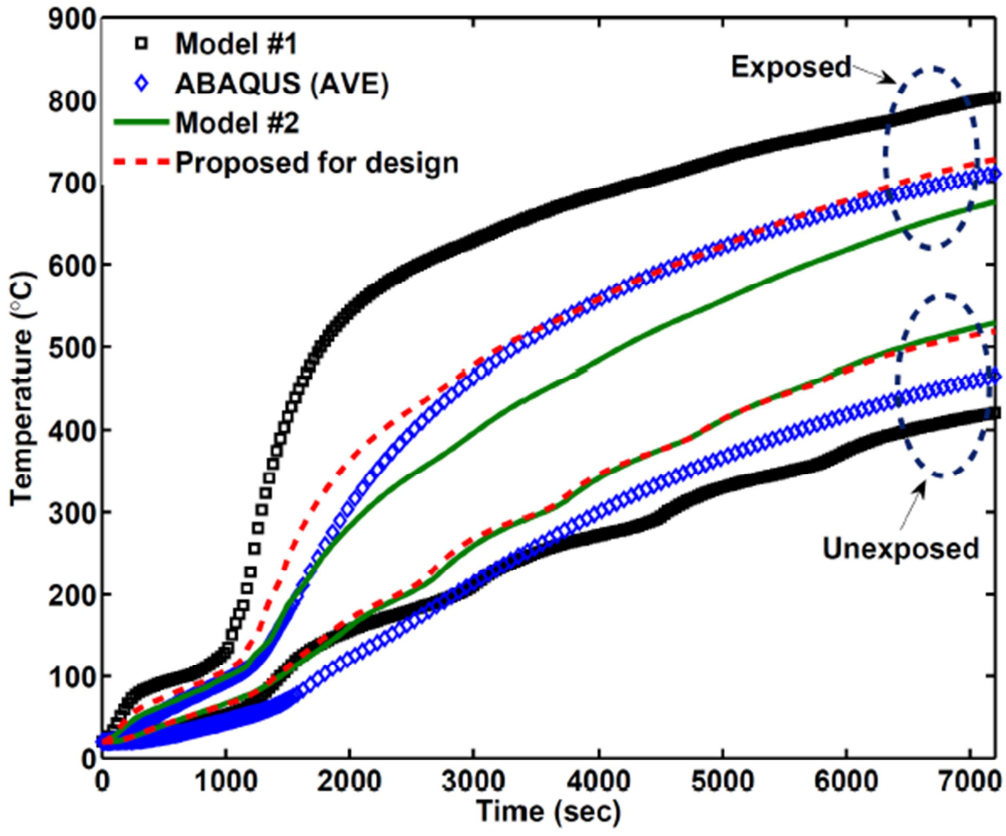

Figure 1.14: Comparison of Temperatures Predicted and Measured By Shahbazian et al [28] (reprinted with permission).

1.6.8 Keerthan and Mahendran

Keerthan and Mahendran [29] conducted experimental and numerical studies on the thermal performance of composite panels under fire conditions. The composite panels were comprised of gypsum boards, mineral wool, glass fibre or cellulose insulations, and wood studs. Suitable thermal properties of these materials were determined and used in the numerical model. A finite element program, SAFIR was used to simulate thermal performance under both standard (temperature-time curve) and Eurocode (another curve similar to the standard temperature-time curve) design fire curves, and the models were then validated by comparing their results with standard fire test results of composite panels. Figure 1.15 shows a comparison between results from a test and the model for one of the wall assemblies. A very good agreement between predicted and measured results was obtained at unexposed (ambient) side of the wall assembly.

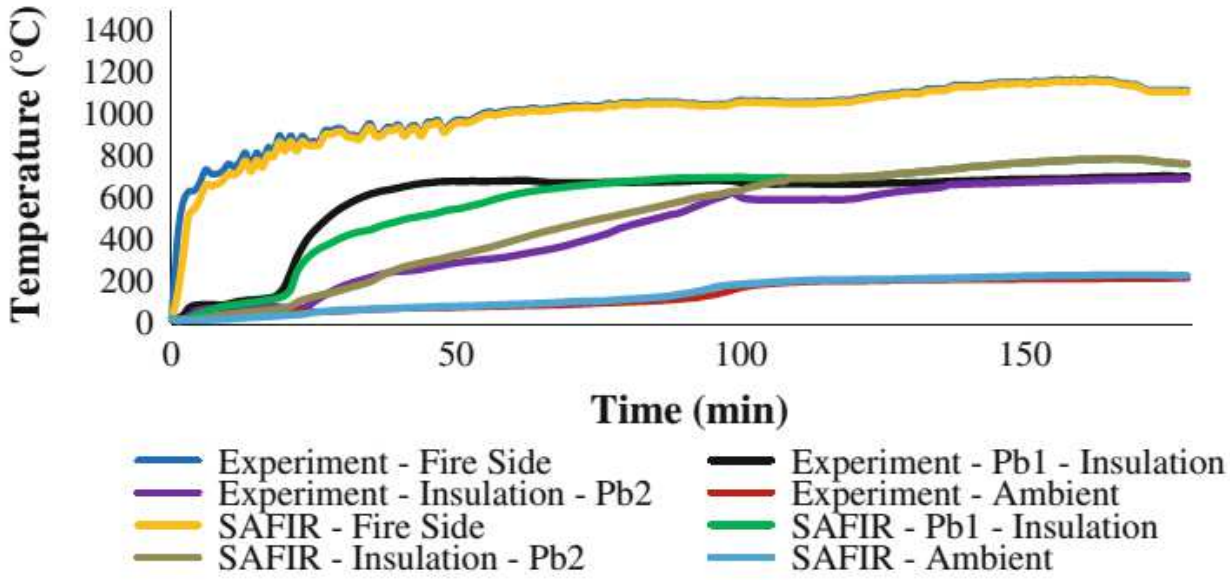

Figure 1.15: Comparison of Temperatures Predicted and Measured By Keerthan and Mahendran [29] (reprinted with permission).

.

1.6.9 Other Models

Hurst and Ahmed

Hurst and Ahmed [7] used a model developed by Portland Cement Association which predicts heat and mass transfer through gypsum board to analyze the thermal response of wood-studs gypsum board assemblies exposed to the ASTM E119 temperature-time curve. A fully implicit finite difference method was used to solve the equations for conservation of mass, momentum and energy. The coupled heat and mass transfer through gypsum board was predicted by the model using the dehydration process and its effect on pore size and mass transport mechanisms. The model results are in good agreement with previous experimental results. The effects of wall studs were not considered in the model. The authors concluded that under positive pressure, the hot gases being forced through cracks and open joints have a significant effect of the fire performance of the wall assemblies.

Craft

Craft [7], developed a two dimensional finite element model called CUWoodFrame to predict the heat and mass transfer through a wood-frame floor assembly exposed to fire. The model uses Arrhenius expressions to predict the calcination process of gypsum and the pyrolysis of wood. The model results were validated using tests conducted in the cone calorimeter, intermediate scale furnace and full scale fire resistance furnace. The comparisons between experimental and numerical predictions show a good agreement for temperatures behind each layer of gypsum board. The temperature at the wall cavity was under-predicted and this resulted in an under-prediction of the temperature at the unexposed side.

1.6.10 Summary of Models

Numerical models of gypsum board wall assemblies subjected to fire discussed in the literature generally demonstrate a good ability to predict fire resistance test results (such as failure times), but models are less successfully able to predict the temperature profiles within a wall assembly. Some of the models presented show a very good agreement between predicted and measured temperatures on the unexposed side of the assembly, while other models show a good agreement at other locations within the wall. The model results presented in the literature also show the difficulty in predicting temperature profiles at all thermocouple locations in the wall assembly. However, the models presented above provide a basis for developing the numerical model used in this research, as well as the choice of thermal properties used in the model.

1.6.11 Related Research at the University of Saskatchewan

Fire research is ongoing at the University of Saskatchewan (UofS) to determine the fire behavior of materials using the cone calorimeter, including the performance of thermal protective fabrics, consumer products and soil. Part of the research at the UofS focuses on using results of small-scale fire tests to predict full-scale fire performance. The cone calorimeter is used in fire testing of materials of 10 cm by 10 cm square. It is referred to as cone calorimeter because of its conical shaped radiant heater which is capable of providing a heat flux in the range of 0-100 kW/m^2. Figure 1.16 shows the cone calorimeter.

Figure 1.16: Cone Calorimeter.

One of the studies into the performance of thermal protective fabrics at the UofS was aimed at developing a heat transfer model of flame resistant fabrics during both heating and cooling after the exposure to fire [30]. Torvi and Threlfall's [30] heat transfer model was used to predict both fabric temperature and skin burn injuries. The model was validated using results from small-scale fabric tests.

Eninful and Torvi [31] developed a numerical heat transfer model to predict temperature profiles in soil during cone calorimeter tests, which simulated wildland fire exposures. Predicted temperature profiles were used to estimate the depth of lethal heat penetration of a wildland fire, the depth to which plants would not be expected to grow after a fire exposure. The model predictions were within the 1-cm accuracy with which the depth of seeds and plant shoots in the soil can be determined.

The burning behavior of polyurethane foam has also been studied by the UofS research group. For example, Ezinwa [32] performed fire tests on polyurethane foam using the cone calorimeter,

and developed a method to scale the fire test results. The test results reveal that the heat flux exposures and the different test arrangements have a significant effect on the fire behavior of the material. Heat release rate (the amount of energy released from the burning specimen) predictions made using a convolution model and a fire protection engineering correlation were compared with results from full-scale fire tests. The model successfully predicted the heat release rates during the early part of the fire growth phase. Predicted and measured peak heat release rates and total heat release were within 10-15% of one another.

1.7 OBJECTIVES AND MAJOR TASKS

Previous research on fire resistance tests of wall assemblies was focused on full scale tests and modeling of wall assemblies. The need for an economical and quick method of testing wall assemblies is important, especially during the design of new building materials and wall assemblies. This research will use the cone calorimeter to determine temperature profiles in wall assemblies and to predict full-scale fire resistance test results. A heat transfer model will be developed to predict expected temperatures profiles and heat transfer through wall assemblies. The main objectives of this research are:

1. To evaluate the ability of the cone calorimeter to test small scale wall assemblies, and to compare temperature measurements in cone calorimeter tests and full-scale fire resistance tests conducted in a furnace for generic assemblies;
2. To develop a heat transfer model to predict behavior of wall assemblies in fire. The development of this model will involve studying and modifying other existing heat transfer models for wall assemblies; and

3. To use cone calorimeter tests and heat transfer models to determine the effects of changes to density, thickness and other design parameters on heat transfer through wall assemblies.

This research will assist manufacturers in using results from cone calorimeter tests to predict the expected fire performance of their materials. This research will significantly reduce the cost of testing since it costs about $100-$150/cone calorimeter test and about $25,000/full-scale wall test. This research will also assist building and fire protection regulators to develop a quick and cost effective means of conducting a preliminary evaluation of new building products as new materials can be quickly tested in the cone calorimeter. The performance of new materials can also be determined using the heat transfer model.

In order to achieve the objectives of this study, cone calorimeter tests of wall assemblies consisting of wood studs, single and double layers of 12.7 mm (1/2 in.) regular and lightweight gypsum board, and 15.9 mm (5/8 in.) type X gypsum board walls, that are uninsulated and insulated with stone wool insulation will be tested using a heat flux of 75 kW/m^2. The effect of heat flux exposure will be determined by testing single layer lightweight gypsum board wall assemblies using heat fluxes of 35, 50 and 75 kW/m^2 in the cone calorimeter.

Single and double layers of regular, lightweight and type X gypsum board, as well as complete wall assemblies, will be tested in this study. A finite difference heat transfer model will be developed to predict temperature profiles within the wall assembly. As will be discussed in the next chapter, the heat transfer through the wall assembly in this model is assumed to be one dimensional, and the effects of moisture movement and the burning of the gypsum board paper are assumed to be negligible.

1.8 OUTLINE OF THESIS

In Chapter One of this thesis, a general introduction to the research project was provided, including background on generic wall assemblies and fire tests. A literature review of selected research dealing with gypsum board, insulation, fire tests and models was presented. The objective for this research was also presented in this Chapter. In Chapter Two, the development of the one dimensional finite difference heat transfer model is presented along with the effects of grid size and time-steps, and the validation of the model. In Chapter Three, the thermal properties of gypsum boards, wood and mineral and stone wool insulation given in the literature and the values adopted for the model are discussed along with numerical results predicted by the model, and the sensitivity of the model to changes in thermal properties of gypsum board and mineral or stone wool insulation. In Chapter Four, the experimental procedure and results are presented along with a comparison of the small scale results to full scale results found in the literature for similar wall assemblies. In Chapter Five, experimental and numerical results of the cone calorimeter tests are compared. In Chapter Six, the conclusions drawn from this study are presented, along with recommendations for future work.

CHAPTER TWO: DEVELOPMENT OF NUMERICAL MODEL

For this study, a one dimensional finite difference model was developed to simulate the transient heat transfer through gypsum board and gypsum board wall assemblies. The derivation of the theoretical model follows a similar procedure as that used by Wang [33]. The objective of the model is to predict temperature development in gypsum board, stone wool insulation and wall assemblies exposed to a constant heat flux and a constant temperature. This chapter will present the development of the one dimensional heat transfer model and the validation of the model.

2.1. GOVERNING EQUATION AND SIMPLIFYING ASSUMPTIONS

From conservation of energy, the governing equation for one-dimensional heat and mass transfer in the control volume, is given by;

$$\rho c_p(T)\frac{\partial T}{\partial t} = \frac{\partial}{\partial x}\left(k(T)\frac{\partial T}{\partial x}\right) + G \qquad (2.1)$$

where:

x is depth of wall from exposed surface (m),

t is time (s),

G is the thermal energy generation rate per unit volume (W/m^3) associated with phase change and thermochemical reactions.

T is the temperature (°C),

k is the thermal conductivity (W/m·K),

ρ is the density (kg/m^3) and

c_p is the specific heat (J/kg·K).

The thermal energy generation rate per unit volume (W/m^3) associated with phase change and thermochemical reactions.is assumed to be accounted for by using the apparent heat capacity method (i.e., is incorporated within the values of density and specific heat). This approach is similar to Torvi [34].

Therefore the governing equation becomes;

$$\rho c_p(T)\frac{\partial T}{\partial t} = \frac{\partial}{\partial x}\left(k(T)\frac{\partial T}{\partial x}\right) \qquad (2.2)$$

Initial and Boundary conditions:

The initial and boundary conditions are based on the tests conducted using a hotplate and cone calorimeter. The initial temperature of the gypsum board as well as the wall assembly is assumed to be uniform and equal to the room temperature before the commencement of the test.

The two boundary conditions used in this study are:

a.) Fixed temperature boundary at the exposed surface of the wall (at, x=0).

b.) Constant heat flux at the exposed surface of the wall (x = 0).

Fixed Temperature Boundary at x=0.

The hotplate is used to heat up the surface of the specimen to a constant temperature. The surface of the specimen is allowed to make contact with the heated surface of the hotplate as shown in Figure 2.1. The unexposed side of the specimen is well insulated to give an insulated boundary condition

$T = T_1$ at (x=0) and

$q_L'' = 0$, for (x=L).

T_1 is a known temperature at the exposed surface(x = 0) of the boundary and q_L'' is the heat flux exchange at x = L.

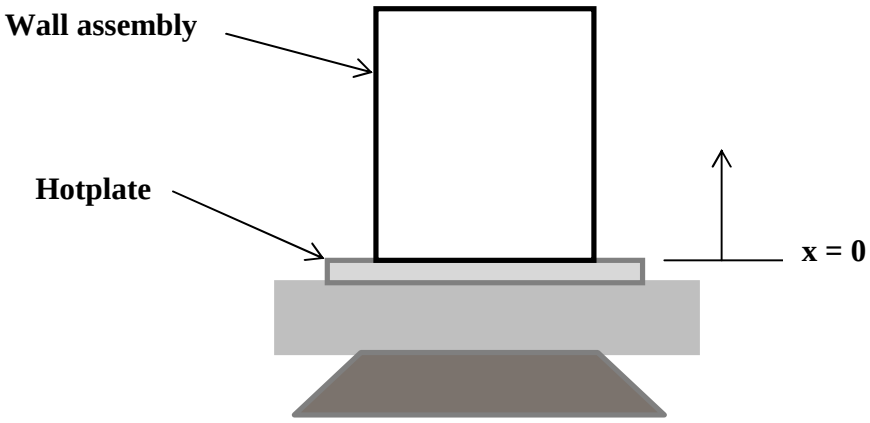

Figure 2.1: Schematic Representation of Wall Sample Exposed to Hotplate.

Constant Heat Flux at x = 0.

The cone calorimeter heater provides a relatively uniform heat flux (q'') to the surface exposed to it. The exposed surface transfers heat to and from the environment by radiation and convection as shown schematically in Figure 2.2. The unexposed surface transfers heat to the surroundings by radiation and convection as well. The mathematical treatment of each of the boundary conditions is outlined below.

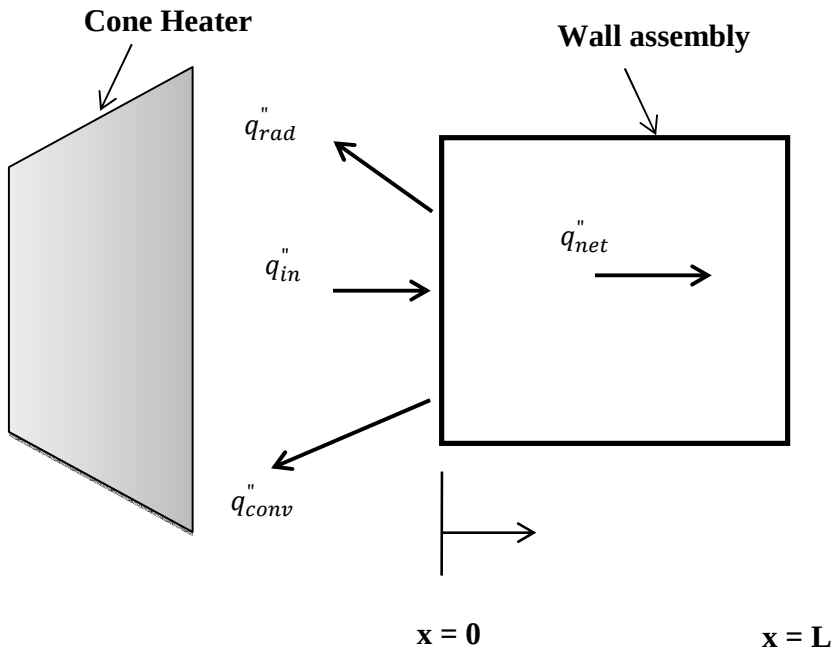

Figure 2.2: Schematic Representation of Wall Sample Exposed to Cone Heater.

Radiative heat flux:

The radiative heat flux exchange q''_{rad}, between the exposed surface of the specimen and the surroundings (assumed to be at ambient temperature) is given by;

$$q''_{rad} = F\varepsilon\sigma(T^4_{x=0} - T^4_a) \qquad (2.3)$$

where:

$\varepsilon =$ emmisivity

σ = Stefan – Boltzmann constant ($W/m^2 \cdot K^4$),

T_a = Temperature of ambient (K),

$T_{x=0}$ = Temperature at the exposed surface of the specimen (K) and

F =View factor

q''_{rad} = Radiative heat flux loses (W/m^2)

Convective heat flux:

The convective heat flux is given by:

$$q''_{conv} = h(T_{x=0} - T_a) \quad (2.4)$$

where:

h = convective heat transfer coefficient ($W/m^2 \cdot K$).

q''_{conv} = Convective heat flux loses (W/m^2)

Net Energy Exchange

The net energy exchange at the exposed surface which gives the boundary condition at the exposed surface (x=0) is given by:

$$q''_{net} = q''_{in} - q''_{rad} - q''_{conv} \quad (2.5)$$

where:

q''_{net} = heat flux conducted into the specimen, (W/m^2),

q''_{in} =, Incident heat flux from cone heater, (W/m^2)

q''_{rad} = Radiative heat flux loses (W/m^2) and

q''_{conv} =Convective heat flux loses (W/m^2)

View Factor

A model for determining the view factor of the radiant interchange between the internal surface of the cone heater and the specimen surface in the cone calorimeter was presented by Yuen et al [35], and Wilson et al [36] as shown in equation (2.7). Figure 2.3 shows the view factor of the interchange between the elemental area dA1 and area 2 and area 4.

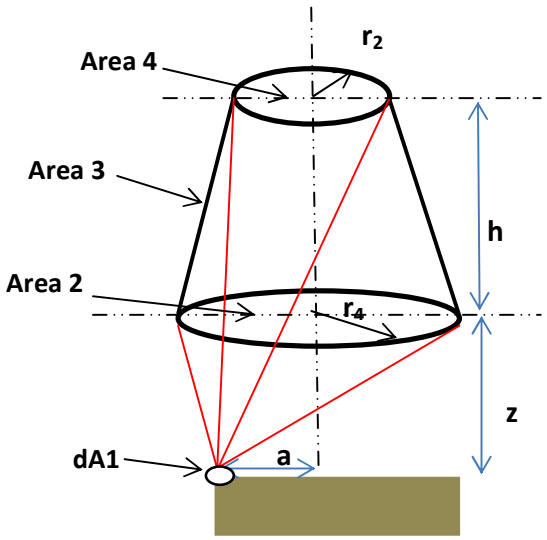

Figure 2.3: Schematic of the internal surface of cone frustum radiating to an elemental surface dA1.

$$F_{d,1-3} = F_{d,1-2} - F_{d,1-4} \tag{2.6}$$

$$F_{d,1-3} = \frac{1}{2}\left[\left(1 - \frac{1 + H_2^2 - R_2^2}{\sqrt{Z_2^2 - 4R_2^2}}\right) - \left(1 - \frac{1 + H_4^2 - R_4^2}{\sqrt{Z_4^2 - 4R_4^2}}\right)\right] \tag{2.7}$$

where: $F_{d,1-2}$ is the view factor between elemental area dA1 and surface 2,

$F_{d,1-3}$ is the view factor between elemental area dA1 and surface 3,

$F_{d,1-4}$ is the view factor between elemental area dA1 and surface 4 and

a, is the distance from centerline

$$R_2 = \frac{r_2}{a}$$

$$R_4 = \frac{r_4}{a}$$

$$H_2 = \frac{z}{a}$$

$$H_4 = \frac{(h+z)}{a}$$

$$Z_2 = 1 + H_2^2 + R_2^2$$

$$Z_4 = 1 + H_4^2 + R_4^2$$

The cone dimensions considered for the model were $r_2 = 4$ cm, $r_4 = 8$ cm, h = 6.8 cm and the cone – specimen distance z, is 2.5 cm. The exposed surface of the specimen is 10 cm by 10 cm which results in a centerline distance (a) of 5 cm. Based on equation (2.7), the view factor $F_{d,1-3}$, is 0.711.

Integrating $F_{d,1-3}$ numerically over the entire surface of the specimen, a value of 0.724 for view factor F_{1-3}, (i.e. a view factor from the specimen to the cone heater surface) was calculated.

The net radiation heat flux to the specimen is the radiation heat transfer from the cone heater divided by the area of the specimen. Therefore, using areas and view factors;

$$q''_{net,3-1} = A_3 \times F_{3-1} \times \varepsilon_3 \sigma (T_3^4 - T_1^4) \quad (2.8)$$

$$q''_{net,3-1} = q_{net,3-1}/A_1$$

By reciprocity,

$$A_3 \times F_{3-1} = A_1 \times F_{1-3}$$

Therefore,

$$q''_{net,3-1} = F_{1-3} \times \varepsilon_1 \sigma (T_3^4 - T_1^4) \quad (2.9)$$

It is assumed that the specimen surface can only see the cone heater and the surroundings, therefore the view factor from the specimen to the surrounding is given as

$$F_{1-surrouding} = 1 - F_{1-3}$$

Therefore the boundary condition for the exposed side is given as;

$$q''_{net,1} = F_{1-3} \times \varepsilon_1 \sigma (T_3^4 - T_1^4) - (1 - F_{1-3}) \times \varepsilon_1 \sigma (T_1^4 - T_a^4) - h(T_1 - T_a) \qquad (2.10)$$

Hence,

$$-\mathrm{k}\frac{\partial \mathrm{T}}{\partial \mathrm{x}} = F_{1-3} \times \varepsilon_1 \sigma (T_3^4 - T_1^4) - (1 - F_{1-3}) \times \varepsilon_1 \sigma (T_1^4 - T_a^4) - h(T_1 - T_a) \qquad (2.11)$$

This is in some ways a simplified treatment of a complex radiation problem which some authors have tried to model in more detail (e.g. Yuen et al [35], Zhang and Delichatsios [37], Boulet et al [38]). However, given the uncertainty in the values of the thermal properties used in the model, which will be discussed later, this approximation is reasonable for the heat transfer model. Based on the assumptions made, this approach may over-estimate the radiation obtained in the cone calorimeter, but it is more suitable for real life fire situations where flame impinges on the exposed surface of the wall assembly. Similar approaches have been used by Spearpoint and Quintere [39], Craft et al [7] and Enninful and Torvi [40], to model the energy exchange between the exposed surface of the sample and the cone heater.

The boundary at the unexposed side is;

$$-k\frac{\partial T}{\partial x} = h(T_{x=L} - T_a) + \varepsilon\sigma[(T_{x=L})^4 - (T_a)^4] \qquad (2.12)$$

Convective heat transfer coefficient

Several authors have developed correlations for determining the convective heat transfer coefficients for different fire scenarios. Incropera et al [41] present convective heat transfer coefficient correlations based on the average temperatures of the ambient and heated surfaces, which can be used for some fire applications. Janssens [42], carried out an experimental and

numerical investigation in order to develop a correlation for the convective heat transfer coefficient for materials tested in the vertical orientation using the cone calorimeter. Based on this investigation, the quadratic expression developed for the convective heat transfer coefficient is presented in equation (2.13)

$$h_c = 1.4 \times 10^{-4}\left(q_e^{"}\right) + 2.4 \times 10^{-6}\left(q_e^{"}\right)^2 \quad (2.13)$$

where:

h_c is the convective heat transfer coefficient (W/m^2·K) and

$q_e^{"}$ is the incident heat flux (kW/m^2).

The correlation presented by Janssens [42] was used here because it best suits the scenario of the heat transfer problem that is being considered. The heat transfer coefficient for the exposed side used in the model was calculated using equation (2.13). Using incident heat fluxes of 35, 50 and 75 kW/m^2, the convective heat transfer coefficient for the exposed side was estimated to be 7.8, 13 and 24 W/m^2·K, respectively.

The convective heat transfer coefficient for the unexposed side is estimated using an empirical correlation for external free convection flow for vertical plates presented by Incropera et al [41]

$$\overline{Nu_L} = \frac{\bar{h}L}{k} \quad (2.14)$$

$$Ra_L = Gr_L Pr = \frac{g\beta(T_s - T_\infty)L^3}{v\alpha} \quad (2.15)$$

$$\overline{Nu_L} = 0.68 + \frac{0.670\, Ra_L^{1/4}}{[1 + (0.429/Pr)^{9/16}]^{4/9}} \qquad (2.16)$$

where Ra_L is the Rayleigh number,

Gr_L is the Grashof number,

$\overline{Nu_L}$ is the Nusselt number,

Pr is the Prandtl's number,

ν is the kinematic viscosity of air (m^2/s),

β is the expansion coefficient of air (K^{-1}),

L is the thickness (m),

g is the acceleration due to gravity([m/s^2) and

α is the thermal diffusivity (m^2/s).

Using a surface temperature T_s, of 130˚C and an ambient temperature T_a, of 24˚C a film temperature T_f, of 77˚C (350 K) is obtained ($T_f = (T_\infty + T_s)/2$). The properties evaluated at this film temperature are [41]:

$\nu = 20.92 \times 10^{-6}$ m^2/s, Pr = 0.7, $\beta = T_f^{-1} = 2.86 \times 10^{-3}$ K^{-1} and $k = 30.0 \times 10^{-3}$ W/m·K, and the Rayleigh number, $Ra_L = 4.97 \times 10^6$.

From equation (2.16), the Nusselt number $Nu_L = 24.89$ and from equation (2.14), the convective heat transfer coefficient value of 7.4 W/m^2·K was calculated.

Using a surface temperature of 25˚C, a convective heat transfer coefficient of 2.6 W/m^2·K was obtained, giving a range of 2.6 – 7.4 W/m^2·K for the convective heat transfer coefficient for the expected temperature range on the unexposed side.

Janssens [42] also presented results for convective heat transfer coefficients based on surface temperatures. For a free flow condition, the convection coefficient ranges from approximately

2.2 W/m^2.K at surface temperature of 25˚C to 5.5 W/m$^2\cdot$K at a surface temperature of 200˚C. Wang [43] used a convective heat transfer coefficient of 4 W/m$^2\cdot$K for the unexposed side which is close to that used by Mehaffey et al [44]. Based on all of these results, a convective heat transfer coefficient of 5 W/m$^2\cdot$K was used for the unexposed side in this model.

Assumptions

The following assumptions were made in this study in order to use the equations outlined above:

1. The heat transfer through the wall assembly at the mid-point is not influenced by the wood studs. Hence, one dimensional heat transfer across the wall assembly is assumed.
2. The burning of the gypsum board paper on the exposed surface of the board during the test occurs within 2-3 min of the start of the test. The burning of the paper is not considered in the model.
3. A perfect thermal contact is assumed between the gypsum board and insulation.
4. Sultan [45] and others [46] have noted that the exposed gypsum boards experience cracks and fall off when the temperature of the mid-thickness exceeds 600˚C. However, in this study the gypsum boards in the wall assembly are assumed to be in place and without cracks for the duration of the simulation.
5. While the energy associated with phase change in the gypsum board is included in the model through the use of the apparent heat capacity, the migration of moisture through the gypsum board is not considered in the model.

2.2 DISCRETIZATION

The explicit finite difference method (FDM) was used to transfer the partial differential equation into a finite difference equation (FDE). Since wall assemblies are made of layered constructions, a finite difference formulation for a multilayered panel described by Wang [33] was modified for the heat transfer problem. To obtain the finite difference form of Equation 2.2, the central-difference approximations to the spatial derivatives and the forward-difference approximation to the time derivatives were employed.

The FDE is comprised of three typical equations, (i indicates the time step);

1. For a boundary node (For example, for a boundary node 1),

$$\frac{\rho_1^i {c_p}_1^{\,i} \Delta x\left(T_1^{i+1} - T_1^i\right)}{2\Delta t} = \frac{k_1^i\left(T_2^i - T_1^i\right)}{\Delta x} + F\varepsilon\sigma\left[(T_{cone}+273)^4 - \left(T_1^i+273\right)^4\right] - (1-F)\left[\left(T_1^i+273\right)^4 - (T_a+273)^4\right] - h\left(T_1^i - T_a\right) \quad (2.17$$

$$T_n^{i+1} = 2F_o\left[T_2^i + \frac{h\Delta x}{k_1^i}T_a + \left(\frac{1}{2F_o} - 1 - \frac{h\Delta x}{k_1^i}\right)T_1^i\right] + F\varepsilon\sigma\left[(T_{cone}+273)^4 - \left(T_1^i+273\right)^4\right] - (1-F)\left[\left(T_1^i+273\right)^4 - (T_a+273)^4\right] \quad (2.18)$$

where;

$$F_o = \frac{k_1^i \Delta t}{\rho_1^i {c_p}_1^{\,i} \Delta x}$$

The most important stability criterion for the FDE is that of the boundary node. This requires that;

$$F_o \leq 0.5\left[1+\frac{h\Delta x}{k_1^i}+\frac{\varepsilon\sigma\Delta x}{k_1^i}.\frac{\left(T_1^i+273\right)^4}{T_1^i}\right]^{-1} \tag{2.19}$$

2. For an interface node;

$$T_n^{i+1}=F_o\left[\frac{2\left(k_1^i\Delta x_2 T_{n-1}^i+k_2^i\Delta x_1 T_{n+1}^i\right)}{k_1^i\Delta x_2+k_2^i\Delta x_1}+T_n^i\left(\frac{1}{F_o}-2\right)\right] \tag{2.20}$$

$$F_o=\left(\frac{k_1^i\Delta x_2+k_2^i\Delta x_1}{\rho_2^i {c_p}_2^i\Delta x_2+\rho_1^i {c_p}_1^i\Delta x_1}\right) \tag{2.21}$$

where subcripts 1,2 represent the 2 materials at the interface.

3. For an interior node n, within a material layer.

$$\frac{\rho_n^i {c_p}_n^i\Delta x\left(T_n^{i+1}-T_n^i\right)}{\Delta t}=\frac{k_{n-1,n}^i\left(T_{n-1}^i-T_n^i\right)}{\Delta x}-\frac{k_{n+1,n}^i\left(T_n^i-T_{n+1}^i\right)}{\Delta x} \tag{2.22}$$

$$T_n^{i+1}=F_o\left[\frac{2\left(k_{n-1,n}^i T_{n-1}^i+k_{n+1,n}^i T_{n+1}^i\right)}{k_{n+1,n}^i+k_{n-1,n}^i}+T_n^i\left(\frac{1}{F_o}-2\right)\right] \tag{2.23}$$

$$F_o=\left(\frac{(k_{n+1,n}^i+k_{n-1,n}^i)\Delta t}{2\rho_n^i {c_p}_n^i(\Delta x)^2}\right) \tag{2.24}$$

In order to ensure stability of the calculation, the coefficient of T_n^i, in equation (2.23) must be greater than zero. Therefore, the stability criterion is given by;

$$\frac{1}{F_o} - 2 \geq 0$$

This implies that; $F_o \leq 0.5$

This restricts the time step.

The conductivities $k_{n+1,n}$, and $k_{n-1,n}$ are evaluated at each time step as;

$$k_{n+1,n}^i = k\left(\frac{T_n^i + T_{n+1}^i}{2}\right)$$

$$k_{n-1,n}^i = k\left(\frac{T_n^i + T_{n-1}^i}{2}\right)$$

2.3 VALIDATION OF MODEL

In order to ensure accuracy of the formulated differential equations and the discretization of the differential equations and coding of the equations, validation exercises were conducted using fixed temperature and heat flux boundary conditions. The validation exercise conducted was for three pieces of regular gypsum boards (12.7 mm each) joined together as shown in Figure 2.4.

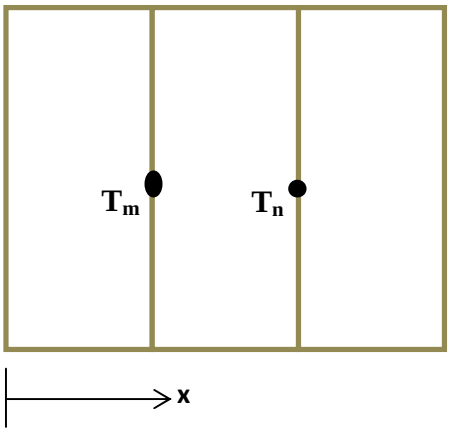

Figure 2.4: Schematic of the gypsum layers and temperature positions.

Constant properties of regular gypsum board used in the simulation are presented in Table 2.1.

Table 2.1: Property of Regular Gypsum Board.

Property	**Value**
Thermal Conductivity, k (W/m·K)	0.168
Specific Heat, c_p (J/kg·K)	950
Density, ρ (kg/m^3)	645.7
Thickness, L (m)	0.0381

2.3.1 Constant Thermal Property – Fixed Temperature Boundary Condition

To validate the accuracy of the finite difference model, an exact solution to equation (2.25) reported by Carslaw and Jaeger's [47] was used to solve for temperature as a function of space and time. This is one dimensional heat transfer in a solid bounded by parallel plates which assumes an initial uniform temperature and fixed temperature boundary conditions

$$\rho c_p \frac{\partial T}{\partial t} = \frac{\partial}{\partial x}\left(k \frac{\partial T}{\partial x}\right) \tag{2.25}$$

The exact solution is given as:

$$T(x,t) = \frac{2}{l}\sum_1^\infty exp\left(\frac{-\alpha n^2\pi^2 t}{l^2}\right).\sin\left(\frac{n\pi x}{l}\right)\left[\int_0^1 f(x')\sin\left(\frac{n\pi x'}{l}\right)dx' + \frac{n\alpha x}{l}\int_0^t exp\left(\frac{\alpha n^2\pi^2\lambda}{l^2}\right)\{\emptyset_1(\lambda) - (-1)^n\emptyset_2(\lambda)\}d\lambda\right] \tag{2.26}$$

where l is the total thickness (m),

α is the thermal diffusivity (m^2/s),

t is time (s),

x is the distance from boundary (m), and

n is the number of layers.

Using a normalized temperature, the exposed surface temperature is fixed at 1, the initial and unexposed temperatures are fixed at 0.

Boundary condition: @ x = 0, T = 1;

@ x = L, T = 0;

Initial condition: @ t = 0, T = 0;

This simplifies equation (2.26) to;

$$T(x,t) = \sum_{1}^{\infty}\left[1 - exp\left(\frac{-\alpha n^2\pi^2 t}{l^2}\right)\right].\frac{\sin(\frac{n\pi x}{l})}{\frac{n\pi}{2}} \qquad (2.27)$$

This approach was used by McCarthy [48] and Spangler [49] to validate heat transfer models. The above simplified case was used to compute the temperature distribution of three layers of gypsum boards with properties presented in Table 2.1. The results are compared with the finite difference solution for the same layers of gypsum as shown in Figure 2.5. The simulation was allowed to run for 30 minutes. Table 2.2 gives a summary of the results from both the exact solution and numerical solution at depths of 12.7 and 25.4 mm. The percentage differences between the exact and numerical solution are in the range of 0 – 3%.

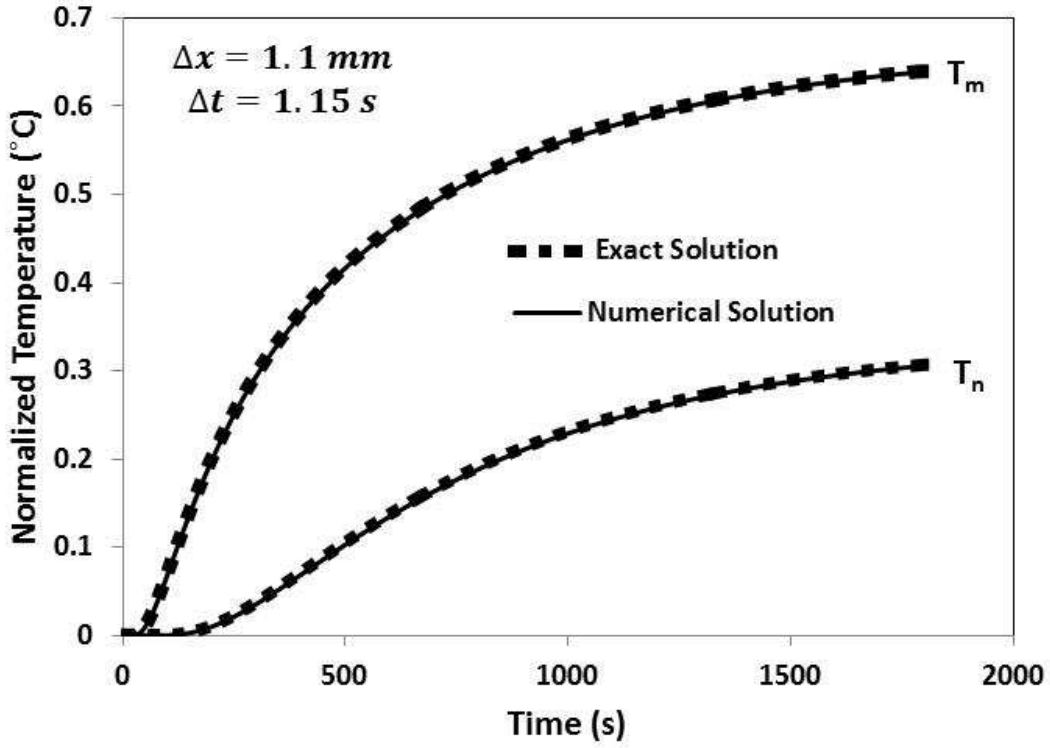

Figure 2.5: Exact Solution vs. Numerical Solution (Δx = node distance and Δt = time step).

Table 2.2: Temperatures Obtained From Exact and Numerical Solution for Duration of 30 min. at Different Depths of 12.7 mm and 25.4 mm.

Time (s)	**Normalized Temperature at Depth 12.7 mm T_m**		**Normalized Temperature at Depth 25.4 mm T_n**	
	Exact Solution	**Numerical Solution**	**Exact Solution**	**Numerical Solution**
300	0.30	0.29	0.04	0.04
600	0.46	0.458	0.14	0.14
900	0.54	0.542	0.21	0.21
1200	0.59	0.591	0.26	0.26
1500	0.62	0.621	0.29	0.29
1800	0.64	0.638	0.31	0.31

2.3.2 Constant Thermal Property – Heat Flux Boundary Condition

To validate the finite difference model, an analytical solution to equation (2.2) reported by Incropera et al [41] was used to solve for temperature as a function of space and time. This is a one dimensional heat transfer in a semi-infinite solid for a constant surface heat flux boundary condition. The validation exercise was conducted at heat fluxes of 35 kW/m^2, 50 kW/m^2 and 75 kW/m^2 for three layers of gypsum boards joined together (Figure 2.4) with properties shown in Table 2.1. Figures 2.6, 2.7 and 2.8 show the comparison between the analytical solution and the

numerical solution at the exposed surface for heat flux exposures of 35 kW/m^2 , 50 kW/m^2 and 75 kW/m^2, respectively, for an exposure time of 5 minutes.

The exact solution is given as:

$$T(x,t) - T_i = \frac{2q_0^{"}\left(\frac{\alpha t}{\pi}\right)^{\frac{1}{2}}}{k} exp\left(\frac{-x^2}{4\alpha t}\right) - \frac{q_0^{"}x}{k} erfc\left(\frac{x}{2\sqrt{\alpha t}}\right) \quad (2.28)$$

where:

$q_0^{"}$ is the incident heat flux $\left(\frac{\text{kW}}{m^2}\right)$

α is the thermal diffusivity (m^2/s)

k is the thermal conductivity ($W/m \cdot k$)

x is the distance from exposed surface (m)

The time-steps and node distance used for the finite difference simulation are:

$\Delta x = 1.1\ mm$

$\Delta t = 1\ s.$

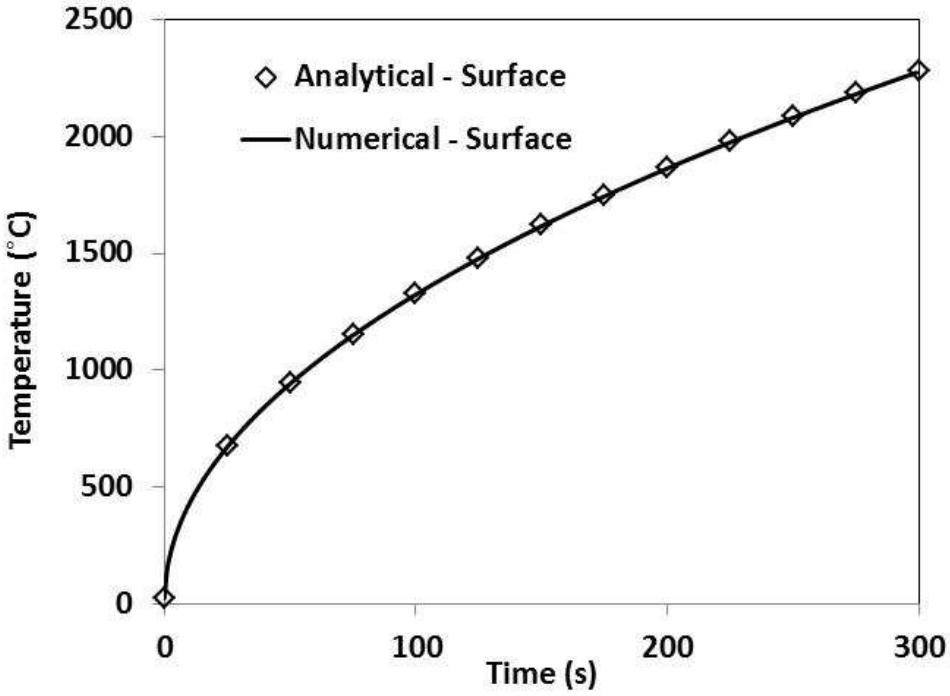

Figure 2.6: Comparison of Numerical and Analytical Results at Surface for Exposure of 5 min. (Irradiance of 35 kW/m^2)

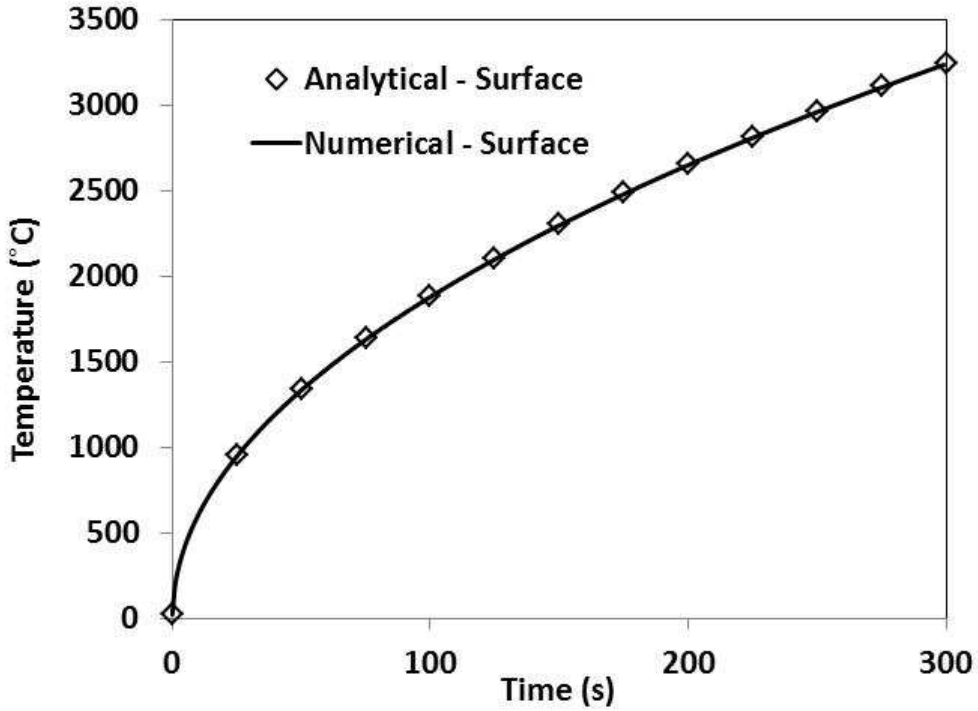

Figure 2.7: Comparison of Numerical and Analytical Results at Surface for Exposure of 5 min. (Irradiance of 50 kW/m^2)

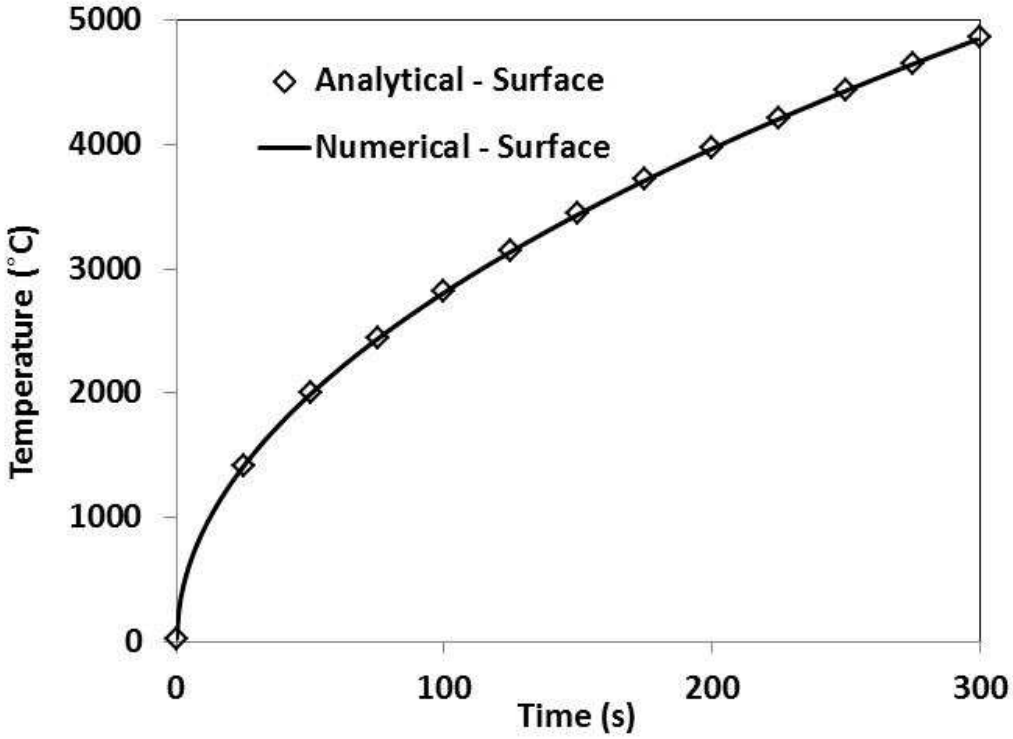

Figure 2.8: Comparison of Numerical and Analytical Results at Surface for Exposure of 5 min. (Irradiance of 75 kW/m^2)

Figures 2.9, 2.10 and 2.11 show the comparison between the analytical solution and the numerical solution at a depth of 25.4 mm from the exposed surface for heat flux exposures of 35kW/m^2 , 50 kW/m^2 and 75 kW/m^2, respectively, for an exposure time of 5 minutes.

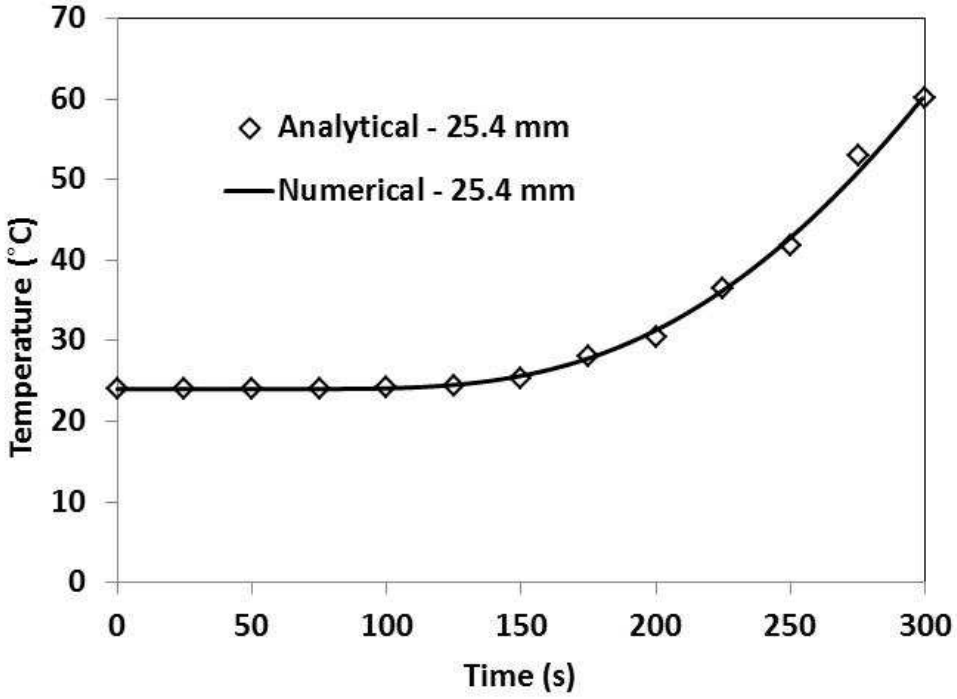

Figure 2.9: Comparison of Numerical and Analytical Results at Depth of 25.4 mm (T_m) for Exposure of 5 min. (Heat Flux of 35 kW/m^2).

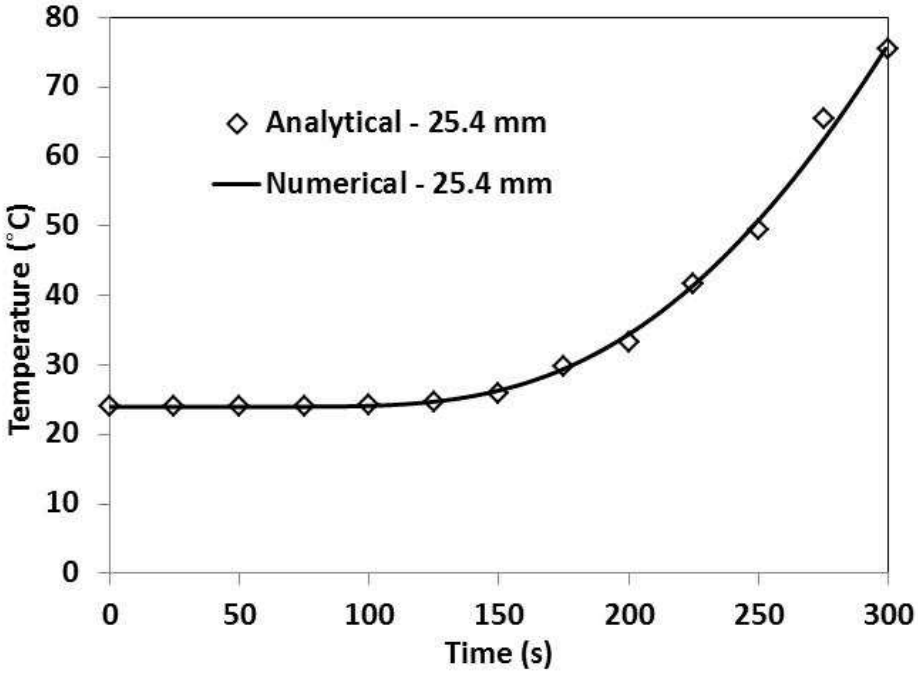

Figure 2.10: Comparison of Numerical and Analytical Results at Depth of 25.4 mm (T_m) for Exposure of 5 min. (Heat Flux of 50 kW/m^2).

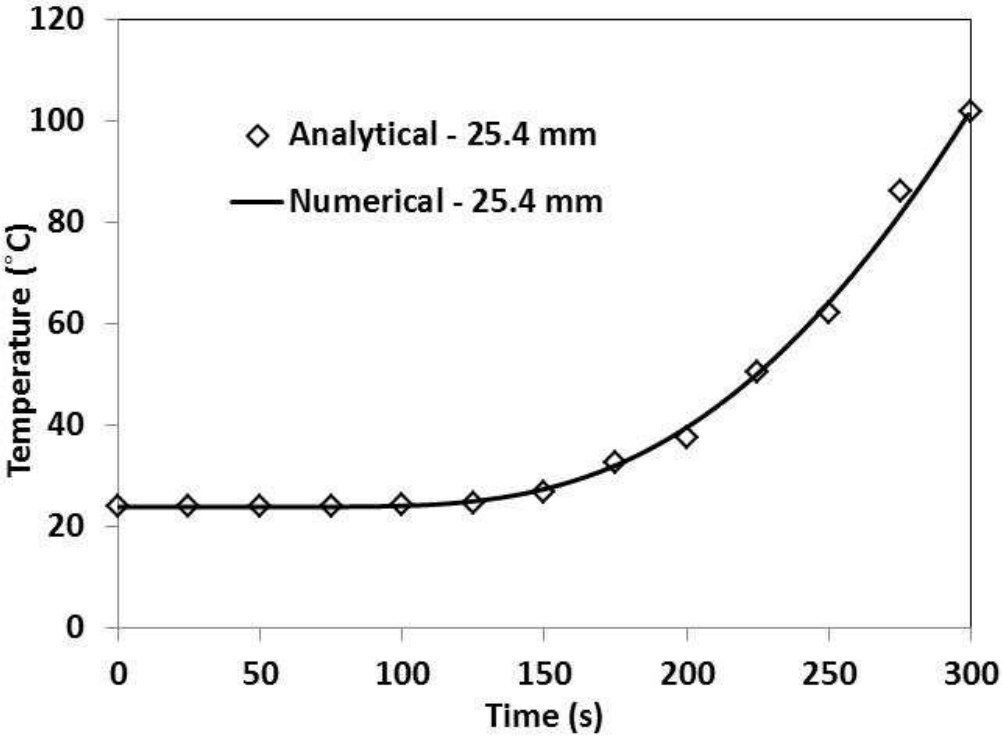

Figure 2.11: Comparison of Numerical and Analytical Results at Depth of 25.4 mm (T_m) for Exposure of 5 min. (Heat Flux of 75 kW/m^2).

Figure 2.6 to 2.11 show a very good agreement between the analytical and numerical results. The variations between the analytical and numerical results were less than 2% throughout the simulation time. Table 2.3 shows a comparison between the analytical and numerical results at different thicknesses within the three layers of gypsum boards at heat flux exposures of 35 kW/m^2, 50 kW/m^2 and 75 kW/m^2 for duration of 5 minutes.

Table 2.3: Temperatures Obtained From Numerical and Analytical Results for Duration of 300 s at Different Depths and Heat Fluxes of 35 kW/m^2, 50 kW/m^2 and 75 kW/m^2 .

Thickness (mm)	**Temperature (˚C)**					
	35 kW/m^2		**50 kW/m^2**		**75 kW/m^2**	
	Numerical	**Analytical**	**Numerical**	**Analytical**	**Numerical**	**Analytical**
Surface	2273.8	2281.1	3237.9	3248.0	4844.9	4860.9
6.35	1095.7	1102.8	1554.9	1565.2	2320.4	2336.0
12.7	449.7	452.9	632.2	636.8	936.4	943.3
19.05	162.3	163.1	221.5	222.8	320.3	322.3
25.4	60.1	60.1	75.6	75.6	101.4	101.9
31.75	31.3	31.3	34.5	34.5	39.7	39.7

The results of the numerical and analytical solution shown in Table 2.3 are in a very good agreement with a variation of less than 2% in all cases. This shows that the discretization of the differential equations and coding of the equations were done correctly, and that the time steps and grid sizes are appropriate.

CHAPTER THREE: NUMERICAL RESULTS

The results from the numerical models formulated in Chapter Two will be presented in this chapter. The predictions made with the models include:

- Heat transfer in wall assemblies exposed to a fixed temperatures of 80˚C;
- Heat transfer in a single layer of gypsum board: Temperature profiles in regular, lightweight and type X gypsum boards exposed to an incident heat flux of 75 kW/m^2 for one hour;
- Heat transfer in a wall assembly (constant properties): Temperature profiles in regular, lightweight and type X gypsum board wall assemblies exposed to an incident heat flux of 75 kW/m^2;
- Heat transfer in a wall assembly (temperature dependent properties): Temperature profiles in single layer lightweight gypsum board wall assemblies exposed to incident heat fluxes of 35 kW/m^2 and 50 kW/m^2;
- Heat transfer in a wall assembly (temperature dependent properties): Temperature profiles in single layer regular, lightweight and type X gypsum board wall assemblies exposed to an incident heat flux of 75 kW/m^2; and
- Heat transfer in a wall assembly (temperature dependent properties): Temperature profiles in double layer regular, lightweight and type X gypsum board wall assemblies exposed to an incident heat flux of 75kW/m^2.

Sensitivity studies will be conducted to determine the effects of the thermal properties on the model results.

3.1 THERMAL PROPERTIES USED IN MODEL

The materials selected for the tests were 12.7 mm thick lightweight, 12.7 mm thick regular and 15.9 mm thick type X gypsum boards, as well as Roxul ComfortBath R-14 (89 mm thick) stone wool insulation. These materials, along with nominal 2x4 wood studs (spruce-pine-fir), were purchased from a home improvement retail store in Saskatoon between January and February, 2013.

The thermal properties used in the model for these materials were derived from data presented in the literature. Several authors have determined the temperature dependent properties of gypsum boards and insulation. The properties used in the model are presented below.

3.1.1 Thermal Conductivity of Gypsum

The thermal conductivity measurements presented by different researchers vary because of the presence of moisture, pores, differences in the microstructure of gypsum board and methods of measurement. The variation in the thermal conductivity measurements is also likely due to changes to gypsum board over the years. Figure 3.1 shows the values of the thermal conductivity of gypsum boards at different temperatures as measured by Harmathy [50], Anderson and Janssen [51], Benichou et al [52, 53] and Mehaffey et al [20]. Harmathy used a relatively small temperature gradient to determine the thermal conductivity with an accuracy within 7%. Andersson and Janssen used the transient hot strip (THS) method to measure the thermal conductivity. This method uses the measured resistance of a metal strip embedded in the material to determine the thermal conductivity. Benichou et al [52, 53]used a TC-31 thermal conductivity meter made by Kyoto Electronics which uses a steady state analysis to determine the thermal conductivity.

Benichou et al [50] defined the thermal conductivity of regular gypsum board using four regions: a constant value from room temperature to 100˚C, a decrease at 100˚C to a value which then remains constant to 400˚C, followed by a rise to 800 ˚C, and finally a steady increase in the slope after 800˚C. Benichou et al [53] defined the thermal conductivity of type X gypsum board using three regions: a steady decrease to a temperature of 200˚C, a constant value between 200˚C and 800˚C and a steep increase after 800˚C. Thomas [51] suggested that the increased thermal conductivity after 800˚C is as a result of the increased radiation which occurs in the openings of cracks in gypsum board at this temperature. Radiation within the cracks increases the effective thermal conductivity of gypsum boards.

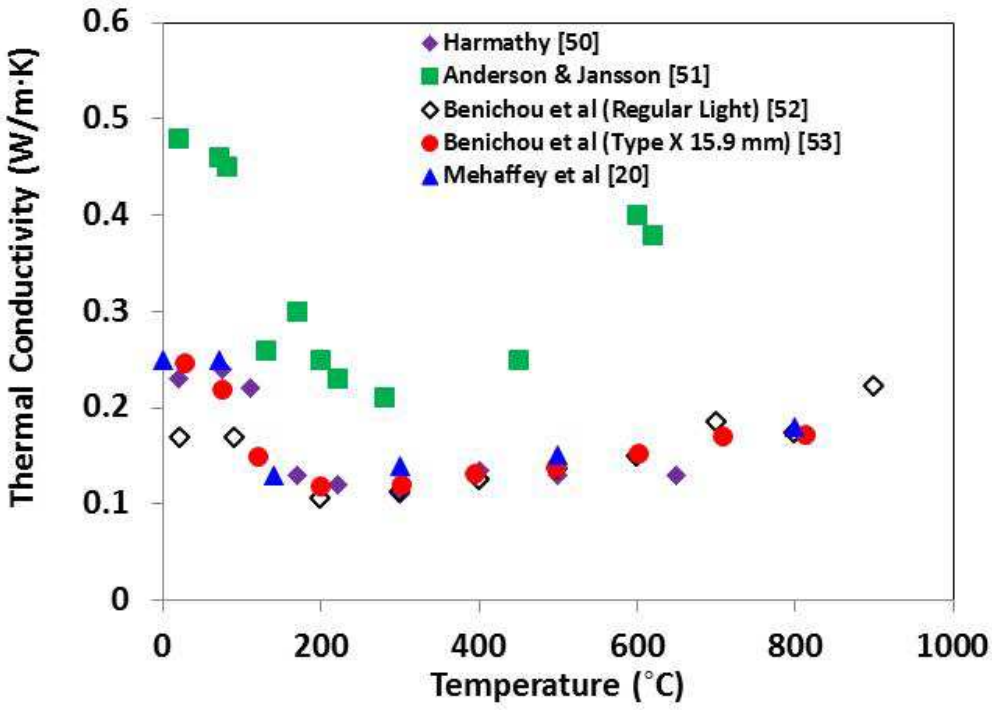

Figure 3.1: Comparison of Thermal Conductivity Values of Gypsum Board from Different Researchers.

The values of the thermal conductivity in Figure 3.1 show a large scatter; however, that reported by Harmathy [50], Mehaffey et al [20] and Benichou [53] are in good agreement. The

temperature dependent thermal conductivity presented by Benichou et al [52] was used in this model for regular and lightweight gypsum boards (Figure 3.2) and that reported by Mehaffey et al [20] was adapted for type X gypsum board (Figure 3.3).

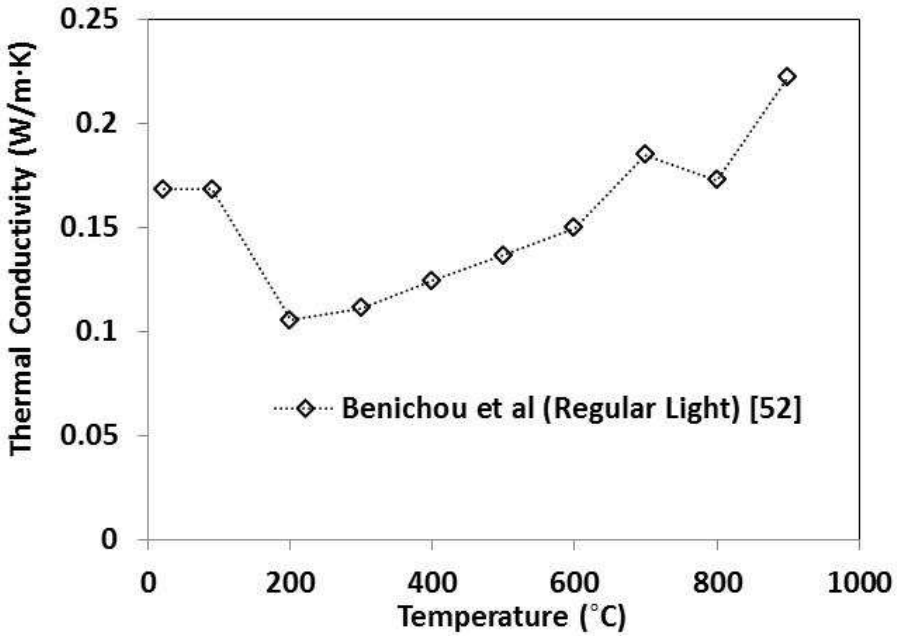

Figure 3.2: Thermal Conductivity of Both Regular and Lightweight Gypsum Board Used in the Model.

The temperature-thermal conductivity correlations drawn from Figure 3.2 for both regular and lightweight gypsum boards are given as follows:

$$
\begin{aligned}
k &= 0.1683 && 0^{\circ}\mathrm{C} < T \leq 90^{\circ}\mathrm{C} \\
k &= -0.00057(T - 90) + 0.1683 && 90^{\circ}\mathrm{C} < T \leq 200^{\circ}\mathrm{C} \\
k &= 0.000055(T - 200) + 0.1056 && 200^{\circ}\mathrm{C} < T \leq 300^{\circ}\mathrm{C} \\
k &= 0.0001283(T - 300) + 0.1111 && 300^{\circ}\mathrm{C} < T \leq 600^{\circ}\mathrm{C} \\
k &= k = 0.000352(T - 600) + 0.1496 && 600^{\circ}\mathrm{C} < T \leq 700^{\circ}\mathrm{C} \\
k &= -0.000121(T - 700) + 0.1848 && 700^{\circ}\mathrm{C} < T \leq 800^{\circ}\mathrm{C} \\
k &= 0.000495(T - 800) + 0.1727 && T > 800^{\circ}\mathrm{C}
\end{aligned}
\tag{3.1}
$$

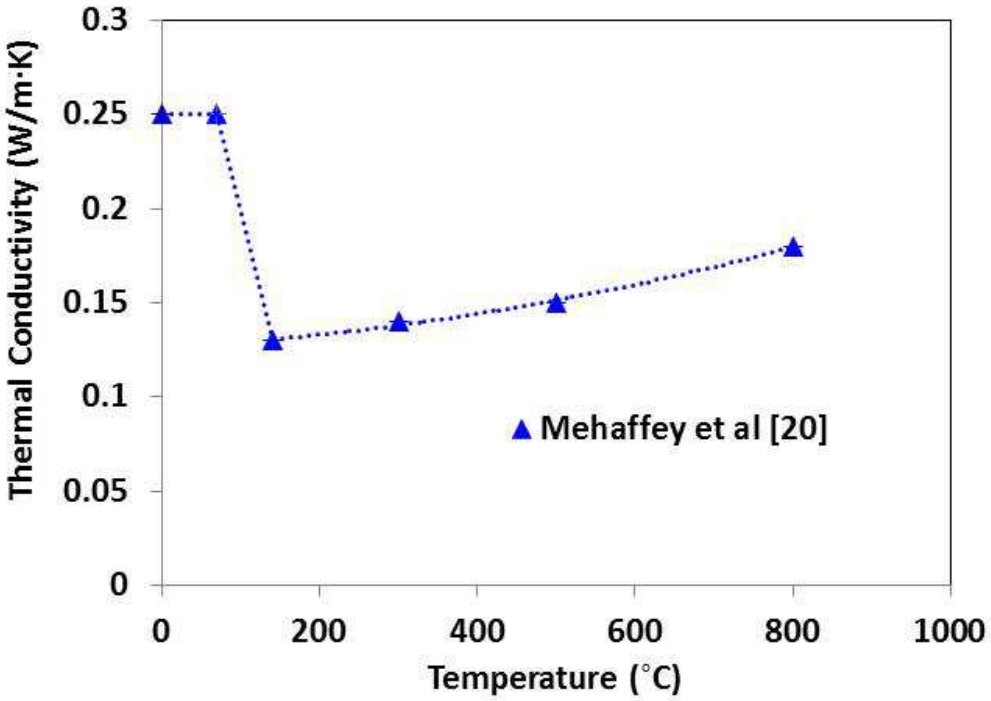

Figure 3.3: Thermal Conductivity of Type X Gypsum Board Used in the Model.

The temperature-thermal conductivity correlations drawn from Figure 3.3 for type X gypsum boards are given as follows:

$$
\begin{aligned}
k &= 0.25 && 0^{\circ}\mathrm{C} < T \leq 70^{\circ}\mathrm{C} \\
k &= -0.0017(T - 70) + 0.25 && 70^{\circ}\mathrm{C} < T \leq 140^{\circ}\mathrm{C} \\
k &= 0.0000625(T - 140) + 0.13 && 140^{\circ}\mathrm{C} < T \leq 300^{\circ}\mathrm{C} \\
k &= 0.00008(T - 300) + 0.14 && T > 300^{\circ}\mathrm{C}
\end{aligned}
\tag{3.2}
$$

3.1.2 Thermal Conductivity of Insulation

Benichou et al [52] conducted a study on the thermal conductivity of millboard and glass fiber insulation as a function of temperature, the results of which are shown in Figure 3.4. A gradual increase in the thermal conductivity is noticed in rock fibre and millboard insulation. A gradual increase in thermal conductivity similar to that obtained for rock fibre and millboard is also

noticed for glass fiber insulation from 0.022 W/m·K at 24°C to 0.204 W/m·K at 515°C. A rapid increase in thermal conductivity is obtained beyond 515°C. Benichou et al [52] attributed the variation in the thermal conductivity of the insulation to the difference in chemical composition of the insulation fiber.

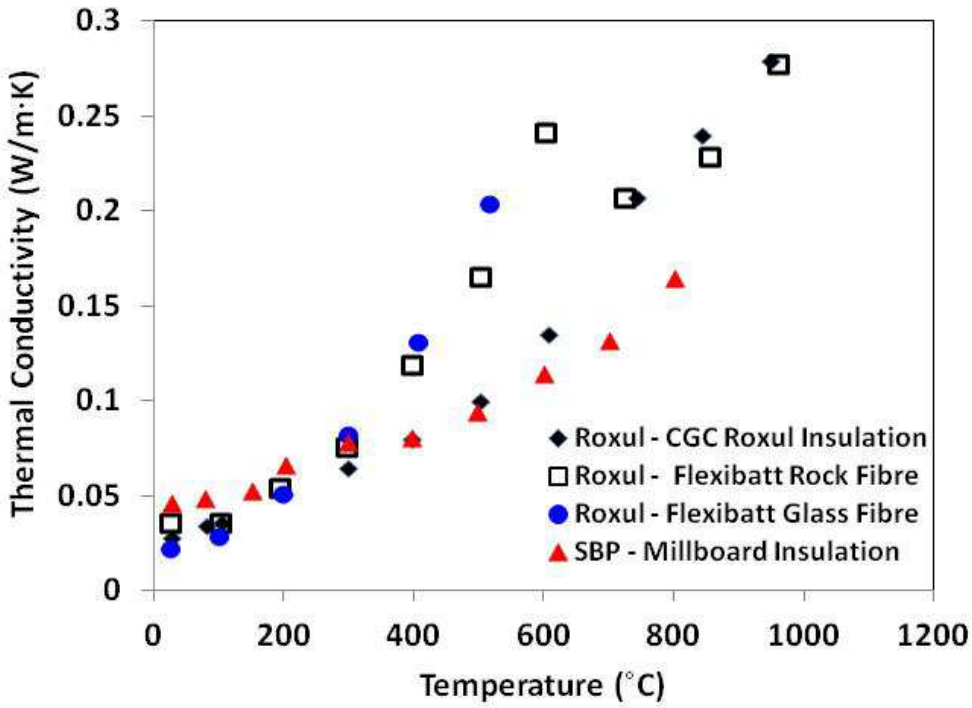

Figure 3.4: Temperature-Dependent Thermal Conductivity of Insulation Benichou et al [52]

Roxul ComfortBath R-14 (89 mm thick) stone wool insulation was used in tests reported in this thesis. Based on the R-value provided by the manufacturer, the thermal conductivity value at room temperature for Roxul ComfortBath R-14 (89 mm thick) stone wool insulation is calculated to be 0.036 W/m·K. Since the thermal conductivity presented by Benichou et al [52] is approximately equal to 0.036, the temperature dependent thermal conductivity data reported by Benichou et al [52] for Roxul insulation (flexibatt) was used as input in the model for stone wool insulation. Figure 3.5 shows the thermal conductivity adopted for the model.

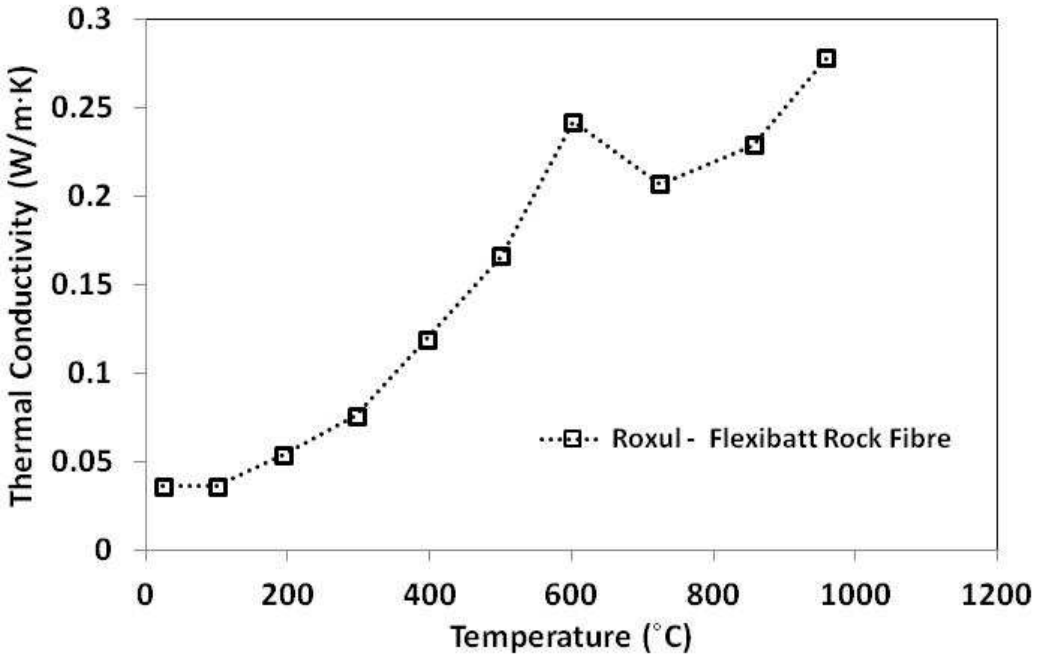

Figure 3.5: Thermal Conductivity of Stone Wool Insulation Used in the Model.

The temperature-thermal conductivity correlations drawn from Figure 3.5 for stone wool insulation are given below:

$$
\begin{aligned}
k &= 0.036 && 0^{\circ}\mathrm{C} < T \leq 101^{\circ}\mathrm{C} \\
k &= 0.000194(T - 101) + 0.036 && 101^{\circ}\mathrm{C} < T \leq 194^{\circ}\mathrm{C} \\
k &= 0.0002135(T - 194) + 0.054 && 194^{\circ}\mathrm{C} < T \leq 297^{\circ}\mathrm{C} \\
k &= 0.0004343(T - 297) + 0.076 && 297^{\circ}\mathrm{C} < T \leq 396^{\circ}\mathrm{C} \\
k &= 0.000447(T - 396) + 0.119 && 396^{\circ}\mathrm{C} < T \leq 501^{\circ}\mathrm{C} \\
k &= 0.0007525(T - 501) + 0.166 && 501^{\circ}\mathrm{C} < T \leq 602^{\circ}\mathrm{C} \\
k &= -0.0002869(T - 602) + 0.242 && 602^{\circ}\mathrm{C} < T \leq 724^{\circ}\mathrm{C} \\
k &= 0.0001667(T - 724) + 0.207 && 724^{\circ}\mathrm{C} < T \leq 856^{\circ}\mathrm{C} \\
k &= 0.0004757(T - 856) + 0.229 && T > 856^{\circ}\mathrm{C}
\end{aligned}
\tag{3.3}
$$

3.1.3 Specific Heat of Gypsum

The specific heat of gypsum board values measured by some researchers is presented in Figure 3.6. The specific heat peaks noticed in Figure 3.6 can be traced to the reactions that occur when gypsum board is exposed to high heat fluxes. The first peak, which generally occurs at 100°C, is traced to the first dehydration (calcination) process of gypsum. The temperature at which the second specific heat peak occurs, and the values obtained by the different researchers, varies. Harmathy [50] gave measurements up to 630°C, with the first specific heat peak value of 7.32 kJ/kg·K obtained at a temperature of 100°C, and a second specific heat peak value of 2 kJ/kg·K obtained at a temperature of 630°C. Anderson and Janssen [51] reported a first peak value of 52.2 kJ/kg.·K at 110°C, and a second peak value of 19.2 kJ/kg·K at 210˚C. Wakili and Hugi [54] mentioned that the second peak obtained by Benichou et al [52, 53] is as a result of the de-carbonization of type X gypsum board at about 700˚C. The specific heat capacity reported by the researchers at ambient temperature is between 0.7–0.95 kJ/kg.·K.

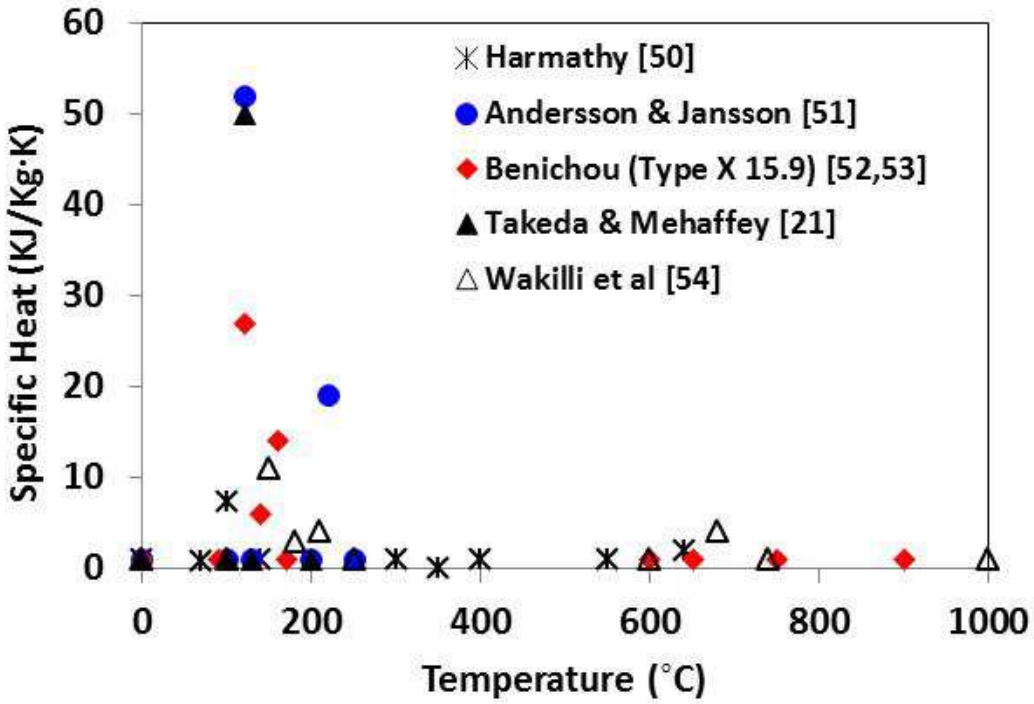

Figure 3.6: Comparison of Specific Heat Values Measured by Different Researchers for Gypsum Board.

The temperature dependent specific heat capacity of gypsum used in the model is that reported by Benichou et al [52] with a specific heat of 950 J/kg·K at room temperature. Mehaffey et al [20] also reported a value of 950 J/kg·K as the specific heat capacity of gypsum board at room temperature. Based on the data presented in Figure 3.6, averages of the temperature dependent specific heat peaks that represent the dehydration and decarbonization processes of gypsum as shown in Figure 3.7 were used in the model.

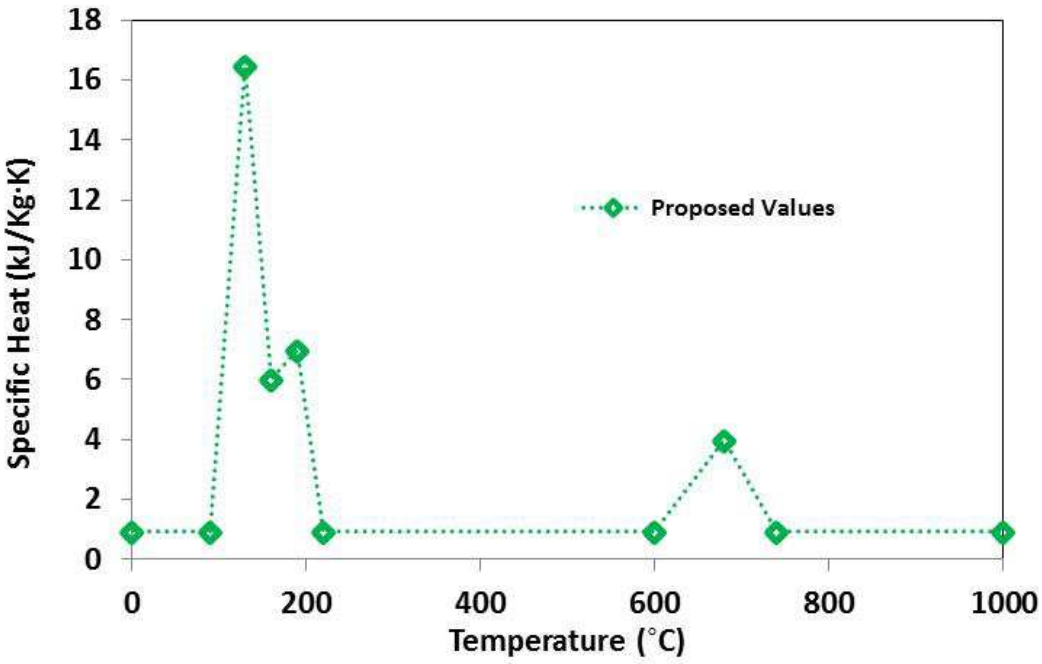

Figure 3.7: Specific Heat of Gypsum Board Used in the Model.

The temperature-specific heat correlations drawn from Figure 3.7 for gypsum board are given as follows:

$$
\begin{aligned}
C_p &= 950 && 0^{\circ}\mathrm{C} < T \leq 90^{\circ}\mathrm{C} \\
C_p &= 388.75(T-90)+950 && 90^{\circ}\mathrm{C} < T \leq 130^{\circ}\mathrm{C} \\
C_p &= -350(T-130)+16500 && 130^{\circ}\mathrm{C} < T \leq 160^{\circ}\mathrm{C} \\
C_p &= 33.333(T-160)+6000 && 160^{\circ}\mathrm{C} < T \leq 190^{\circ}\mathrm{C} \\
C_p &= -201.67(T-190)+7000 && 190^{\circ}\mathrm{C} < T \leq 220^{\circ}\mathrm{C} \\
C_p &= 950 && 220^{\circ}\mathrm{C} < T \leq 600^{\circ}\mathrm{C} \\
C_p &= 38.125(T-600)+950 && 600^{\circ}\mathrm{C} < T \leq 680^{\circ}\mathrm{C} \\
C_p &= -50.833(T-680)+4000 && 680^{\circ}\mathrm{C} < T \leq 740^{\circ}\mathrm{C} \\
C_p &= 950 && T > 740^{\circ}\mathrm{C}
\end{aligned}
\tag{3.4}
$$

3.1.4 Specific Heat of Insulation

Benichou et al [52] carried out specific heat measurements of rock fiber insulation, mineral wool, glass fiber and SBP – Millboard fiber insulation using a Differential Scanning Calorimeter (DSC) at a heating rate of 5˚C/min in Nitrogen with results shown in Figure 3.8. Over regions where there are phase changes or reactions, specific heats measured by the DSC would account for energies associated with these phase changes or reactions, in a similar way to how these energies are treated using the apparent heat capacity described in Section 2.1. A gradual increase in specific heat capacity up to temperatures of about 300 – 350˚C is observed in all insulations tested. Beyond 330˚C to 470˚C a rapid decrease in specific heat is noticed, followed by a rapid increase to 600˚C, then a slight variation in specific heat after 600˚C. The negative values of specific heat were attributed to the exothermic reaction in the material which was as a result of the applied heating rate, where the rate of absorption of the material is less than the rate of evolution due to reactions. The variation in the specific heat of the insulation was attributed to the difference in the composition of the insulation from one product to another.

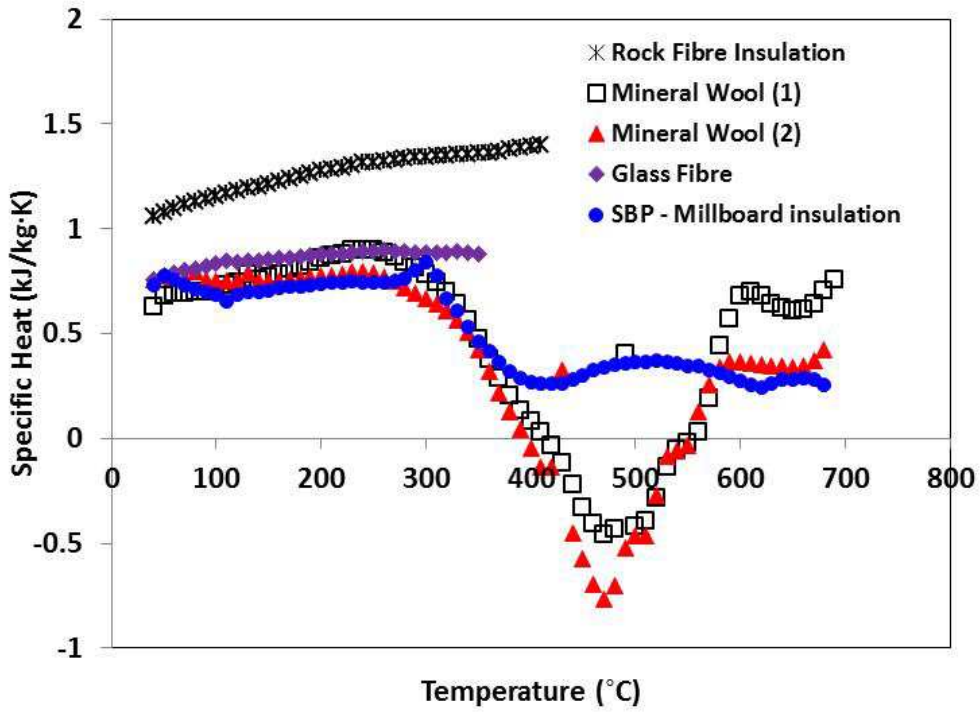

Figure 3.8: Temperature Dependent Specific Heat of Insulation (Benichou et al [52])

As will be discussed in the next section, previous research has indicated that there are relatively small changes in mass for the type of insulation used in this study over the expected temperature range. There is also considerably less data in the literature on specific heat values of stone wool insulation than there are for gypsum board. Therefore, a constant specific heat value of 0.7 kJ/kg·K was used in the model for stone wool.

3.1.5 Density of Gypsum Board

The density of gypsum board influences the thermal performance of the boards when exposed to high temperature. Table 3.1 shows some examples of the density measurements reported in the literature for some gypsum boards.

Table 3.1: Comparison of Density Values of Gypsum by Different Researchers.

Authors	**Type of Board**	**Nominal Thickness (mm)**	**Density (kg/m^3)**
Craft et al [8]	Regular	12.7	620
	Type X	15.9	690
Thomas et al [17]	Regular	12.7	612
	Type X	15.9	687 – 750
Mehaffey et al[18]	Type X	15.9	648

Mass Loss of Gypsum Board

The mass loss of gypsum board as a function of temperature has been reported by some authors. The mass loss results of type X and type C gypsum board presented by Thomas et al [19] and Benichou et al [52-53] were similar with the mass loss for all specimens beginning at approximately 100˚C. Mehaffey et al [44] report that between 100˚C and 160˚C the cores of the gypsum lost about 18% mass, while Takeda and Mehaffey [55] report that between 100˚C and 150˚C a mass loss of 15% was obtained. Benichou et al [52] report that between 100˚C and 160˚C the mass loss for different boards was between 15% and 17%. The mass loss of four Canadian gypsum boards conducted at a heating rate of 5˚C per minute by Craft et al [8] reveals that a total of 15 to 17% of the total mass was lost between 100˚C and 160˚C.

Thermal gravimetric analysis involves the measurement of the mass change of a specimen with a thermo-balance while the specimen is subjected to a controlled change in temperature. Thermal gravimetric analysis (TGA) was conducted for the three types of gypsum boards considered in

this study. Thermal gravimetric analysis (TGA) tests of the three types of drywall were conducted in air using a Q5000 thermal gravimetric analyzer (TA Instruments, New Castle, DE) at a heating rate of 20˚C/ min. The test was conducted at the Department of Chemistry Laboratory, University of Saskatchewan. The TGA results obtained provides information on the thermal stability of gypsum boards along with the thermal degradation temperatures.

The result of the thermal gravimetric analysis tests of the three different types of gypsum board in dry air at a heating rate of 20˚C/min is shown in Figure 3.9.

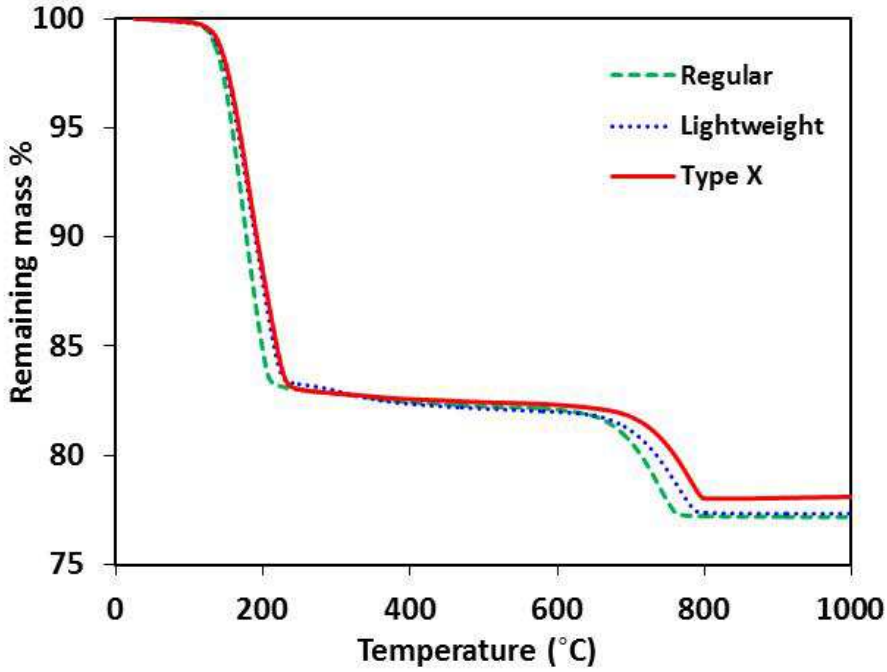

Figure 3.9: Thermo gravimetric Analysis (TGA) Curves for Regular, Lightweight and Type X Gypsum Board.

The TGA results for the three types of gypsum board, shown in Figure 3.9, were similar as the significant mass losses occurred over approximately the same range of temperatures for each material. There were two significant mass losses, which represent the reactions described in Equations 1.1-1.3. The first significant mass loss, which is due to calcination (Equations 1.1 and 1.2), began at about 140-150˚C. This mass loss was approximately 17-18% of the initial mass for

each of the three types of gypsum board. The second mass loss started at about 730-750˚C and was due to decarbonation (Equation 1.3). This second mass loss was approximately 6-7% of the initial mass for each of the three types of gypsum board.

The values of density of the gypsum board at room temperature used in the model are presented in Table 3.2.

Table 3.2: Description of Gypsum Board

Material	**Description**
Regular Gypsum Board	Thickness = 12.7 mm (1/2 in.) Density = 645.7 kg/m^3
Lightweight Gypsum Board	Thickness = 12.7 mm (1/2 in.) Density = 564.3 kg/m^3
Type X Gypsum Board	Thickness = 15.9 mm (5/8 in.) Density = 724.8 kg/m^3

The TGA results were used to extrapolate the density as a percentage of the original density of gypsum at room temperature. Rahmanian [56] reports that at temperatures below 900˚C, the volume change in gypsum is insignificant; hence the heat transfer analysis does not include the effect of volume change on density but takes the relative change in density to be equal to the change in the mass. Figure 3.10 shows the density of regular and type X gypsum boards, respectively used in the model.

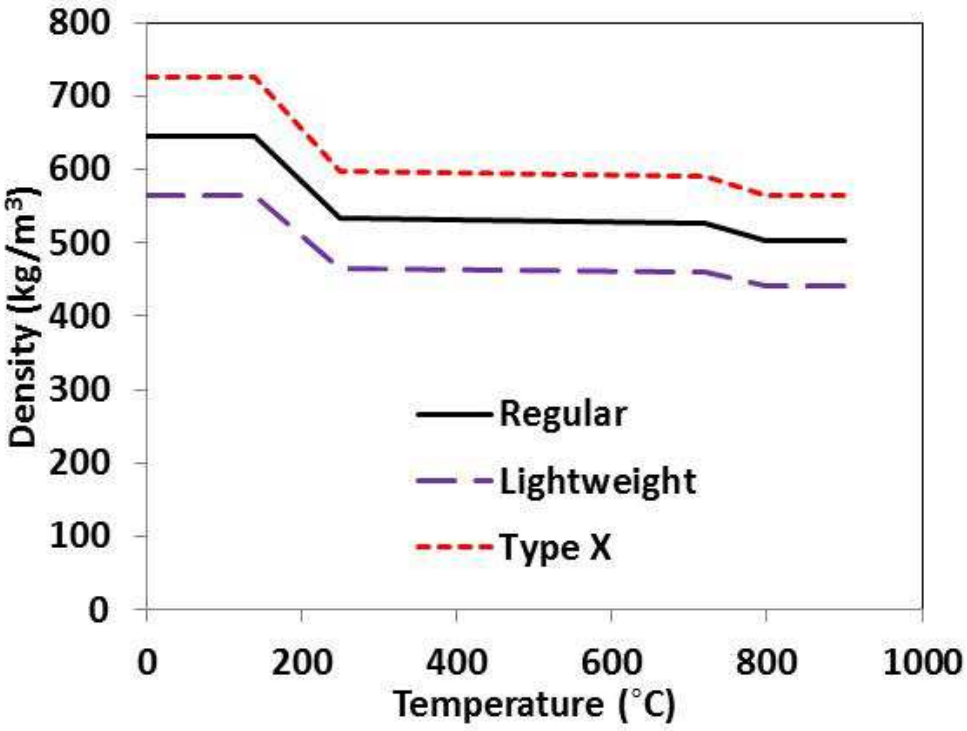

Figure 3.10: Density of Gypsum Boards Used in the Model.

The temperature-density correlation drawn from Figure 3.10 for the regular gypsum board is given as follows:

$$\begin{aligned}
\rho &= 645.7 && 0^{\circ}\mathrm{C} < T \leq 140^{\circ}\mathrm{C} \\
\rho &= -1.02725T + 789.515 && 140^{\circ}\mathrm{C} < T \leq 250^{\circ}\mathrm{C} \\
\rho &= -0.0137T + 536.13 && 240^{\circ}\mathrm{C} < T \leq 720^{\circ}\mathrm{C} \\
\rho &= -0.3632T + 787.75 && 720^{\circ}\mathrm{C} < T \leq 800^{\circ}\mathrm{C} \\
\rho &= 497.189 && T > 800^{\circ}\mathrm{C}
\end{aligned} \tag{3.5}$$

The temperature-density correlation drawn from Figure 3.10 for the lightweight gypsum board is given as follows:

$$\rho = 564.3 \qquad 0^{\circ}C < T \leq 140^{\circ}C$$

$$\rho = -0.8977T + 689.98 \qquad 140^{\circ}C < T \leq 250^{\circ}C$$

$$\rho = -0.012T + 468.55 \qquad 250^{\circ}C < T \leq 720^{\circ}C$$

$$\rho = -0.2469T + 637.7 \qquad 720^{\circ}C < T \leq 800^{\circ}C$$

$$\rho = 440.15 \qquad T > 800^{\circ}C$$

(3.6)

The temperature-density correlation drawn from Figure 3.10 for the type X gypsum board is given as follows:

$$\rho = 724.8 \qquad 0^{\circ}C < T \leq 140^{\circ}C$$

$$\rho = -1.1531T + 886.23 \qquad 140^{\circ}C < T \leq 250^{\circ}C$$

$$\rho = -0.0154T + 601.82 \qquad 250^{\circ}C < T \leq 720^{\circ}C$$

$$\rho = -0.317T + 819.02 \qquad 720^{\circ}C < T \leq 800^{\circ}C$$

$$\rho = 565.344 \qquad T > 800^{\circ}C$$

(3.7)

3.1.6 Density of Insulation

Mass Loss of Insulation

The mass loss test results from thermal gravimetric analysis of rock fiber insulation and glass fiber insulation presented by Benichou et al [52] are shown in Figure 3.11. From Figure 3.11, 6% mass of rock fiber insulation was lost from 25˚C to 1000˚C and 6% mass of glass fiber insulation was also lost from 36˚C to 310˚C after which the mass remains constant.

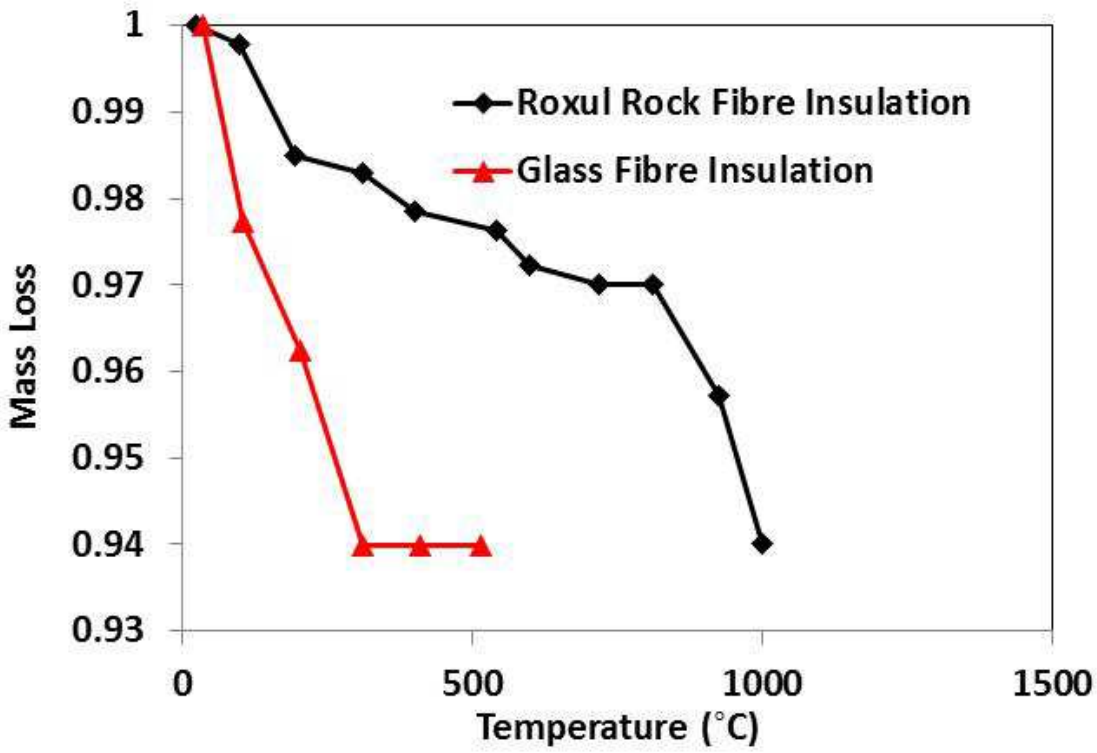

Figure 3.11: Mass Loss of Insulation [14].

The density of insulation used in the model was 32 kg/m^2, taken from Roxul technical data sheet for Roxul ComfortBatt R-14 (89 mm thick) stone wool insulation [57]. As was done for the specific heat, a constant density value for stone wool insulation was used in the model.

3.2 GRID SIZE AND TIME-STEP

The heat transfer model described in Chapter Two will be stable result as long as the stability criterion is met; however the optimal grid size and time step to be used in the model will be investigated. The effect of time step on temperature at the unexposed side (depth of 12.7 mm) of a single regular gypsum board is shown in Figure 3.12 for a heat flux of 75 kW/m^2. Figure 3.12 shows that the time step has less significant effect on the predicted temperature at the unexposed end of the board (depth of 12.7 mm).

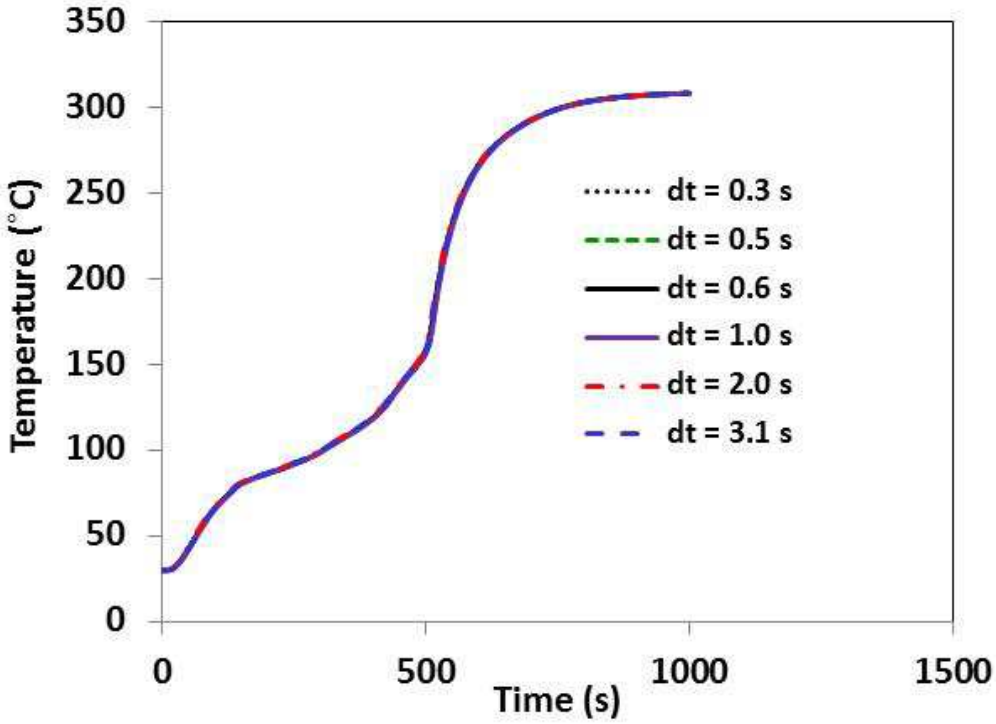

Figure 3.12: Effect of Time-step on Temperature Measurements on the Unexposed End (12.7 mm) of a Regular Gypsum Board.

The choice of the grid size and time step were chosen by considering the effects at the exposed surface of the board. Figure 3.13 compares the results of the heat transfer analysis at a time-step of 0.5 s for different gird sizes and Figure 3.14 compares the results of the heat transfer analysis at a mesh size of 1.6 mm (8 layers) for different time steps. From Figures 3.13 and 3.14, 8 layers corresponding to a grid size of 1.6 mm and a time step of 0.5 s were chosen as the optimal grid size and time step for further analysis. There were only small differences between the results within the first minute of the exposure predicted using this time step and grid size, and predicted using the next smaller time step and grid size. As results after longer time periods are of most interest in this research, it was also noted that at the end of a 60 min. exposure, the duration used in this study, there was a difference of only about 0.3-1% between the numerical results

predicted using any of the different time steps and grid sizes shown in Figures 3.13 and 3.14.The finite difference method used the same grid size for both gypsum board and insulation.

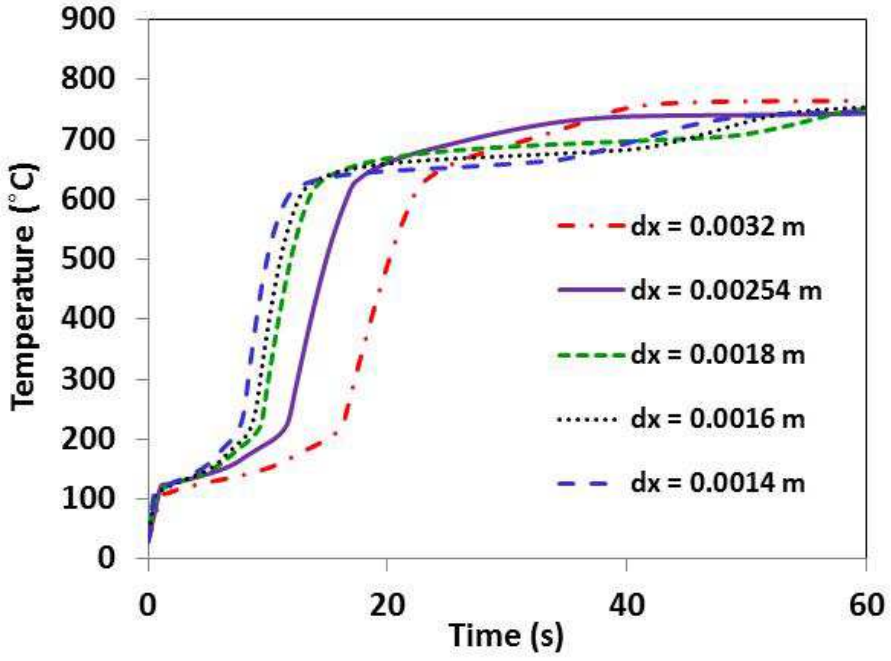

Figure 3.13: Effect of Grid Size on Exposed Surface Temperature Prediction of Gypsum Board (Time-Step = 0.5 s)

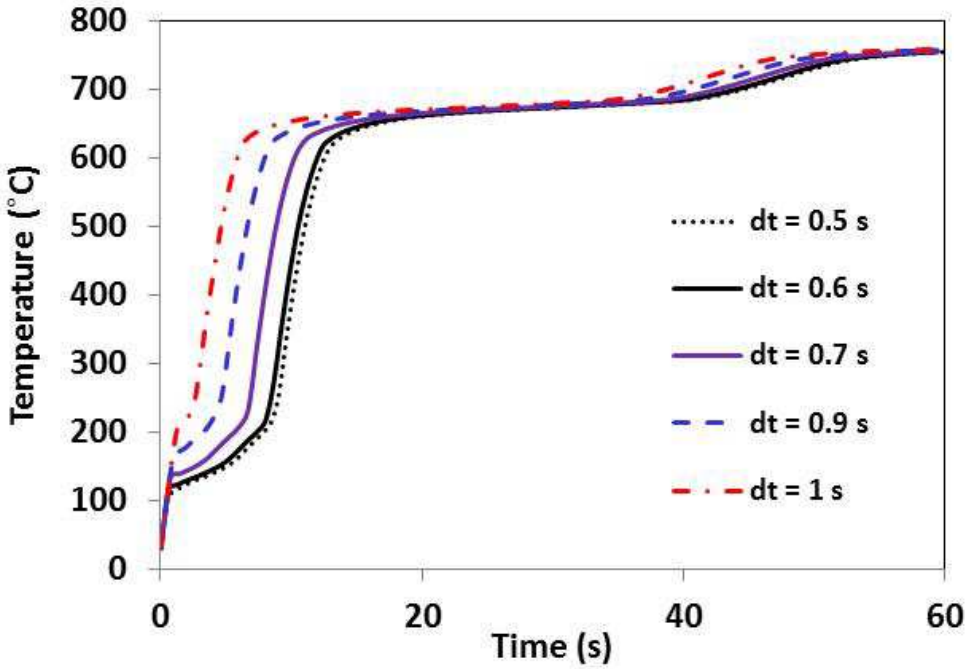

Figure 3.14: Effect of Time-step on Temperature Prediction (Grid size = 1.6 mm)

3.3 NUMERICAL RESULTS

The points of temperature prediction within the wall assembly are shown in Figure 3.15. From Figure 3.15, Point A is the temperature prediction between the unexposed side of the exposed board and insulation, point B is approximately 30 mm from the exposed board (point A) and Point C is approximately 30 mm from point B. Point D is the temperature prediction between the insulation and the exposed end of the unexposed board. Point E is the temperature prediction at the unexposed end of the wall assembly and point M is the midpoint in the insulation. Locations A,B,C, D and E were chosen to compare with experimental results.

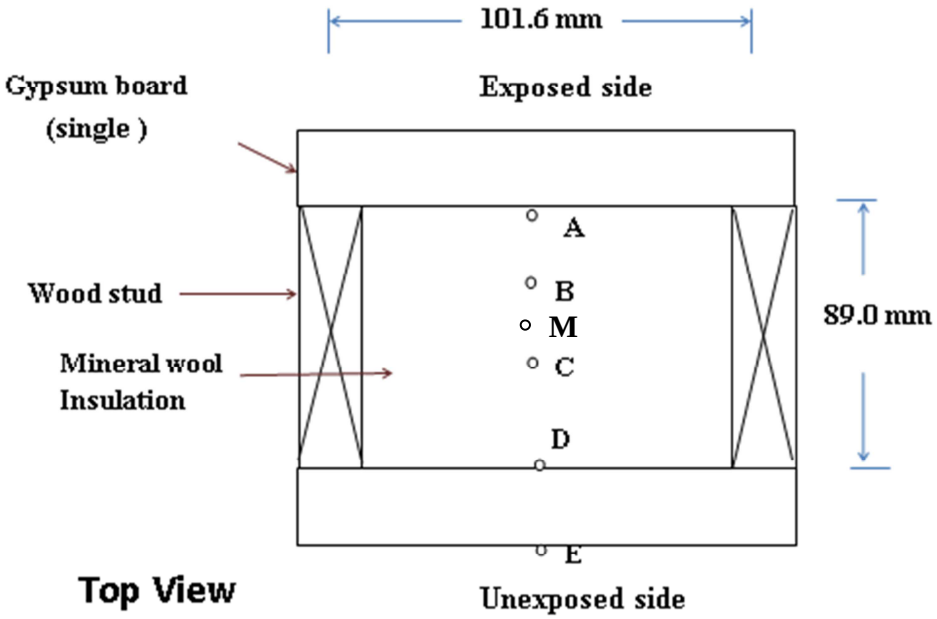

Figure 3.15: Positions of Temperature Predictions in Wall Assemblies.

3.3.1 Heat Transfer in Wall Assemblies Exposed to a Fixed Temperature Boundary

The temperature profiles within regular and type X wall assemblies exposed to a fixed temperature of 80˚C are presented in Figure 3.16 and 3.17, respectively. Thermal properties in the literature reveal that the thermal properties of gypsum and mineral wool are constant up to about 80˚C of exposure. Hence constant properties were used in the model.

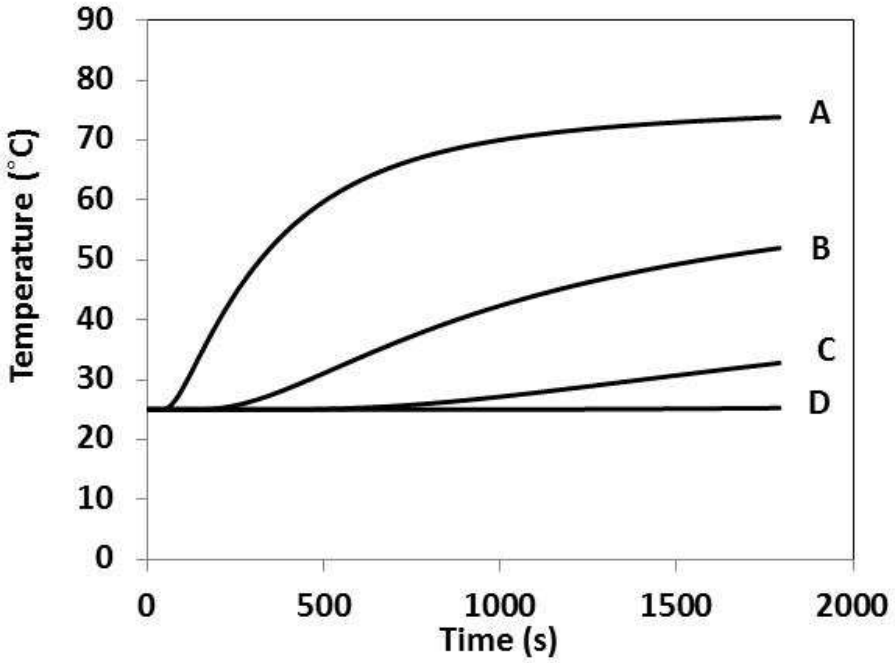

Figure 3.16: Temperatures Predicted by the Model for Regular Board Wall Assembly Exposed to a Fixed Temperature of 80˚C.

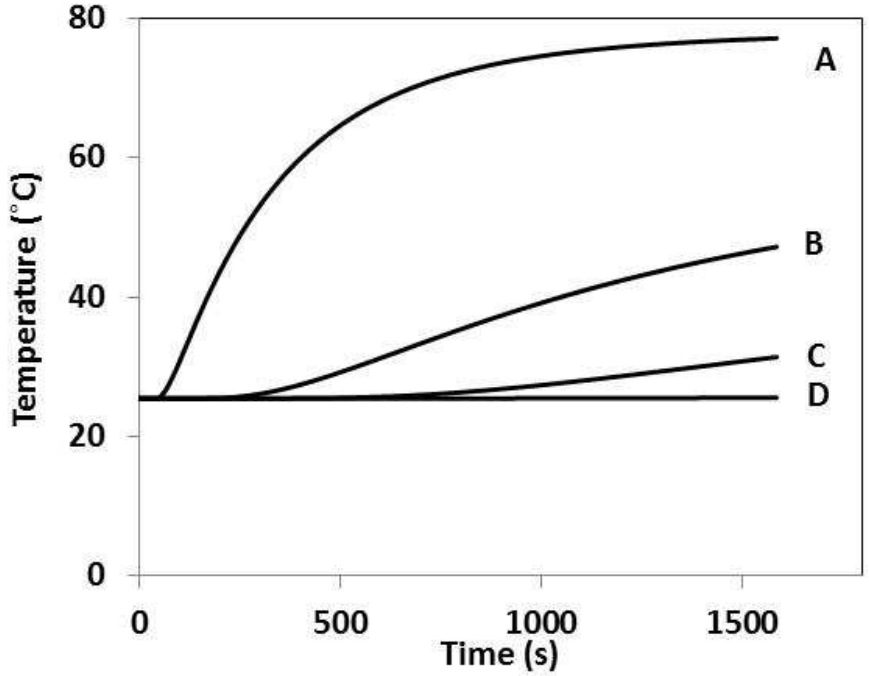

Figure 3.17: Model Prediction of Type X Board Wall Assembly Exposed to a Fixed Temperature of 80˚C.

3.3.2 Heat Transfer in a Single Layer of Gypsum Board

The temperature profile on the exposed and unexposed side of a single layer of regular, lightweight and type X gypsum board exposed to an incident heat flux of 75 kW/m^2 are presented in Figures 3.18, 3.19 and 3.20, respectively. The temperature dependent properties of gypsum board were used in the model. The MATLAB code for the model is presented in APPENDIX A.

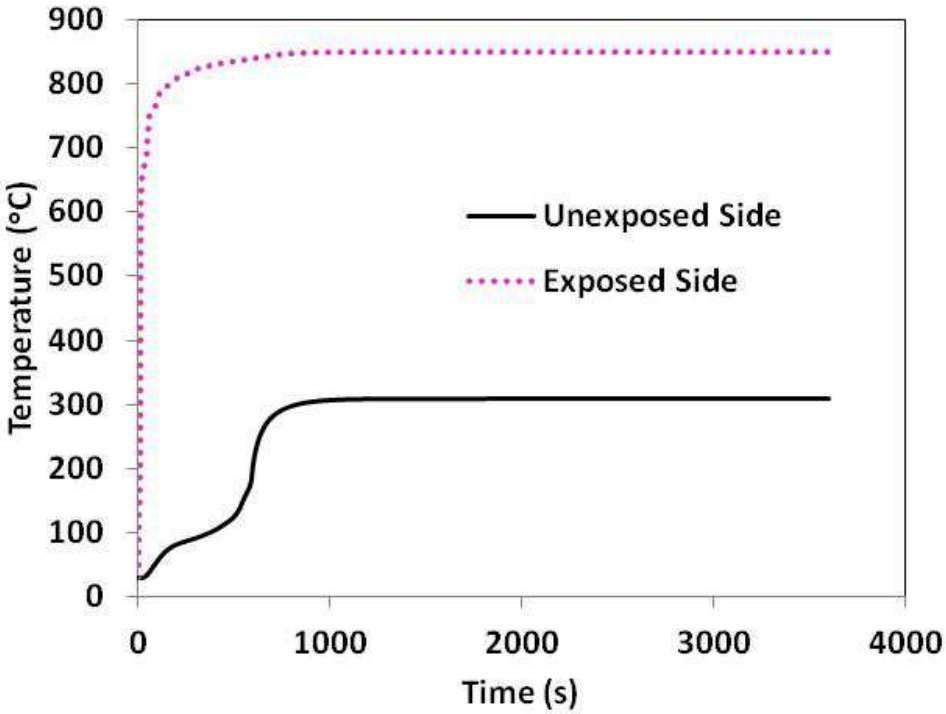

Figure 3.18: Temperature Prediction for a 12.7 mm Regular Gypsum Board Exposed to a Heat Flux of 75 kW/m^2.

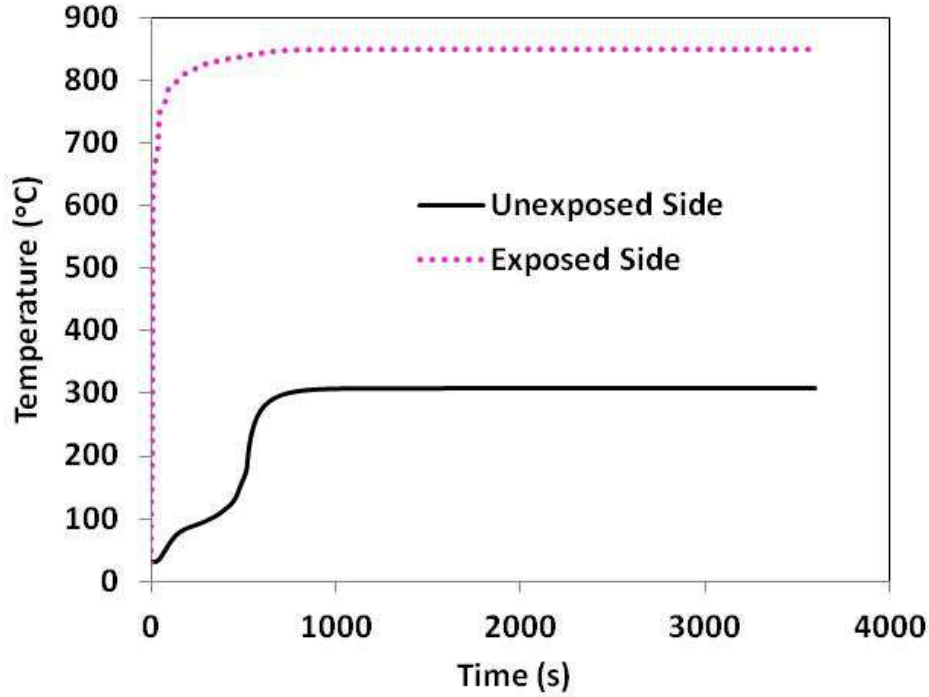

Figure 3.19: Temperature Prediction for a 12.7 mm Lightweight Gypsum Board Exposed to a Heat Flux of 75 kW/m^2.

.

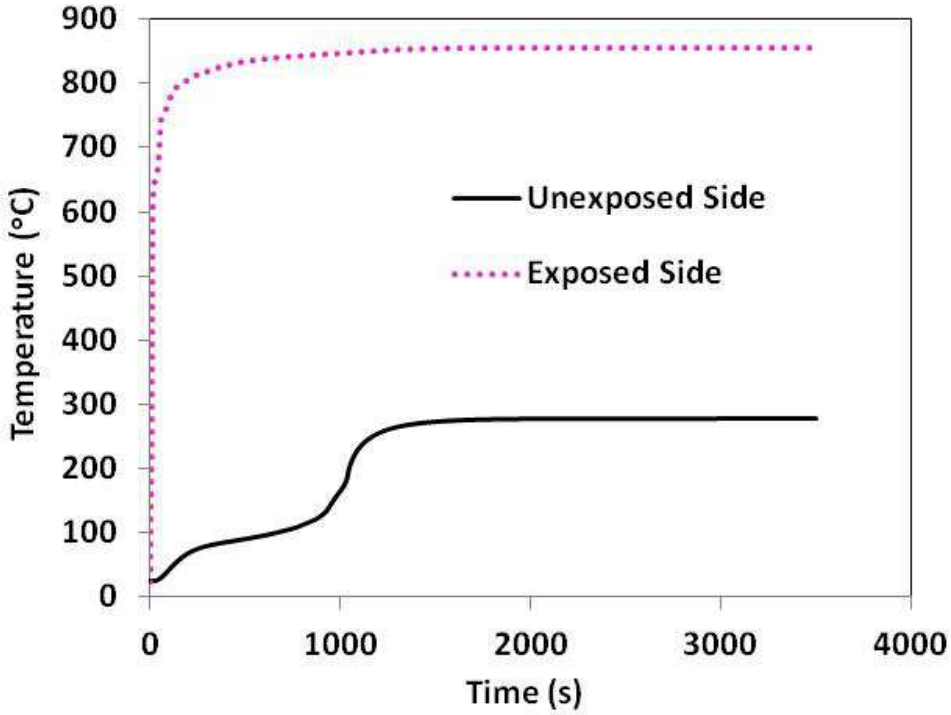

Figure 3.20: Temperature Prediction for a 15.9 mm Type X Gypsum Board Exposed to a Heat Flux of 75 kW/m^2.

.

A comparison of predicted temperatures on the unexposed side of a single layer 12.7 mm regular, lightweight and 15.9 mm type X gypsum boards is presented in Figure 3.21

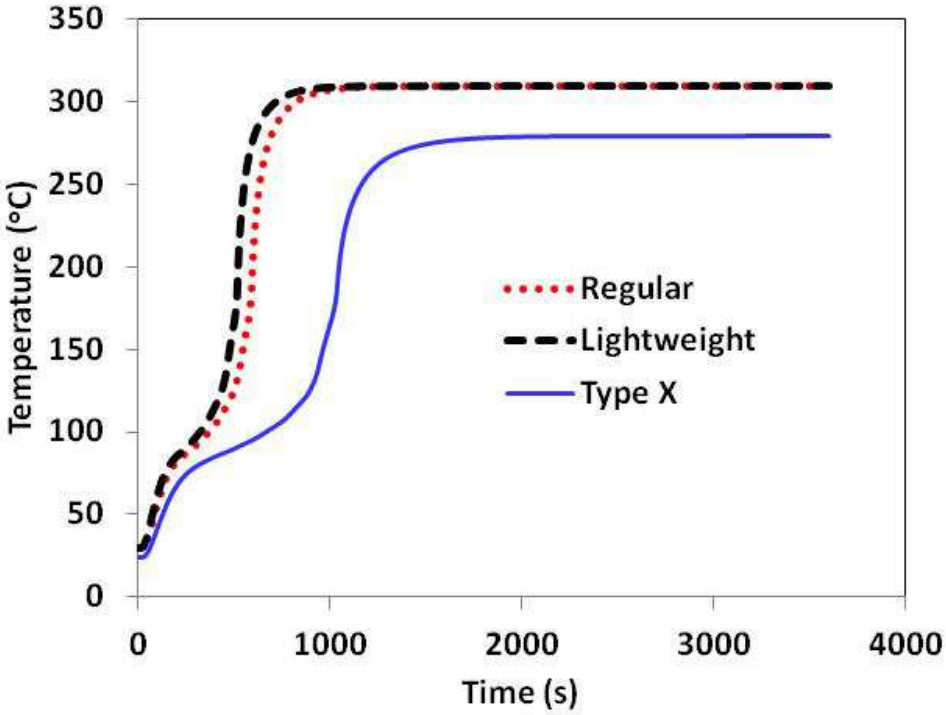

Figure 3.21: Temperature Prediction for a Single Layer 12.7 mm Regular and Lightweight and a Single Layer 15.9 mm Type X Gypsum Board Exposed to a Heat Flux of 75 kW/m^2.

3.3.3 Heat Transfer in a Double Layer of Gypsum Board

The temperature profile on the interface and unexposed side of double layers regular, lightweight and type X gypsum board exposed to an incident heat flux 75 kW/m^2 are presented in Figures 3.22, 3.23 and 3.24, respectively. The temperature dependent properties of gypsum board were used in the model.

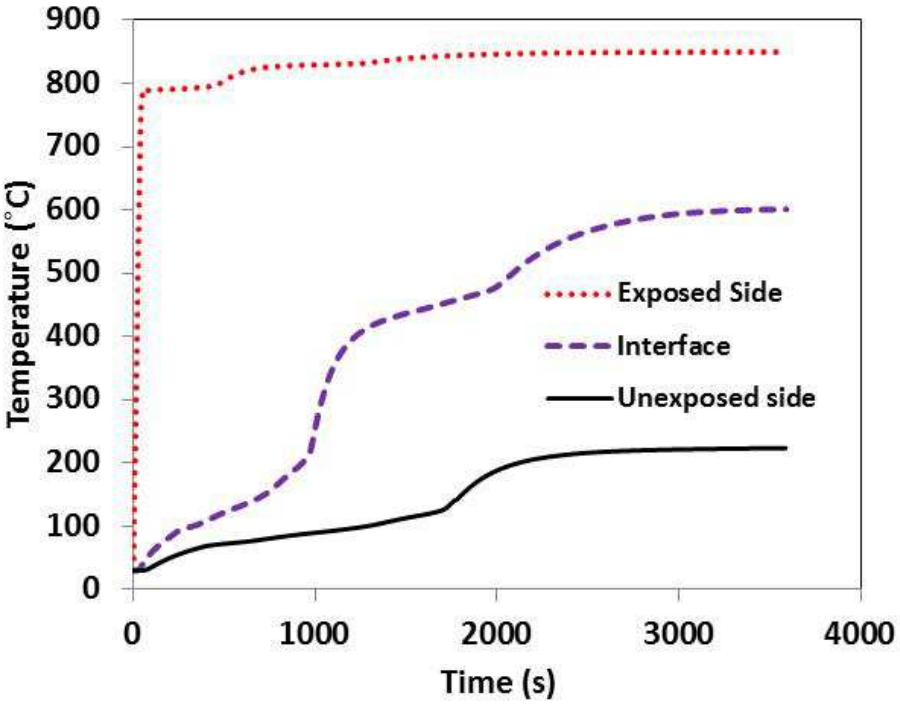

Figure 3.22: Temperature Prediction at the Exposed Side, Interface and Unexposed Side of a Double Layer 12.7 mm Regular Gypsum Board Exposed to a Heat Flux of 75 kW/m^2.

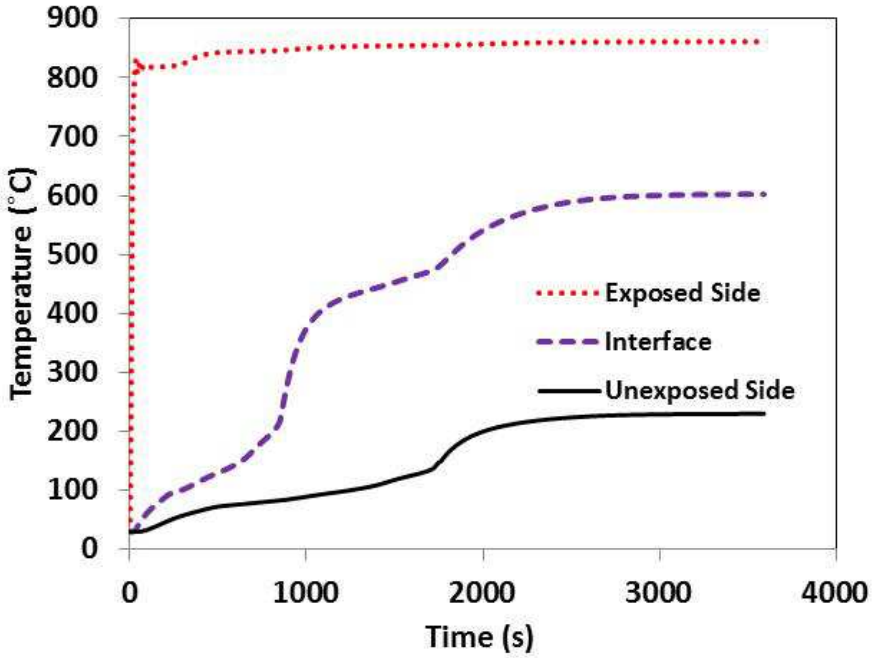

Figure 3.23: Temperature Prediction at the Exposed Side, Interface and Unexposed Side of a Double Layer 12.7 mm Lightweight Gypsum Board Exposed to a Heat Flux of 75 kW/m^2.

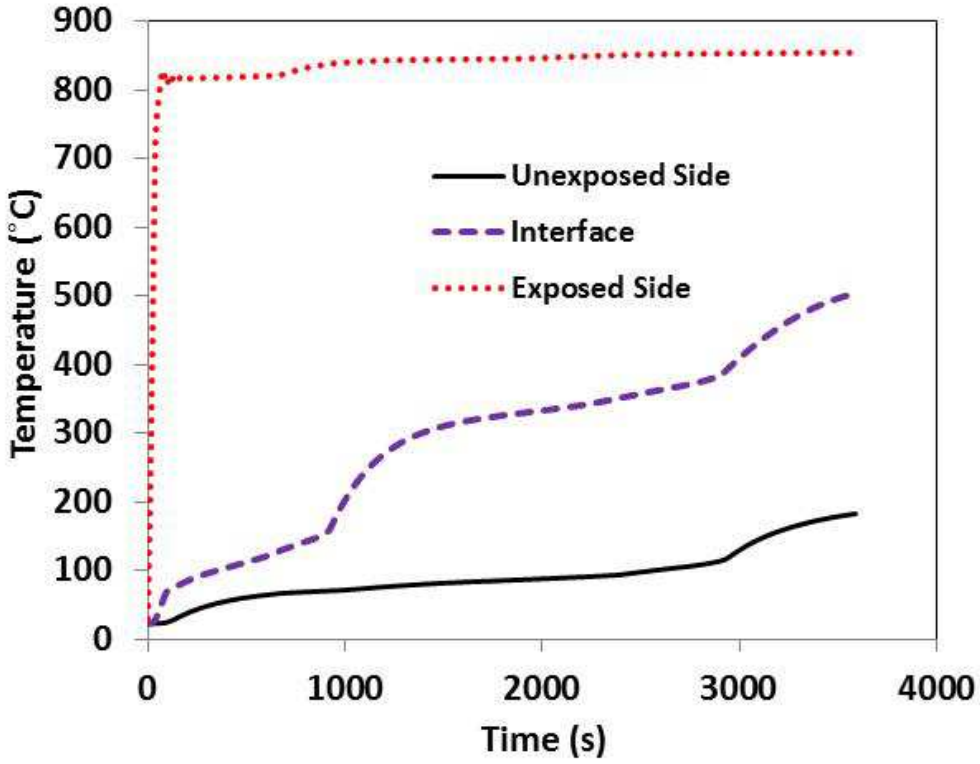

Figure 3.24: Temperature Prediction at the Exposed Side, Interface and Unexposed Side of a Double Layer 15.9 mm Type X Gypsum Board Exposed to a Heat Flux of 75 kW/m^2.

The comparison of predicted temperatures on the unexposed side of a double layer 12.7 mm regular, lightweight and 15.9 mm type X gypsum boards is presented in Figure 3.25.

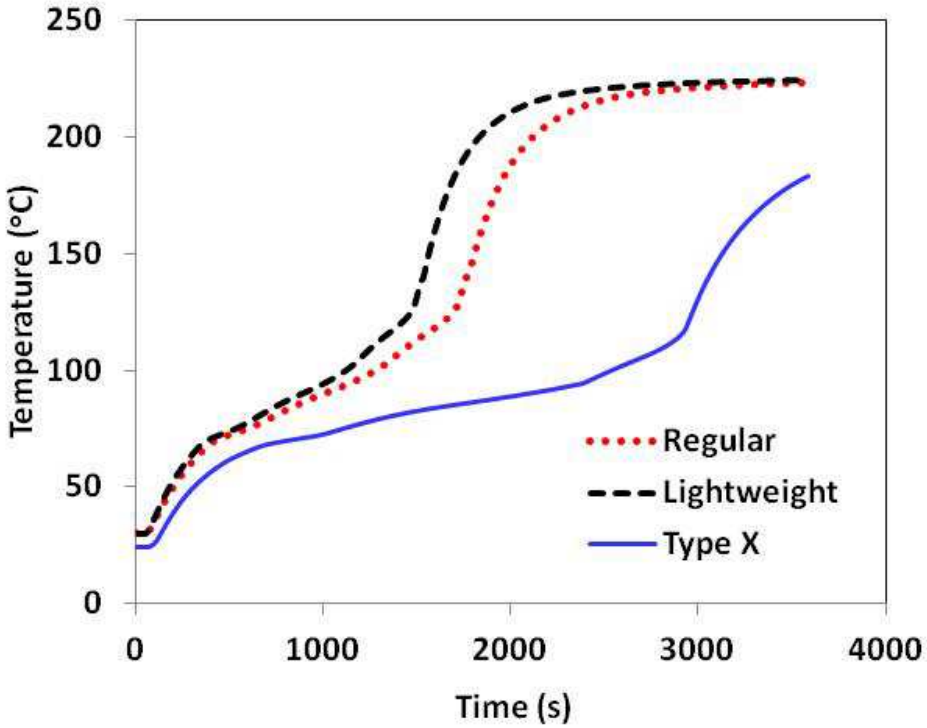

Figure 3.25: Temperature Prediction on the Unexposed Side of Double Layer 12.7 mm Regular and Lightweight and a Double Layer 15.9 mm Type X Gypsum Board Exposed to a Heat Flux of 75 kW/m^2.

3.3.4 Heat Transfer in Wall Assembly with Constant Properties:

Temperature predictions using constant thermal properties of materials for regular, lightweight and type X gypsum (single layer) wall assemblies exposed to an incident heat flux of 75 kW/m^2 are presented in Figures 3.26, 3.27 and 3.28, respectively. Constant properties of the wall materials were used in the model.

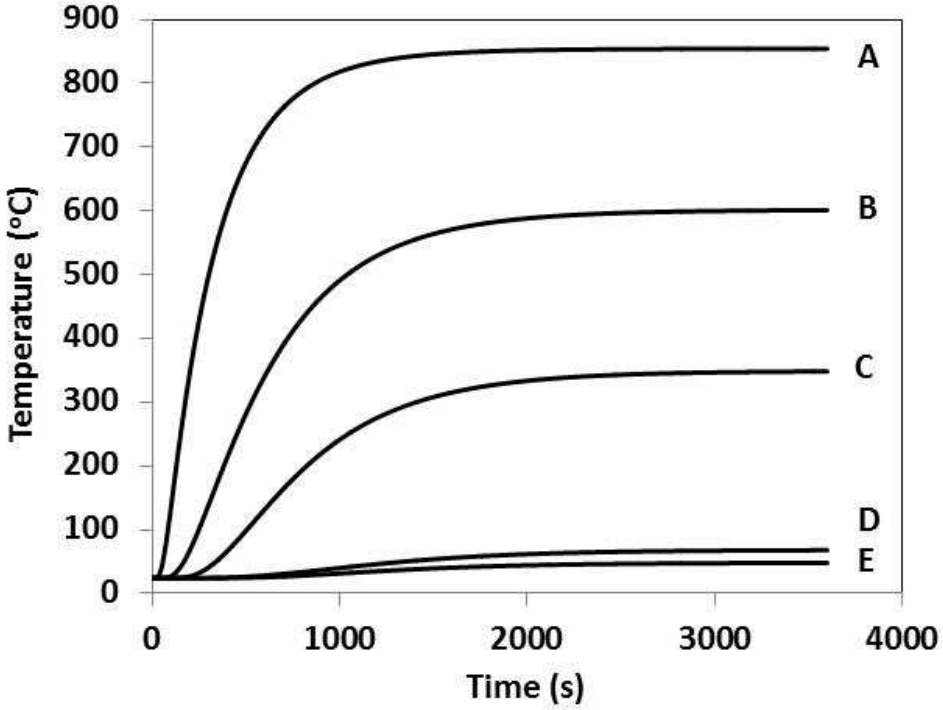

Figure 3.26: Temperature Predictions for a Regular Gypsum Board Wall Assembly Exposed to a Heat Flux of 75 kW/m^2. (Constant Thermal Properties).

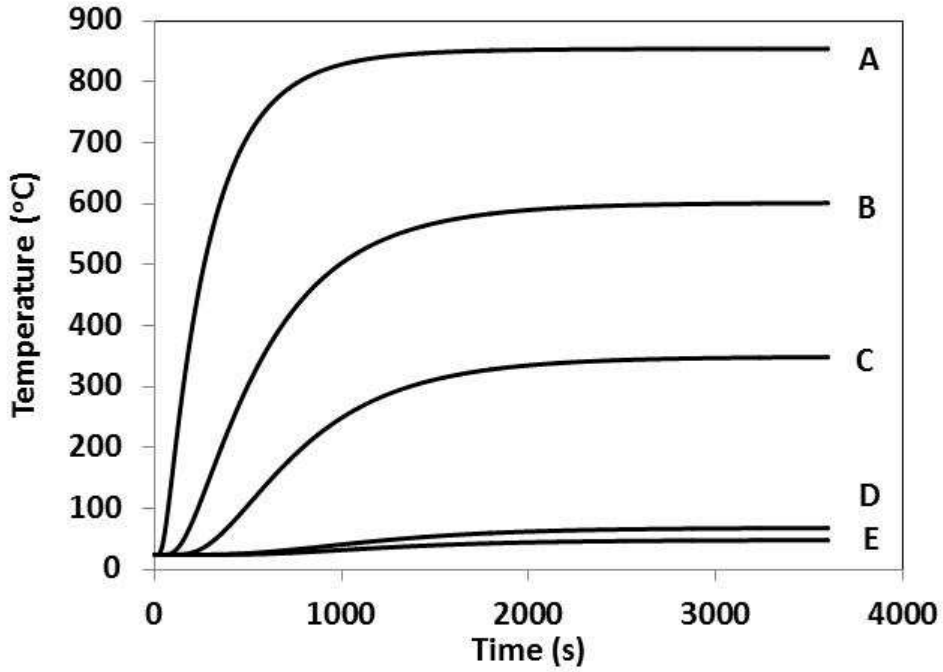

Figure 3.27: Temperature Prediction for a Lightweight Gypsum Board Wall Assembly Exposed to a Heat Flux of 75 kW/m^2. (Constant Thermal Properties).

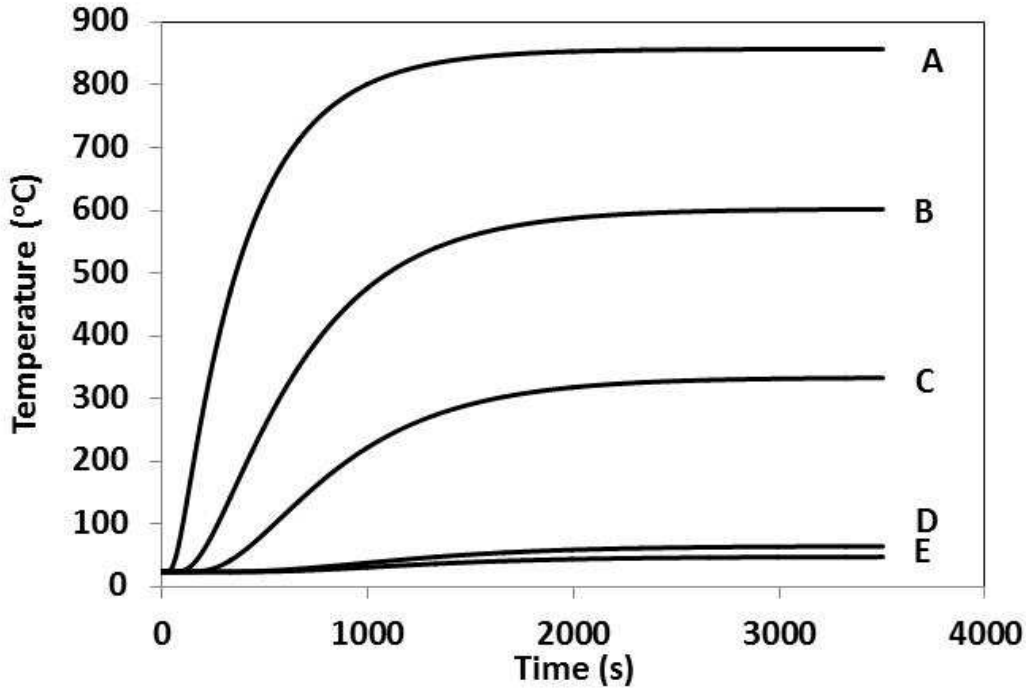

Figure 3.28: Temperature Prediction for a Type X Gypsum Board Wall Assembly Exposed to a Heat Flux of 75 kW/m^2. (Constant Thermal Properties).

3.3.5 Heat Transfer in Wall Assembly with Temperature Dependent Properties.

The temperature profile in a single layer regular, lightweight and type X gypsum wall assembly exposed to an incident heat flux 75 kW/m^2 are presented in Figures 3.29, 3.30 and 3.31, respectively. The temperature dependent properties of gypsum and stone wool insulation were used in the model. The MATLAB code for the model is presented in APPENDIX B.

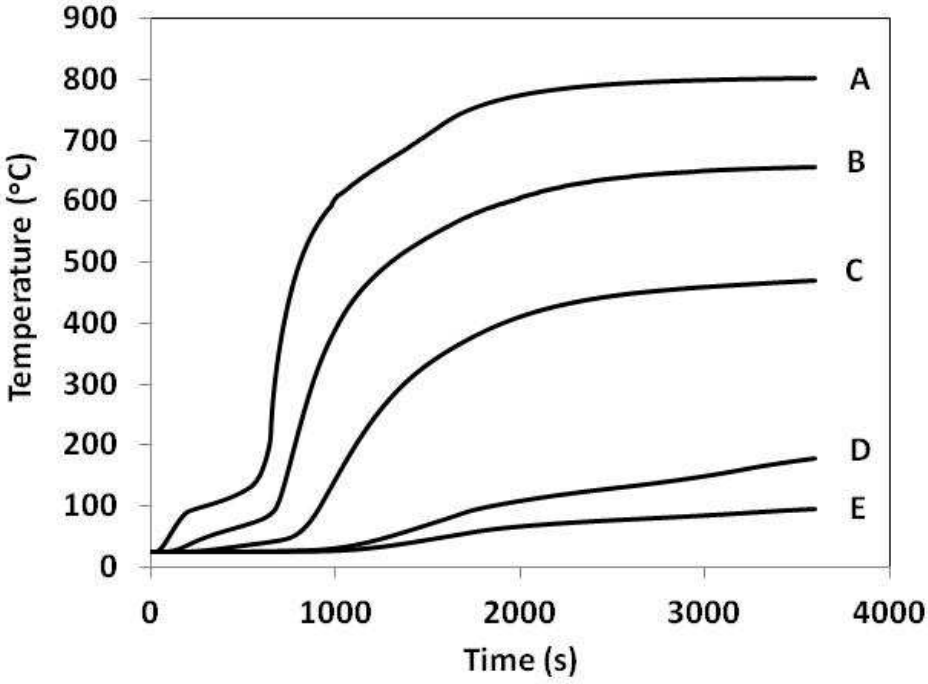

Figure 3.29: Temperature Prediction for a Regular Gypsum Board Wall Assembly Exposed to 75 kW/m^2 (Temperature Dependent Thermal Properties).

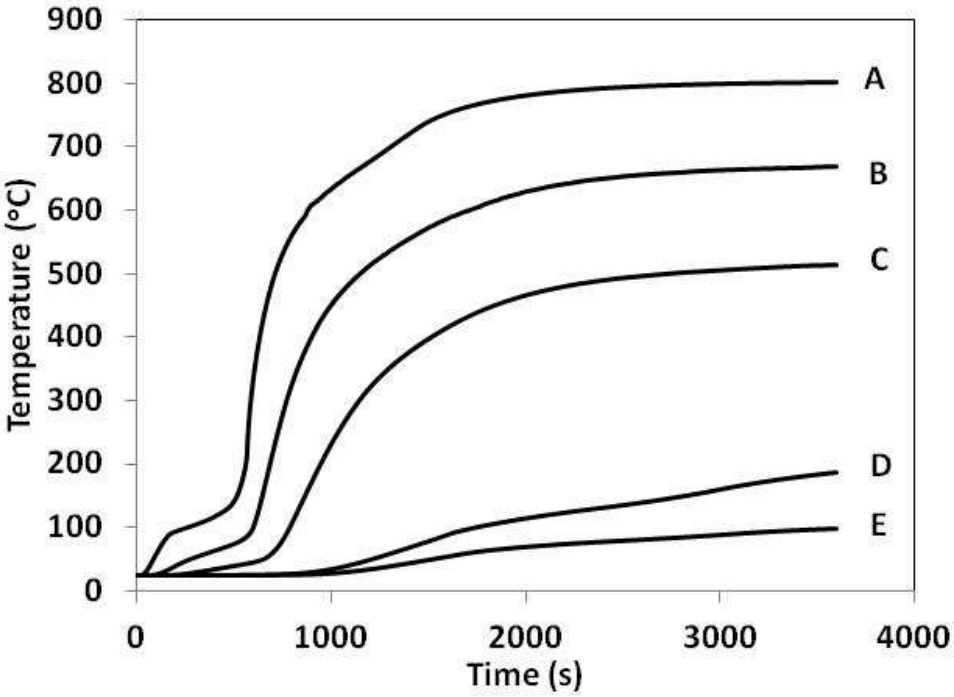

Figure 3.30: Temperature Prediction for a Lightweight Gypsum Board Wall Assembly Exposed to 75 kW/m^2 (Temperature Dependent Thermal Properties).

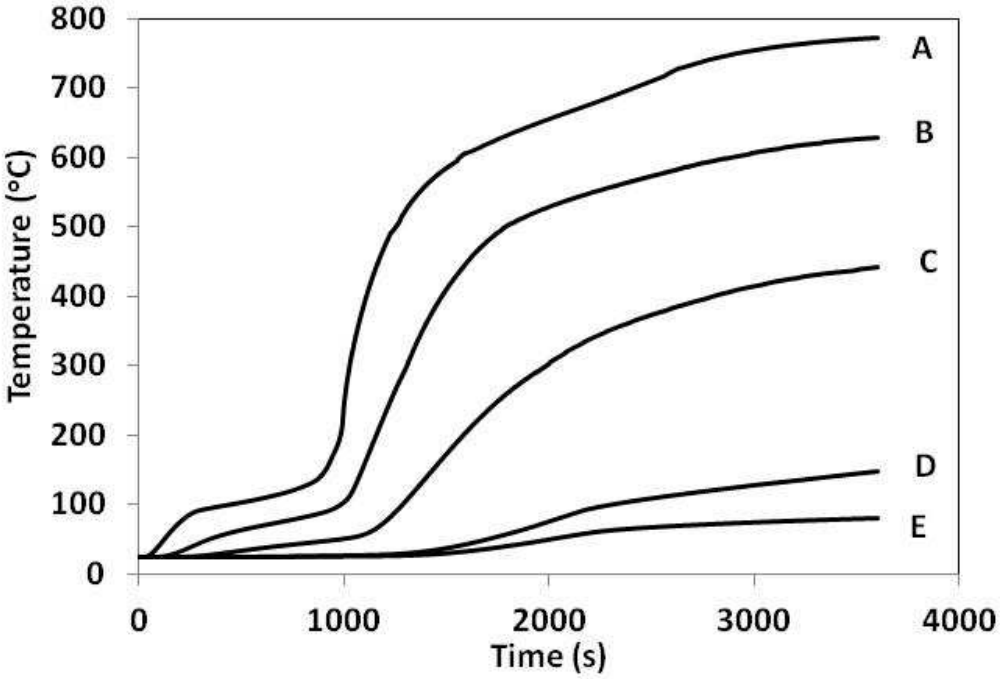

Figure 3.31: Temperature Prediction for a Type X Gypsum Board Wall Assembly Exposed to 75 kW/m^2 (Temperature Dependent Thermal Properties).

The temperature profiles in a single layer lightweight gypsum board wall assembly exposed to incident heat fluxes of 35 and 50 kW/m^2 are presented in Figure 3.32 and 3.33, respectively. The temperature dependent properties of gypsum and stone wool insulation were used in the model.

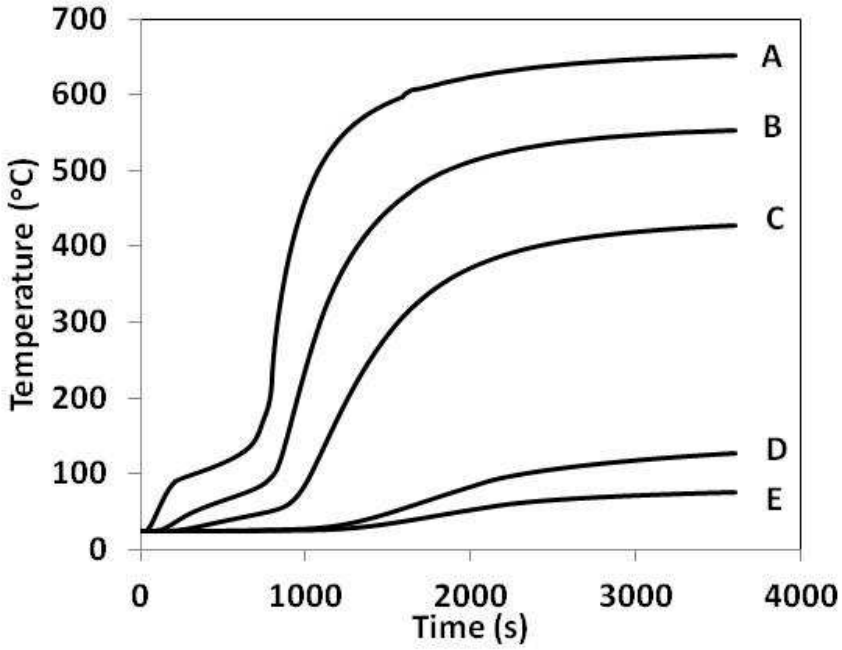

Figure 3.32: Temperature Prediction for a Lightweight Gypsum Board Wall Assembly Exposed to 35 kW/m^2 (Temperature Dependent Thermal Properties).

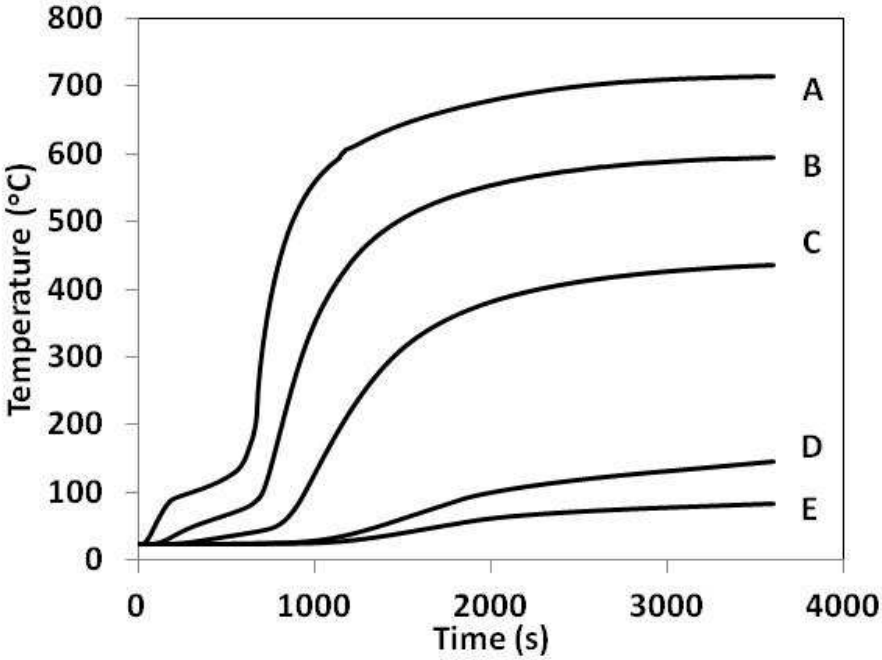

Figure 3.33: Temperature Prediction for a Lightweight Gypsum Board Wall Assembly Exposed to 50 kW/m^2 (Temperature Dependent Thermal Properties).

The temperature profile in double layer regular, lightweight and type X gypsum wall assemblies exposed to an incident heat flux of 75 kW/m^2 are presented in Figures 3.34, 3.35 and 3.36, respectively.

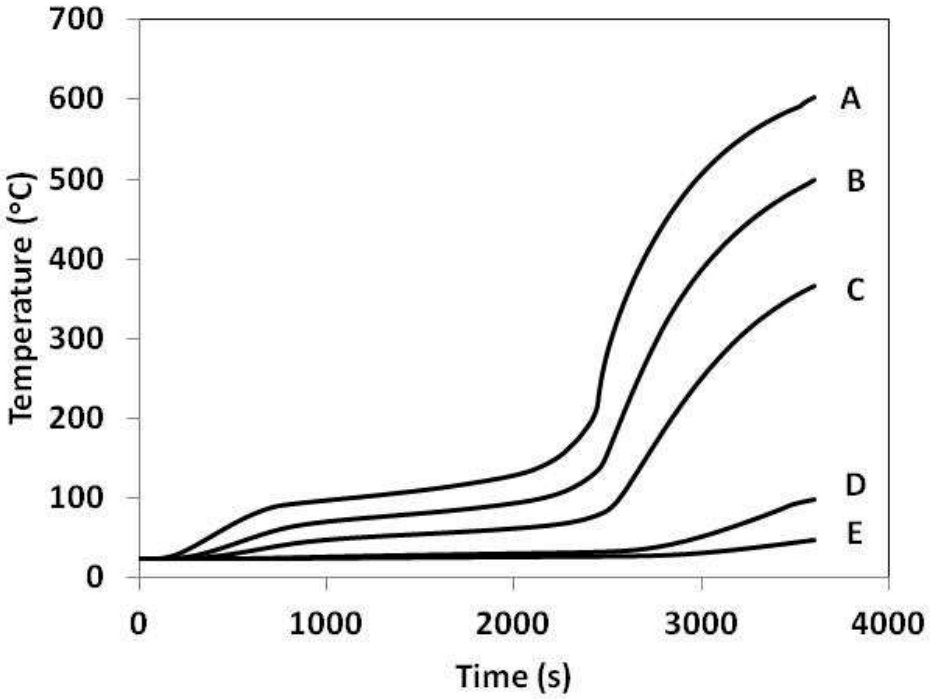

Figure 3.34: Temperature for a Double Layer Regular Gypsum Board Wall Assembly Exposed to75 kW/m^2 (Temperature Dependent Thermal Properties).

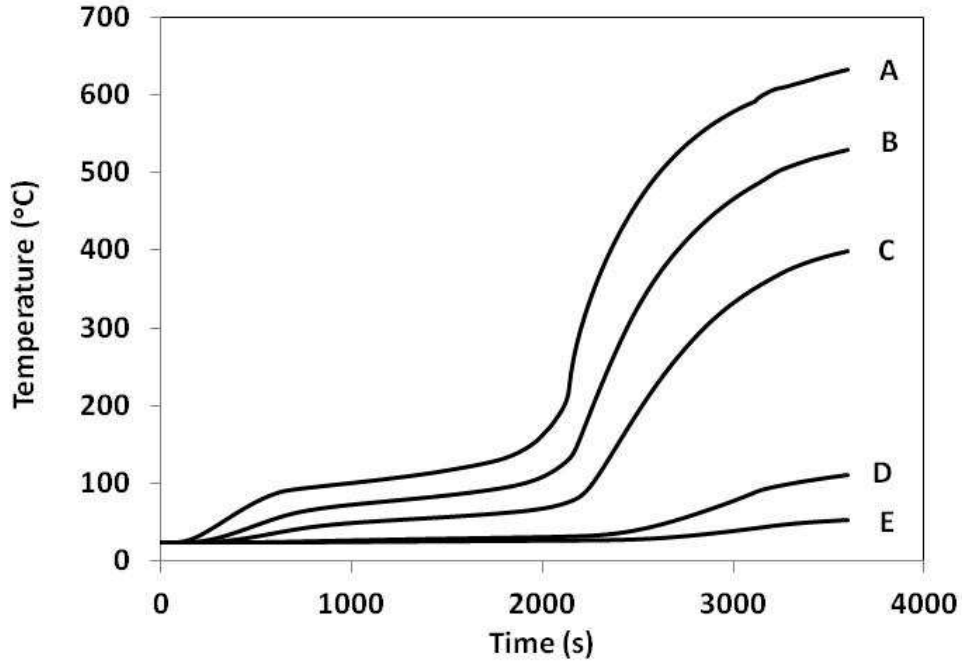

Figure 3.35: Temperature Prediction for a Double Layer Lightweight Gypsum Board Wall Assembly Exposed to75 kW/m^2 (Temperature Dependent Thermal Properties).

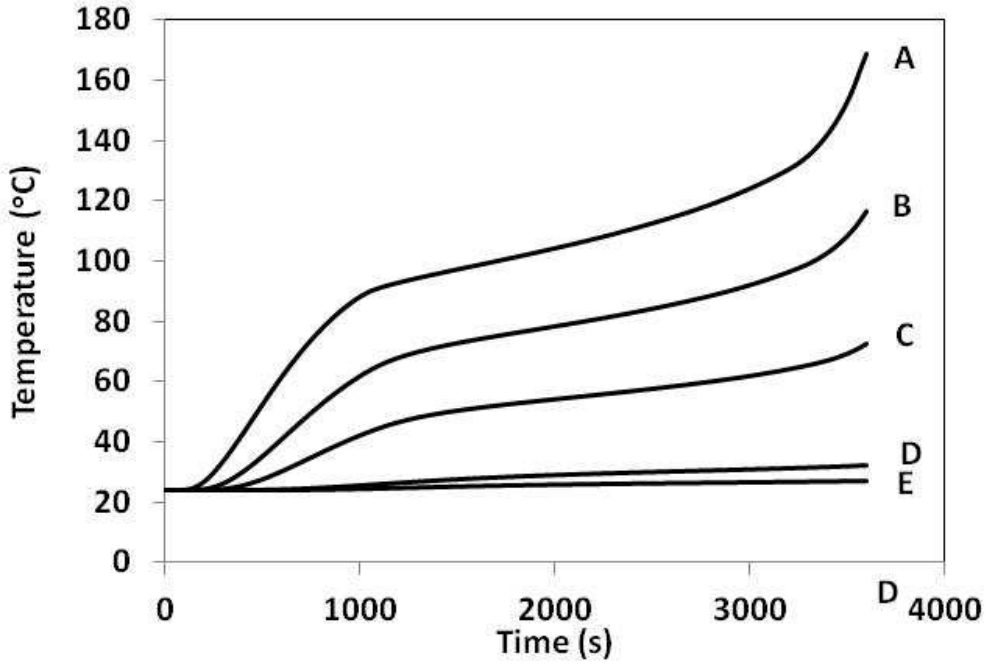

Figure 3.36: Temperature Prediction for a Double Layer Type X Gypsum Board Wall Assembly Exposed to75 kW/m^2 (Temperature Dependent Thermal Properties).

3.4 SENSITIVITY STUDY

A sensitivity study was performed to determine the property or properties that have the most important impact on the numerical results. This study helps to quantify the influence of the uncertainties in material properties on the numerical results. The sensitivity of the temperature in a wood stud, 12.7 mm regular gypsum board with stone wool insulation wall assembly to ±20% changes in thermal conductivity, specific heat and density of both gypsum and insulation for the temperature dependent model is presented in this section.

3.4.1 Specific Heat of Gypsum and Stone Wool

The ± 20% changes to the temperature dependent specific heat of gypsum are shown in Figure 3.37. The sensitivity of the temperature to ± 20% changes in specific heat of gypsum in the temperature dependent model for the wall assembly at location A (depth of 12.7 mm from exposed side), M (middle of insulation) and E (unexposed side) is presented in Figure 3.38. Figure 3.39 shows the temperature variation on the unexposed side (E).

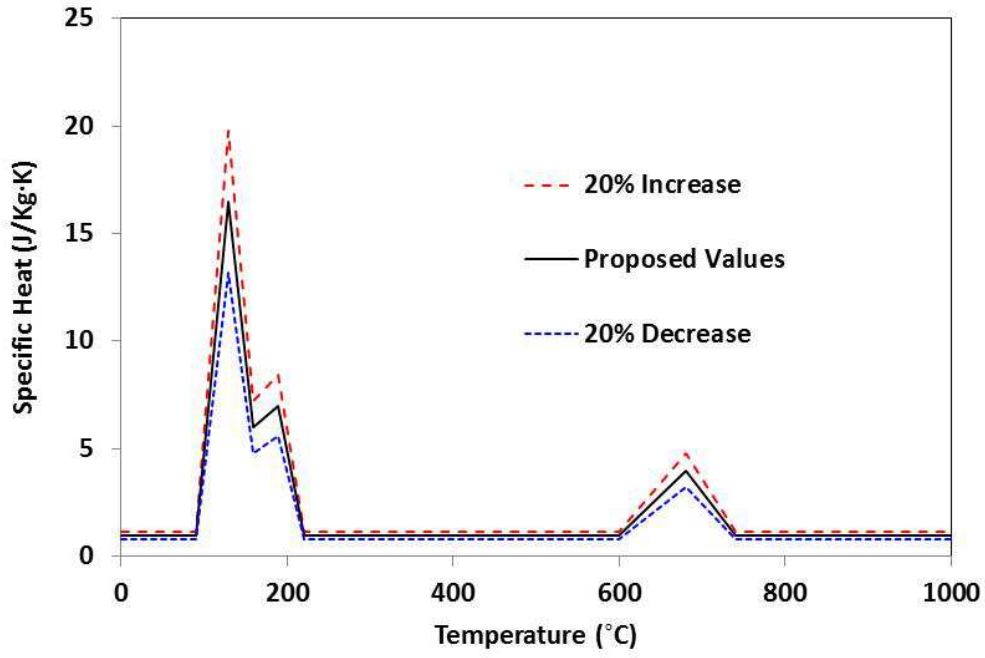

Figure 3.37: Changes to Specific Heat of Gypsum

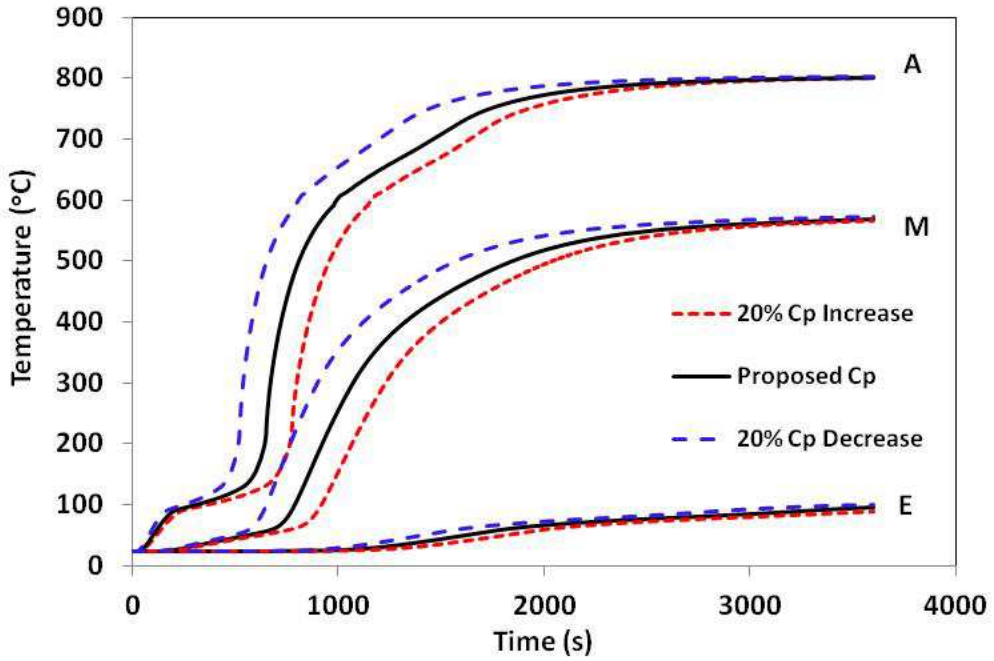

Figure 3.38: Sensitivity of Temperature to ± 20% Changes in Specific Heat of Gypsum for Location A (Depth of 12.7 mm from Exposed Side), M (Middle of Insulation) and E (Unexposed Side). – Temperature Dependent Property Model

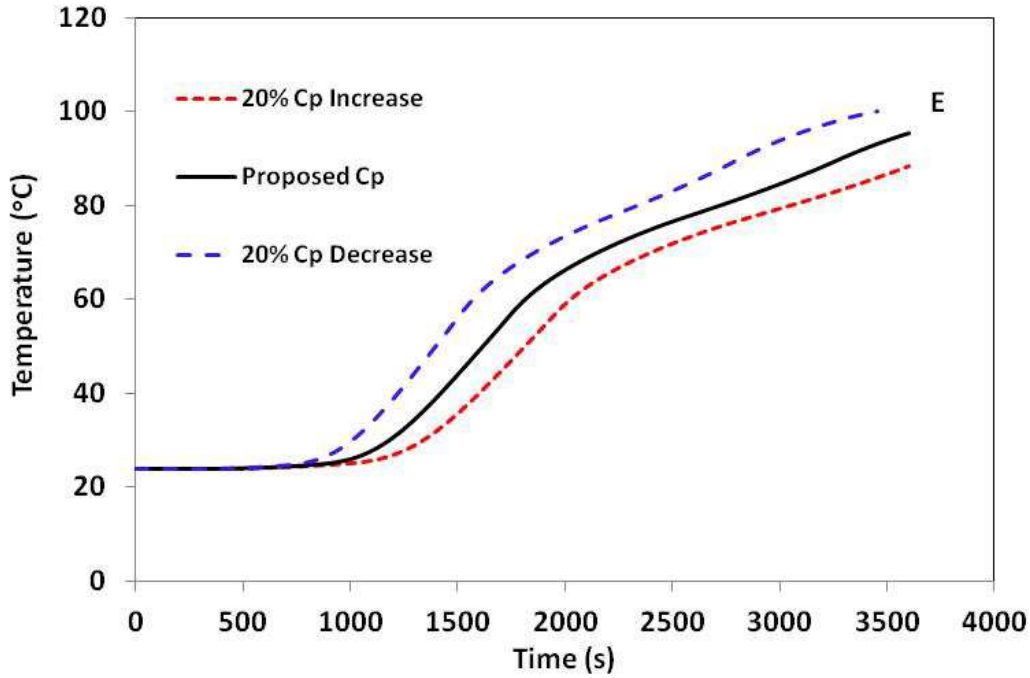

Figure 3.39: Sensitivity of Temperature to ± 20% Changes in Specific Heat of Gypsum for Location E (Unexposed Side). – Temperature Dependent Property Model

The ± 20% changes to the constant specific heat value of stone wool is shown in Table 3.3. The sensitivity of the temperature to ± 20% changes in specific heat of stone wool in the temperature dependent model for the wall assembly at location A (depth of 12.7 mm from exposed side), M (middle of insulation) and E (unexposed side) is presented in Figure 3.40. Figure 3.41 shows the temperature variation at the unexposed end (E).

Table 3.3: Changes to Specific Heat of Stone Wool Insulation

Specific Heat of Stone Wool Insulation (J/kg.K)		
Proposed Value	20% Increase	20% Decrease
700	840	560

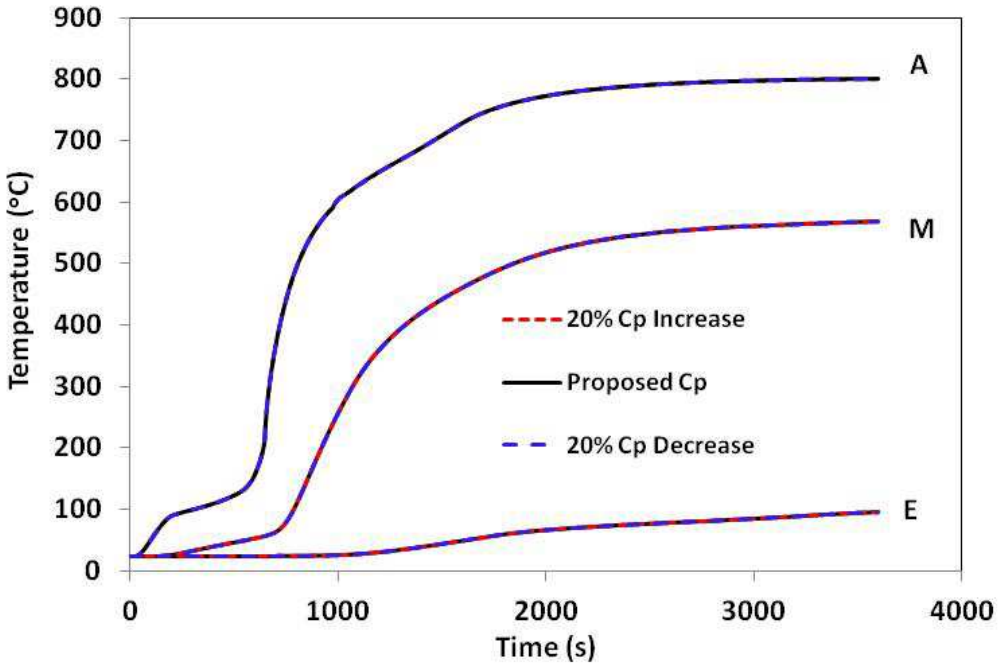

Figure 3.40: Sensitivity of Temperature to ± 20% Changes in Specific Heat of Stone Wool Insulation for Location A (Depth of 12.7 mm from Exposed Side), M (Middle of Insulation) and E (Unexposed Side). – Temperature Dependent Property Model

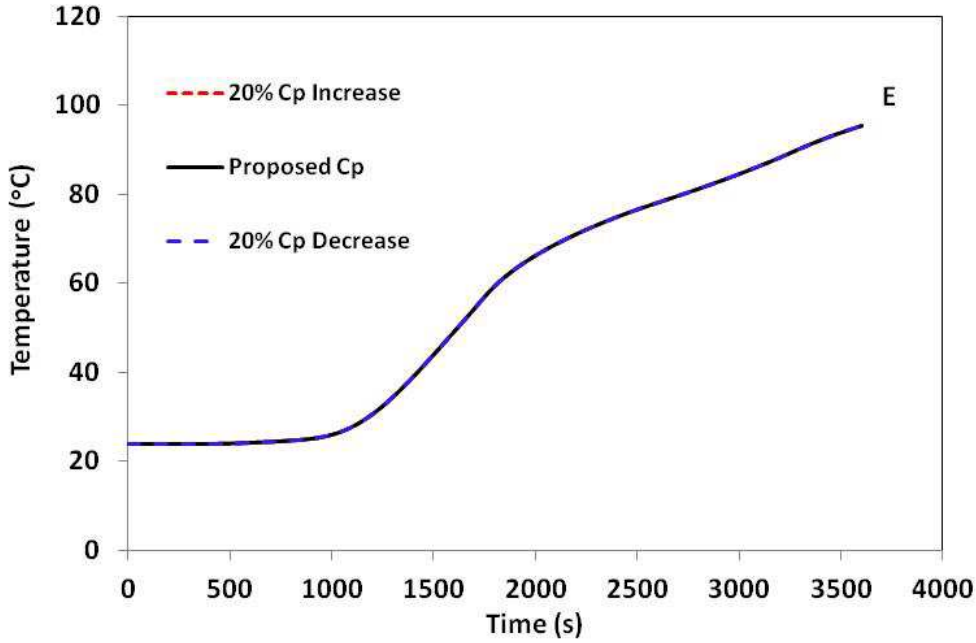

Figure 3.41: Sensitivity of Temperature to ± 20% Changes in Specific Heat of Stone Wool Insulation for Location E (Unexposed Side). – Temperature Dependent Property Model.

3.4.2 Thermal Conductivity of Gypsum and Stone Wool Insulation

The ± 20% changes to the thermal conductivity of gypsum are shown in Figure 3.42 The sensitivity of the temperature to ± 20% changes in thermal conductivity of gypsum in the temperature dependent model for the wall assembly at location A (depth of 12.7 mm from exposed side), M (middle of insulation) and E (unexposed side) is presented in Figure 3.43. Figure 3.44 shows the temperature variation at the unexposed end (E).

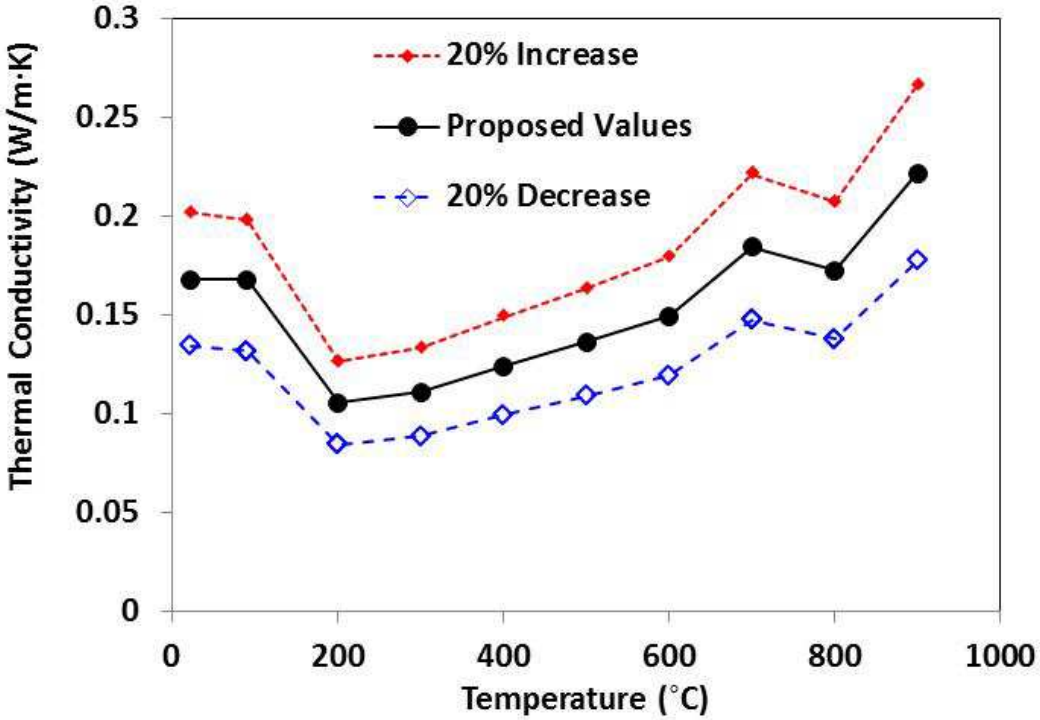

Figure 3.42: Changes to Thermal Conductivity of Gypsum Board

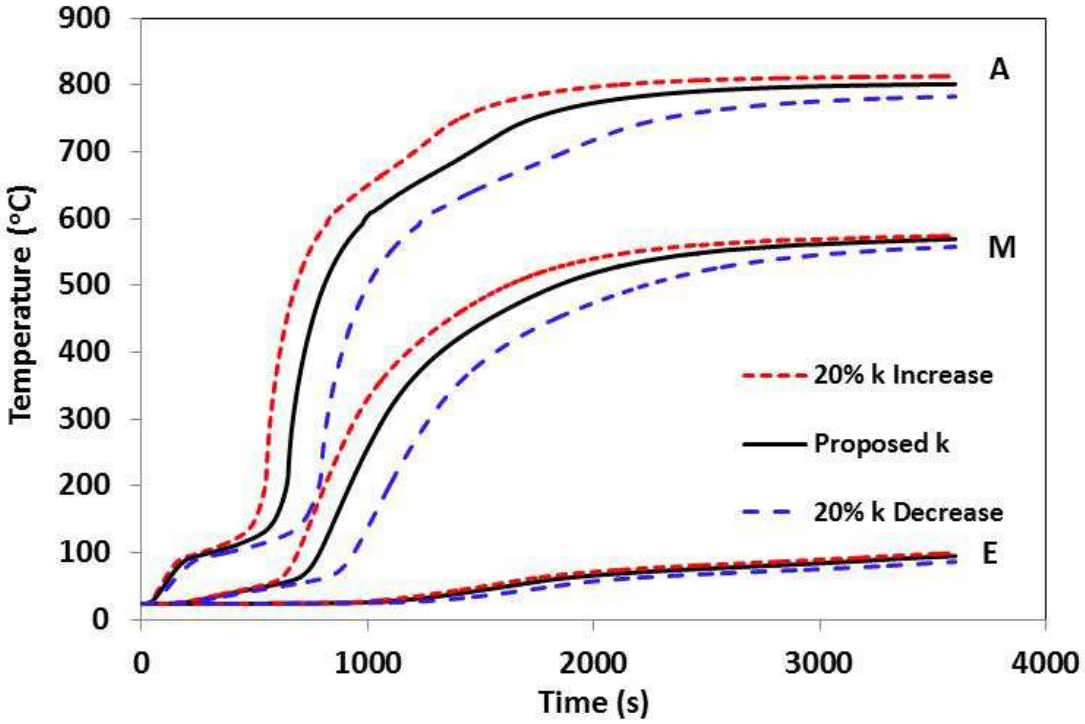

Figure 3.43: Sensitivity of Temperature to ± 20% Changes in Thermal Conductivity of Gypsum Board for Location A (Depth of 12.7 mm from Exposed Side), M (Middle of Insulation) and E (Unexposed Side). – Temperature Dependent Property Model

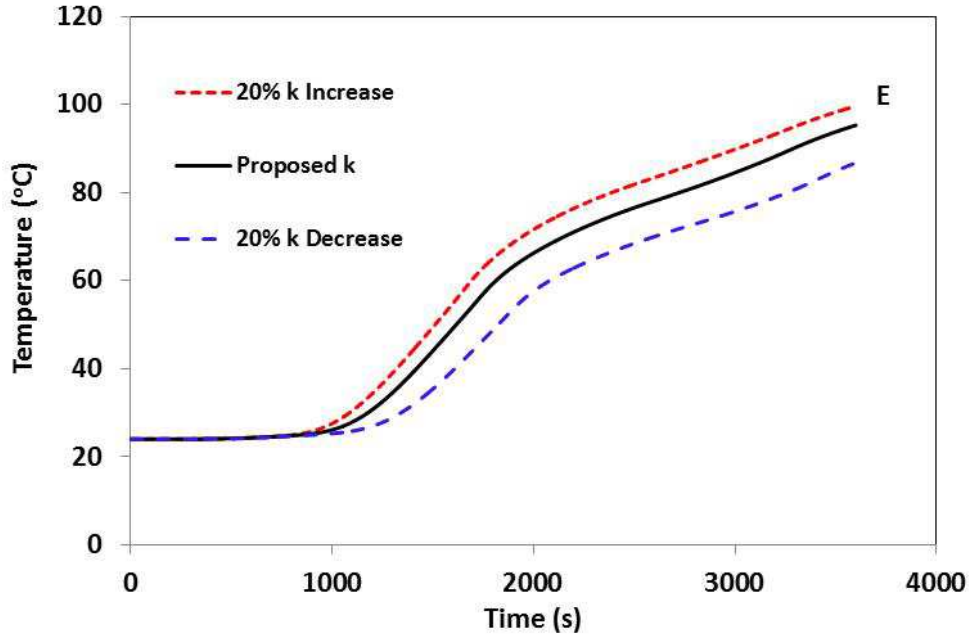

Figure 3.44: Sensitivity of Temperature to ± 20% Changes in Thermal Conductivity of Gypsum Board for Location E (Unexposed Side). – Temperature Dependent Property Model

The ± 20% changes to the temperature dependent thermal conductivity of stone wool insulation are shown in Figure 3.45. The sensitivity of the temperature to ± 20% changes in thermal conductivity of insulation in the temperature dependent model for the wall assembly at location A (depth of 12.7 mm from exposed side), M (middle of insulation) and E (unexposed side) is presented in Figure 3.46. Figure 3.47 shows the temperature variation at the unexposed end (E).

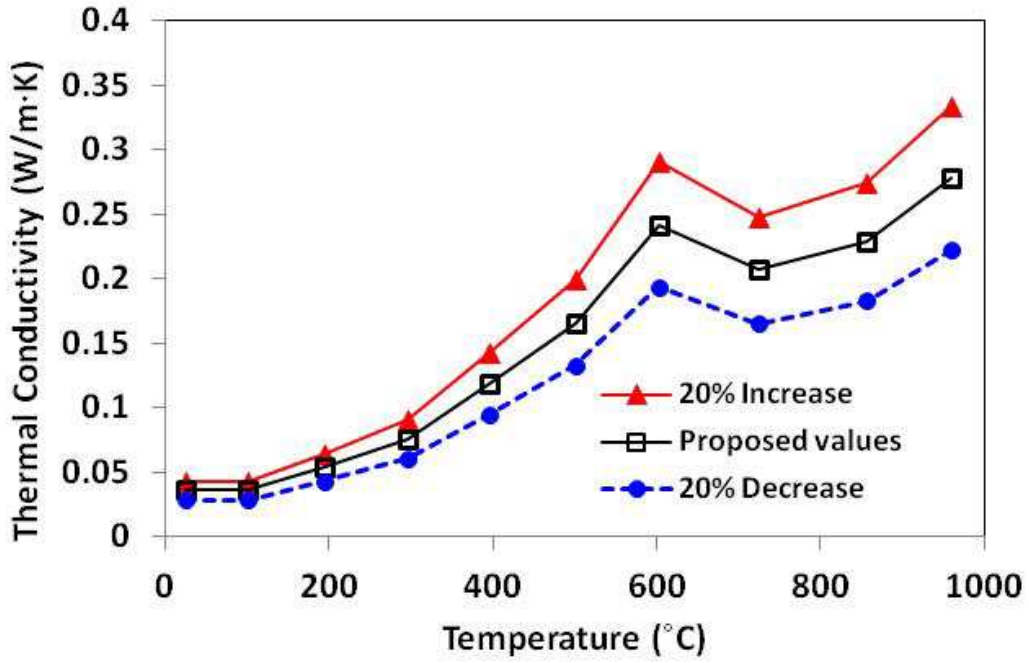

Figure 3.45: Changes to Thermal Conductivity of Stone Wool Insulation

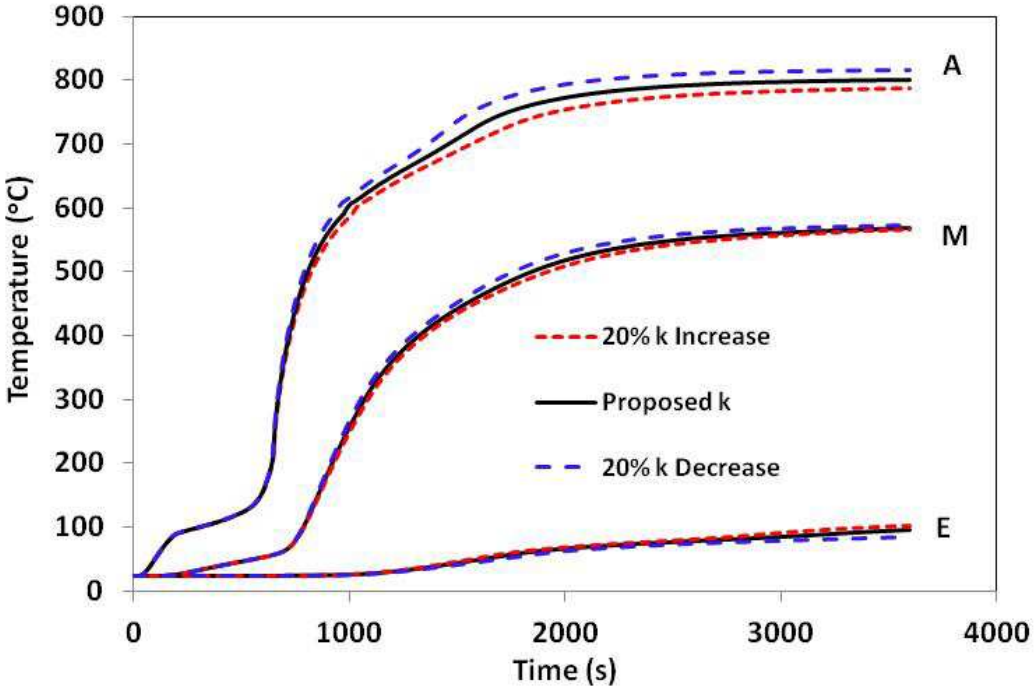

Figure 3.46: Sensitivity of Temperature to ± 20% Changes in Thermal Conductivity of Stone Wool Insulation for Location A (Depth of 12.7 mm from Exposed Side), M (Middle of Insulation) and E (Unexposed Side). – Temperature Dependent Property Model

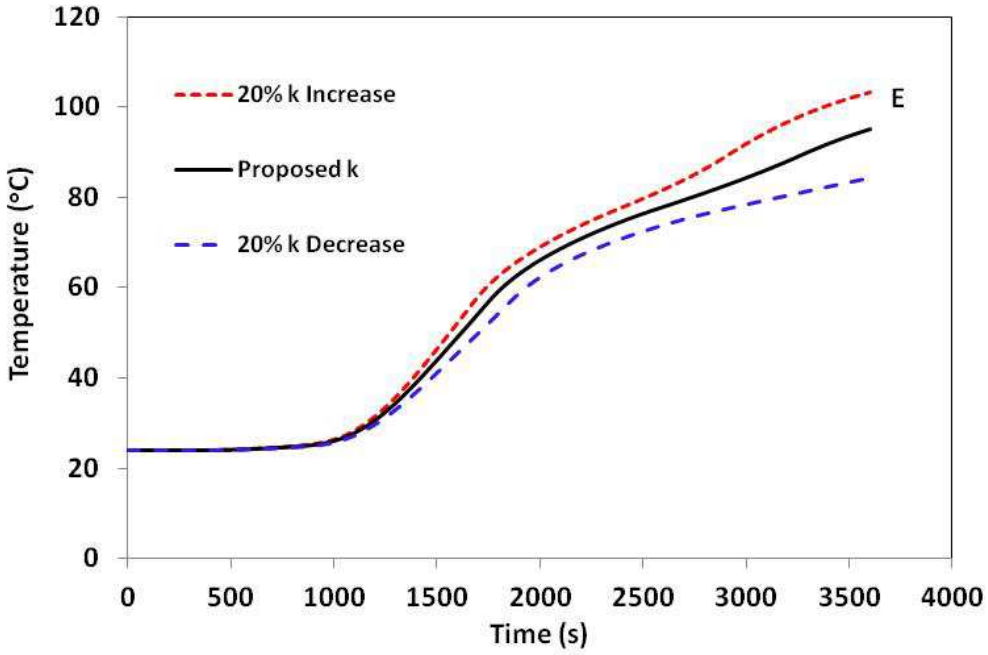

Figure 3.47: Sensitivity of Temperature to ± 20% Changes in Thermal Conductivity of Stone Wool Insulation for Location E (Unexposed Side). – Temperature Dependent Property Model

3.4.3 Density of Gypsum Board and Stone Wool Insulation

The ± 20% changes to the temperature dependent density of gypsum board are shown in Figure 3.48. The sensitivity of the temperature to ± 20% changes in density of gypsum board in the temperature dependent model for the wall assembly at location A (depth of 12.7 mm from exposed side), M (middle of insulation) and E (unexposed side) is presented in Figure 3.49. Figure 3.50 shows the temperature variation at the unexposed end (E).

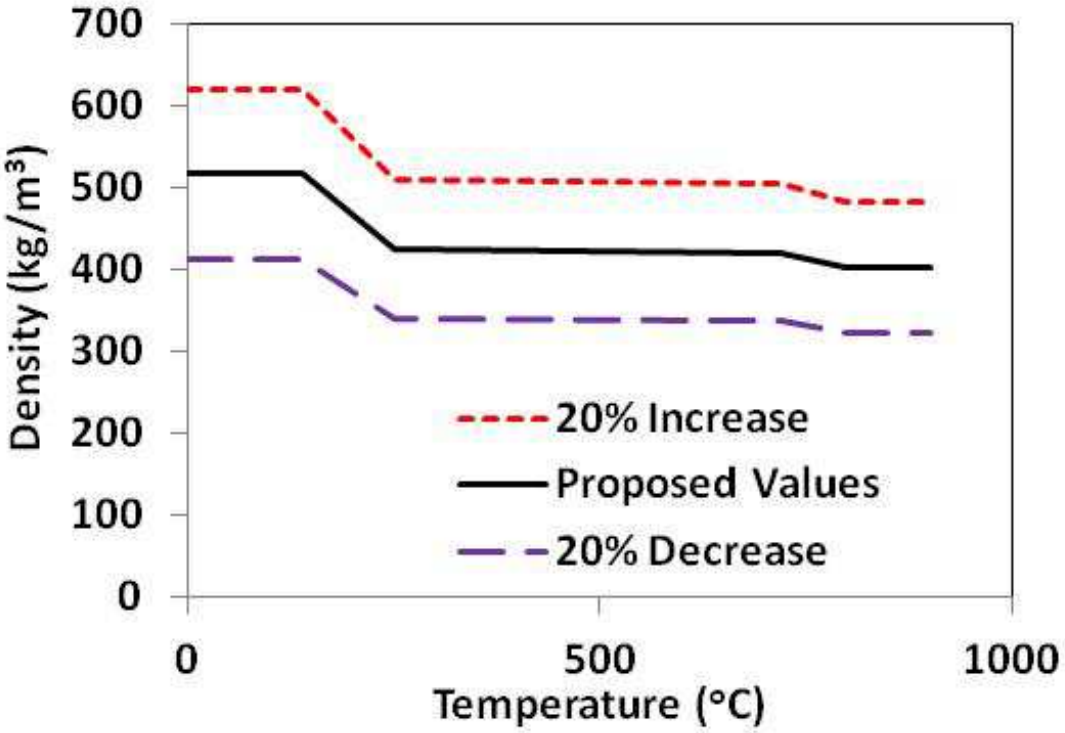

Figure 3.48: Changes to Density of Gypsum Board

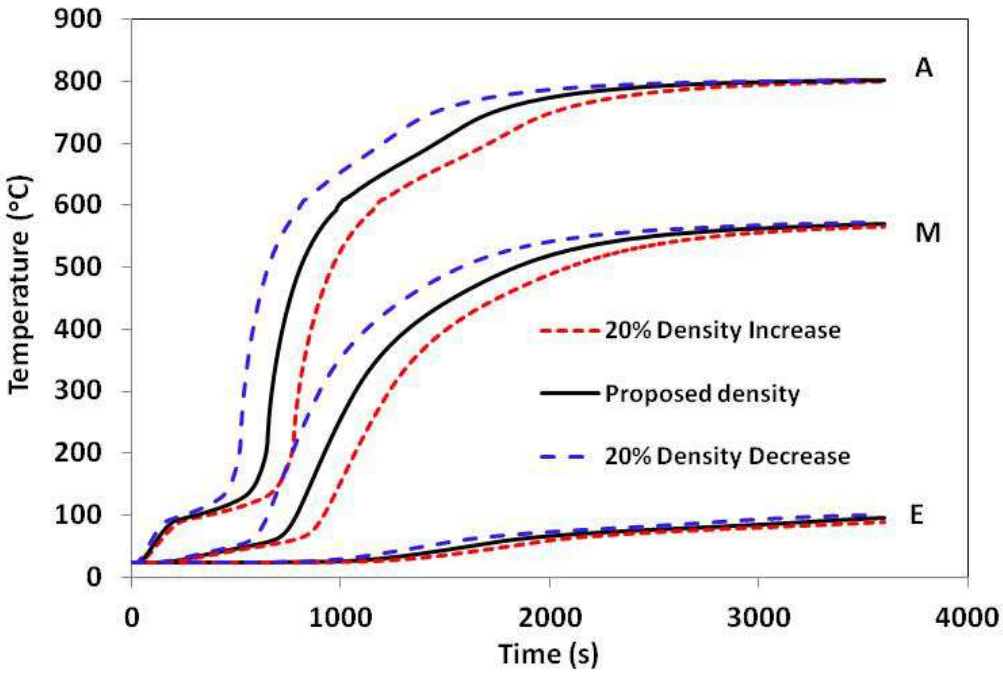

Figure 3.49: Sensitivity of Temperature to ± 20% Changes in Density of Gypsum Board for Location A (Depth of 12.7 mm from Exposed Side), M (Middle of Insulation) and E (Unexposed Side). – Temperature Dependent Property Model

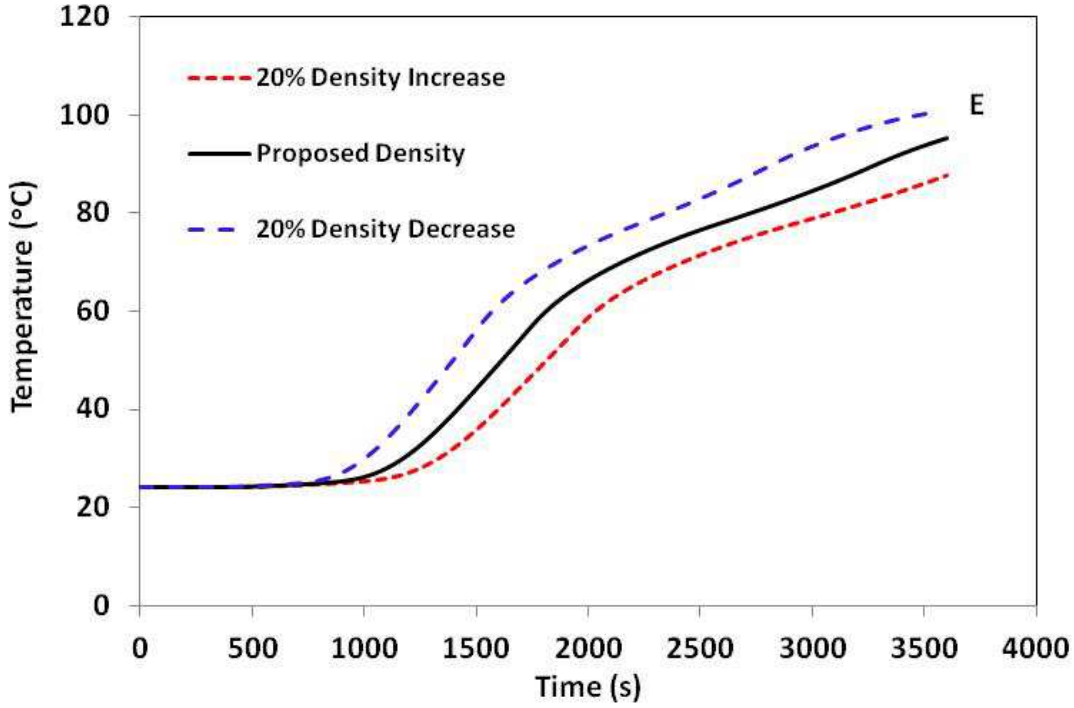

Figure 3.50: Sensitivity of Temperature to ± 20% Changes in Density of Gypsum Board for Location E (Unexposed Side). – Temperature Dependent Property Model

The ± 20% changes to the constant value of the density of stone wool insulation is shown in Table 3.4. The sensitivity of the temperature to ± 20% changes in density of stone wool in the temperature dependent model for wall assembly at location A (depth of 12.7 mm from exposed side), M (middle of insulation) and E (unexposed side) is presented in Figure 3.51. Figure 3.52 show the temperature variation at the unexposed end (E).

Table 3.4: Changes to Density of Stone Wool Insulation

Density of Stone Wool (kg/m^3)		
Proposed Value	20% Decrease	20% Increase
31.3	25.1	37.6

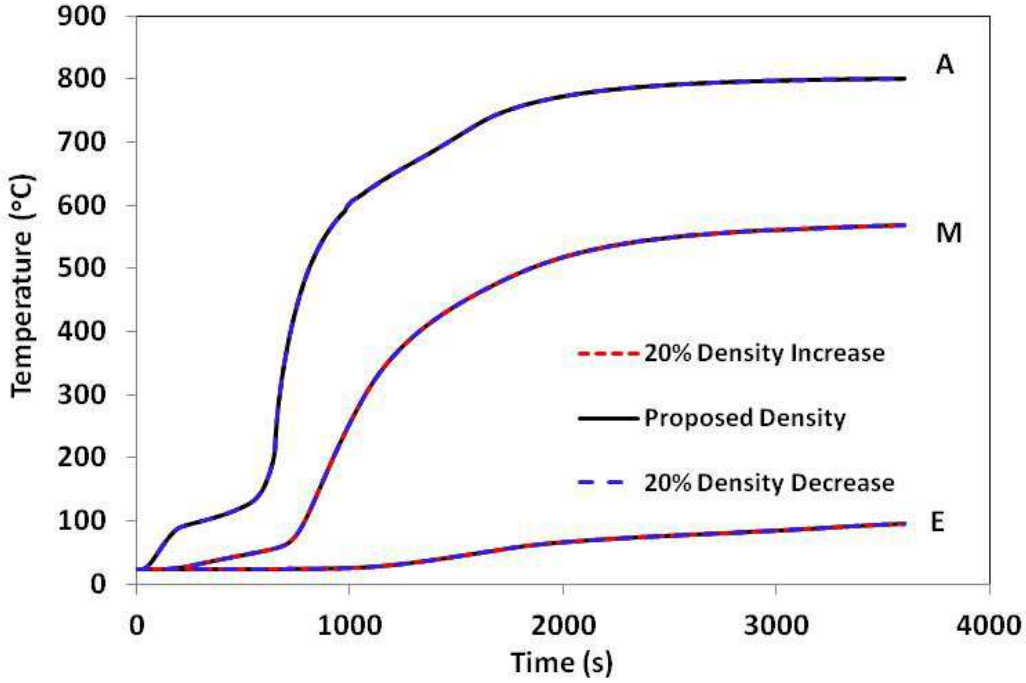

Figure 3.51: Sensitivity of Temperature to ± 10% and ± 20% Changes in Density of Stone Wool Insulation for Location A (Depth of 12.7 mm from Exposed Side), M (Middle of Insulation) and E (Unexposed Side). – Temperature Dependent Property Model.

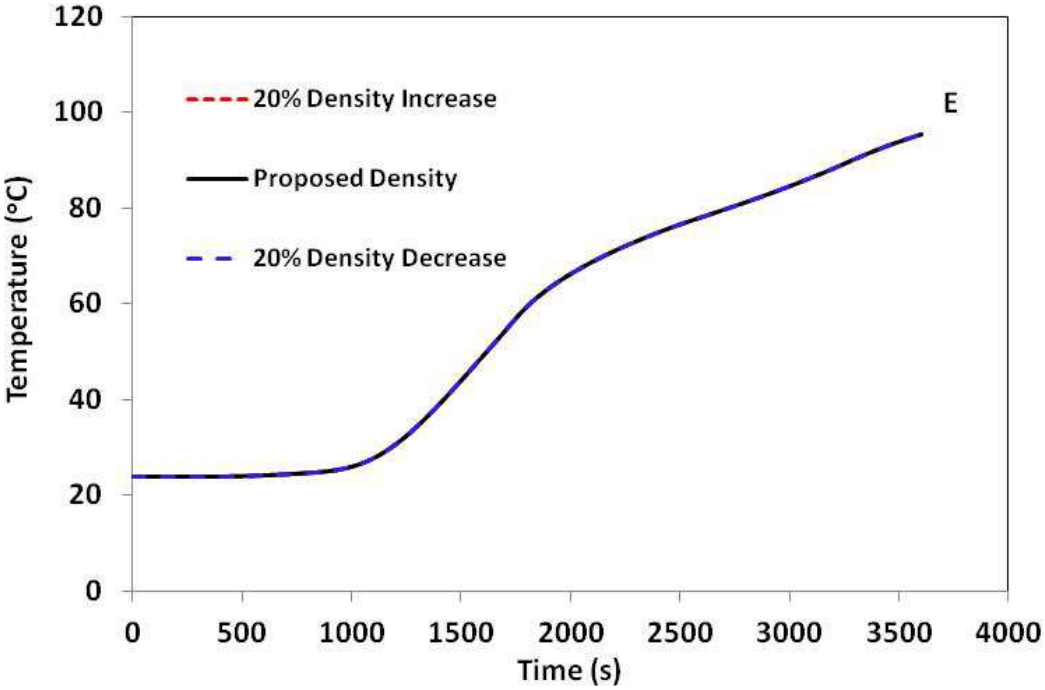

Figure 3.52: Sensitivity of Temperature to ± 20% Changes in Density of Stone Wool Insulation for Location E (Unexposed Side). – Temperature Dependent Property Model

The sensitivity of the temperature increase after 40 min. of exposure on the unexposed side of the wall assembly to ± 20% changes to specific heat, thermal conductivity and density for both gypsum board and stone wool insulation is shown in Table 3.5.

Table 3.5: Sensitivity Results for Temperature Increase at Location E (Unexposed Side) at 40 Minutes of Exposure for Temperature Dependent Property Model.

Property	**20% Decrease**		**Original**	**20% Increase**	
	(˚C)	% diff	(˚C)	(˚C)	% diff
Specific Heat (Gypsum Board)	57.1	11.5	50.9	45.9	-10.3
Thermal Conductivity (Gypsum Board)	42.7	-17.5	50.9	56.1	9.7
Density (Gypsum Board)	57.1	11.5	50.9	45.8	-10.5
Specific Heat (Stone Wool Insulation)	50.9	0	50.9	50.9	0
Thermal Conductivity (Stone Wool Insulation)	47.1	-7.8	50.9	53.8	5.5
Density (Stone Wool Insulation)	50.9	0	50.9	50.9	0

3.4.4 Sensitivity Study Results

The results of the study of the sensitivity of temperature increase after 40 min. of exposure on the unexposed side of the wall assembly to ± 20% changes to specific heat, thermal conductivity and density of both gypsum board and stone wool insulation show that the property that the temperature is most sensitive to is the thermal conductivity of the gypsum board. The sensitivity study also shows that the temperature is significantly affected by the changes in the specific heat and density of gypsum board and moderately affected by the changes to the thermal conductivity of stone wool insulation. The specific heat and density of stone wool insulation is seen to have a negligible effect on the temperature.

A 17.5% decrease in temperature at the unexposed side is obtained for a 20% decrease in the thermal conductivity of gypsum board. A 7.8% decrease in temperature at the unexposed side is obtained for a 20% decrease in the thermal conductivity of stone wool insulation. A 5.5% increase in temperature at the unexposed side is obtained for a 20% increase in the thermal conductivity of stone wool insulation. The sensitivity of the temperature at the unexposed side to ± 20% changes to specific heat of stone wool is negligible.

CHAPTER FOUR: EXPERIMENTAL RESULTS[1]

In this chapter the experimental apparatus, sample, procedures and results are discussed. The experiments were designed to measure heat transfer through gypsum boards and wall assemblies using a hotplate and cone calorimeter. The following experiments were conducted:

- Heat transfer through insulated, wood stud single layer gypsum board wall assemblies using a hotplate;
- Heat transfer through single and double layers of gypsum board using the cone calorimeter;
- Heat transfer through insulated, wood stud single and double layer gypsum board wall assemblies using a cone calorimeter; and
- Heat transfer through non-insulated, wood stud single and double layer gypsum board wall assemblies using a cone calorimeter.

4.1 EXPERIMENTAL APPARATUS

The apparatus used in this study included: a thermal gravimetric analyzer, a hotplate, a cone calorimeter, an Agilent data acquisition system, a sample holder, and temperature transducers.

4.1.1 Hot Plate

To determine the heat transfer through wall assemblies during low temperature exposures with a constant temperature boundary condition, a procedure similar to the ASTM Standard Test Method for Thermal Protective Performance of Materials for Protective Clothing for Hot Surface

[1] *A version of portions of this chapter has been previously published: Aire C.T., Torvi D.A., Weckman E.J., 2013, Heat Transfer in Cone Calorimeter Tests of Generic Wall Assemblies, Proceedings of the ASME International Mechanical Engineering Conference and Exposition, Paper No. IMECE2013-63981, San Diego, CA, USA.*

Contact (ASTM F 1060) [58] was used. This standard uses a hotplate at a constant temperature to provide a thermal exposure. A 6.4 mm (0.25 in) thick, 140 by 140 mm (5.5 by 5.5 in.) wide, T-1100 aluminum surface plate was placed on the HP72625 MIRAK ^{TM} hotplate (Barnstead International, Iowa, USA). The aluminum plate has a 2.4 mm (3/32 in.) hole drilled from the edge to the centre of the plate. A mass of 3.89 kg was placed on the specimen to ensure a contact pressure of 3 kPa. The setup for the hotplate experiment is shown in Figure 4.1. The control knob on the hot plate was adjusted when necessary to keep the temperature constant at 80˚C. Insulating boards were used to prevent loss of temperature to the surrounding during the tests and also to attempt to ensure one dimensional heat transfer.

Figure 4.1: Hotplate Experimental Setup

4.1.2 Cone Calorimeter

The cone calorimeter is one of the small-scale pieces of fire equipment used extensively for research purposes, as it measures the heat release of materials using the oxygen consumption principle. This principle states that for each kilogram of oxygen that is consumed in a combustion reaction for a wide range of combustibles, a heat value of 13.1 MJ is released with an accuracy of ±5% [59]. The capability of the cone calorimeter in measuring the heat release rate was not used in this thesis as only the cone heater was used. As shown in Figure 4.2, the cone calorimeter comprises a radiant electric heater which has a shape of a truncated cone (frustum) which is capable of providing a heat flux in the range of 0 – 100 kW/m^2 to a 10 x 10 cm square sample. The cone calorimeter can be used to conduct tests in both the vertical and horizontal orientations.

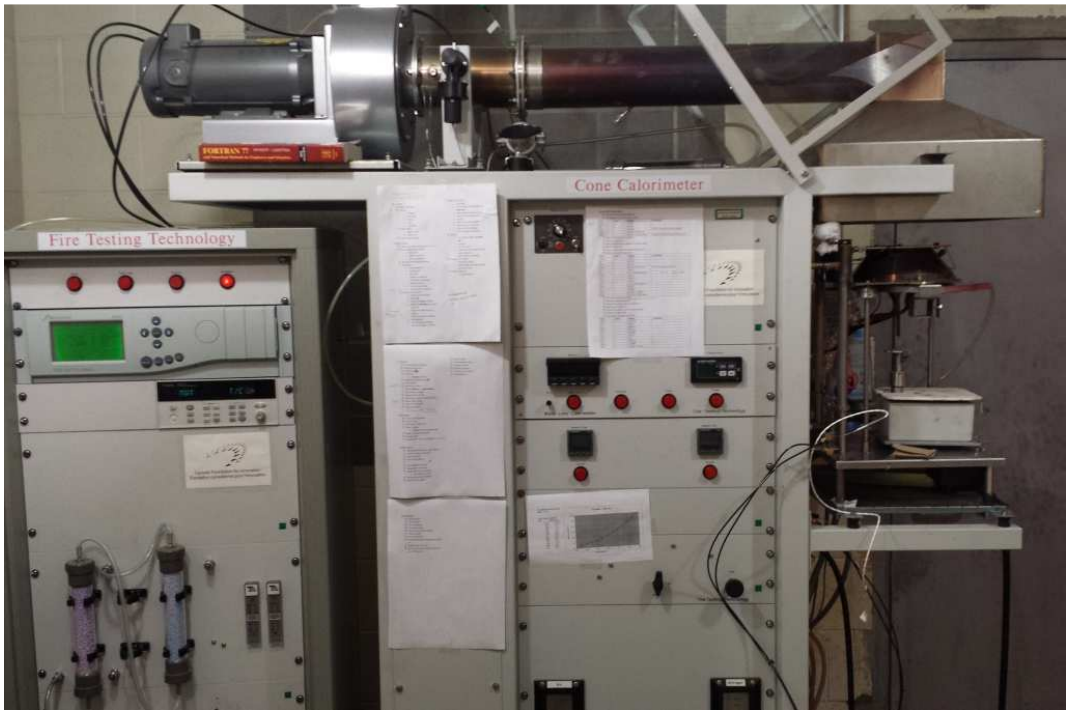

Figure 4.2: Cone Calorimeter

For this research, tests were performed using a cone calorimeter (Fire Testing Technology, East Grinstead, U.K.) with the cone heater in the vertical orientation as shown in Figure 4.3. The cone heater alone was used to conduct tests for this research. The heat release rate in gypsum boards and wall assemblies were not considered in this research because the relatively long duration of the tests.

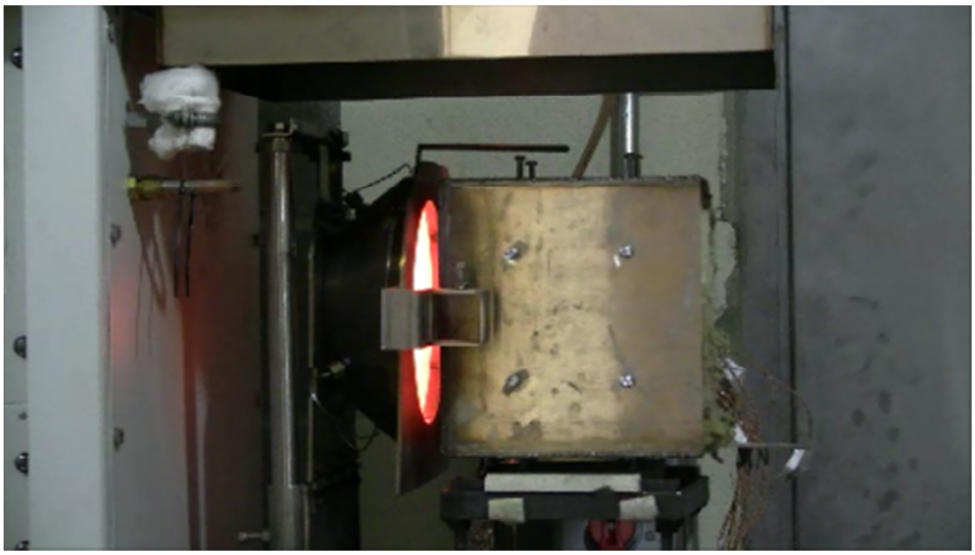

Figure 4.3: Cone Heater in Vertical Orientation

4.1.3 Sample Holder

Due to the size of the specimens tested, the sample holder used with the cone calorimeter in this study is not the standard sample holder specified in ASTM E 1354 [59]. The sample holder consists of a 190.5 mm (7.5 in.) by 190.5 mm (7.5 in.) by 177.8 mm (7 in.) deep stainless steel box with an opening so that an area of 101.6 mm (4 in.) by 101.6 mm (4 in.) was exposed to the cone heater, as shown in Figure 4.4. A box was built out of 12.7 mm (0.5 in.) cement board to hold the test specimen. This cement board box was centered within the stainless steel box and the

space between the two boxes was filled with stone wool insulation. This arrangement was used to reduce heat losses from the sides of the test specimen.

Figure 4.4: Sample Holder (Clockwise from Upper Left – Without Specimen and Insulation, Without Specimen, With Specimen (Rear View), With Specimen (Front View))

4.1.4 Temperature Measurements

The Agilent 34970A data acquisition system manufactured by Hewlett Packard, Santa Clara, CA was used to record temperature readings within the test specimens during experiments at an interval of 1 s. This data logger has 16 channels and has the capability of recording signals (e.g.

temperatures, voltages) for long periods of time. Figure 4.5 shows a photograph of the Agilent data acquisition system.

Figure 4.5: Agilent 34902A Data Acquisition System.

Temperature measurements were taken by attaching 24 AWG (0.51 mm (0.02 in.) diameter) Type K (chromel-alumel) thermocouples at different locations on the gypsum boards with an adhesive prior to conditioning of the specimen. Thermocouples were also inserted into the insulation. The thermocouples were connected to an Agilent 34970A data acquisition system (HP Agilent, Santa Clara, CA), and temperature data were collected at an interval of 1 s. Infra-red photographs of the unexposed surface were taken using an InfraCAM ™ camera (FLIR SYSTEMS, Burlington, ON). Figure 4.6 shows the InfraCAM ™ camera used.

Figure 4.6: Infra-red Camera

An infrared thermometer (Cyclops 300AF, Minolta/Land, Dronfield, UK) shown in Figure 4.7 was used to take the temperature measurements of the unexposed side of the gypsum boards at an interval of 1 s.

Figure 4.7: InfraRed Thermometer

4.2 TEST SPECIMEN

Test specimens are shown in Figures 4.8 and 4.9. The scaled wall assemblies were 111.1 mm (4.375 in.) by 111.1 mm (4.375 in.) and consisted of single or double layers of gypsum board, stone wool insulation and spruce-pine-fir (SPR) studs. The specimens were designed to represent a one-quarter scale model of a common wall design, with studs spaced at a centre-to-centre distance of 406.4 mm (16 in.).

Three different types of gypsum board were used: 12.7 mm (0.5 in.) regular gypsum board, 12.7 mm (0.5 in.) lightweight gypsum board and 15.9 mm (0.625 in.) type X gypsum board. The wood studs were made by cutting nominal 2x4 studs (38 mm by 89 mm) into 9.25 mm by 89 mm (0.375 in. by 3.5 in.) pieces. The scaled studs were spaced at a centre-to-centre distance of 101.6 mm (4 in.). 6D finishing nails (2.33 mm (0.092 in.) diameter) were used to fasten single or double layers of the gypsum board to the wood studs (Figure 4.9). Nails of length 50.8 mm (2.0 in.) were used for the assemblies with double layers of type X gypsum board; the nails were cut to shorter lengths for other assemblies in order to provide a minimum penetration depth of 20 mm into the wood as prescribed in the National Building Code of Canada [60]. The nails were spaced at 98.4 mm (3.875 in.) as shown in Figure 4.9. More information on the materials tested is presented in Table 4.1. The temperature measurement locations were picked so as to determine the temperature at which wall failure occurs. These locations are similar to the temperature measurement locations used in full scale testing to determine the performance of wall assemblies.

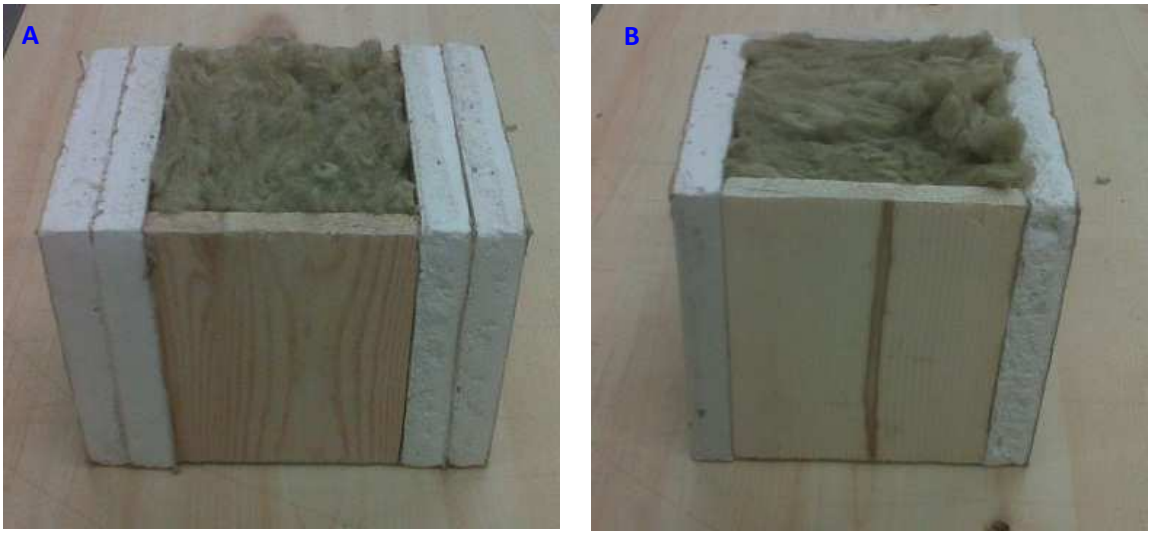

Figure 4.8: Wall Assembly Specimen (A – Double Layers of Gypsum Board, B – Single Layer of Gypsum Board)

Table 4.1: Description of Materials Used

Material	**Description**
Regular Gypsum Board	Thickness = 12.7 mm (0.5 in.) Density = 645.7 kg/m^3
Lightweight Gypsum Board	Thickness = 12.7 mm (0.5 in.) Density = 564.3 kg/m^3
Type X Gypsum Board	Thickness = 15.9 mm (0.625 in.) Density = 724.8 kg/m^3
R-14 Stone Wool Insulation	Thickness = 89 mm (3.5 in.) Nominal Thermal Resistance: R-14
Studs	9.25 mm (0.375 in.) by 111.1 mm (4.375 in.) by 89.0 mm (3.5 in.) Cut from Spruce-Pine-Fir (SPR) 2x4's

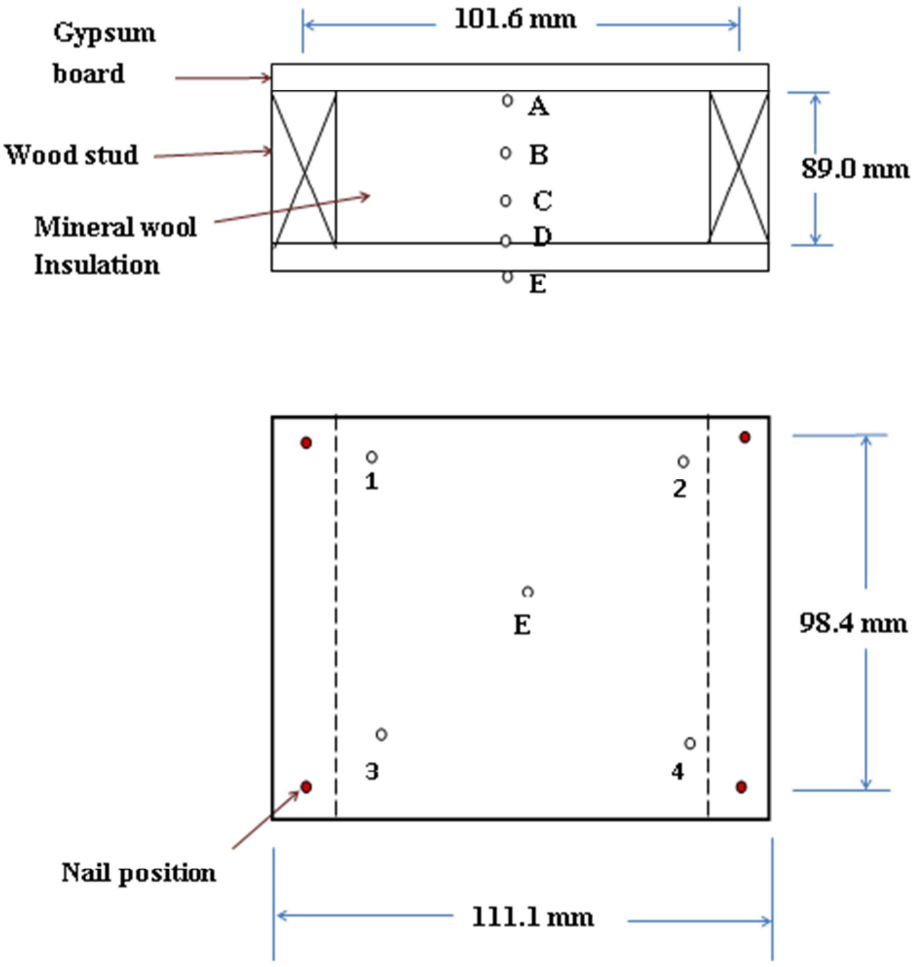

Figure 4.9: Schematic Diagram of the Specimen Showing Locations of Thermocouples (A-E, 1-4) and Nails

4.3 EXPERIMENTAL PROCEDURE

4.3.1. Instrumentation

For the wall assemblies, five thermocouples were located on the centerline of the specimen at various depths (Figure 4.9). One thermocouple was placed on the back of the exposed gypsum board(s). Two thermocouples were placed within the insulation, such that there was a distance of approximately 30 mm between thermocouples A and B, B and C, and C and D in Figure 4.9. One thermocouple was placed on the surface of the gypsum board that was in contact with the

insulation, and one thermocouple was placed on the unexposed surface of the assembly. Four additional thermocouples were placed on the unexposed surface of the assembly, as shown in Figure 4.9 (thermocouples 1-4).

Tests were also conducted in which only the gypsum board was tested, using either single or double layers. In these tests an infrared thermometer (Cyclops 300AF, Minolta/Land, Dronfield, UK) was used to take the temperature measurements of the unexposed side at an interval of 1 s. For the double layer tests, a single thermocouple was also placed between the two layers of the gypsum board.

Specimens were placed inside the cement board box, within the stainless steel box. The specimen was then exposed to the cone heater for a period of 70 min. After testing the specimen was removed and inspected.

4.3.2 Conditioning of Specimen

The wall assembly specimens were conditioned for at least 24 hours in a chamber (shown in Figure 4.10), which was kept at a temperature of 23±2°C and a relative humidity of 50±3%, as specified in ASTM E 1354 [59]. The relative humidity within the chamber was controlled using a non-saturated salt solution of magnesium chloride ($MgCl_2$). A saturated aqueous salt solution of magnesium chloride will produce an equilibrium relative humidity value of 32.8±0.2% at a temperature of 25°C [61]. The salt was mixed with water until the desired relative humidity of 50±5% was achieved and sustained within the chamber. An Anton Paar (DMA 4500 M) densitometer was used to determine the density and specific gravity of the salt solution. The density of the salt solution was 1.27 g/cm^3 and specific gravity was 1.28. During testing, the laboratory ambient conditions were 23±3°C and 35±7% relative humidity.

Figure 4.10: Pictures of conditioning chamber.

4.3.3. Heat Flux Exposures

One of the limitations of the cone heater is its inability to produce a high enough heat flux to replicate the full-scale fire test furnace environment [62]. These furnaces follow a standard temperature-time curve, which produce heat fluxes of up to 150 kW/m^2 [6]. The cone calorimeter can only produce a maximum heat flux of 100 kW/m^2. In this study, the small scale wall specimens were tested using an incident heat flux of 75 kW/m^2. The effect of heat flux was also investigated by conducting wall tests using assemblies that contained single layers of lightweight gypsum board with and without insulation at heat fluxes of 35 and 50 kW/m^2.

4.4 EXPERIMENTAL RESULTS

4.4.1. Hot Plate Experiments

Hot plate experiments on wall assemblies comprising of Regular and Type X gypsum board and stone wool insulation were conducted at a constant exposure temperature of 80^{o}C. Three tests were conducted for both regular and type X wall assemblies. Figure 4.11 gives an indication of the repeatability as well as the variation of the temperature of the aluminum plate. Figure 4.12 compares the temperature measurement at different depths in the wall assembly. Comparisons of the average temperature at different depths and times are presented in Table 4.2

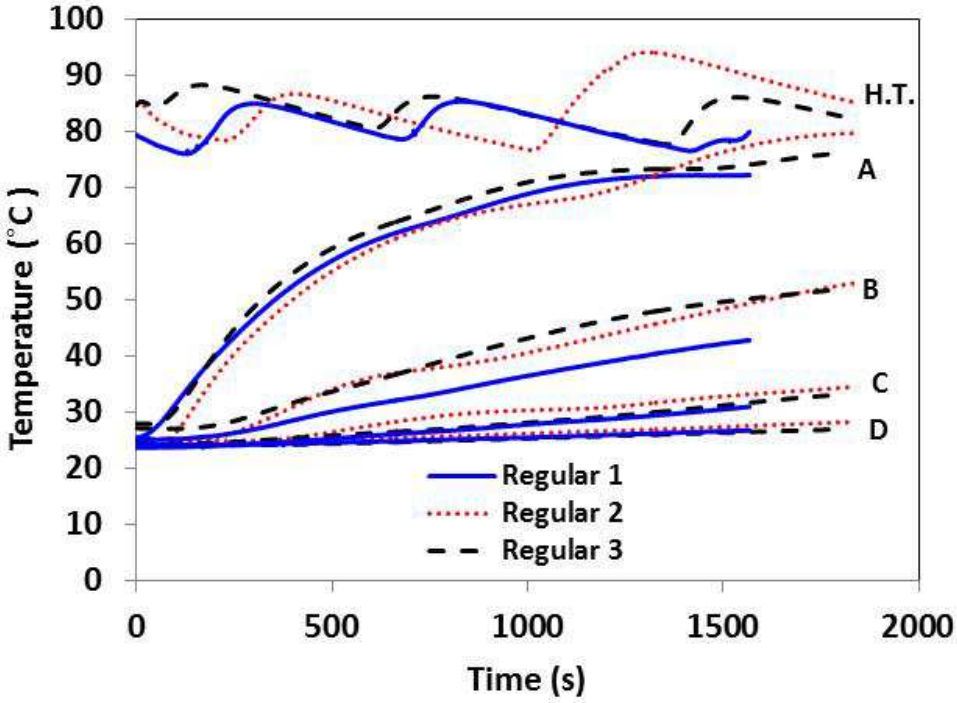

Figure 4.11: Temperature Measurements in Regular Gypsum Board Wall Assembly Exposed to Hotplate Temperature of 80˚C. (H.T. – Hotplate Temperature)

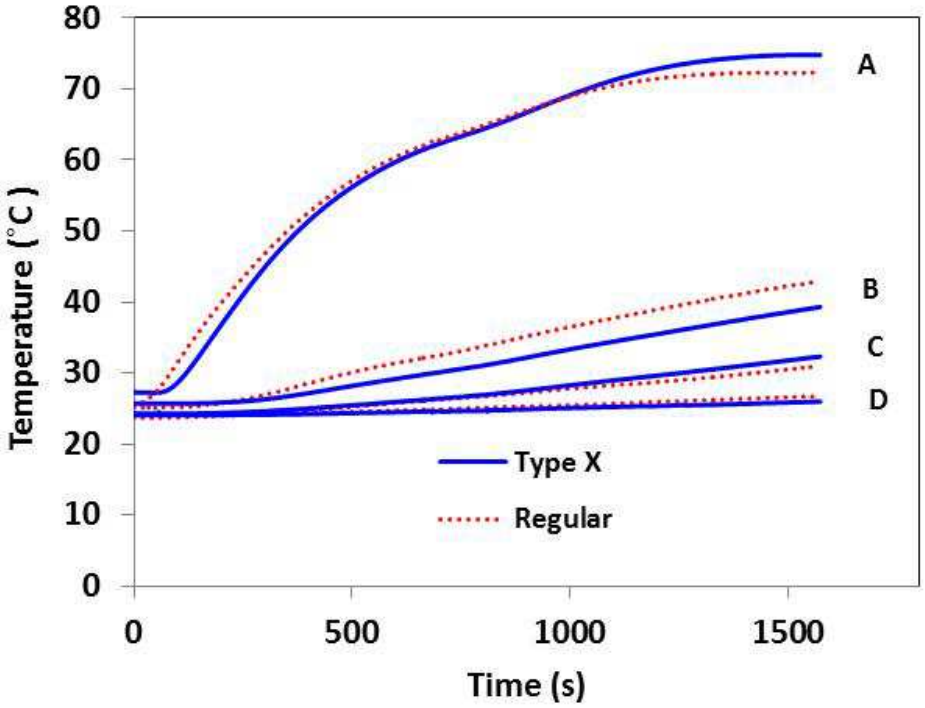

Figure 4.12: Temperature Measurements in Regular and Type X Gypsum Board Wall Assemblies Exposed to Hotplate Temperature of 80˚C.

Table 4.2: Average Temperature Increase after 10, 15 and 25 Min. of Exposure Measured at Four Locations During Hotplate Tests of Wall Assemblies..

Type of Gypsum Board Used in Wall Assembly	Maximum Temperature Increase (^{o}C)							
	Back of exposed board(s) (A)		Insulation: 30 mm from point A (s) (B)		Insulation: 30 mm from point B (s) (C)		Front of unexposed board(s) (D)	
	Ave.	(σ)	Ave.	(σ)	Ave.	(σ)	Ave.	(σ)
Single Regular 12.7 mm (0.5 in.) at 10 minutes	34.9	(0.3)	8.8	(2.3)	2.6	(0.8)	0.5	(0.08)
Single Regular 12.7 mm (0.5 in.) at 15 minutes	45.5	(0.3)	17.5	(2.6)	5.6	(0.9)	1.8	(0.01)
Single Regular 12.7 mm (0.5 in.) at 25 minutes	48.3	(3.0)	21.2	(2.9)	5.9	(1.2)	2.4	(0.07)
Single Type X 15.9 mm (0.625 in.) at 10 minutes	33.8	(1.0)	5.1	(1.2)	2.0	(0.2)	0.5	(0.1)
Single Type X 15.9 mm (0.625 in.) at 15 minutes	46.2	(0.7)	12.0	(1.6)	5.6	(0.5)	1.5	(0.2)
Single Type X 15.9 mm (0.625 in.) at 25 minutes	47.9	(1.2)	15.3	(1.8)	7.5	(0.6)	2.1	(0.3)

The test results in Figures 4.11 and 4.12 indicate a good level of repeatability and the variation in the results is primarily as a result of the variation in the hotplate temperature (H.T.) since it was difficult to keep the temperature of the hot plate constant. The knob of the hotplate was used to control the temperature within the desired range and an exposed temperature range of 80±10˚C

was attained during the test. The large variation in test results at location B is attributed to the shifting of the thermocouple position within the stone wool insulation. The nature of the stone wool insulation is such that it is difficult to maintain a consistent temperature measurement location within the insulation from test to test. Table 4.2 gives more information on the repeatability as well as the temperature increase at locations A, B, C, and D at 10, 15 and 25 min of exposure. From Table 4.2, the temperature increases in regular gypsum board wall assemblies are higher than temperature increases in type X wall assemblies at location B within the insulation. Similar temperature increases are observed at the other locations shown in Table 4.2. There is very little temperature increase at the unexposed side (location E) of either wall assembly.

4.4.2. Cone Calorimeter Experiments

Gypsum boards

The three different types of gypsum boards were first tested on their own, using either single or double layers. Three tests were conducted at a heat flux of 75 kW/m^2 for both single and double layers of gypsum board. Measurements of the temperature at the centre of the unexposed side of a single layer of gypsum board (location E in Figure 4.9) are shown in Figure 4.13. Figure 4.14 shows the temperatures measured between the two boards in the double layer tests, along with the temperatures measured on the unexposed side.

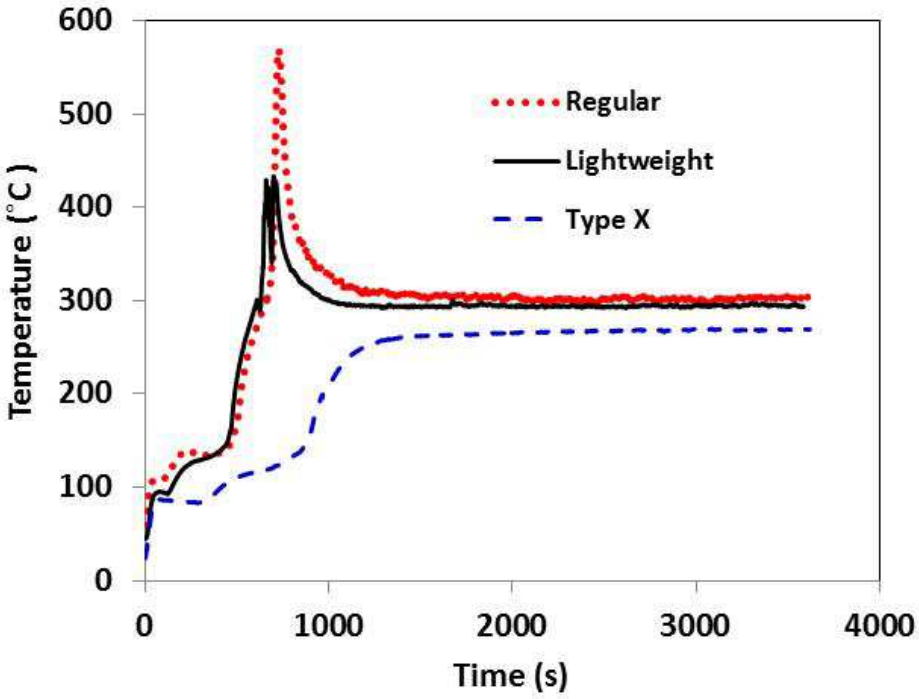

Figure 4.13: Comparison of Temperature Measurements at Centre of Unexposed Side of Single Layer of Regular, Lightweight and Type X Gypsum Boards

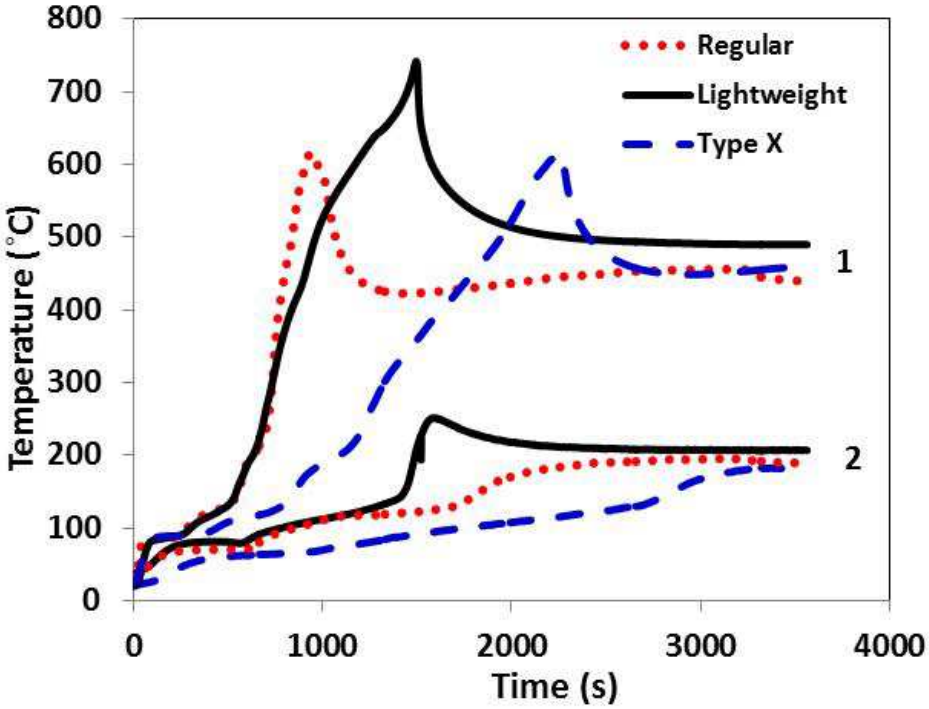

Figure 4.14: Comparison of Temperature Measurements at Interface Between Two Layers of Gypsum Board (1) and Unexposed Side of Gypsum Boards (2) for Tests of Double Layers of Regular, Lightweight and Type X Gypsum Board

The burning of the gypsum board paper occurred 20-30 s after exposure of the sample to the cone heater and it lasted for about 10-15 s after which products of combustion were released from the specimen and heating of the specimen continued. A comparison of the temperatures shown in Figure 4.13 for the tests of a single layer of gypsum board with the TGA results shown in Figure 3.9 (Section 3.1.5) indicates that calcination began quickly in all tests and that the length of time required to complete this process was much shorter for the two 12.7 mm (1/2 in.) gypsum boards (approximately 340 s) than for the thicker type X gypsum board (approximately 840 s). For the two 12.7 mm (1/2 in.) gypsum board types, there was a sharp increase to a maximum temperature, which lasted for a relatively short time, after which the temperature decreased until it reached its steady state value of about 300 ˚C. Temperatures of the type X board did not show the same behavior, but instead increased at a slower rate to a steady state value of about 280˚C.

Temperature measurements on the unexposed side of the assembly in the double layer gypsum board tests (Figure 4.14) exhibited a different behavior from the tests of the three types of single boards shown in Figure 4.13. It took a much longer time for calcination to occur throughout the two layers (from about 1400 s to more than 3000 s, depending on the type of drywall) than for a single layer. The maximum temperature increases on the unexposed side of the double layer of gypsum board were 33-68% lower than the values for a single layer of the three types of gypsum board. The temperature between the two layers of gypsum board (labeled 1 in Figure 4.14) rose to a peak and then decreased. This observation is similar to that obtained by [7] and this peak was attributed to the oxidation of the paper between the two surfaces after complete pyrolysis. While there were some similarities between the temperatures measured behind the exposed layer (Figure 4.14) and the temperatures measured behind a single layer (Figure 4.13), peaks were

considerably broader in Figure 4.14, and maximum temperatures for the lightweight and type X boards were significantly higher. Differences in temperature measurements would be expected due to the differences in heat transfer and availability of oxygen between the two cases.

Insulated Wall Assembly

Six different insulated wall assemblies, using single or double layers of the three types of gypsum board, were tested. Three individual tests were performed for each of these six assembly designs. Figure 4.15 provides an indication of the repeatability of the temperature measurements. This particular example is for a wall assembly consisting of double layers of 12.7 mm (0.5 in.) regular gypsum board, wood studs and stone wool insulation. Temperature measurements in other test series displayed similar repeatability.

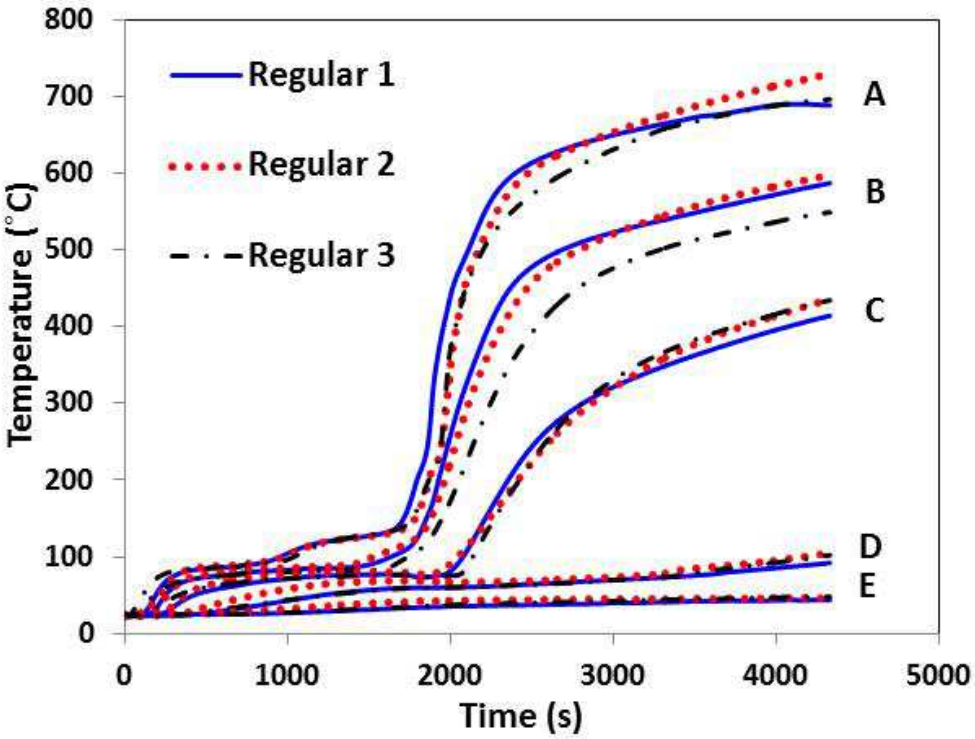

Figure 4.15: Temperature Measurements During Three Tests of Wall Assembly Containing Double Layers of Regular Gypsum Board

The temperature measurements at location A, D and E are much more repeatable compared to locations B and C because the thermocouples are well attached to the gypsum boards, while, as noted earlier, at locations B and C there is likely variation in the exact thermocouples position within the insulation from test to test.

Experimental Results for Walls with Different Gypsum Board Types

Figure 4.16 compares temperatures measured at three locations in wall assemblies that use single layers of the three types of gypsum board. A similar comparison is shown in Figure 4.17 for the wall assemblies that use double layers of the three types of gypsum board.

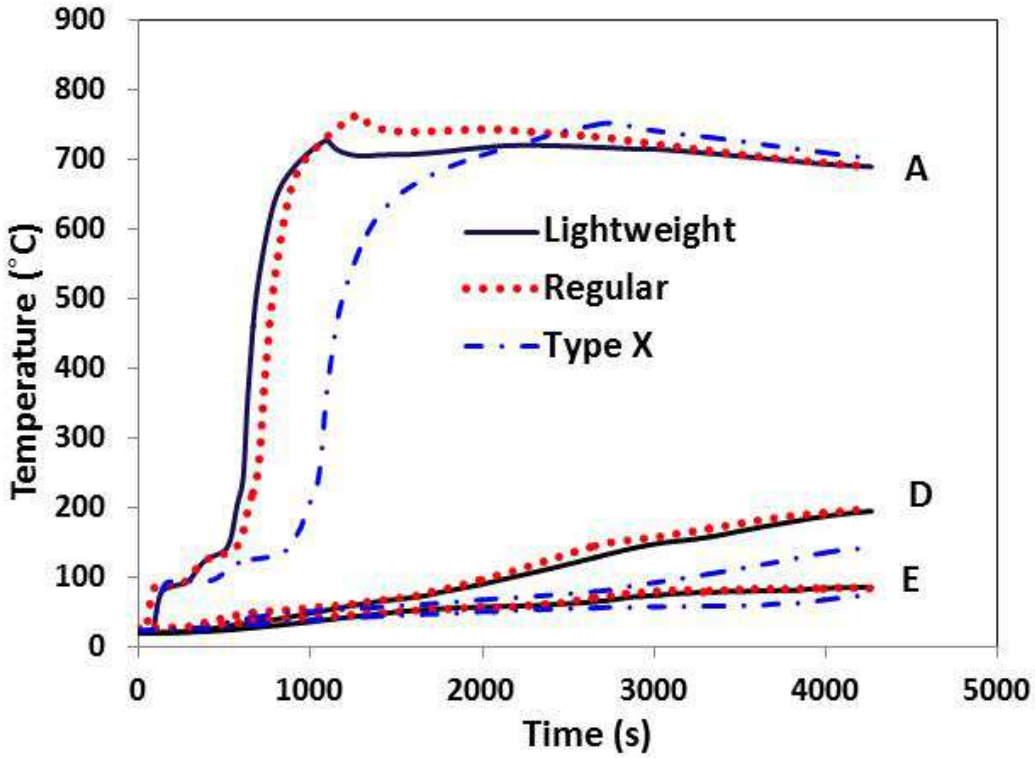

Figure 4.16: Comparison of Temperature Measurements Made During Tests of Wall Assemblies Containing Regular, Lightweight and Type X Gypsum Board (Single Layer)

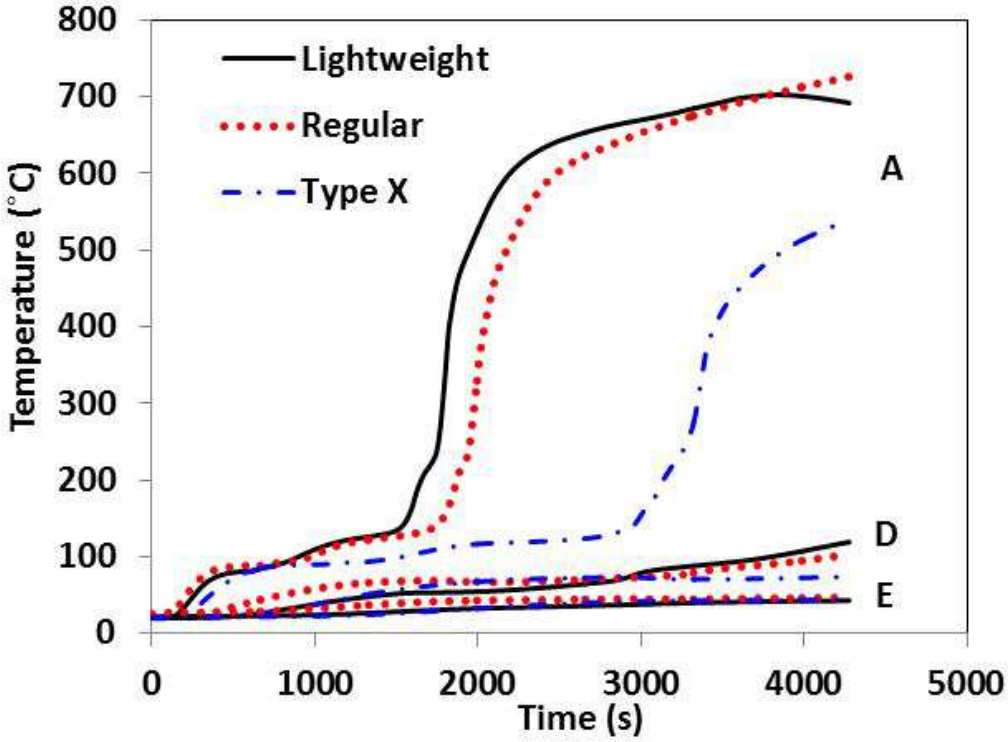

Figure 4.17: Comparison of Temperature Measurements Made During Tests of Wall Assemblies Containing Regular, Lightweight and Type X Gypsum Board (Double Layers)

Experimental Results for Single vs. Double Layer Walls

Figures 4.18-4.20 compare the temperatures measured at three locations in wall assemblies that use single and double layers of each of the three types of gypsum board.

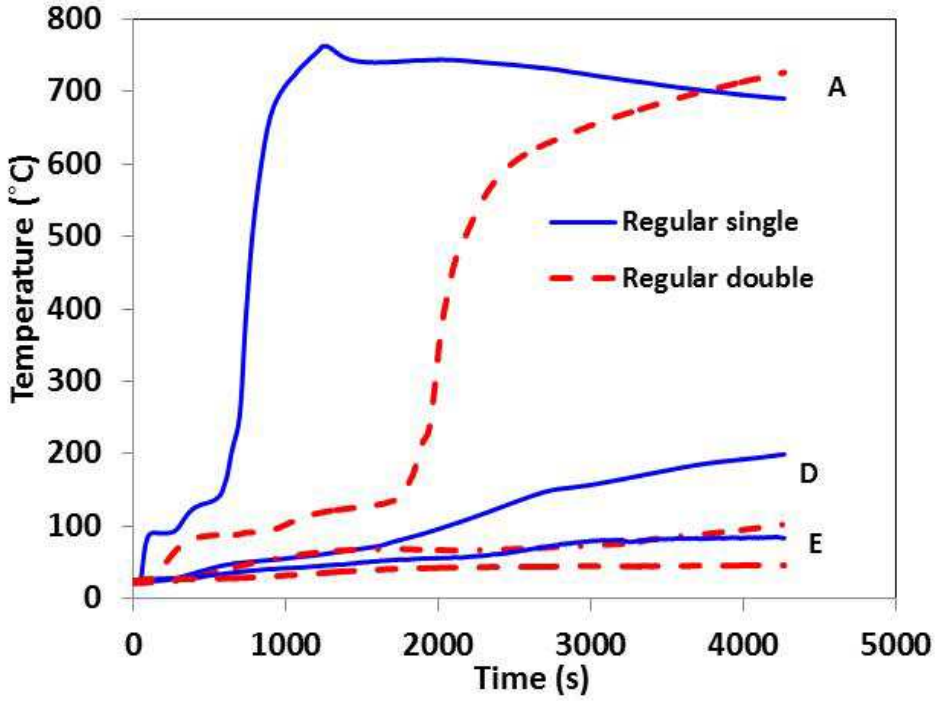

Figure 4.18: Comparison of Temperature Measurements Made During Tests of Wall Assemblies Containing Single and Double Layers of Regular Gypsum Board

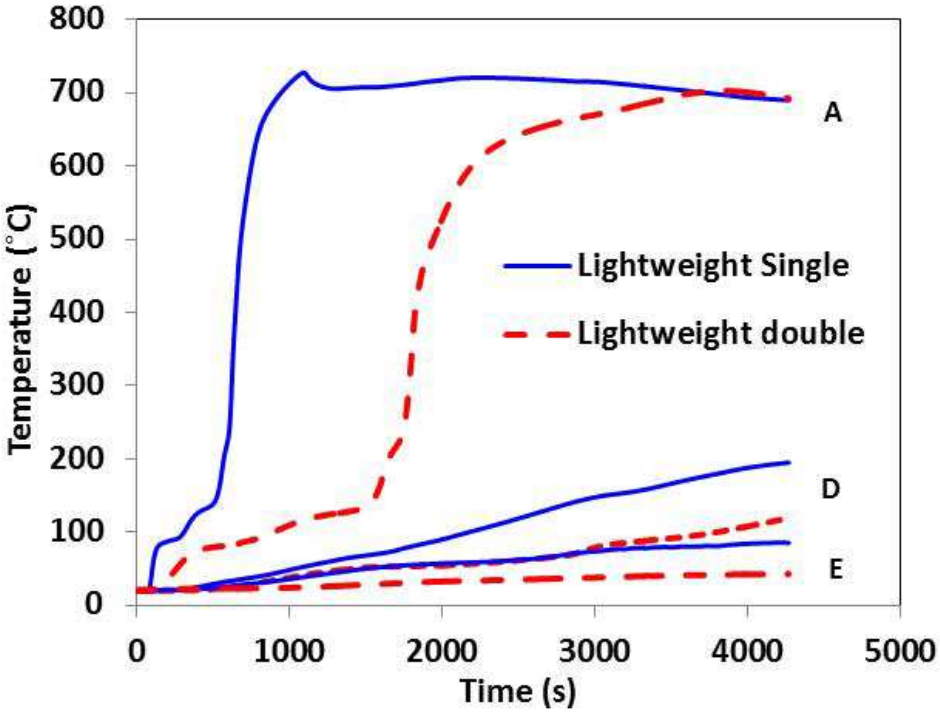

Figure 4.19: Comparison of Temperature Measurements Made During Tests of Wall Assemblies Containing Single and Double Layers of Lightweight Gypsum Board

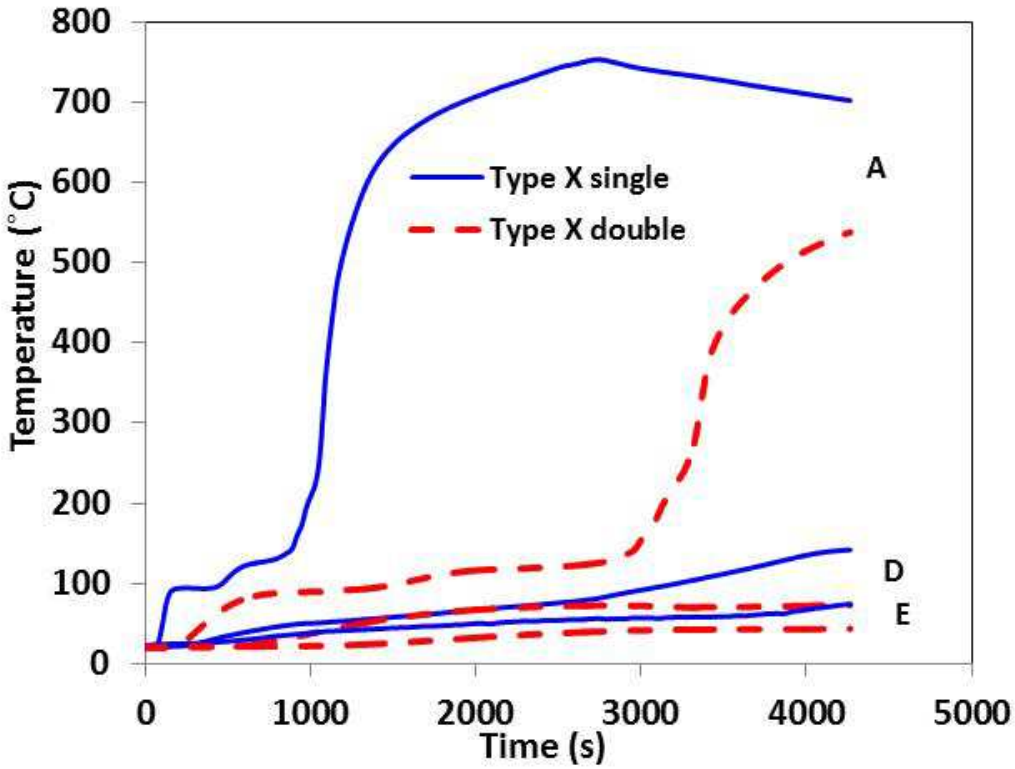

Figure 4.20: Comparison of Temperature Measurements Made During Tests of Wall Assemblies Containing Single and Double Layers of Type X Gypsum Board

Comparisons of the average maximum temperature increase at three locations within the specimen for the six wall assembly designs are shown in Table 4.3. The average times for the temperature of the unexposed side of the gypsum board layer(s) closest to the cone heater to reach particular temperatures are compared in Table 4.4 for the six wall designs.

Table 4.3: Average Maximum Temperature Increase Measured at Three Locations During Tests of Insulated Wall Assemblies (Heat Flux of 75 kW/m^2)

Type of Gypsum Board Used in Wall Assembly	**Maximum Temperature Increase (^{o}C)**					
	Back of exposed board(s) (A)		**Front of unexposed board(s) (D)**		**Back of unexposed board (E)**	
	Ave.	**(σ)**	**Ave.**	**(σ)**	**Ave.**	**(σ)**
Single Regular 12.7 mm (0.5 in.)	733.0	(6.0)	182.0	(17.1)	59.0	(1.2)
Single Lightweight 12.5 mm (0.5 in.)	712.9	(10.3)	189.5	(10.6)	66.2	(4.8)
Single Type X 15.9 mm (0.625 in.)	701.4	(22.4)	145.0	(19.6)	48.3	(2.5)
Double Regular 12.7 mm (0.5 in.)	682.3	(17.8)	76.8	(6.1)	23.7	(1.4)
Double Lightweight 12.7 mm (0.5 in.)	686.2	(4.1)	112.4	(8.4)	25.6	(3.5)
Double Type X 15.9 mm (0.625 in.)	542.6	(17.9)	54.8	(2.2)	22.8	(0.46)

Table 4.4: Average Time to Reach 100°C, 200°C, 250°C and Maximum Recorded Temperature on Back of Exposed Gypsum Board Layer(s) in Tests of Insulated Wall Assemblies

Type of Gypsum Board Used in Wall Assembly	**Average Time to Reach Temperature on Back of Exposed Gypsum Board Layer(s) (Location A) (s)**			
	100°C	**200°C**	**250°C**	**Maximum Temperature**
Single Regular 12.7 mm (0.5 in.)	300	660	720	1680
Single Lightweight 12.5 mm (0.5 in.)	270	564	588	1488
Single Type X 15.9 mm (0.625 in.)	444	960	1020	2940
Double Regular 12.7 mm (0.5 in.)	990	1836	1920	*
Double Lightweight 12.7 mm (0.5 in.)	906	1656	1740	*
Double Type X 15.9 mm (0.625 in.)	1518	3048	3168	*

* for double layers, temperatures were still increasing at end of 4200 s (70 min.) tests

In the tests of the insulated wall assemblies, there was a similar rate of rise in temperature on the back of the exposed board(s) (location A in Figures 4.18-4.19) for insulated single and double layer wall assembly, for all types of gypsum board up to a temperature of about 100 ˚C, when calcination began. The temperature on the back of the exposed board of the lightweight board wall assembly rose quicker than the regular and type X board wall assemblies. It can be seen from Table 4.4, as noted earlier, that the time required to reach a temperature of 100˚C at location A is dependent on the thickness and number of layers of the board as it took about 4–8 min for the single layer walls and 15–25 min for the double layer walls to attain this temperature.

Figures 4.18-4.20 all show a plateau in temperature at about 100 ˚C on the back of the exposed board(s) (location A). This is as a result of the energy that is required for the dehydration or calcination of the gypsum board. The duration of this plateau will depend on the type of gypsum board, the thickness, and number of layers and presence of insulation in the wall. A rapid rise in temperature followed the end of the calcination process. The rate of this temperature increase is again dependent on the type and thickness of the gypsum board as well as presence of insulation in the wall assembly. For insulated wall assemblies, temperature increased most rapidly in the assemblies containing the two types of 12.7 mm (1/2 in.) gypsum board, and temperatures increased quickest in the assemblies containing the lightweight gypsum board. These differences in heating rates can also be observed in Table 4.4, which compares the times required to reach temperatures of 200 ˚C, 250 ˚C and the maximum recorded temperature.

Figures 4.18-4.20 compare the temperatures measured in assemblies with single and double layers of the three types of gypsum board for insulated wall assembly. The figures clearly show that a higher level of fire protection can be obtained by using double layers of gypsum board in wall assemblies, as adding the second layer of drywall to each side of the assembly significantly decreases the rate of increase in temperature on the unexposed side of the assembly. Table 4.3 indicates that maximum temperatures on the exposed side of the insulated double layer specimens were 53-61% lower than the maximum temperatures at the same location for the insulated single layer specimens. Table 4.4 indicates that the times required to reach 100, 200 or 250 ˚C on the back of the exposed gypsum board layer were 170-240% longer for the insulated double layer specimens than the insulated single layer specimens. Figures 4.18-4.20 all demonstrate that temperatures measured on the back of the wall assemblies were relatively low. This is due to the performance of the gypsum boards and the stone wool insulation. As with other

temperature measurements, Table 4.3 indicates that the highest temperatures were recorded in tests that used lightweight gypsum board, and the lowest temperatures were recorded in tests that used the type X gypsum board.

Experimental Results of Insulated Lightweight Wall Assembly Exposed to Different Heat Flux

Cone calorimeter tests of insulated wall assemblies with a single layer of lightweight gypsum board were conducted at 35, 50 and 75 kW/m^2 in order to determine the effects of heat flux. Figure 4.21 compares the effect of heat flux exposure on temperature measurements in lightweight wall assemblies.

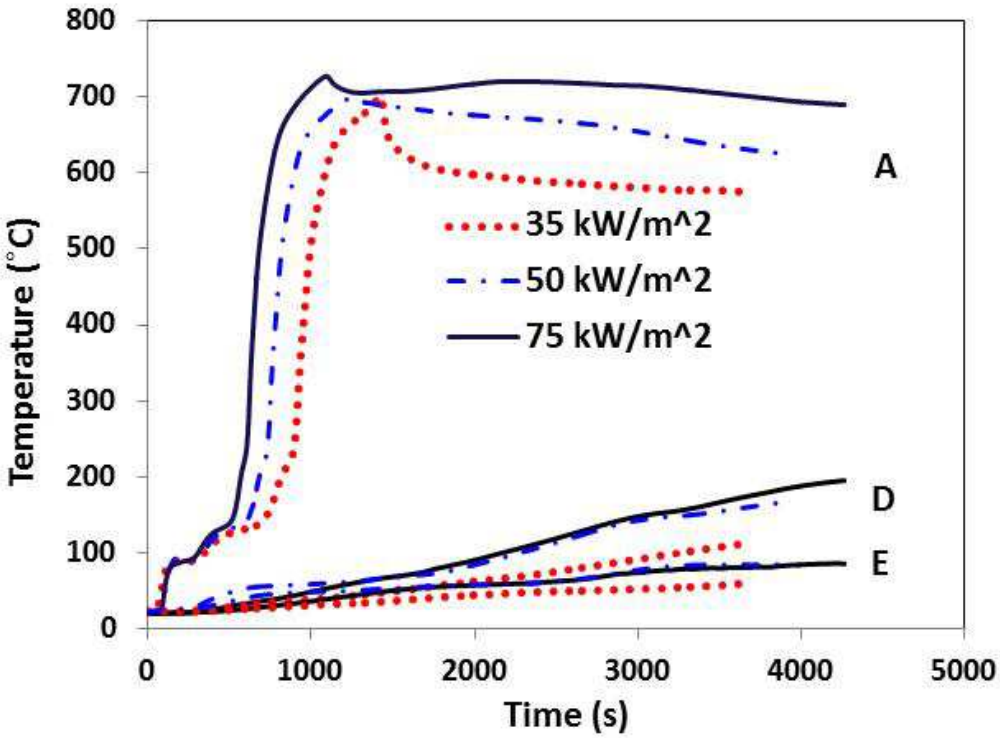

Figure 4.21: Temperature Measurements in Insulated Single Layer Lightweight Board Wall Assembly Exposed to Heat Fluxes of 35, 50 and 75 kW/m^2.

Comparisons of the average maximum temperature increase at three locations within the specimen for the insulated single layer lightweight wall assembly exposed to 35, 50 and 75 kW/m^2 are shown in Table 4.5.

Table 4.5: Average Maximum Temperature Increase Measured at Three Locations During Tests of Insulated Single Layer Lightweight Wall Assemblies Exposed to Heat Flux of 35, 50 and 75 kW/m^2

Insulated Single 12.5 mm (0.5 in.) Lightweight Gypsum Board Wall Assembly						
Heat Flux Exposure (kW/m^2)	**Maximum Temperature Increase (^{o}C)**					
	Back of exposed board(s) (A)		**Front of unexposed board(s) (D)**		**Back of unexposed board (E)**	
	Ave.	**(σ)**	**Ave.**	**(σ)**	**Ave.**	**(σ)**
35	661.6	(29)	101.0	(12.8)	41.1	(13.2)
50	683.4	(21.0)	138.3	(5.3)	47.3	(0.6)
75	712.9	(10.3)	189.5	(10.6)	66.2	(4.8)

From Figure 4.21 and Table 4.5, it is seen that higher temperatures at all locations (A, D, E) were recorded for tests with the higher heat flux exposures

Temperature Distribution in Unexposed Side of Wall Assembly

Figures 4.22-4.23 provide an indication of the temperature distribution on the unexposed side of the wall assembly. Figure 4.22 includes temperatures measurements made using thermocouples attached to the unexposed side, while Figure 4.23 includes examples of infrared photos taken of the unexposed side of the assembly at various times throughout a test of one layer of type X gypsum board.

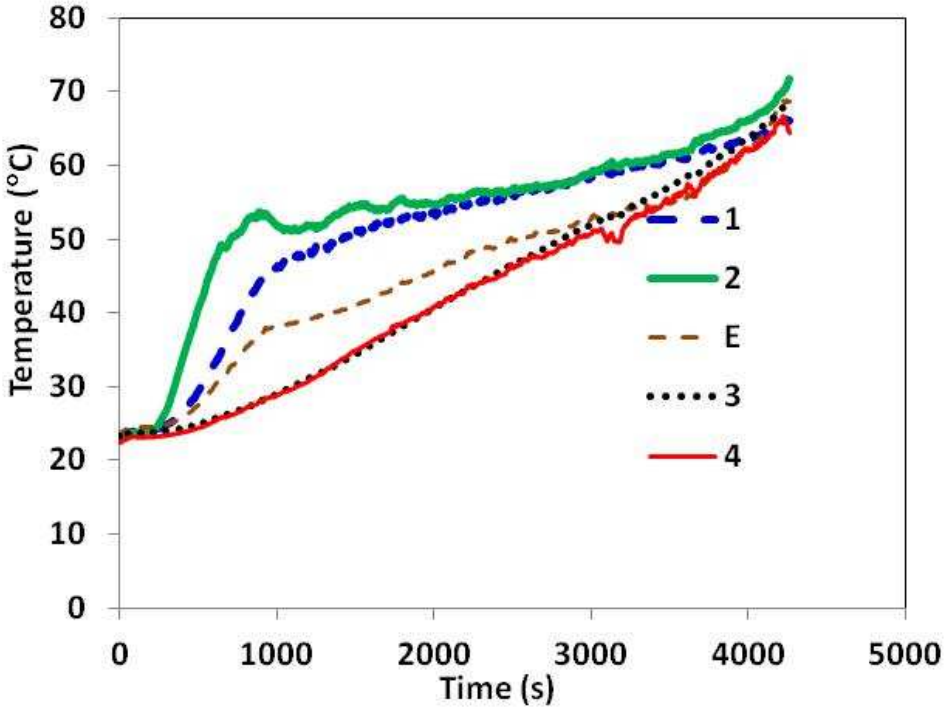

Figure 4.22: Temperature Measurements Made at Five Locations On Unexposed Side During Test of a Single Layer of Type X Gypsum Board

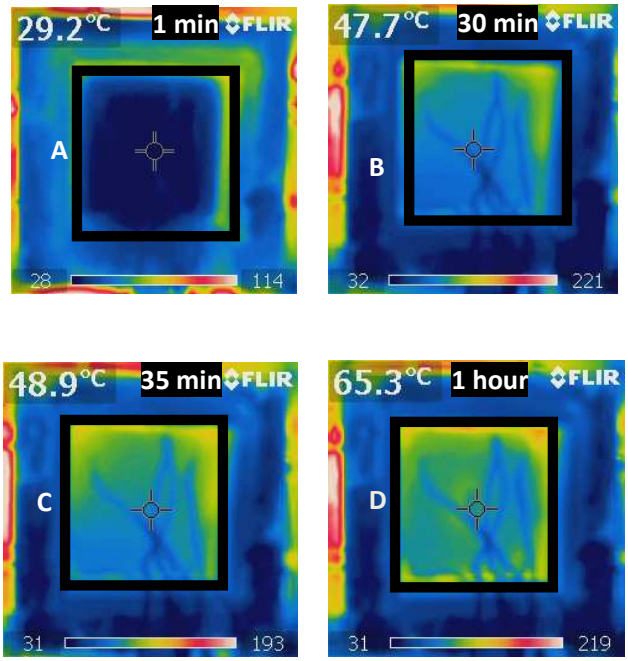

Figure 4.23: IR Photographs Taken During Test of a Single Layer of Type X Gypsum Board. (Black Square Shows Boundary of Specimen).

One issue is whether one-dimensional heat transfer models will be sufficiently accurate to model these exposures. Therefore, the temperature distribution on the unexposed side of the wall specimen was investigated. Figures 4.22 and 4.23 provide an indication of the temperature distribution on the unexposed side of the specimen (see Figure 4.9 for thermocouple locations). It should be noted that higher temperatures were measured by thermocouples 1 and 2. However, this was mainly due to the release of combustion products during the tests, which flowed close to these thermocouple locations. Thermocouples 3 and 4 were in closer agreement to the centre thermocouple (E). The centre thermocouple (E) (mid-point), was used for comparison with predictions made using the numerical model.

Uninsulated Wall Assembly

Six different uninsulated wall assemblies, using single or double layers of the three types of gypsum board, were tested. Three individual tests were performed for each of these six assembly designs. Figure 4.24 provides an indication of the repeatability of the temperature measurements. This particular example is for a wall assembly consisting of double layers of 12.7 mm (0.5 in.) regular gypsum board, wood studs and stone wool insulation. In Figure 4.24, L1 is the temperature profile at the interface of the exposed gypsum boards, L2 is the temperature profile at the interface of the unexposed gypsum boards. Temperature measurements in other test series displayed similar repeatability.

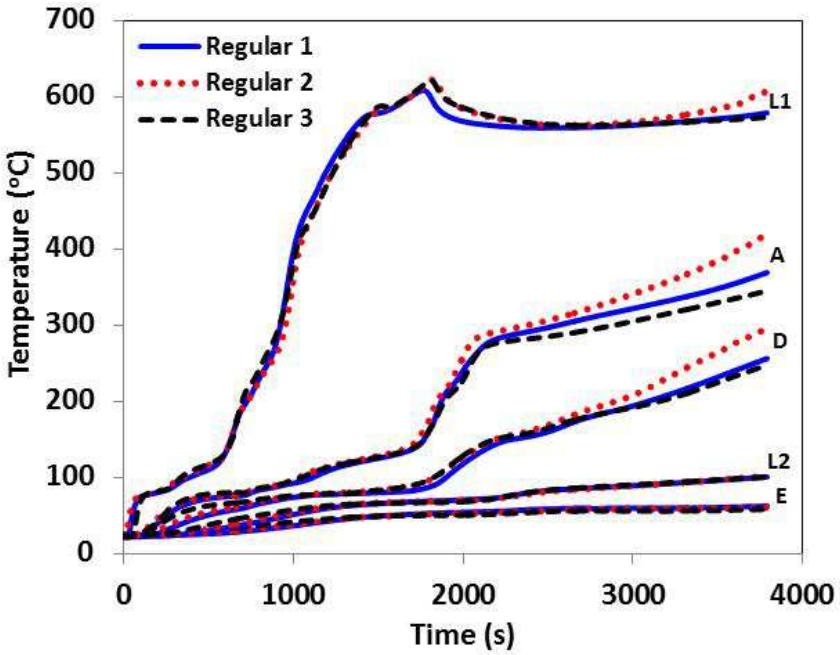

Figure 4.24: Temperature Measurements During Three Tests of Wall Assembly Containing Non Insulated Double Layers of Regular Gypsum Board (Uninsulated)
(L1 is the temperature profile at the interface of the exposed gypsum boards,
L2 is the temperature profile at the interface of the unexposed gypsum boards)

Experimental Results for Walls with Different Gypsum Board

Figure 4.25 compares temperatures measured at three locations in wall assemblies that use single layers of the three types of gypsum board. A similar comparison is shown in Figure 4.26 for the wall assemblies that use double layers of the three types of gypsum board.

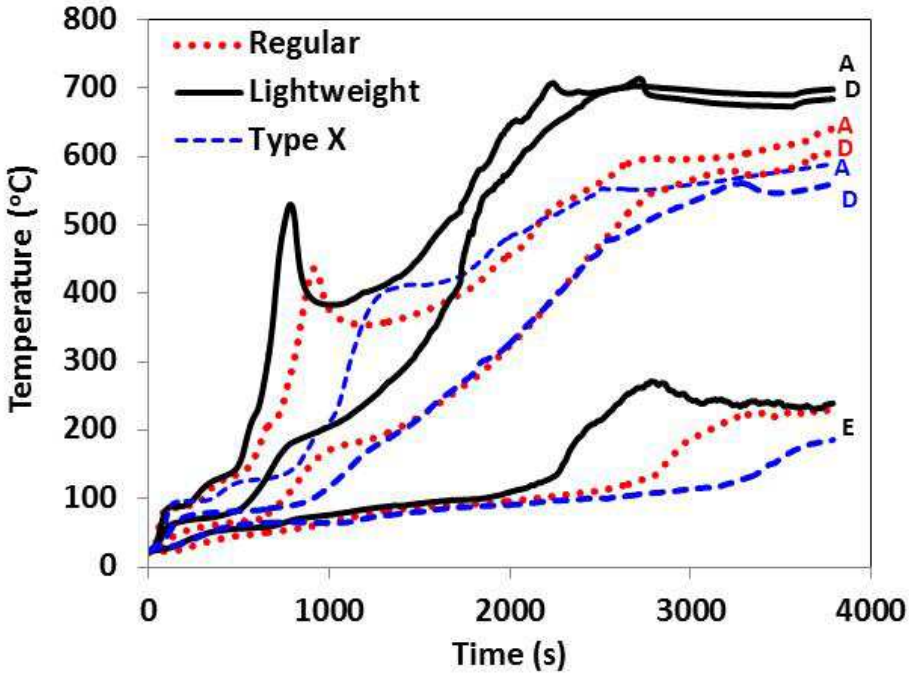

Figure 4.25: Comparison of Temperature Measurements Made During Tests of Uninsulated Wall Assemblies Containing Regular, Lightweight and Type X Gypsum Board (Single Layer)

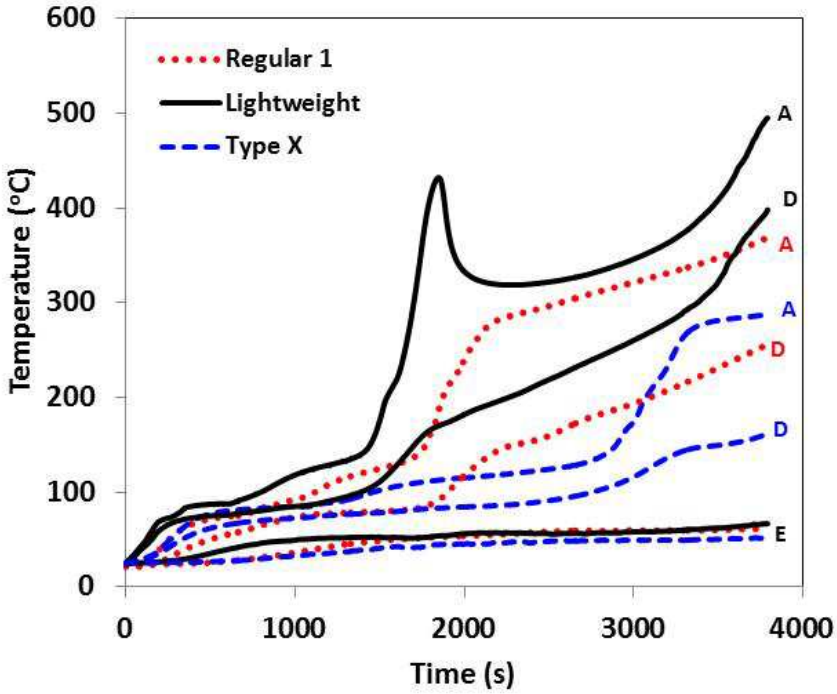

Figure 4.26: Comparison of Temperature Measurements Made During Tests of Uninsulated Wall Assemblies Containing Regular, Lightweight and Type X Gypsum Board (Double Layers)

Experimental Results for Single vs. Double Layer Walls

Figures 4.27-4.29 compare the temperatures measured at three locations in wall assemblies that use single and double layers of each of the three types of gypsum board.

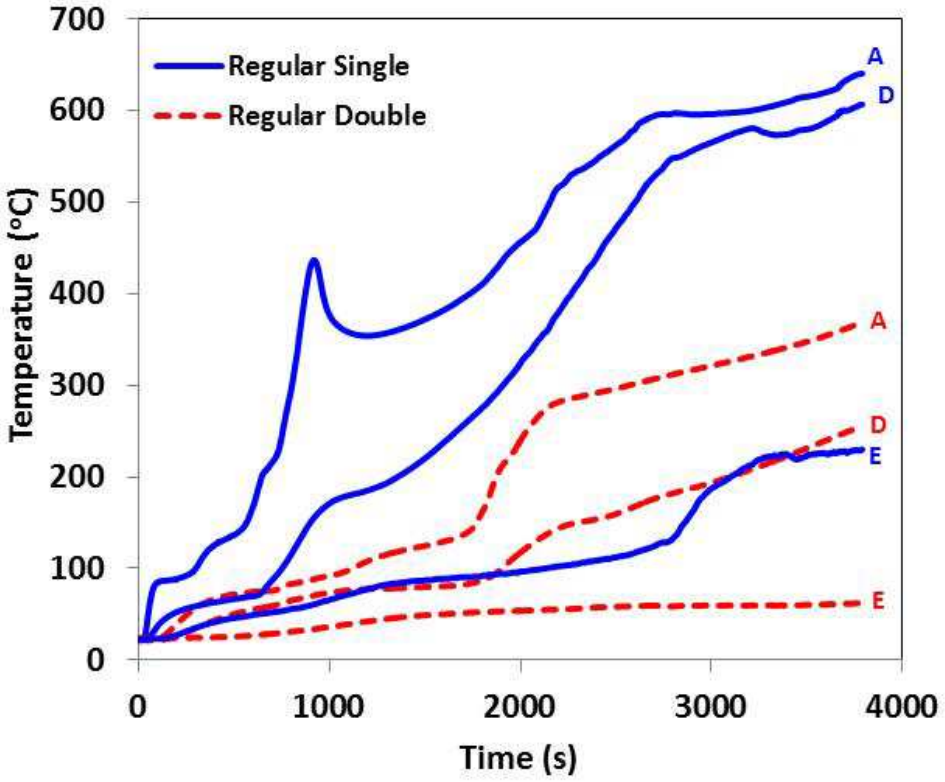

Figure 4.27: Comparison of Temperature Measurements Made During Tests of Uninsulated Wall Assemblies Containing Single and Double Layers of Regular Gypsum Board

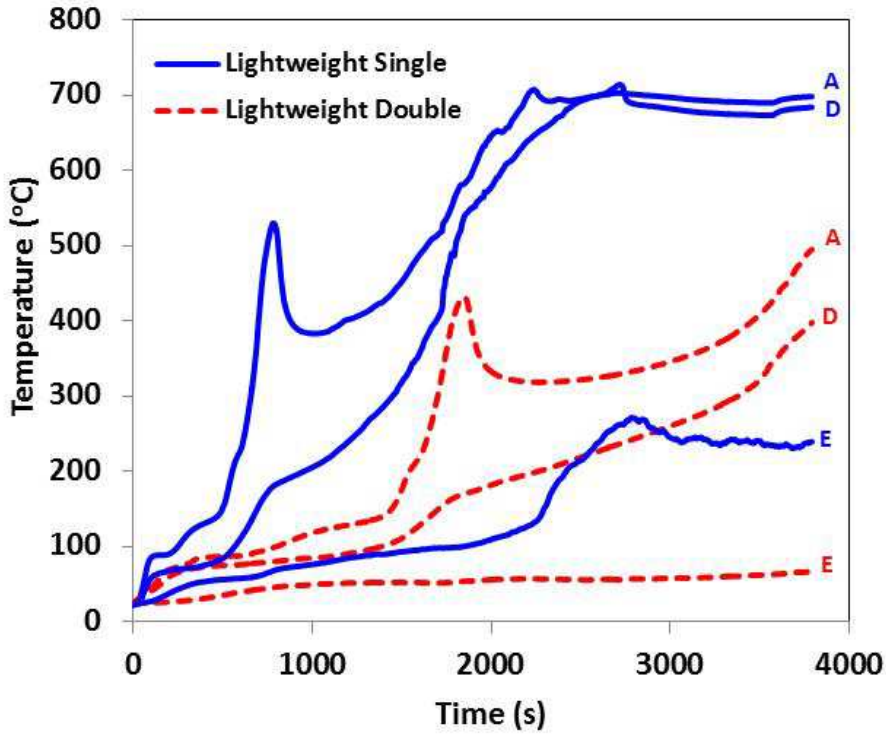

Figure 4.28: Comparison of Temperature Measurements Made During Tests of Uninsulated Wall Assemblies Containing Single and Double Layers of Lightweight Gypsum Board

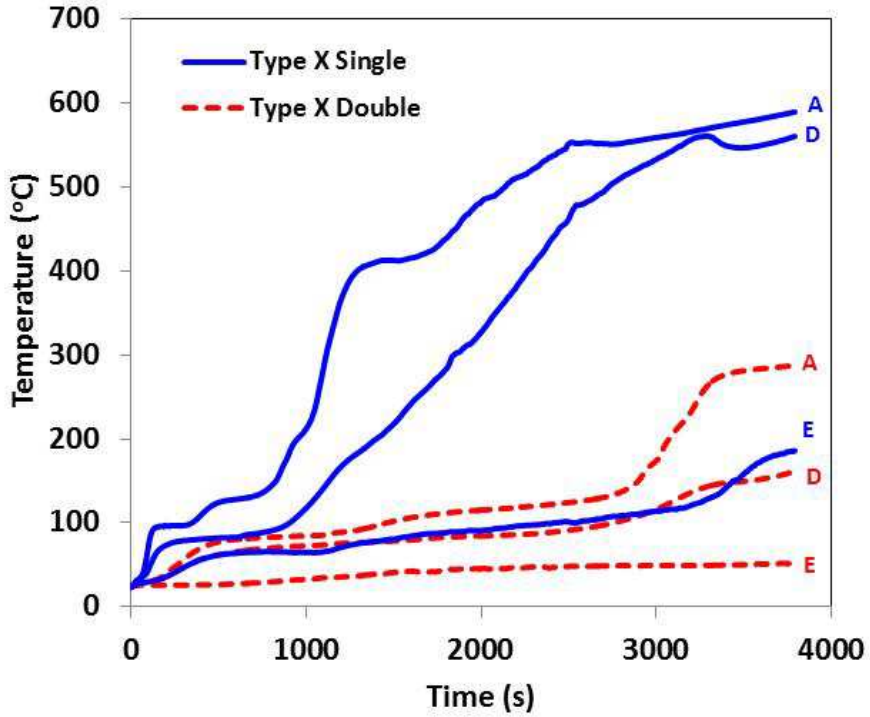

Figure 4.29: Comparison of Temperature Measurements Made During Tests of Uninsulated Wall Assemblies Containing Single and Double Layers of Type X Gypsum Board.

Comparisons of the average maximum temperature increase at three locations within the specimen for the six wall assembly designs are shown in Table 4.6. The average times for the temperature of the unexposed side of the gypsum board layer(s) closest to the cone heater to reach particular temperatures are compared in Table 4.7 for the six wall designs.

Table 4.6: Average Maximum Temperature Increase Measured at Three Locations During Tests of Uninsulated Wall Assemblies

Type of Gypsum Board Used in Wall Assembly	**Maximum Temperature Increase (˚C)**					
	Back of exposed board(s) (A)		**Front of unexposed board(s) (D)**		**Back of unexposed board (E)**	
	Ave.	**(σ)**	**Ave.**	**(σ)**	**Ave.**	**(σ)**
Single Regular 12.7 mm (0.5 in.)	586.0	(25.9)	549.0	(29.2)	188.0	(18.3)
Single Lightweight 12.5 mm (0.5 in.)	679.6	(4.0)	686.1	(6.2)	258.6	(7.1)
Single Type X 15.9 mm (0.625 in.)	532.5	(25.3)	494.0	(31.4)	120.4	(29.5)
Double Regular 12.7 mm (0.5 in.)	355.5	(31.8)	243.9	(21.2)	36.0	(1.8)
Double Lightweight 12.7 mm (0.5 in.)	449.3	(28.4)	356.0	(32.7)	43.5	(1.9)
Double Type X 15.9 mm (0.625 in.)	276.3	(9.5)	597.6	(9.1)	28.5	(0.95)

Table 4.7: Average Time to Reach 100°C, 200°C, 250°C and Maximum Recorded Temperature on Back of Exposed Gypsum Board Layer(s) in Tests of Uninsulated Wall Assemblies

Type of Gypsum Board Used in Wall Assembly	**Average Time to Reach Temperature on Back of Exposed Gypsum Board Layer(s) (Location A) (s)**			
	100˚C	**200˚C**	**250˚C**	**Maximum Temperature**
Single Regular 12.7 mm (0.5 in.)	314	656	750	*
Single Lightweight 12.5 mm (0.5 in.)	248	562	625	*
Single Type X 15.9 mm (0.625 in.)	382	987	1103	*
Double Regular 12.7 mm (0.5 in.)	1070	1871	2022	*
Double Lightweight 12.7 mm (0.5 in.)	816	1557	1662	*
Double Type X 15.9 mm (0.625 in.)	1472	3064	3223	*

* for double layers, temperatures were still increasing at end of 4200 s (70 min.) tests

As expected, the temperature measurements in the uninsulated wall assemblies were different from those in the insulated wall assemblies. The average maximum temperature increase at the back of the exposed board (location A) in the insulated wall assembly (Table 4.3) was generally higher than that of the uninsulated wall (Table 4.6) for all single and double layer wall assemblies. The average maximum temperature increase at the back of the exposed board of the uninsulated single layer lightweight, regular and type X wall assembly were 20%, 4.7% and 24% respectively less than that of the insulated wall assemblies (Table 4.3). The average maximum temperature increase at the back of the exposed board of the uninsulated double layer

lightweight, regular and type X wall assembly were 47.8%, 34.5% and 49%, respectively, less than that of the insulated wall assemblies (Table 4.3). The lower temperature increase at the back of the exposed board is as a result of increased heat losses in the wall cavity as compared to the insulation. From Table 4.4 and 4.7, the percentage difference in the average time to reach 100˚C at the back of the exposed board of insulated and uninsulated wall assembly is in the range of 4.5-15% for single layer wall and 7-10.5% for double layer wall assembly. The percentage difference in the average time to reach 200˚C at the back of the exposed board of insulated and uninsulated wall assembly is in the range of 0.3-2.8% for single layer wall and 0.5-1.9% for double layer wall assembly. The percentage difference in the average time to reach 250˚C at the back of the exposed board of insulated and uninsulated wall assembly is in the range of 4.7-7.8% for single layer wall and 1.7 - 5.2% for double layer wall assembly.

The average maximum temperature increase at the front of the unexposed board (location D) and at the back of the unexposed board (location E) in the insulated wall assembly (Table 4.3) were generally lower than that of the uninsulated wall (Table 4.6) for all single and double layer wall assemblies. The average maximum temperature increase at the front of the unexposed board of the insulated single layer lightweight, regular and type X wall assemblies (Table 4.3) were 66.8%, 72.3% and 70.6%, respectively less than that of the uninsulated wall assemblies (Table 4.6). The average maximum temperature increase at the back of the exposed board of the insulated double layer lightweight, regular and type X wall assemblies were 68.4%, 68.5% and 90.8%, respectively less than that of the uninsulated wall assemblies. The average maximum temperature increase at the back of the unexposed board of the insulated single layer lightweight, regular and type X wall assemblies (Table 4.3) were 68.6%, 74.5% and 60%, respectively, less than that of the uninsulated wall assemblies (Table 4.6). The average maximum temperature

increase at the back of the exposed board of the insulated double layer lightweight, regular and type X wall assemblies were 33.3%, 19.3% and 90.8%, respectively, less than that of the uninsulated wall assemblies. The lower temperature increase at the front and back of the unexposed board in the insulated wall assembly is due to the fire protection provided by the insulation in the wall cavity.

Experimental Results of Uninsulated Lightweight Wall Assembly Exposed to Different Heat Flux

Cone calorimeter tests of uninsulated wall assemblies containing lightweight gypsum board were conducted at 35, 50 and 75 kW/m^2 in order to determine the effects of heat flux. Figure 4.30 compares the effect of heat flux exposure on temperature measurements in uninsulated lightweight wall assembly.

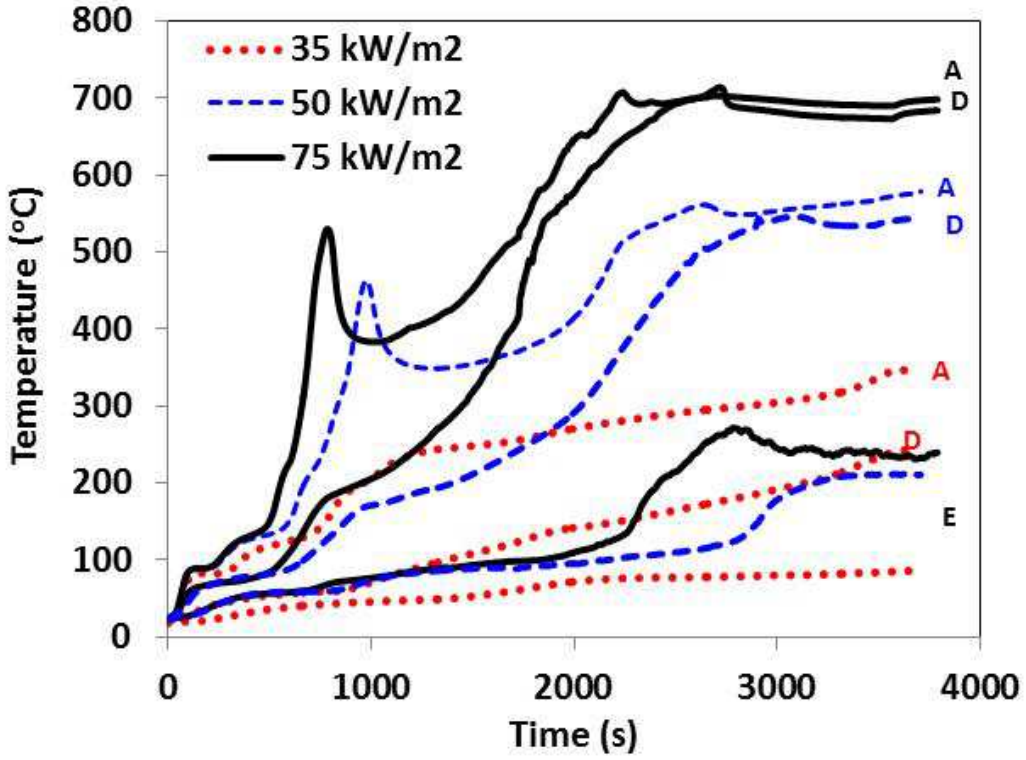

Figure 4.30: Temperature Measurements in Uninsulated Single Layer Lightweight Board Wall Assembly Exposed to Heat Fluxes of 35, 50 and 75 kW/m^2.

Comparisons of the average maximum temperature increase at three locations within the specimen for the uninsulated single layer lightweight wall assembly exposed to 35, 50 and 75 kW/m^2 are shown in Table 4.8. From Figure 4.30 and Table 4.8, it is seen that higher temperatures at all locations (A, D, E) were recorded for tests with higher heat flux exposures.

Table 4.8: Average Maximum Temperature Increase Measured at Three Locations During Tests of Uninsulated Sinlge Layer Lightweight Wall Assemblies Exposed to Heat Flux of 35, 50 and 75 kW/m^2

Uninsulated Single Lightweight 12.5 mm (0.5 in.)Gypsum Board Wall Assembly						
Heat Flux Exposure (kW/m^2)	**Maximum Temperature Increase (^{o}C)**					
	Back of exposed board(s) (A)		**Front of unexposed board(s) (D)**		**Back of unexposed board (E)**	
	Ave.	**(σ)**	**Ave.**	**(σ)**	**Ave.**	**(σ)**
35	337	(15.1)	235	(21.9)	78.1	(14.2)
50	573.8	(64.1)	553.2	(74.1)	188.9	(42.5)
75	679.6	(4.0)	686.1	(6.2)	258.6	(7.1)

4. 5 CONE CALORIMETER, INTERMEDIATE AND FULL SCALE TESTS RESULTS

Full scale tests are often required to determine the fire resistance performance of wall and floor assemblies formed with new materials and construction methods. These tests are very expensive and time consuming and as a result of this, design engineers seek alternative solution in order to save cost and time. The National Research Council of Canada (NRCC) developed an intermediate scale furnace which is a simpler and less expensive test method and capable of reflecting the full scale test results. Some results of the intermediate and full scale tests of wall assemblies conducted at the NRCC are compared with some results of the cone calorimeter tests

of wall assemblies reported in this Chapter in Figures 4.32-4.36. The average furnace temperature in the intermediate and full scale followed very closely the CAN/ULC-S101-M89 [1] standard temperature-time curve which is similar to the ASTM E 119 curve [3]. Figure 4.31 shows the heat flux-time distribution used in the furnaces and that used in the cone calorimeter. Table 4.9 compares the dimensions of the specimen tested in the furnaces and cone calorimeter. Results of single and double layer non-insulated wall assemblies tested in the furnaces and cone calorimeter are compared below.

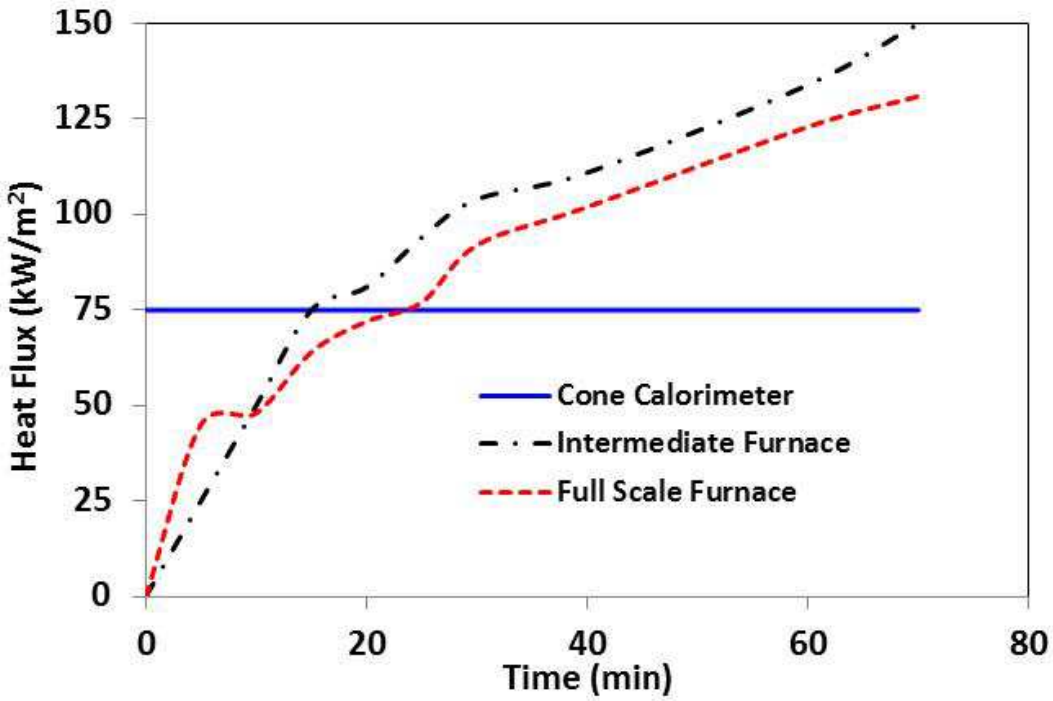

Figure 4.31: Comparison of Heat Flux Distribution in the Furnace and Cone Calorimeter.

Table 4.9: Comparison of Cone Calorimeter, Intermediate and Full Scale Wall Assembly Specimens.

	Cone Calorimeter Specimen	**Full Scale Specimen [12]**	**Intermediate Scale Specimen [15]**
Gypsum Board	12.7 mm Regular	12.7 mm Regular	12.7 mm Regular
Wood Studs	9.25mm x 89 mm SPF	38 mm x 89 mm SPF	38 mm x 89 mm SPF
Studs Spacing	101.6 mm O.C.	Single layer: (F-01) 400 mm O.C Double layer: (F-04) 600 mm O.C.	Double layer: 600 mm O.C.
Screws	6D finishing nails, 2.33 mm diameter, with 20 mm minimum penetration depth	Single layer : 41 mm long Type S drywall screws Double layer: 41 mm long Type S drywall screws	Double layer: 41 mm long Type S drywall screws
Wall Size	111.1 mm x 111.1 mm	3048 mm x 3658 mm	914 mm x 914 mm

Full Scale vs. Cone Calorimeter Test - Single Layer Wall Test.

The results from cone calorimeter tests of single layer uninsulated regular gypsum board wall assembly and that from the full scale furnace test of the loaded single layer non-insulated regular gypsum board wall assembly (test F-01) reported by Sultan et al [12], are compared in Figure 4.32. Figure 4.33 shows the temperature measurements at the unexposed side.

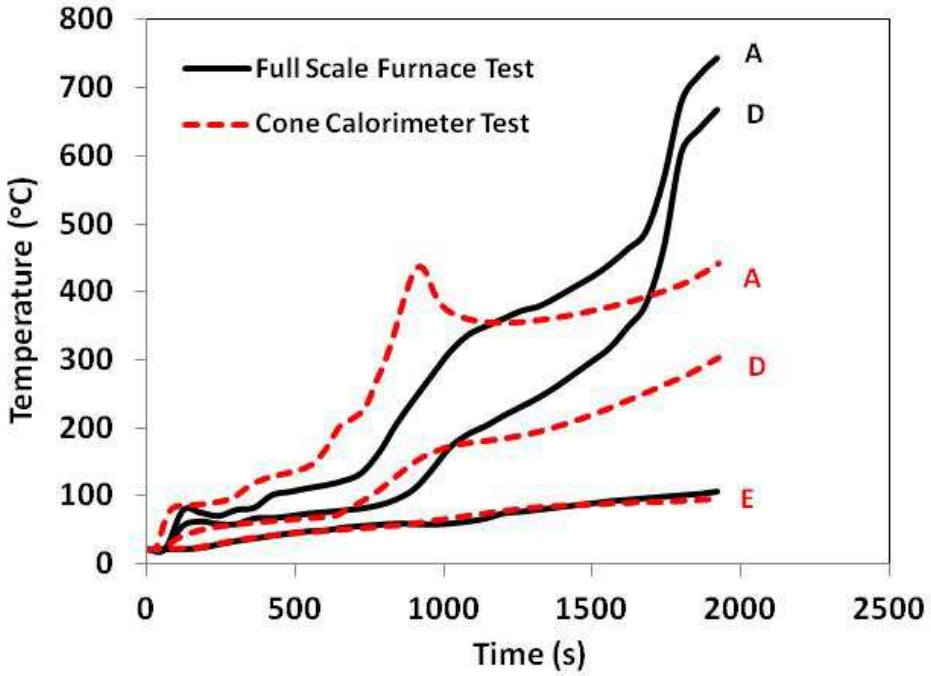

Figure 4.32: Comparison Between Full-scale Furnace Test Results and Cone Calorimeter Tests Results of Uninsulated Single Layer Regular Gypsum Board Wall Assembly.

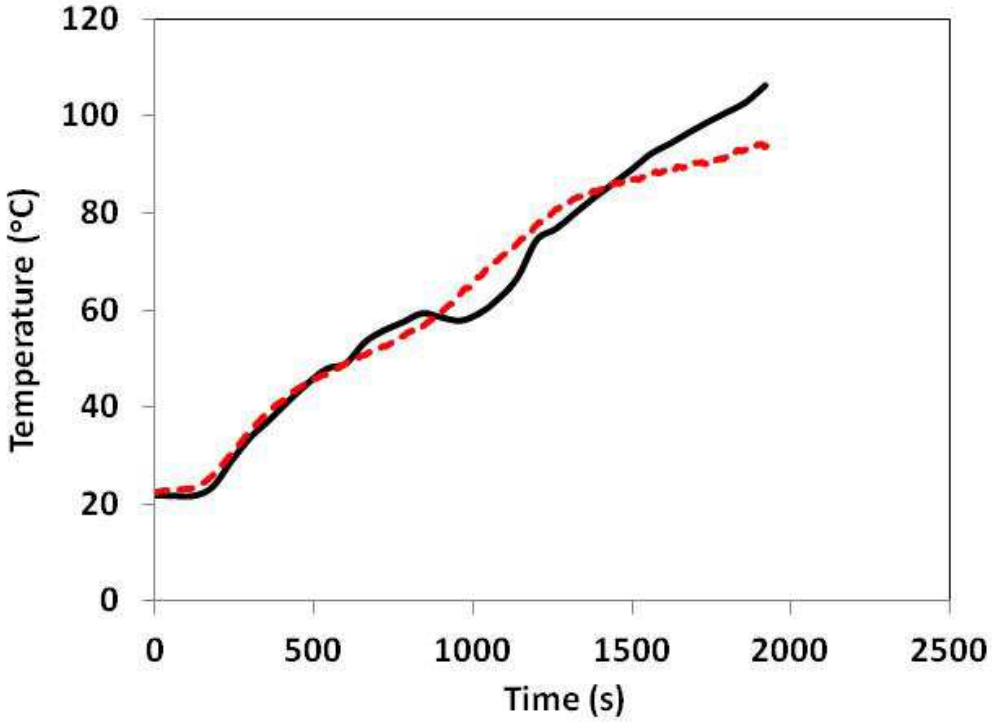

Figure 4.33: Comparison Between Temperature Measurements in Full-scale Furnace Test Results and Cone Calorimeter Tests Results For Uninsulated Regular Gypsum Board Wall Assembly (Unexposed side – E).

Comparisons of the average maximum temperature increase at three locations within the specimen for the full scale tests and the cone calorimeter tests of uninsulated single layer regular wall assembly are shown in Table 4.10. The average times for the temperature of the back of the exposed board (A) to reach particular temperatures are compared in Table 4.11 for the full scale tests and the cone calorimeter tests of uninsulated single layer regular wall assembly.

Table 4.10: Average Maximum Temperature Increase Exposure Measured at Three Locations During Full Scale and Cone Calorimeter Tests of Uninsulated Single Layer Regular Gypsum Board Wall Assemblies

Type of Test	**Maximum Temperature Increase (^{o}C)**		
	Back of exposed board(s) (A) (°C)	**Front of unexposed board(s) (D) (°C)**	**Back of unexposed board (E) (°C)**
Cone Calorimeter	423.2	287.4	93.1
Full Scale	718.5	639.5	102.9

Table 4.11: Average Time to Reach 100°C, 200°C, 250°C and Maximum Recorded Temperature on Back of Exposed Gypsum Board Layer(s) in Full Scale and Cone Calorimeter Tests of Uninsulated Single Layer Regular Gypsum Board Wall Assemblies

Type of Test	**Average Time to Reach Temperature on Back of Exposed Gypsum Board Layer(s) (Location A) (s)**			
	100°C	**200°C**	**250°C**	**Maximum Temperature**
Cone Calorimeter	300	646	756	1860*
Full Scale	420	835	910	1860*

*temperatures were still increasing at end of 1800 s (30 min.) tests

Intermediate vs. Full Scale vs. Cone Calorimeter Test - Double Layer Wall Test.

The results from cone calorimeter tests of a double layer uninsulated regular gypsum board wall assembly and that from a full scale furnace test of loaded double layer uninsulated regular gypsum board wall assembly (test F-04) reported by Sultan et al [12], are compared in Figure 4.34. The results from cone calorimeter tests of a double layer uninsulated regular gypsum board wall assembly and that from an intermediate scale furnace test of an unloaded double layer non-insulated regular gypsum board wall assembly (test S-02) reported by Sultan et al [15], are compared in Figure 4.35. Figure 4.36 shows the temperature measurements on the unexposed side of the wall assemblies tested in the cone calorimeter, intermediate furnace and the full scale furnace.

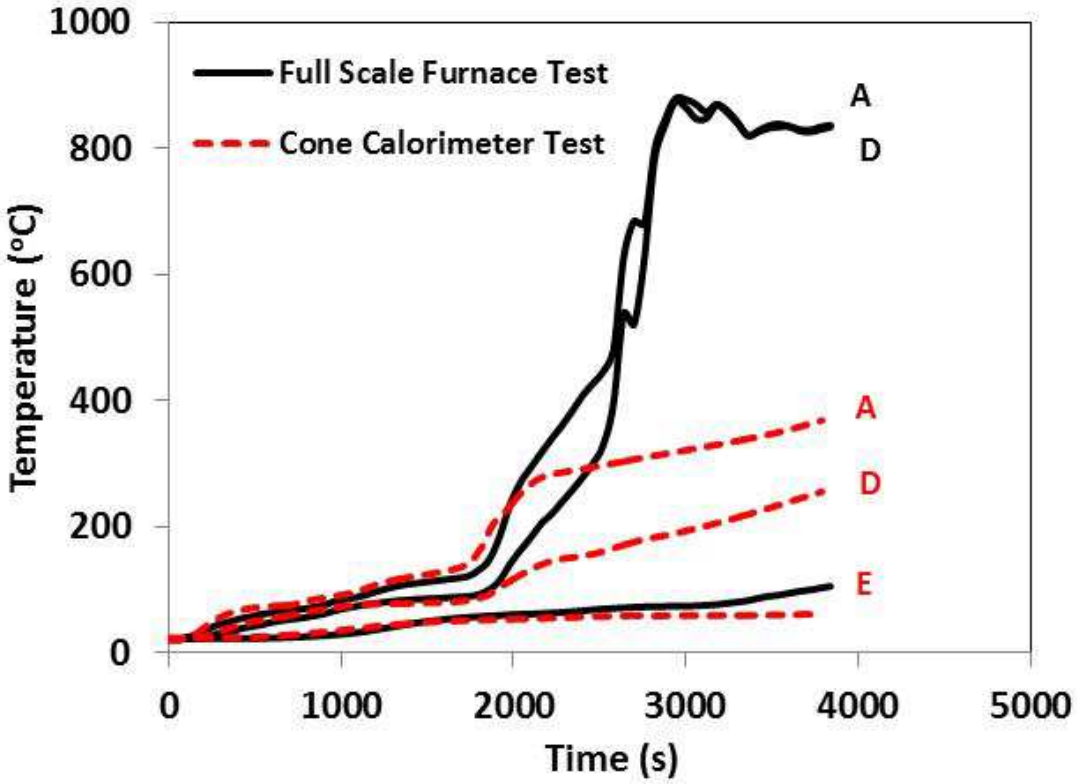

Figure 4.34: Comparison Between Full-scale Furnace Test Results and Cone Calorimeter Tests Results of Uninsulated Double Layer Regular Gypsum Board Wall Assembly.

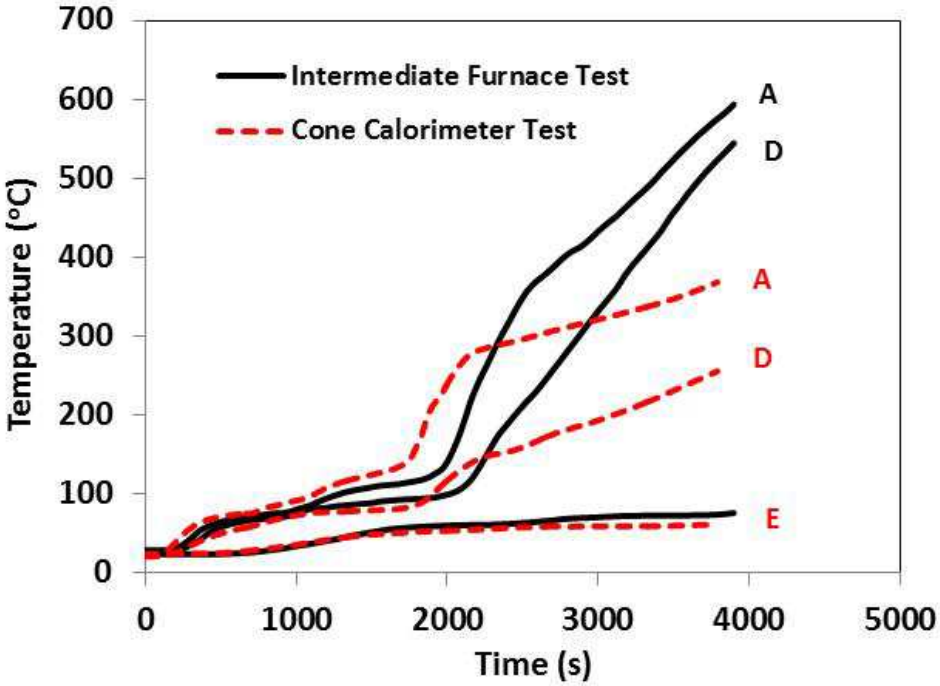

Figure 4.35: Comparison Between Temperature Measurements in Intermediate and Cone Calorimeter Tests Results of Uninsulated Single Layer Regular Gypsum Board Wall Assembly.

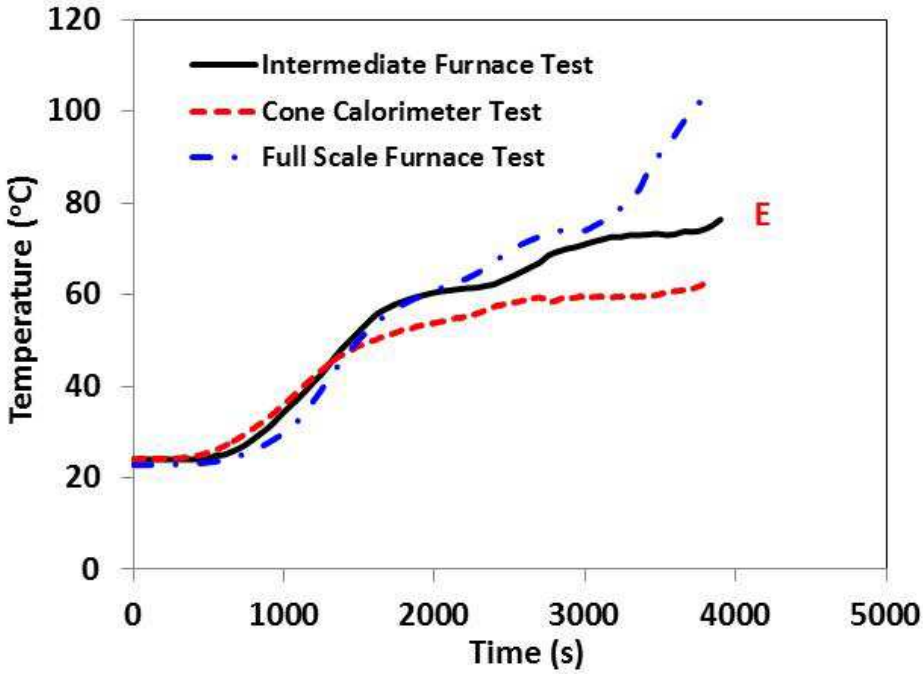

Figure 4.36: Comparison Between Unexposed Side Temperature Measurements in Full-scale Furnace, Intermediate and Cone Calorimeter Tests Results of Uninsulated Single Layer Regular Gypsum Board Wall Assembly.

Comparisons of the average maximum temperature increase at three locations within the specimen for the intermediate, full scale and the cone calorimeter tests of uninsulated double layer regular wall assembly are shown in Table 4.12. The average times for the temperature of the back of the exposed board (A) to reach particular temperatures are compared in Table 4.13 for the intermediate, full scale and the cone calorimeter tests of uninsulated double layer regular wall assembly.

Table 4.12: Average Maximum Temperature Increase Exposure Measured at Three Locations During Intermediate, Full Scale and Cone Calorimeter Tests of Uninsulated Double Layer Regular Gypsum Board Wall Assemblies

Type of Test	**Maximum Temperature Increase (^{o}C)**		
	Back of exposed board(s) (A) (°C)	**Front of unexposed board(s) (D) (°C)**	**Back of unexposed board (E) (°C)**
Cone Calorimeter	354.2	239.9	60.8
Intermediate Scale	594.0	545.0	73.2
Full Scale	879.0	874.0	95.0

Table 4.13: Average Time to Reach 100°C, 200°C, 250°C and Maximum Recorded Temperature on Back of Exposed Gypsum Board Layer(s) in Intermediate, Full Scale and Cone Calorimeter Tests of Uninsulated Double Layer Regular Gypsum Board Wall Assemblies

Type of Test	**Average Time to Reach Temperature on Back of Exposed Gypsum Board Layer(s) (Location A) (s)**			
	100°C	**200°C**	**250°C**	**Maximum Temperature**
Cone Calorimeter	1120	1874	2032	3600*
Intermediate Scale	1320	2130	2230	3600*
Full Scale	1250	1935	2020	2940

* temperatures were still increasing at end of 3600 s (60 min.) tests

The comparison between full scale, intermediate and cone calorimeter tests of uninsulated single and double layer wall assemblies presented in Figures 4.32-4.36 show higher temperatures in the cone calorimeter tests than in the full-scale tests for the first 20 – 25 min of exposure. The temperature difference is larger for the single layer wall than the double layer wall assembly. The higher temperatures observed for cone calorimeter tests up to the first 20-25 min of exposure is as a result of the higher heat flux of exposure in the cone calorimeter for the first 20-25 min as shown in Figure 4.31. The temperature measurements from the intermediate and full scale tests rise above that of the cone calorimeter tests after 20-25 min of exposure as a result of the higher heat flux of exposures than that of the cone calorimeter after this time (Figure 4.31). The maximum temperature at location D in the full scale test is 67.7% higher than the maximum temperature at location A in the cone calorimeter test. A low percentage difference of 10% in

maximum temperature between the cone calorimeter and full scale tests is observed for the unexposed side (location E).

The full scale, intermediate scale and cone calorimeter tests results for double layer non insulated wall assembly show a very good agreement for the first 20 to 25 min as seen in Figures 4.34-4.36. The full scale and cone calorimeter tests results for the non-insulated double wall assembly in Figure 4.34 are in good agreement at the unexposed side (E) for up to 25 min of exposure. The maximum temperatures at locations A, D and E in Table 4.12 shows a higher temperature in full scale tests than the cone calorimeter tests for all locations with a percentage difference of 51.7% for location A and a percentage difference of 75.9% for location D. The maximum temperatures on locations A, D and E in Table 4.13 also show a higher temperature in full scale tests compared to the intermediate and cone calorimeter tests for all locations. The maximum temperature in the intermediate scale test is 67.7% higher at location A, 127.2% higher at location D and 20.4% higher at location E than the maximum temperature in the cone calorimeter test. The maximum temperature in the full scale test is 148.2% higher at location A, 264.3% higher at location D and 56.3% higher at location E than the maximum temperature in the cone calorimeter test.

Generally the difference in temperature measurements within the wall assemblies in full scale, intermediate scale and cone calorimeter tests is as a result of the difference in the incident heat fluxes as shown in Figure 4.31 and the inability of the tests to adequately represent all of the phenomena exhibited in large-scale wall assemblies, such as the fire performance of joints in a drywall system. From Figures 4.33 and 4.36, the unexposed side temperatures showed a good agreement even though the heat of exposures and condition of testing are different. This demonstrates that cone calorimeter tests may have the potential to be used as indicators of the

performance of wall assemblies in standard full-scale fire tests. Additional research is necessary to develop scaling relationships for these tests.

4.6 SUMMARY OF CHAPTER

The experimental procedure, specimen and apparatus used to obtain results have been presented in this Chapter. The heat transfer through small-scale specimens that are representative of generic wall assemblies was investigated in this chapter using the cone calorimeter and a hotplate. Wall assemblies tested in the hotplate were exposed to a temperature of 80˚C. Insulated and uninsulated assemblies that use 12.7 mm (1/2 in.) regular and lightweight gypsum board, and 15.9 mm (5/8 in.) Type X gypsum board, were tested in the cone calorimeter using an incident heat flux of 35, 50 and 75 kW/m^2. Temperature measurements were dependent on the type and number of layers of gypsum board used. Temperatures increased most rapidly in assemblies that used lightweight gypsum board and most slowly in assemblies that used Type X gypsum board. Adding a second layer of gypsum board on each side of the assembly reduced the maximum temperature on the unexposed side by 53-61%. The results obtained from cone calorimeter tests of wall assembly specimen conducted in this study were also compared with similar intermediate and full scale tests conducted at the NRCC.

CHAPTER FIVE: COMPARISON OF NUMERICAL AND EXPERIMENTAL RESULTS

In this chapter the numerical results presented in Chapter Three will be compared to the experimental results presented in Chapter Four. The main comparisons in this chapter will include the following:

- comparison of hotplate experimental results with numerical results of wall assemblies exposed to a fixed temperature boundary condition;
- comparison of cone calorimeter test results with numerical results for single layer regular, lightweight and type X gypsum boards exposed to a heat flux of 75 kW/m^2;
- comparison of cone calorimeter test results with numerical results for double layer regular, lightweight and type X gypsum boards exposed to a heat flux of 75 kW/m^2;
- comparison of cone calorimeter test results with numerical results for wall assemblies that include single layers of lightweight gypsum board exposed to heat fluxes of 35, 50 and 75 kW/m^2;
- comparison of cone calorimeter test results and numerical results for wall assemblies that include single layers of regular and type X gypsum board exposed to a heat flux of 75 kW/m^2; and
- comparison of cone calorimeter test results and numerical results for wall assemblies that include double layers of lightweight, regular and type X gypsum board exposed to a heat flux of 75 kW/m^2.

5.1. COMPARISON OF NUMERICAL AND HOTPLATE EXPERIMENTAL RESULTS

The temperature profiles from the hotplate experiment discussed in Section 4.4.1 are compared to the numerical results with constant properties and fixed temperature boundary discussed in Section 3.3.1. Temperature profiles predicted by the numerical model and those measured in the experiments for an exposure to 80^{o}C are presented in Figure 5.1 and 5.2.

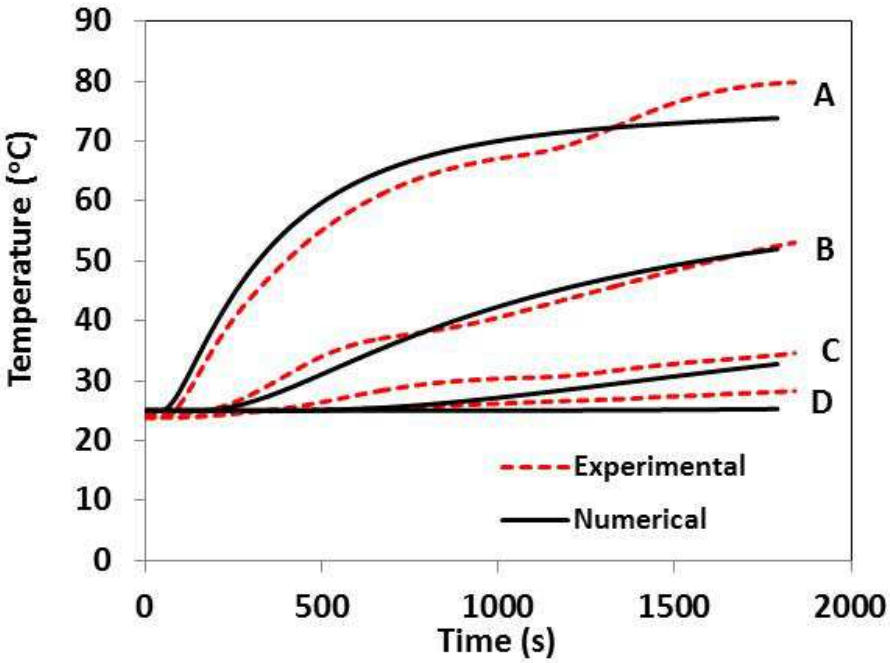

Figure 5.1: Comparison of Numerical and Hotplate Experimental Results for Regular Gypsum Wall Assembly.

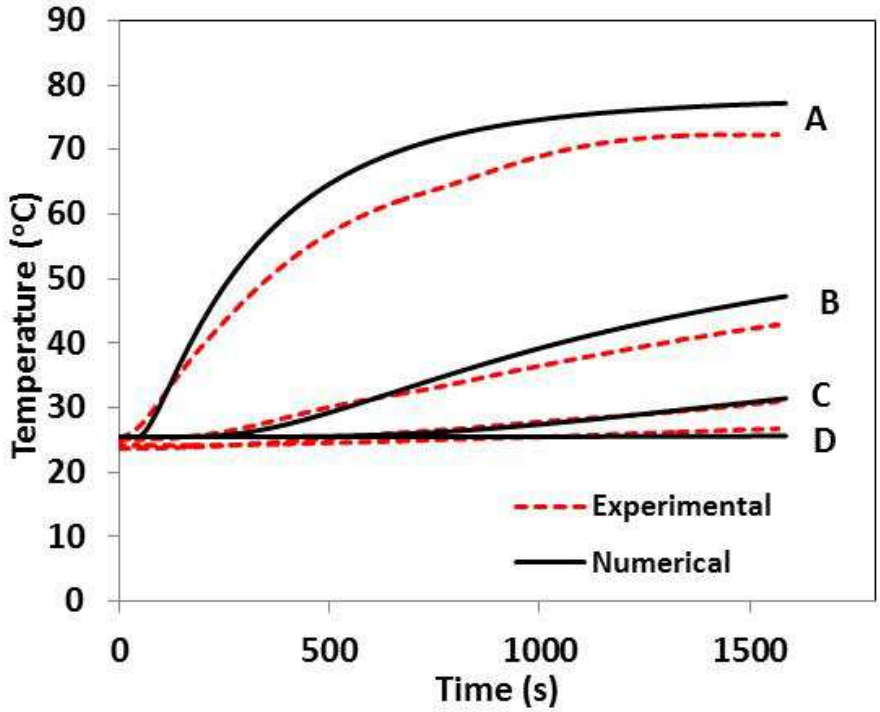

Figure 5.2: Comparison of Numerical and Hotplate Experimental Results for Type X Gypsum Wall Assembly.

The tests conducted using the hotplate were used to determine the temperature profiles in the wall assembly before major reactions begin. Thermal properties at room temperature were used in the model. This exercise was to evaluate the model and the choice of thermal properties at room temperature. The results show a fair level of agreement between predicted and measured temperatures. The variation between the numerical and experimental results is expected to be mainly a result of the variation in the hot plate temperature shown in Figure 4.11 (Section 4.4.1). It was difficult to keep the temperature of the hotplate constant at 80˚C, as the knob was controlled to get the desired temperature and a temperature of about 80±7˚C was achieved. The uncertainty in thermal properties is also expected to be responsible for the differences between numerical and experimental results. The effects of uncertainty in thermal properties will be discussed later in this chapter.

5.2. COMPARISON OF NUMERICAL RESULTS AND CONE CALORIMETER TEST RESULTS OF GYPSUM BOARD.

Single Layer Gypsum Board

Temperature profiles on the unexposed side measured during the cone calorimeter experiments in which single layer regular, lightweight and type X gypsum boards were exposed to a heat flux of 75 kW/m^2 (Section 4.4.2) are compared with predictions made using the numerical model (Section 3.3.2) in Figures 5.3, 5.4 and 5.5, respectively.

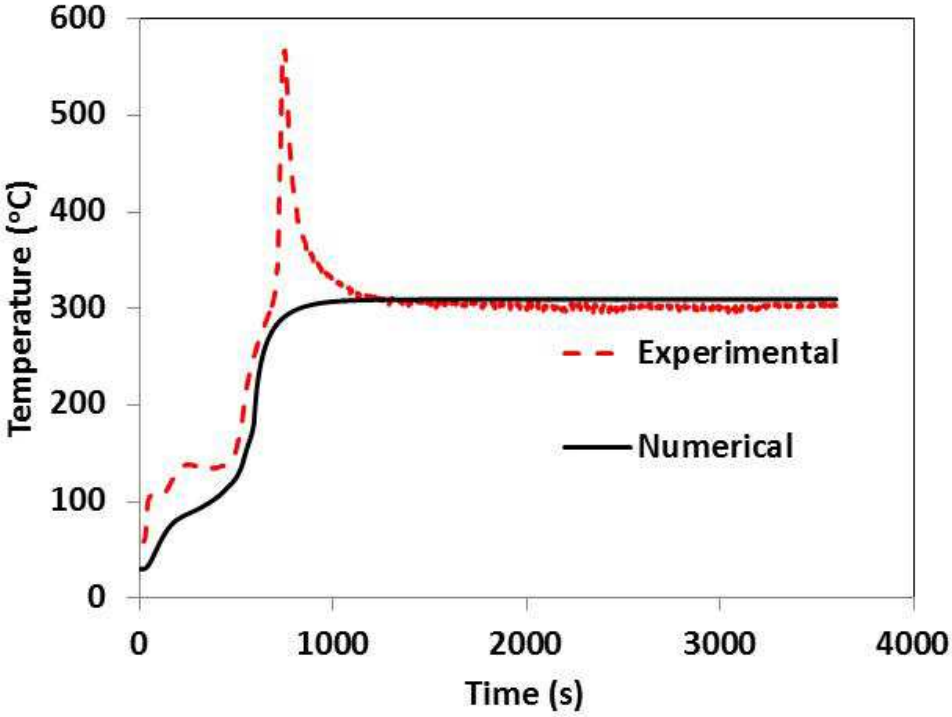

Figure 5.3: Comparison of Numerical and Experimental Results at Unexposed Side of (12.7 mm) Regular Gypsum Board

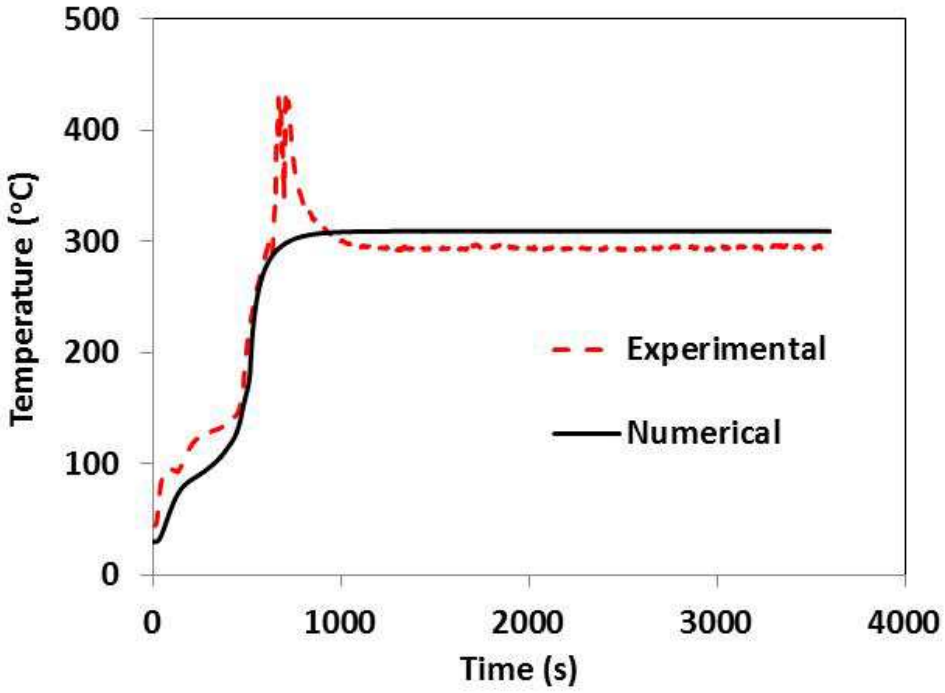

Figure 5.4: Comparison of Numerical and Experimental Results at Unexposed Side of 12.7 mm Lightweight Gypsum Board

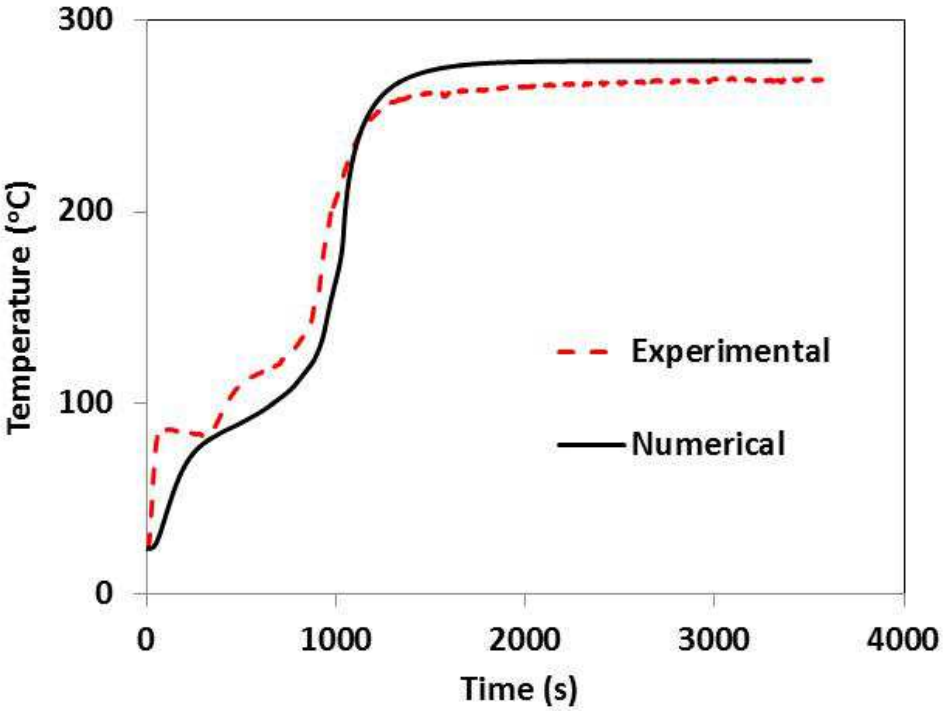

Figure 5.5: Comparison of Numerical and Experimental Results for 15.9 mm Type X Gypsum Board

The results presented in Figures 5.3-5.5 indicate that the model is fairly successful in predicting the expected temperatures profiles seen in the experimental results. While the model did a good job of predicting the initial temperature increase and the steady-state portion later in the test, the model is unable to predict the sudden rise in temperature beyond 300˚C for both regular and lightweight boards as seen in Figures 5.3 and 5.4. This is likely attributed to moisture movement within the 12.7 mm board which is not considered in this study. The sensitivity study conducted in Section 3.4 also shows how changes in specific heat, thermal conductivity density of gypsum boards affect the temperature profiles within the wall assembly, and demonstrate how the variation between the predicted and measured temperatures in Figures 5.3-5.5 is expected to be largely as a result of the uncertainty in the thermal properties used for the gypsum boards. As noted in Chapter 3, the properties used in the model were largely taken from the literature, rather than being measured for the specific materials used in this study.

Double Layer Gypsum Board

Temperature profiles at the interface and on the unexposed side measured during the cone calorimeter experiments in which double layer regular, lightweight and type X gypsum boards were exposed to a heat flux of 75 kW/m^2 (Section 4.4.2) are compared with predictions made using the numerical model (Section 3.3.3) in Figures 5.6, 5.7 and 5.8, respectively.

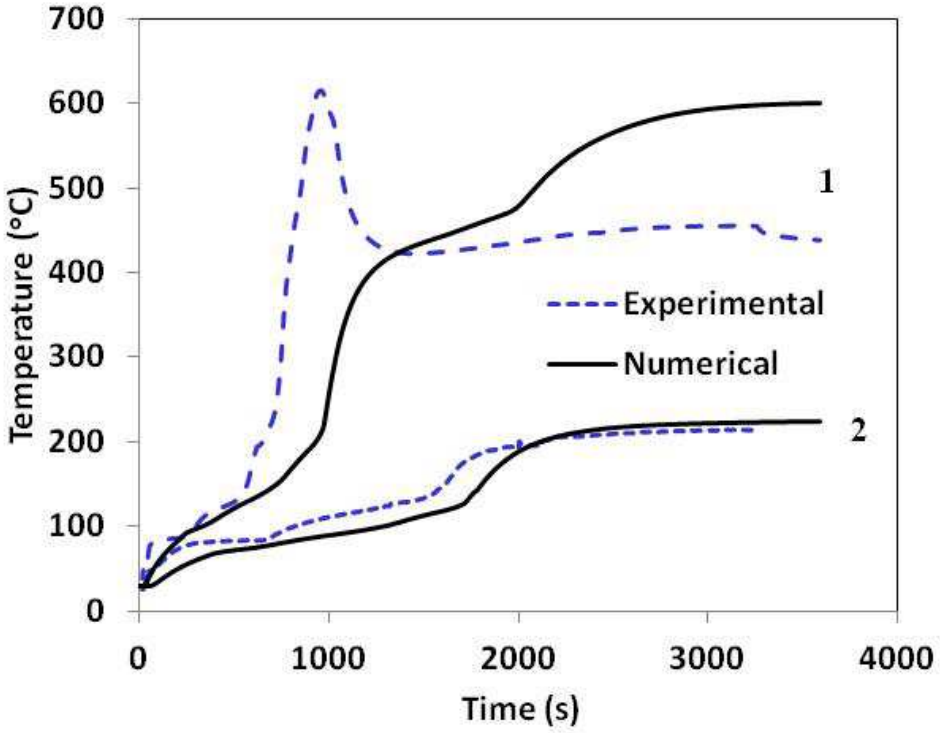

Figure 5.6: Comparison of Numerical and Experimental Results at the Middle (1) and Unexposed Side (2) of Double Layers of 12.7 mm Regular Gypsum Board

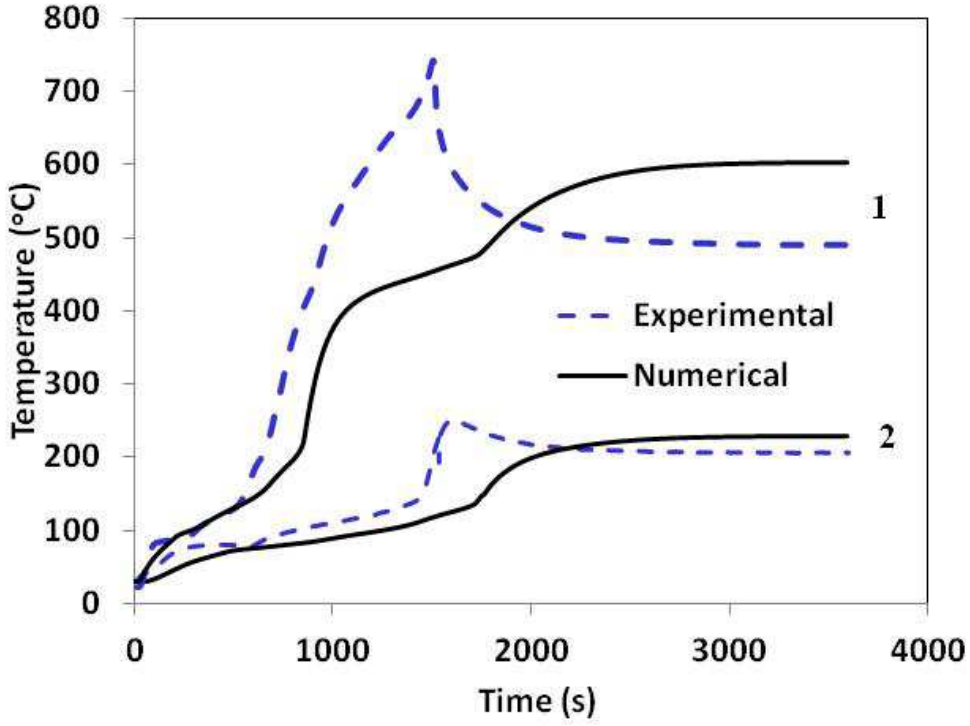

Figure 5.7: Comparison of Numerical and Experimental Results at the Middle (1) and Unexposed Side (2) of Double Layers of 12.7 mm Lightweight Gypsum Board

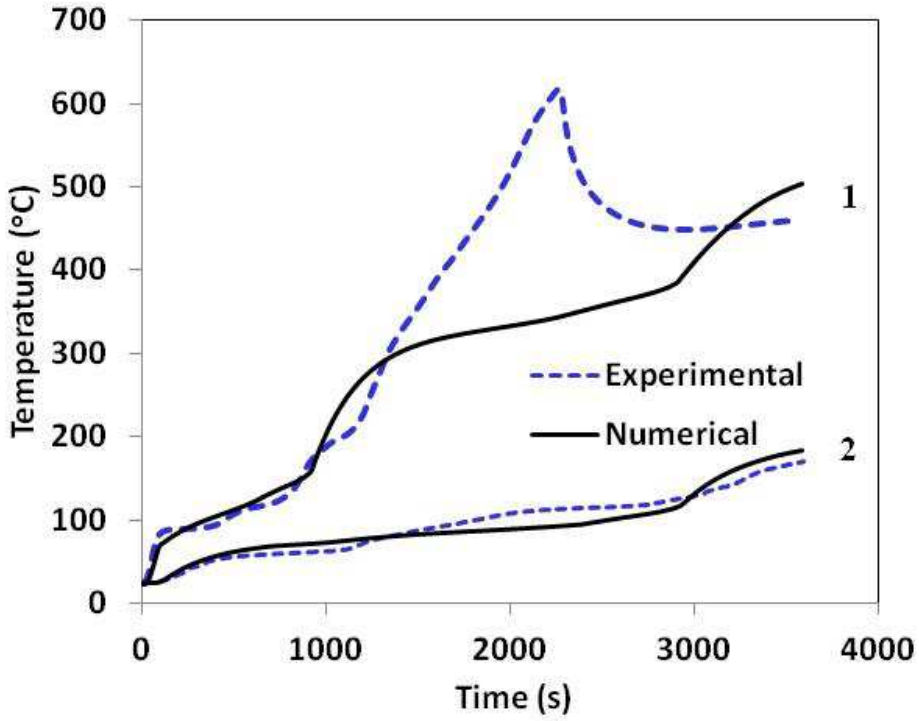

Figure 5.8: Comparison of Numerical and Experimental Results at Unexposed Side of Double Layers of 15.9 mm Type X Gypsum Board

The results presented in Figures 5.6-5.8 again indicate the model is fairly successful in predicting the temperatures obtained in the experiment, especially on the unexposed surface of the test specimen. The variation in the temperature prediction may once again be attributed to the moisture movement within the gypsum boards and other physical phenomenon not captured in the model (e.g. release of hot gases from the specimen through the sample holder). The temperature predictions at the interface of the boards show a very good agreement with the experimental temperature profiles during the first 6-12 min of testing. The larger variation in the temperature between the predicted and measured temperatures at the interface later in the tests can be as a result of the contact resistance at the interface of the boards, and the fact that phenomena such as burning of the paper at this interface are not included in the model.

5.3. COMPARISON OF NUMERICAL RESULTS AND CONE CALORIMETER TEST RESULTS OF WALL ASSEMBLIES

Lightweight Gypsum Board Wall Assembly

Temperature profiles within the wall assemblies measured during the cone calorimeter experiments in which single layer lightweight gypsum board wall assemblies were exposed to heat fluxes of 35, 50 and 75 kW/m^2 (Section 4.4.2) are compared with predictions made using the numerical model (Sections 3.3.5 and 3.3.6) in Figures 5.9, 5.10 and 5.11, respectively. The time at which the back of the exposed board reaches 100, 250 and 600˚C and the maximum temperature increase at the back of the unexposed board of the wall assembly are presented in Tables 5.1, 5.2 and 5.3 for lightweight wall assemblies exposed to 35, 50 and 75 kW/m^2, respectively.

Single Layer Lightweight Gypsum Board Wall

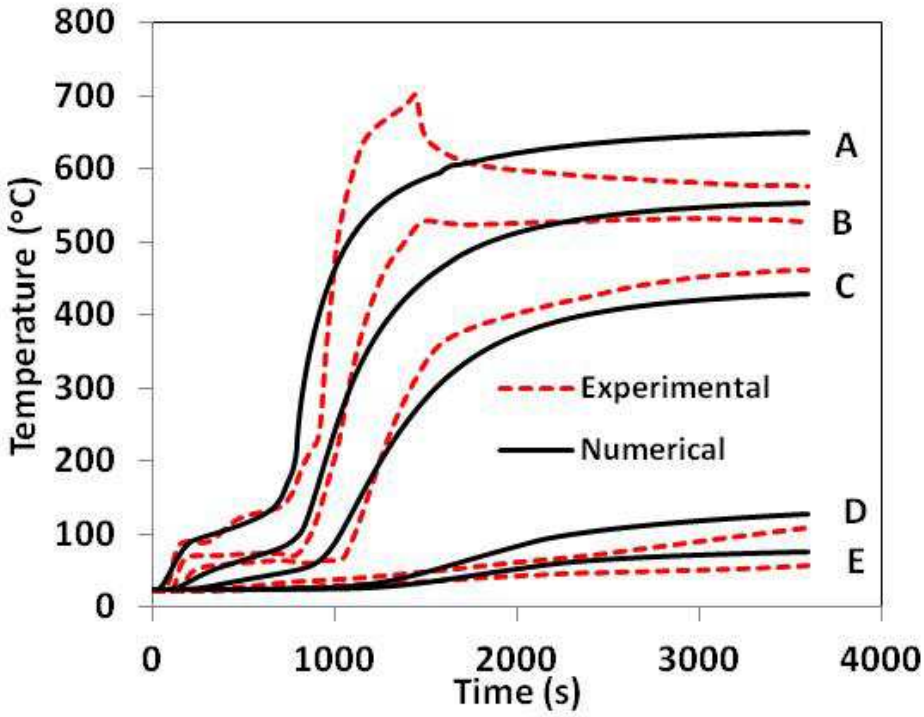

Figure 5.9: Comparison of Numerical and Experimental Results for Single Lightweight Gypsum Wall Assembly Exposed to 35 kW/m^2.

Table 5.1: Comparison Between Experimental and Numerical Results – Single Layer Lightweight Gypsum Board Wall Assembly (35 kW/m^2 Exposure)

Back of exposed board(s) **(A)**	**Experimental** **Ave. (s)**	**σ**	**Numerical** (s)
Time to 100^{o}C	360	7.3	328
Time to 250^{o}C	912	6.3	800
Time to 600^{o}C	1108	9.2	1599
Back of unexposed board **(E)**	**Ave. (˚C)**	**σ**	**Ave. (˚C)**
Maximum Temperature Increase	38.4	4.1	46.0

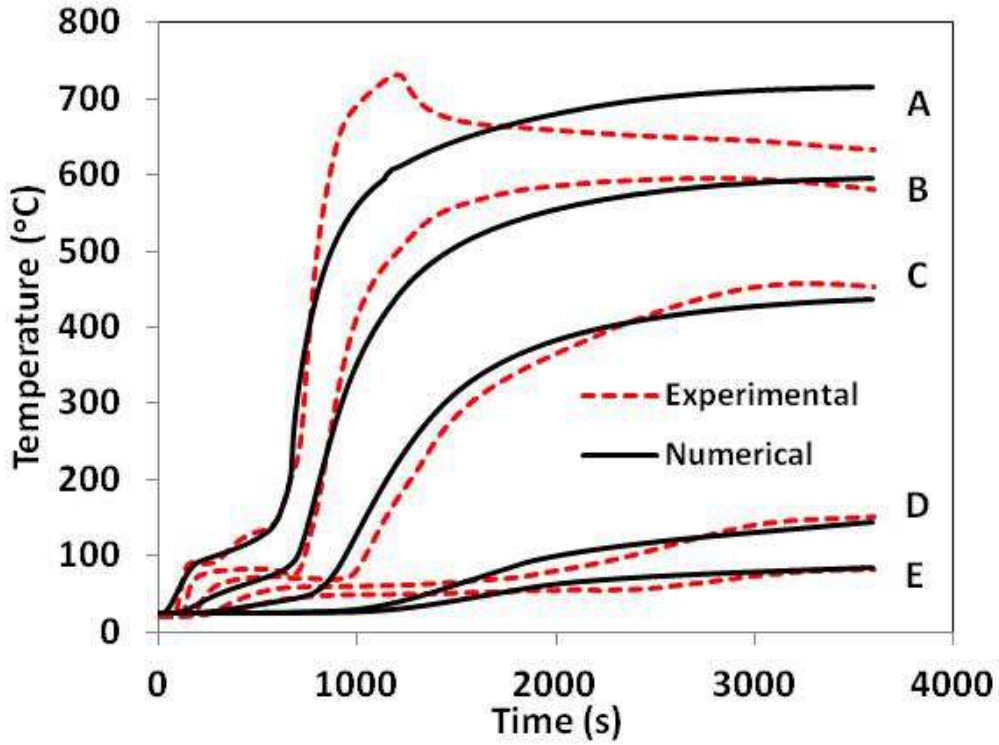

Figure 5.10: Comparison of Numerical and Experimental Results for Single Lightweight Gypsum Wall Assembly Exposed to 50 kW/m^2.

Table 5.2: Comparison Between Experimental and Numerical Results – Single Layer Lightweight Gypsum Board Wall Assembly (50 kW/m^2 Exposure)

Back of exposed board(s) **(A)**	**Experimental** Ave. (s)	**(σ)**	**Numerical** (s)
Time to 100°C	323	(27)	295
Time to 250°C	700	(50)	678
Time to 600°C	864	(40)	1152
Back of unexposed board **(E)**	Ave. (˚C)	**(σ)**	(˚C)
Maximum Temperature Increase	62.8	(0.9)	59.5

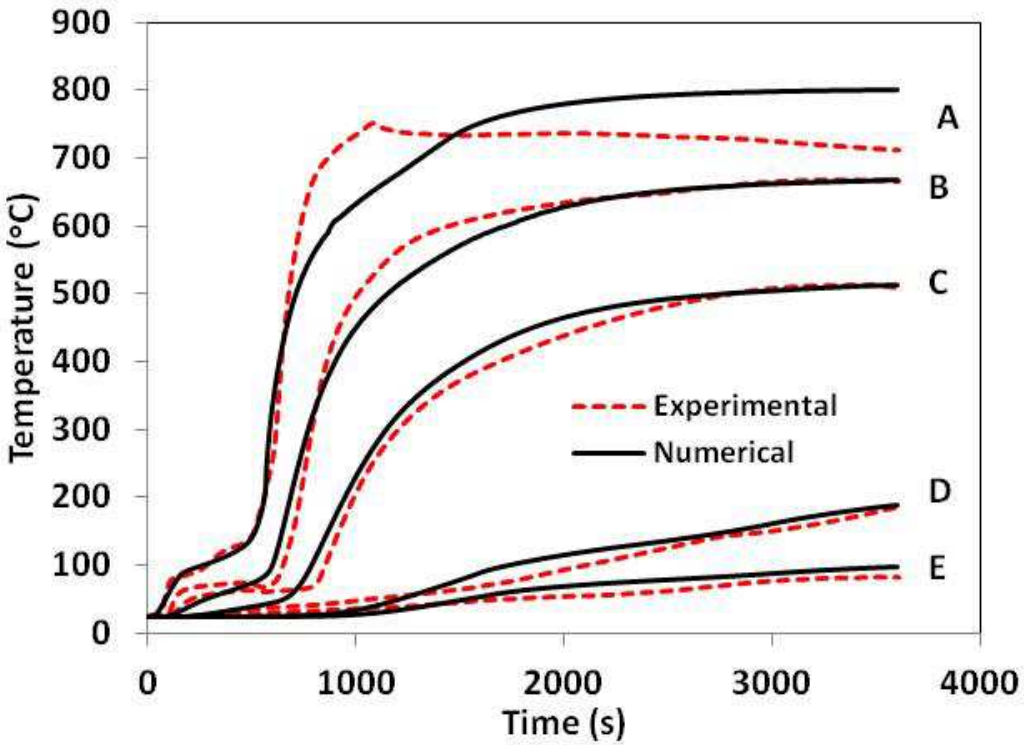

Figure 5.11: Comparison of Numerical and Experimental Results for Single Lightweight Gypsum Wall Assembly Exposed to 75 kW/m^2.

Table 5.3: Comparison Between Experimental and Numerical Results – Single Layer Lightweight Gypsum Board Wall Assembly (75 kW/m^2 Exposure)

Back of exposed board(s) **(A)**	**Experimental** Ave. (s)	**(σ)**	**Numerical** (s)
Time to 100^{o}C	273	(28.3)	265
Time to 250^{o}C	585	(19.3)	573
Time to 600^{o}C	729	(15.1)	880
Back of unexposed board **(E)**	Ave. (˚C)	**(σ)**	(˚C)
Maximum Temperature Increase	55	(5.2)	74.2

Double Layer Lightweight Gypsum Board Wall Assembly

Temperature profiles on the unexposed side measured during the cone calorimeter experiments in which double layer lightweight gypsum board wall assemblies were exposed to 75 kW/m^2 (Section 4.4.2) are compared with predictions made using the numerical model (Section 3.3.6) in Figure 5.12. The time at which the back of the exposed board reaches 100, 200 and 250˚C and the maximum temperature increase at the back of the unexposed board of the wall assembly are presented in Table 5.4.

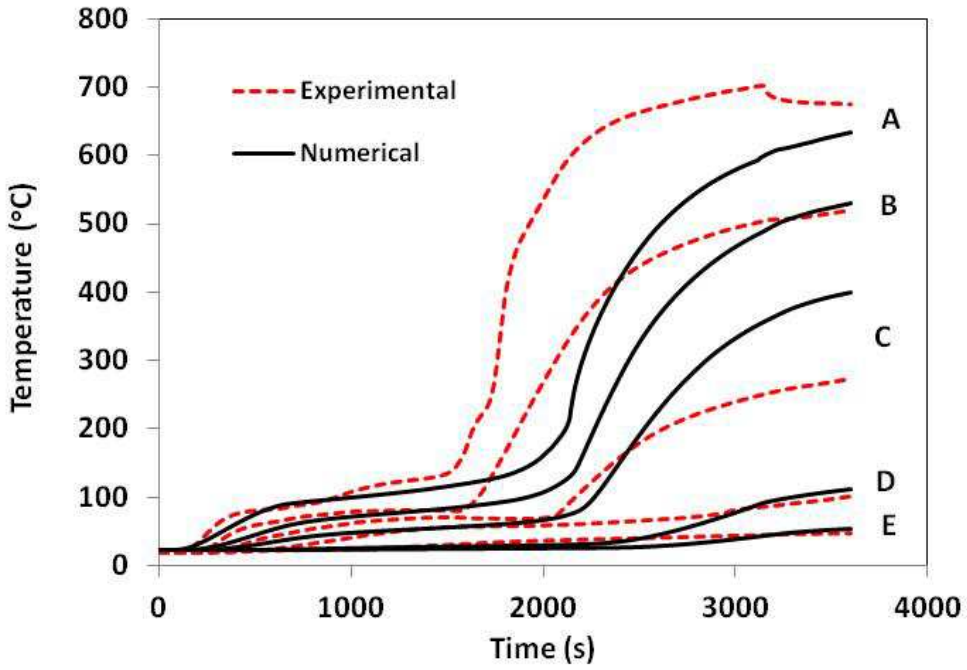

Figure 5.12: Comparison of Numerical and Experimental Results for Double Lightweight Gypsum Board Wall Assembly Exposed to 75 kW/m^2.

Table 5.4: Comparison Between Experimental and Numerical Results – Double Layer Lightweight Gypsum Board Wall Assembly (75 kW/m^2 Exposure)

Back of exposed board(s) **(A)**	**Experimental** Ave. (s)	**(σ)**	**Numerical** (s)
Time to 100°C	908	(5.4)	975
Time to 200°C	1644	(6.7)	2114
Time to 250°C	1740	(11.7)	2156
Back of unexposed board **(E)**	Ave. (˚C)	**(σ)**	(˚C)
Maximum Temperature Increase	24.9	(3.5)	30.5*

*temperature still increasing at the end of 3600 s (60 min.)

Regular Gypsum Board Wall Assemblies

Temperature profiles on the unexposed side measured during the cone calorimeter experiments in which single layer regular gypsum board wall assemblies were exposed to 75 kW/m^2 (Section 4.4.2) are compared with predictions made using the numerical model (Section 3.3.6) in Figure 5.13. The time to 100˚C, 250˚C and 600˚C at location A as well as the maximum temperature increase at the back of the unexposed board (E) are presented in Table 5.5.

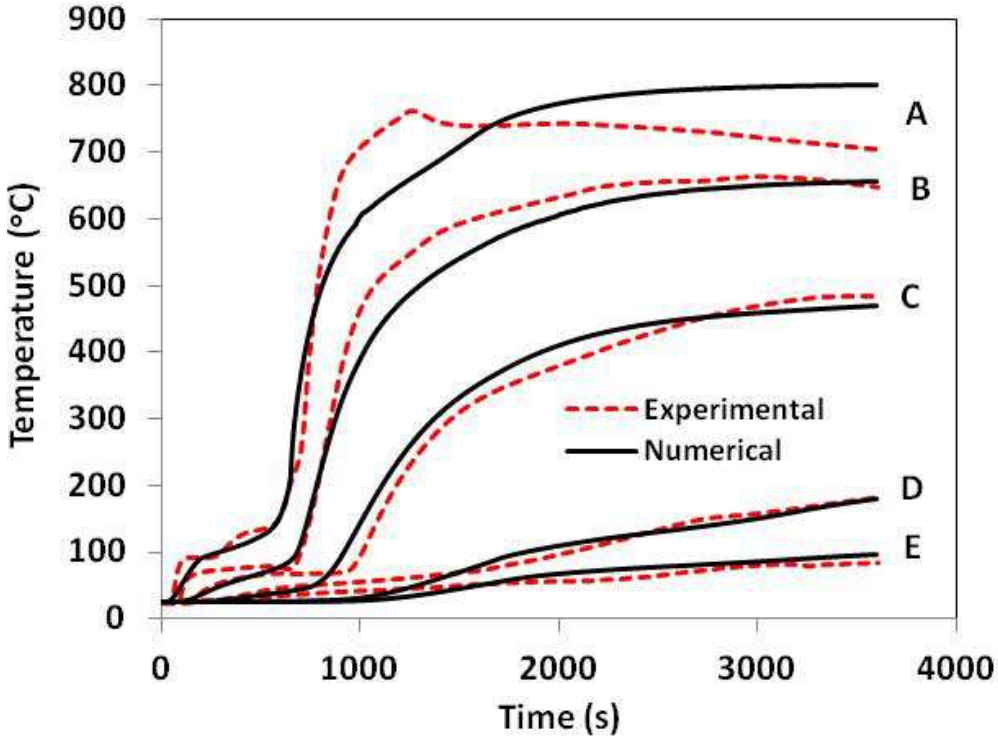

Figure 5.13: Comparison of Numerical and Experimental Results for Single Regular Gypsum Wall Assembly Exposed to 75 kW/m^2.

Table 5.5: Comparison Between Experimental and Numerical Results – Single Layer Regular Gypsum Board Wall Assembly (75 kW/m^2 Exposure)

Back of exposed board(s) **(A)**	**Experimental** Ave. (s)	**(σ)**	**Numerical** (s)
Time to 100^{o}C	302	(14.3)	301
Time to 250^{o}C	694	(18.8)	655
Time to 600^{o}C	843	(20.4)	990
Back of unexposed board **(E)**	Ave. (˚C)	**(σ)**	(˚C)
Maximum Temperature Increase	57	(2.5)	71.3

Double Layer Regular Gypsum Board Wall Assembly

Temperature profiles on the unexposed side measured during the cone calorimeter experiments in which single layer regular gypsum board wall assembly were exposed to 75 kW/m^2 (Section 4.4.2) are compared with predictions made using the numerical model (Section 3.3.6) in Figure 5.14. The time at which the back of the exposed board reaches 100, 200 and 250˚C and the maximum temperature increase at the back of the unexposed board of the wall assembly are presented in Tables 5.6.

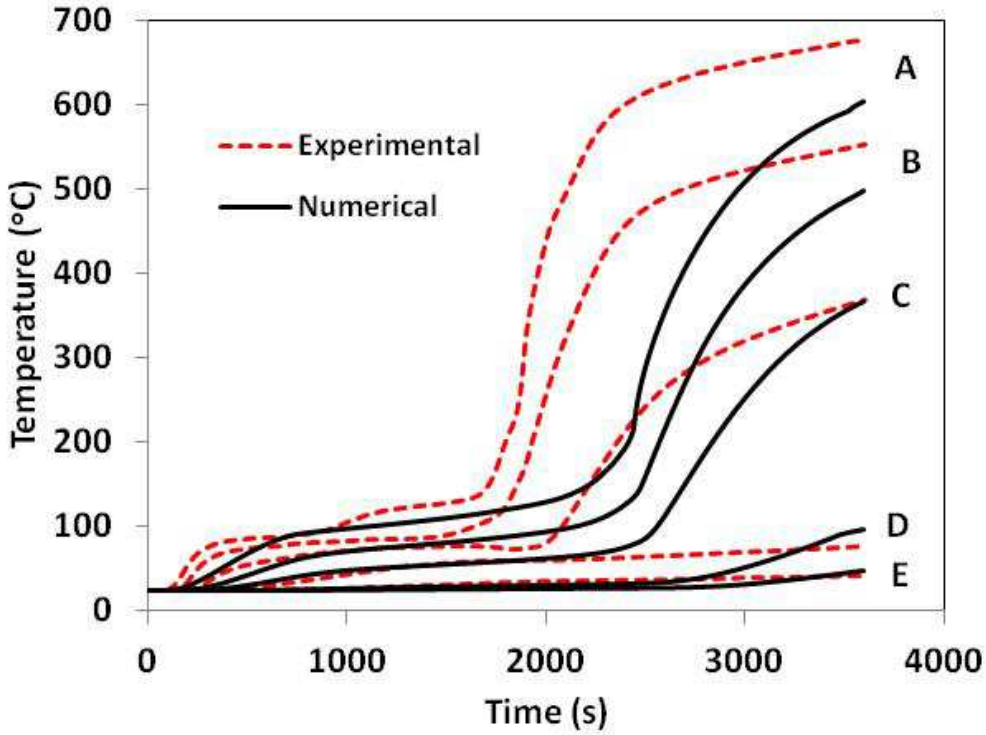

Figure 5.14: Comparison of Numerical and Experimental Results for Double Layer Regular Gypsum Wall Assembly Exposed to 75 kW/m^2.

Table 5.6: Comparison Between Experimental and Numerical Results – Double Layer Regular Gypsum Board Wall Assemblies (75 kW/m^2 Exposure)

Back of exposed board(s) **(A)**	**Experimental** Ave. (s)	**(σ)**	**Numerical** (s)
Time to 100°C	957	(35.9)	1112
Time to 200°C	1845	(33.4)	2417
Time to 250°C	1920	(38.7)	2464
Back of unexposed board **(E)**	Ave. (˚C)	**(σ)**	(˚C)
Maximum Temperature Increase	21.3	(1.4)	24.0*

*temperature still increasing at end of 3600 s (60 min.) tests

Type X Gypsum Board Wall Assemblies

Temperature profiles on the unexposed side measured during the cone calorimeter experiments in which single layer type X gypsum board wall assemblies were exposed to 75 kW/m^2 (Section 4.4.2) are compared with predictions made using the numerical model (Section 3.3.6) in Figure 5.15. The time to 100˚C, 250˚C and 600˚C at location A as well as the maximum temperature increase at the back of the unexposed board (E) are presented in Table 5.7.

Single Layer Type X Gypsum Board Wall Assembly

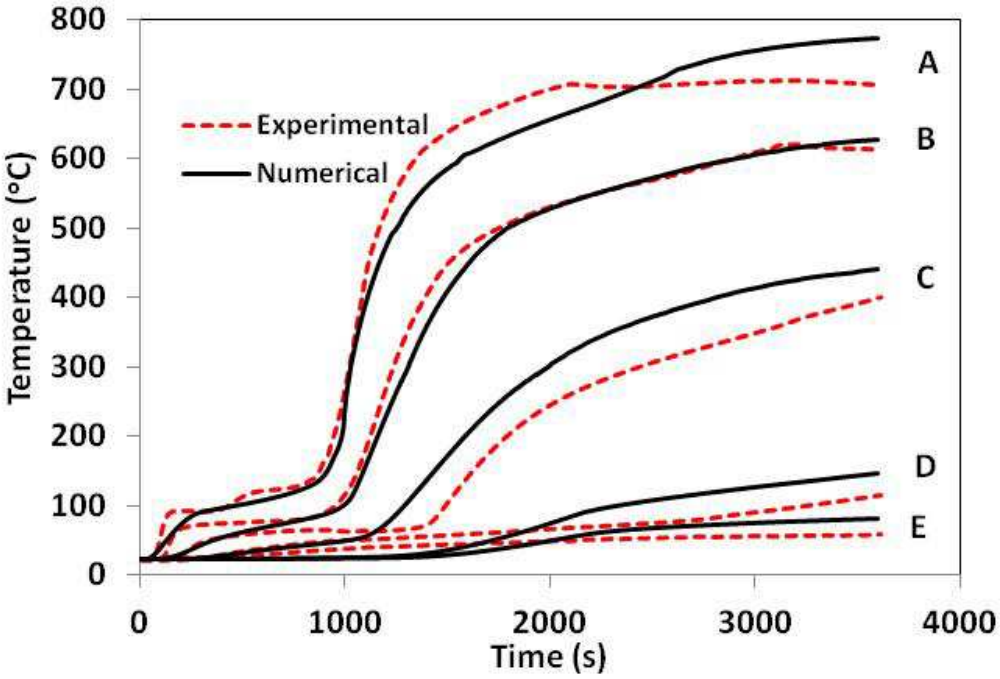

Figure 5.15: Comparison of Numerical and Experimental Results for Type X Gypsum Wall Assembly Exposed to 75 kW/m^2.

Table 5.7: Comparison Between Experimental and Numerical Results – Single Layer Type X Gypsum Board Wall Assembly (75 kW/m^2 Exposure)

Back of exposed board(s) **(A)**	**Experimental** Ave. (s)	**(σ)**	**Numerical** (s)
Time to 100^{o}C	444	(17.5)	449
Time to 250^{o}C	1010	(29)	1003
Time to 600^{o}C	1334	(7.3)	1562
Back of unexposed board **(E)**	Ave. (˚C)	**(σ)**	(˚C)
Maximum Temperature Increase	37	(5.3)	57.8

Double Layer Type X Gypsum Board Wall Assembly

Temperature profiles on the unexposed side measured during the cone calorimeter experiments in which single layer type X gypsum board wall assemblies were exposed to 75 kW/m^2 (Section 4.4.2) are compared with predictions made using the numerical model (Section 3.3.6) in Figure 5.16. The time at which the back of the exposed board reaches 100, 200 and 250˚C and the maximum temperature increase at the back of the unexposed board of the wall assembly are presented in Tables 5.8.

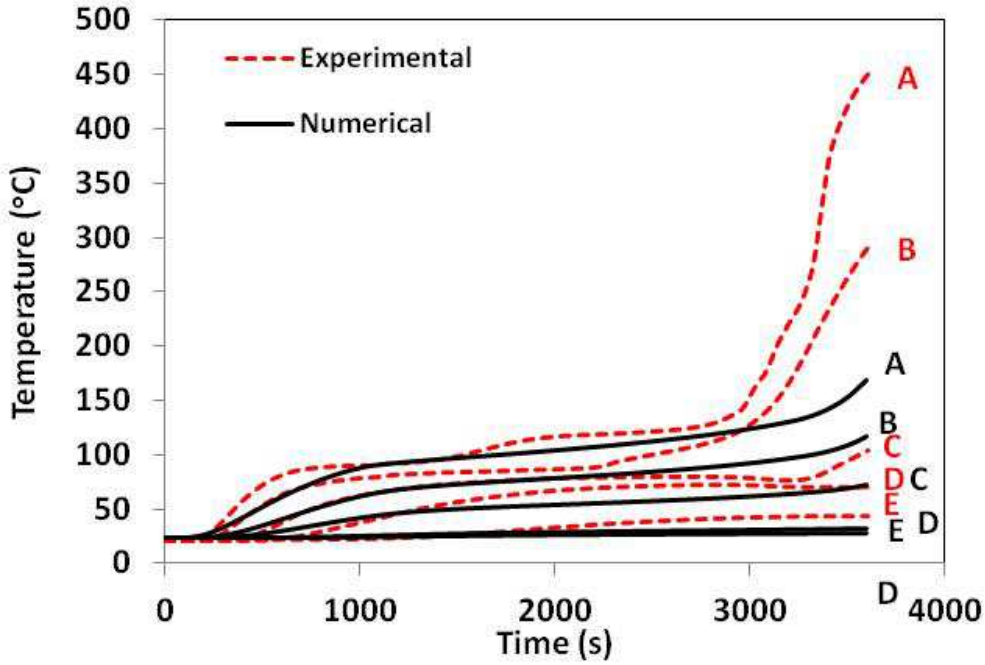

Figure 5.16: Comparison of Numerical and Experimental Results for Double Type X Gypsum Wall Assembly Exposed to 75 kW/m^2.

Table 5.8: Comparison Between Experimental and Numerical Results – Double Layer Type X Gypsum Board Wall Assembly (75 kW/m^2 Exposure)

Back of exposed board(s) **(A)**	**Experimental** Ave. (s)	**(σ)**	**Numerical** (s)
Time to 100°C	1538	(19.8)	1701
Time to 200°C	3049	(63.8)	**
Time to 250°C	3167	(81.02)	**
Back of unexposed board **(E)**	Ave. (˚C)	**(σ)**	(˚C)
Maximum Temperature Increase	22.6	(0.3)	3.3

** Temperature not attained

Discussion

The comparisons between the numerical and experimental time-temperature profiles for single layer wall tests in Figures 5.9-5.11, and Figures 5.13 and 5.15 further validates the finite difference model as the agreement between experimental and numerical results is reasonably good at all locations. The larger variations between the temperature predictions made using the model and the experimental results at locations B and C are attributed to the difficulty in keeping the thermocouple at the exact position predicted by the model as a result of the loose nature of stone wool insulation. Tables 5.1-5.3, Table 5.5 and 5.7 give information about the predicted and measured times to 100˚C (calcination), 250˚C and 600˚C (fall off of exposed gypsum board) at location A for all wall tests. The agreement between the numerical and experimental results (single wall) for the calcination of the gypsum (predictions to 100˚C at location A), the time to 250˚C, and the time to 600˚C (fall off of the exposed gypsum board) was reasonably good with a percentage difference in the range of 0.3 -36% for all the results in Tables 5.1-5.3, Table 5.5 and 5.7. Tables 5.1-5.3, Table 5.5 and 5.7 also give information on the maximum predicted and measured temperature increase at the back of the unexposed board (E). The agreement was reasonably good with a percentage difference in the range of 5-43%.

The comparison between the time-temperature profiles in experimental and numerical results for double layer wall tests are presented in Figures 5.12, 5.14 and 5.16.The predicted and measured results show good agreement at the earlier stages (initial heating and calcination process) of the tests but show a poor level of agreement after the calcination process is complete. For all double wall temperature predictions, the time for calcination was overestimated by the model.

Tables 5.4, 5.6 and 5.8 gives information about the time to 100˚C (calcination), 200˚C and 250˚C at location A and the maximum temperature at location E for all wall tests. The comparison

between the numerical and experimental results (double wall) for the calcination of the gypsum (predictions to 100˚C at location A) and predictions to 200˚C were reasonably good. The percentage difference between predicted and measured time to 100˚C at location A for lightweight, regular and type X gypsum board wall assembly is 7.1%, 15% and 10.1%, respectively. The percentage difference between predicted and measured time to 200˚C at location A for lightweight and regular gypsum board wall assemblies is 25% and 27%, respectively. The percentage difference between predicted and measured time to 250˚C at location A for lightweight and regular gypsum board wall assemblies is 21% and 24.8%, respectively. The predicted temperature at location A for type X wall assemblies did not attain 200˚C and 250˚C. Tables 5.4, 5.6 and 5.8 also give information on the maximum numerical and experimental temperature increase at the back of the unexposed board (E). The percentage difference between predicted and measured maximum temperatures at the unexposed side (location E) for lightweight, regular and type X gypsum board wall assemblies is 10.1%, 20.2% and 149%, respectively. This very high percentage difference in temperature increase on the unexposed side for the double layer type X gypsum board wall assembly is because the other predicted temperatures in the wall assembly did not increase enough to cause the unexposed temperature to rise.

The fact that the model was not as successful in predicting temperatures in the double layer wall assemblies is expected, as the model had more difficulties in predicting temperatures within the specimens that contained two layers of drywall than in predicting temperatures in the specimens that contained only a single layer of drywall. These comparisons and possible reasons for the

difficulties in predicting temperatures within double layers of drywall were discussed in Section 5.2.

A major reason for the differences between all of the predicted and measured results was the choice of thermal properties, which were taken from the literature rather than being measured. In particular the sensitivity study presented in Section 3.4 demonstrated that the thermal conductivity, and to a lesser degree the specific heat, of the gypsum board had the largest effect on the predicted temperatures. Comparing the figures in Section 3.4 with those in this section, the magnitude of the differences between numerical and experimental results are similar to the magnitude of the differences in temperatures when the properties of the gypsum board were changed.

The model was also unable to predict the temperature peaks in Figures 5.3 and 5.4 which are largely due to moisture movement which was not considered in this thesis research. To investigate the possible effect of the energy transfer associated with moisture movement within the wall assembly, the specific heat curve shown in Figure 5.17 was used in the model for gypsum board. While most of this curve was based on the values used in the model, three points at 159, 191 and 220°C were introduced in order to look at the effects of including negative specific heat values in the model, as negative values are seen in some measurements reported in the literature. The negative values represent exothermic reactions, or in this case, energy transfer to the inner parts of the gypsum board as the moisture is driven through the assembly. Using this specific heat curve resulted in a better prediction of the temperature peak noticed in the gypsum board tests shown in Figures 5.18 and 5.19. These results are further evidence that in order to obtain a better prediction of the temperature profiles in wall assemblies the correct thermal property data and the effect of moisture movement need to be included in the numerical model.

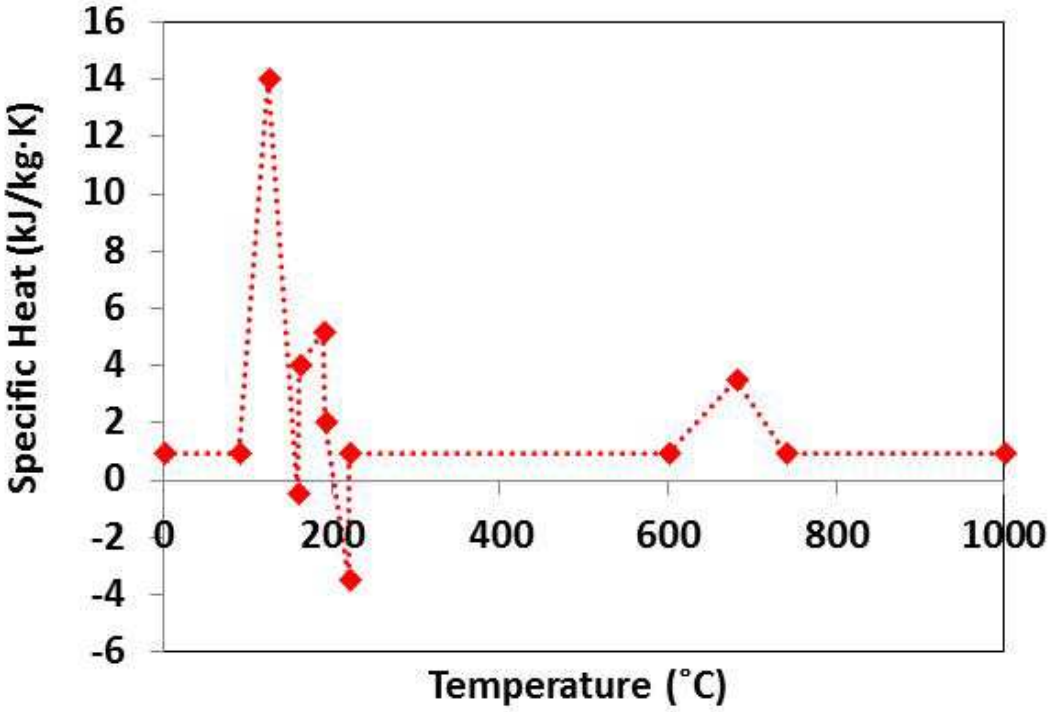

Figure 5.17: A Modified Specific Heat of Gypsum Board to Account for Energy Associated with Moisture Movement

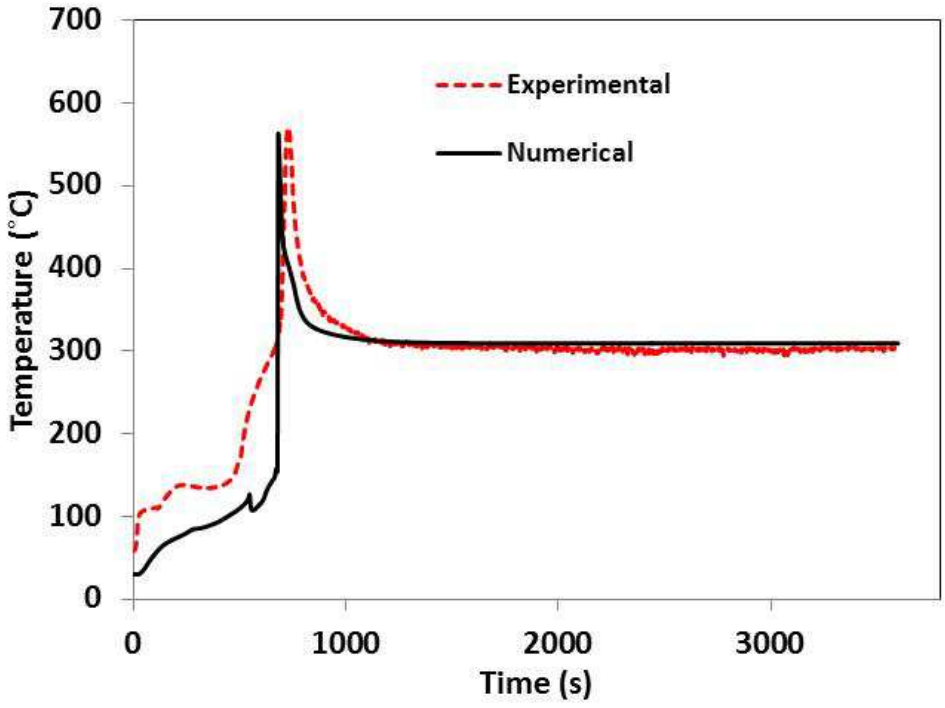

Figure 5.18: Comparison of Numerical and Experimental Results at Unexposed Side of Single Regular Gypsum Board (Using Specific Heat in Figure 5.17)

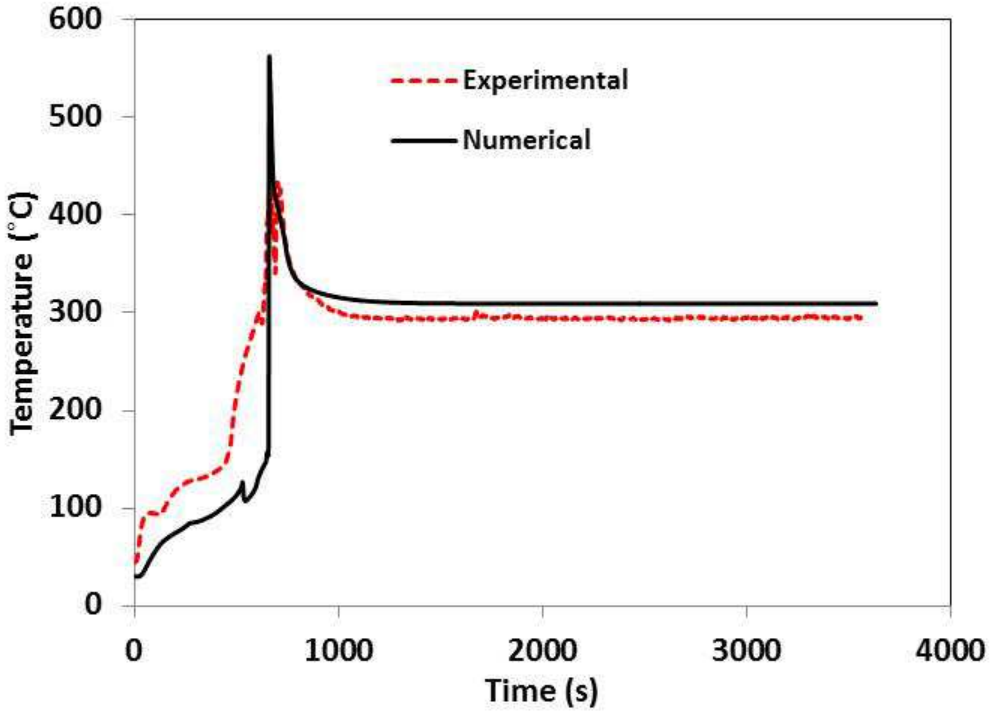

Figure 5.19: Comparison of Numerical and Experimental Results at Unexposed Side of Single Lightweight Gypsum Board (Using Specific Heat in Figure 5.17

CHAPTER SIX: CONCLUSIONS AND RECOMMENDATIONS

6.1. CONCLUSIONS

The following conclusions can be made as a result of this research.

- Temperatures predicted using the one dimensional conduction heat transfer model developed in this study show a varying degree of agreement with measured temperatures for insulated single layer wall assemblies. Predicted and measured times for temperatures to reach 100°C and 250°C on the unexposed side of the gypsum board layer closest to the cone heater were generally within 10%. There was less agreement between predicted and measured times to reach 600°C at this location, and the temperature increase on the unexposed side of the test specimen. The model did not do a good job in predicting temperatures in the insulated double layer walls. Based on these comparisons, it was felt that the heat transfer model showed good potential for predicting temperature in cone calorimeter tests of wall assemblies, but more development work is needed.

- Experimental and numerical results demonstrated that temperatures increased most rapidly in assemblies that used lightweight gypsum board and most slowly in assemblies that used Type X gypsum board. Adding a second layer of gypsum board on each side of the assembly reduced the maximum temperature on the unexposed side and insulated wall assemblies provided better fire protection than uninsulated wall assemblies.

- The results of the sensitivity of temperature to ± 20% changes to specific heat, thermal conductivity and density of both gypsum board and stone wool insulation showed that the

thermal conductivity of gypsum board has the most significant impact on the predicted temperatures with the specific heat of gypsum board having a significant impact as well.

- In the comparison of cone calorimeter, intermediate and full scale test results, the temperatures on the back of the exposed gypsum board and front of the unexposed board showed good agreement up to the first 20-25 min of exposure. The temperature on the unexposed side of the assembly showed a good agreement up to about 45-50 min of testing even though the incident heat fluxes and conditions of testing are different. This demonstrates that cone calorimeter tests may have the potential to be used as indicators of the performance of wall assemblies in standard full-scale fire tests. One limitation is that the cone calorimeter tests only used a heat flux of 75 kW/m^2, while the full scale tests produce heat fluxes of up to 150 kW/m^2.

6.2. RECOMMENDATIONS FOR FUTURE WORK

Based on the experiments, the following recommendations are made to improve cone calorimeter tests of wall assemblies:

- A temperature dependent cone calorimeter should be used to simulate the temperature distribution of the standard temperature time curve; and
- More cone calorimeter tests of wall assemblies with similar gypsum board arrangement and stud types as in the full scale tests should be conducted in order to develop a scaling model.

Based on the development of the numerical model, the following recommendations are made to improve heat transfer models of wall assemblies.

- The numerical model should be further improved to include the effects of moisture movement across the wall section, structural failure, and shrinkage of gypsum boards. For example, a porous media model should be used for the gypsum board and insulation.
- The use of the differential scanning calorimeter (DSC) should be employed to determine the temperature dependent thermal properties of gypsum board and insulation over a large range of temperature so as to arrive at a better prediction of the experimental results.
- It should be noted that when the specimens were inspected after testing there was evidence that the wood studs had partially burned during the exposures. Therefore, this phenomenon may need to be taken into account in modeling these tests. While temperatures of the wood studs were not recorded in these tests, future tests may be necessary to record this information for use in developing numerical models.

LIST OF REFERENCES

[1] CAN/ULC-S101, 2007, Standard Methods of Fire Endurance Tests of Building Construction and Materials, Underwriters' Laboratories of Canada, Toronto, ON.

[2] ASTM E 176, 2007, Standard Terminology of Fire Standards, American Society for Testing and Materials, West Conshohocken, PA.

[3] ASTM E 119, 2007, Standard Test Method for Fire Tests of Building Construction and Materials, American Society for Testing and Materials, West Conshohocken, PA.

[4] ISO 834, 2002, Fire Resistance Tests – Elements of Building Construction, International Standard Organization; Geneva, Switzerland.

[5] Sultan M.A., Benichou N., 2004, Heat Exposure Measurements in Fire Resistance Wall and Floor Test Furnaces, Internal Report No. 46893, Institute for Research in Construction, National Research Council, Ottawa, ON.

[6] Sultan M.A., Benichou N., Min B.Y., 2003, Heat Exposure in Fire Resistance Furnaces: Full-Scale vs. Intermediate Scale, Internal Report No. 46106, Institute for Research in Construction, National Research Council, Ottawa, ON.

[7] Craft S. T., 2009, CUWood Frame – A Heat and Mass Transfer Model for Light-Framed Wood Floors Exposed to Fire, Ph.D. Thesis, Department of Civil and Environmental Engineering, Carleton University, Ottawa, ON.

[8] Craft S. T., Hadjisophocleous G., Isgor B., Mehaffey J., 2006, Predicting the Fire Resistance of Light-Framed Wood Floor Assemblies, Proceedings 4th International Structures in Fire Workshop, Aveiro, Portugal, pp. 936–950.

[9] Wakili K. J., Hugi E., Wullschleger L., Frank T., 2007, Gypsum Board in Fire – Modeling and Experimental Validation, Journal of Fire Sciences, Vol. 25, pp. 267–282.

[10] Sultan M.A., 1996, A Model for Predicting Heat Transfer through Non-insulated Unloaded Steel-stud Gypsum-Board/Wood-Stud Walls Exposed to Fire, Fire Technology, Vol. 32, pp. 239-259.

[11] ASHRAE Handbook Fundamentals, 2009, American Society of Heating, Refrigeration and Air-Conditioning Engineers, Atlanta, GA.

[12] Sultan M.A., Lougheed G.D., Denham M., Monette R.C., MacLaurin J.W., 1994, Temperature Measurements in Full-Scale Fire Resistance Tests on Non-Insulated Regular Gypsum Board Wall Assemblies. Internal Report No. 674, Institute for Research in Construction, National Research Council, Ottawa, ON.

[13] Kodur V.K.R., Sultan M.A., Denham M., 1996, Temperature Measurements in Full-Scale Wood Stud Shear Walls, Internal Report No. 729, Institute for Research in Construction, National Research Council, Ottawa, ON.

[14] Sultan M.A., Lougheed G.D., Denham M., Monette R.C., MacLaurin J.W., 1994, Temperature Measurements in Fire Resistance Tests on Insulated and Non-Insulated Small-Scale Wall Assemblies Protected by Type X Gypsum Board, Internal Report No. 677, Institute for Research in Construction, National Research Council, Ottawa, ON.

[15] Sultan M.A., Denham E.M.A., Monette R.C., Morwick D.W., 1994, Temperature Measurements in Fire Resistance Tests on Small-Scale Insulated and Non-Insulated Regular Gypsum Board Assemblies. Internal Report No. 671, Institute for Research in Construction, National Research Council, Ottawa, ON.

[16] Park S., Manzello S.L., Bundy M.F., Mizukami T., 2011, Experimental Study on the Performance of a Load-bearing Steel Stud Gypsum Board Wall Assembly Exposed to a Real Fire. Fire Safety Journal, Vol. 46, pp. 497-505.

[17] Kontogeorgos D.K., Wakili G., Hugi E., Founti M., 2011, Heat and Moisture Through a Steel Stud Gypsum Board Assembly Exposed to Fire. Construction and Building Materials, Vol. 26, pp. 746-754.

[18] Urbas J., Shaw J.R., 1993, Testing Wall Assemblies on an Intermediate-Scale Calorimeter, Weyerhaeuser Fire Technology Laboratory, Longview, Washington, USA.

[19] Jones B.H. Performance of Gypsum Plasterboard Assemblies Exposed to Real Building Fires. M.Eng Thesis, Department of Civil Engineering, University of Canterbury, Christchurch, New Zealand.

[20] Thomas G.C., 1997. Fire Resistance of Light Timber Framed Walls and Floors. PhD. Thesis, Department of Civil Engineering, University of Canterbury, Christchurch, New Zealand.

[21] Takeda H., Mehaffey J.R., 1998. WALL2D: A Model for Predicting Heat Transfer through Wood-Stud Walla Exposed to Fire. Fire and Materials Vol.22, pp. 133-140.

[22] Takeda H., 2003, A Model to Predict Fire Resistance of Non-load Bearing Wood-Stud Walls. Fire and Materials Vol. 27, pp. 19-39.

[23] Clancy P. 1999, Time and Probability of Failure of Timber Framed Walls in Fire. Ph.D. Thesis, Centre for Environmental Safety and Risk Engineering, Victoria University of Technology, Victoria, Australia.

[24] Clancy P., 2001, Advances in Modelling Heat Transfer Through Wood Framed Walls in Fire. Fire and Materials, Vol.25, pp. 241-254.

[25] Clancy P. 2002, A Parametric Study on the Time-to-Failure of Wood Framed Walls in Fire. Fire Technology Vol.38, pp. 243-269.

[26] Collier, P. 1996, A Model for Predicting the Fire Resisting Performance of Small-Scale Cavity Walls in Realistic Fires. Fire Technology Vol.32, pp. 120-136.

[27] Alfawakhiri F., Sultan M.A., Benichou N., 2001, A Model for Predicting Heat Transfer Through Insulated Steel-Stud Wall Assemblies Exposed to Fire Proceedings, Fire and Materials Conference, San Francisco, CA, pp.495-506.

[28] Shahbazian A., Wang Y.C., 2012, A Simplified Approach for Calculating Temperatures in Axially Loaded Cold-formed Thin-walled Steel Studs in Wall Panel Assemblies Exposed to Fire from One Side. School of Mechanical, Aerospace and Civil Engineering, University of Manchester, UK.

[29] Keerthan P., Mahendran M., 2012, Thermal Performance of Composite Panels Under Fire Conditions Using Numerical Studies: Plasterboards, Rockwool, Glass Fibre and Cellulose Insulations. Fire Technology, Vol. 49, pp. 329-356.

[30] Torvi D.A., Threlfall T.G., 2006, Heat Transfer Model of Flame Resistant Fabrics During Cooling After Exposure to Fire, Fire Technology, Vol. 42, pp. 27-48.

[31] Enninful E.K., Torvi D.A., 2008, A Variable Property Heat Transfer Model for Predicting Soil Temperature Profiles during Simulated Wildlife Fire Conditions. International Journal of Wildland Fire, Vol. 17, pp. 205-213.

[32] Ezinwa J.U., 2009, Modeling Full-Scale Fire Test Behaviour of Polyurethane Foams Using Cone Calorimeter Data, M.Sc. Thesis, Department of Mechanical Engineering, University of Saskatchewan, Saskatoon, SK.

[33] Wang H., 1995, Heat Transfer Analysis of Components of Construction Exposed to Fire – A Theoretical, Numerical and Experimental Approach. Ph.D. Thesis, Department of Civil and Construction, University of Salford, Manchester, England.

[34] Torvi D.A., 1997, Heat Transfer in Thin Fibrous Materials Under High Heat Flux Conditions, Ph.D Thesis, Department of Mechanical Engineering, University of Alberta, Edmonton, AB.

[35] Yuen R.K.K, Yeoh G.H., de Vahl Davis G., Leonardi E., 2007, Modelling the Pyrolysis of Wet Wood – II. Three-dimensional Cone Calorimeter Simulation. International Journal of Heat and Mass Transfer, Vol. 50, pp. 4387-4399.

[36] Wilson M.T., Dlugogorski B.Z., and Kenedy E.Z., 2003,Uniformity of Radiant Heat Fluxes in Cone Calorimeter, Proceedings Seventh International Symposium on Fire Safety Science, Vol. 7, pp. 815-827.

[37] Zhang J., Delichatsios M., 2010, Further Validation of a Numerical Model for Prediction of Pyrolysis of Polymer Nanocomposites in the Cone Calorimeter, Fire Technology, Vol. 46, pp. 307-319.

[38] Boulet P., Parent G., Acem Z., Rogaume T., Fateh T., Zaida J., Richard F., 2012, Characterization of the Radiative Exchanges When Using a Cone Calorimeter for the Plywood Pyrolysis, Fire Safety Journal, Vol. 51, pp.53-60.

[39] Spearpoint M.J., Quintier J.G., 2001, Predicting the Piloted Ignition of Wood in the Cone Calorimeter Using an Integral Model – Effect of Species, Grain Orientation and Heat Flux, Fire Safety Journal, Vol. 36, pp. 391-415.

[40] Enninful E.K, Torvi D.A, 2008, A Variable Property Heat Transfer Model for Predicting Soil Temperature Profiles during Simulated Wildlife Fire Conditions. International Journal of Wildland Fire, Vol. 17, pp. 205-213.

[41] Incropera F.P., Dewitt D.P., Bergman T.L., Lavine A.S., Fundamentals of Heat and Mass Transfer, Sixth Edition, John Wiley and Sons, Hoboken, NJ.

[42] Janssens M.L., 2003, Improved Method for Analysing Ignition Data From the Cone Calorimeter in the Vertical Orientation, Proceedings Seventh International Symposium on Fire Safety Science , pp. 803-814.

[43] Wang Y.C., 2002. Steel and Composite Structures: Behavior and Design for Fire Safety, Spon Press London, UK.

[44] Mehaffey J.R., Cuerrier P., Carisse G., 1994. A Model for Predicting Heat Transfer Through Gypsum-Board/Wood-Stud Walls Exposed to Fire. Fire and Materials Vol. 18, pp. 297-305.

[45] Sultan M.A., 2010, Comparison of Gypsum Board Fall-off in Wall and Floor Assemblies Exposed to Furnace Heat, Report No. NRCC 50843, Institute for Research in Construction, National Research Council, Ottawa, ON.

[46] Eleweni E., Sultan M.A., Hadjisophocleous G.V., 2007, Gypsum Board Fall-off in Floor Assemblies Exposed to A Standard Fire. Report No. NRCC 45420, Institute for Research in Construction, National Research Council, Ottawa, ON.

[47] Carslaw H., Jaeger J., 1956, Conduction of Heat in Solids, Second Edition, Oxford University Press, Oxford, UK.

[48] McCarthy L.K., 2010, Evaluation of The Thermal Performance of Fire Fighters Protective Clothing With The Addition of Phase Change Material, M.Sc. Thesis, Department of Fire Protection Engineering, University of Maryland, Baltimore, MD.

[49] Spangler K., 2008, Energy Transport in Firefighter Protective Clothing, M.Sc. Thesis Department of Fire Protection Engineering, University of Maryland, College Park, MD.

[50] Harmathy T.Z., 1995, Properties of Building Materials. Internal Report No. 1580 Institute for Research in Construction, National Research Council, Ottawa, ON.

[51] Thomas G., 2002, Thermal Properties of Gypsum Plasterboard at High Temperatures, Fire and Materials, Vol. 26, pp. 37-45.

[52] Benichou N., Sultan M. A., MacCallum C., Hum J.K., 2001, Thermal Properties of Wood, Gypsum and Insulation at Elevated Temperatures. Internal Report No. 710, Institute for Research in Construction, National Research Council, Ottawa, ON.

[53] Benichou N., Sultan M.A., 2005, Thermal Properties of Lightweight-Framed Construction Components at Elevated Temperatures. Fire and Materials, Vol. 25, pp. 165-179.

[54] Wakili K., Hugi E., 2009, Four Types of Gypsum Plaster Boards and their Thermo-physical Properties under Fire Condition. Journal of Fire Sciences, Vol. 27, pp. 27-43.

[55] Takeda H., Mehaffey J.R., 1998. WALL2D: A Model for Predicting Heat Transfer through Wood-Stud Walla Exposed to Fire. Fire and Materials, Vol. 22, pp. 133-140.

[56] Rahmanian I., 2011, Thermal and Mechanical Properties of Gypsum Boards and Their Influence on Fire Resistance of Gypsum Based Systems, Ph.D. Thesis, Faculty of Engineering and Physical Sciences, University of Manchester, Manchester, UK.

[57] Roxul, Roxul Comfort Batt Technical Product Information; http://www.roxul.com/files/RX-NA_EN/pdf/Technical%20Data%20Sheets%20updated/COMFORTBATT_CDAwithSS.pdf, accessed July, 2013.

[57] ASTM F 1060, 2007, Standard Test Method for Thermal Protective Performance of Materials for Protective Clothing for Hot Surface Contact, American Society for Testing and Materials, West Conshohocken, PA.

[59] ASTM E 1354, 2007, Standard Test Method for Heat and Visible Smoke Release Rates for Materials and Products Using an Oxygen Consumption Calorimeter, American Society for Testing and Materials, West Conshohocken, PA.

[60] National Building Code of Canada, 2010, Canadian Commission on Building and Fire Codes, Institute for Research in Construction, National Research Council Ottawa, ON.

[61] ASTM E 104, 2012, Standard Practice for Maintaining Constant Relative Humidity by Means of Aqueous Solution, American Society for Testing and Materials, West Conshohocken, PA.

[62] Crewe R. J., Staggs E. J., and Phylaktou H. N., 2010, Temperature –dependent Cone Calorimeter: An Approximate Alternative to Furnace Testing, Journal of Fire Sciences, Vol. 29, pp. 131-151.

APPENDIX A

```
%*************************************************************************
***************
% COMPUTER CODE FOR SINGLE GYPSUM BOARD
%*************************************************************************
% THIS COMPUTER CODE SOLVES ONE-DIMENSIONAL TRANSIENT HEAT CONDUCTION
% EQUATION USING A FINITE DIFFERENCE APPROACH.
%*************************************************************************

clc;
% Single Layer Gypsum Board

%PROPERTIES

L= 0.0127*1;      %thickness (SINGLE GYPSUM BOARD = 12.7 mm, DOUBLE = 12.7*2)
St=5.669*10^-8;         %stefan boltzmann constant
Tini = 30;              %Initial temperature
Tamb = 30;              % ambient temperature
Tout = 30;              % outside temperature
Tcone = 894;            % cone temperature (894 C for 75 kW/m2, 690C = 35
kW/m2, 780C = 50 kW/m2)
F = 0.72;               % view factor
hc=24;               %convective heat transfer coeffient at the exposed side)
hco=5;            % convective heat transfer coeffient at the unexposed side)
emo=0.9;                % emmisivity
em = 0.9;               %emmisivity
        % GYPSUM BOARD PROPERTIES = REGULAR GYPSUM BOARD

k=0.1683;               %thermal conductivity at room temperature
p=645.7;                % density at room temperature
cp=950;                 %specific heat at room temperature
            %grid properties
N = 8;                 % number of divisions (N+1 = total number of nodes)
dx = L/N;              % thickness of each division
 dtime=p*cp*dx^2/(2*hc*dx+2*k+2*em*St*dx*(Tini+273.15)^3); % stability
criterion (max. time)
dt=dtime/4;            % setting up for stability and timestep
 tspace = (0:dt:3600)'; % time increaement and duration of test
[sp,sy] = size(tspace);

T = zeros(sp,sy);      %Initialize temperature matrix

for j=2:1:sp;
    n=N+1;  % total number of nodes including surface temperatures
            T(1,1)=0;
    for ny=1:n;
         T(1,ny)=Tini;
    end

        for x=1:1:n

         if x<=1;   % FIRST NODE
            % THERMAL CONDUCTIVITY
            Tm1=(T(j-1,x+1)+T(j-1,x))/2;
```

```
if Tm1<=90;
k1=0.1683;
elseif Tm1<=200;
k1=-0.00057*(Tm1-90)+0.1683;
elseif Tm1<=300;
k1=0.000055*(Tm1-200)+0.1056;
elseif Tm1<=600;
k1=0.0001283*(Tm1-300)+0.1111;
elseif Tm1<=700;
k1=0.000352*(Tm1-600)+0.1496;
 elseif Tm1<=800;
k1=-0.000121*(Tm1-700)+0.1848;
 elseif Tm1>800;
k1=0.000495*(Tm1-800)+0.1727;
end
         % DENSITY
if T(j-1,x)<=140;
 p1=645.7;
elseif T(j-1,x)<=250;          %Regular
p1=-1.02725*T(j-1,x)+789.515;
elseif T(j-1,x)<=720;
p1=-0.0137*T(j-1,x)+536.13;
elseif T(j-1,x)<=800;
p1=-0.3632*T(j-1,x)+787.75;
elseif T(j-1,x)>800;
p1=497.189;
end
         %  SPECIFIC HEAT
if T(j-1,x)<=90;
cp1=950;
elseif T(j-1,x)<=130;
cp1=388.75*(T(j-1,x)-90)+950;
elseif T(j-1,x)<=160;
cp1=-350*(T(j-1,x)-130)+16500;
elseif T(j-1,x)<=190;
cp1=33.333*(T(j-1,x)-160)+6000;
elseif T(j-1,x)<=220;
cp1=-201.67*(T(j-1,x)-190)+7000;
elseif T(j-1,x)<=600;
cp1=950;
elseif T(j-1,x)<=680;
cp1=38.125*(T(j-1,x)-600)+950;
elseif T(j-1,x)<=740;
cp1=-50.833*(T(j-1,x)-680)+4000;
elseif T(j-1,x)>740;
cp1=950;
end

 syms T1

EQ1= hc*(T(j-1,x)-Tamb)+F*em*St*((Tcone+273)^4-(T(j-1,x)+273)^4)-(1-
F)*em*St*((T(j-1,x)+273)^4-(Tamb+273)^4)+k1*(T(j-1,x+1)-T(j-1,x))/dx-
p1*cp1*(dx/2)*(T1-T(j-1,x))/(dt);
[T1]=solve(EQ1);
T(j,x)= T1;
clear T1
clear EQ1
```

```
clear k1
clear p1
clear cp1
   %INTERIOR NODES
elseif x<n;

T2l=(T(j-1,x-1)+T(j-1,x))/2;

%conductivity
if T2l<=90;
k2l=0.1683;
elseif T2l<=200;
k2l=-0.00057*(T2l-90)+0.1683;
elseif T2l<=300;
k2l=0.000055*(T2l-200)+0.1056;
elseif T2l<=600;
k2l=0.0001283*(T2l-300)+0.1111;
elseif T2l<=700;
k2l=0.000352*(T2l-600)+0.1496;
elseif T2l<=800;
k2l=-0.000121*(T2l-700)+0.1848;
elseif T2l>800;
k2l=0.000495*(T2l-800)+0.1727;
end

T2r=(T(j-1,x+1)+T(j-1,x))/2;

%conductivity
if T2r<=90;
k2r=0.1683;
elseif T2r<=200;
k2r=-0.00057*(T2r-90)+0.1683;
elseif T2r<=300;
k2r=0.000055*(T2r-200)+0.1056;
elseif T2r<=600;
k2r=0.0001283*(T2r-300)+0.1111;
elseif T2r<=700;
k2r=0.000352*(T2r-600)+0.1496;
elseif T2r<=800;
k2r=-0.000121*(T2r-700)+0.1848;
elseif T2r>800;
k2r=0.000495*(T2r-800)+0.1727;
end

% density
if T(j-1,x)<=140;
 p2=645.7;
elseif T(j-1,x)<=250;          %Regular
p2=-1.02725*T(j-1,x)+789.515;
elseif T(j-1,x)<=720;
p2=-0.0137*T(j-1,x)+536.13;
elseif T(j-1,x)<=800;
p2=-0.3632*T(j-1,x)+787.75;
elseif T(j-1,x)>800;
p2=497.189;
end
```

```
        %  specific heat
        if T(j-1,x)<=90;
        cp2=950;
        elseif T(j-1,x)<=130;
        cp2=388.75*(T(j-1,x)-90)+950;
        elseif T(j-1,x)<=160;
        cp2=-350*(T(j-1,x)-130)+16500;
        elseif T(j-1,x)<=190;
        cp2=33.333*(T(j-1,x)-160)+6000;
        elseif T(j-1,x)<=220;
        cp2=-201.67*(T(j-1,x)-190)+7000;
        elseif T(j-1,x)<=600;
        cp2=950;
        elseif T(j-1,x)<=680;
        cp2=38.125*(T(j-1,x)-600)+950;
        elseif T(j-1,x)<=740;
        cp2=-50.833*(T(j-1,x)-680)+4000;
        elseif T(j-1,x)>740;
        cp2=950;
        end

        syms T2
        EQ2=k2l*(T(j-1,x-1)-T(j-1,x))/dx+k2r*(T(j-1,x+1)-T(j-1,x))/dx-
p2*cp2*(dx)*(T2-T(j-1,x))/(dt);
        [T2]=solve(EQ2);
        T(j,x)=T2;
        clear T2
        clear EQ2
        clear k2l
        clear k2r
        clear cp2
        clear p2

        elseif x>=n;
            T7l=(T(j-1,x-1)+T(j-1,x))/2;

        %conductivity
        if T7l<=90;
        k7=0.1683;
        elseif T7l<=200;
        k7=-0.00057*(T7l-90)+0.1683;
        elseif T7l<=300;
        k7=0.000055*(T7l-200)+0.1056;
        elseif T7l<=600;
        k7=0.0001283*(T7l-300)+0.1111;
        elseif T7l<=700;
        k7=0.000352*(T7l-600)+0.1496;
        elseif T7l<=800;
        k7=-0.000121*(T7l-700)+0.1848;
        elseif T7l>800;
        k7=0.000495*(T7l-800)+0.1727;

        end

        % density
        if T(j-1,x)<=140;
         p7=645.7;
```

```
        elseif T(j-1,x)<=250;          %Regular
        p7=-1.02725*T(j-1,x)+789.515;
        elseif T(j-1,x)<=720;
        p7=-0.0137*T(j-1,x)+536.13;
        elseif T(j-1,x)<=800;
        p7=-0.3632*T(j-1,x)+787.75;
        elseif T(j-1,x)>800;
        p7=497.189;
        end

        %  specific heat
        if T(j-1,x)<=90;
        cp7=950;
        elseif T(j-1,x)<=130;
        cp7=388.75*(T(j-1,x)-90)+950;
        elseif T(j-1,x)<=160;
        cp7=-350*(T(j-1,x)-130)+16500;
        elseif T(j-1,x)<=190;
        cp7=33.333*(T(j-1,x)-160)+6000;
        elseif T(j-1,x)<=220;
        cp7=-201.67*(T(j-1,x)-190)+7000;
        elseif T(j-1,x)<=600;
        cp7=950;
        elseif T(j-1,x)<=680;
        cp7=38.125*(T(j-1,x)-600)+950;
        elseif T(j-1,x)<=740;
        cp7=-50.833*(T(j-1,x)-680)+4000;
        elseif T(j-1,x)>740;
        cp7=950;
        end

        % STABILITY...

        dtimel=p7*cp7*dx^2/(2*hco*dx+2*k7+2*emo*St*dx*(Tout+273.15)^3); %
maximum time for instablity
         dtl=dtimel/2;

        syms T7

        EQ7=k7*(T(j-1,x-1)-T(j-1,x))/dx-hco*(T(j-1,x)-Tout)-emo*St*((T(j-
1,x)+273.15)^4-(Tout+273.15)^4)-p7*cp7*(dx/2)*(T7-T(j-1,x))/(dtl);
        [T7]=solve(EQ7);
        T(j,x)=T7;
        clear T7
        clear EQ7
        clear T7l
        clear k7
        clear cp7
        clear p7

       end
       end


end
% OBTAIN RESULTS FROM MATLAB WORKSPACE (T).
plot (tspace,T(:,n),'-b','LineWidth',3)
```

APPENDIX A

```
%************************************************************************
% COMPUTER CODE FOR INSULATED SINGLE GYPSUM BOARD WALL ASSEMBLY
%************************************************************************
**************
% THIS COMPUTER CODE SOLVES ONE-DIMENSIONAL TRANSIENT HEAT CONDUCTION
% EQUATION USING A FINITE DIFFERENCE APPROACH.
%************************************************************************


%REGULAR WALL ASSEMBLY....

%PROPERTIES

L= 0.1143;       %total thickness of wall in m (GYPSUM BOARD = 12.7 mm,
INSULATION CAVITY = 89 mm)
St=5.669*10^-8;  %stefan boltzmann constant
Tini = 24;         %Initial temperature
Tamb = 24;          % ambient temperature
Tout = 24;             % outside temperature
Tcone = 894;            % cone temperature (894 C for 75 kW/m2, 690C = 35
kW/m2, 780C = 50 kW/m2)
F = 0.72;               % view factor
hc=24;                  %convective heat transfer coeffient at the exposed
side)
hco=5;                  % convective heat transfer coeffient at the unexposed
side)
emo=0.9;                % emmisivity
em = 0.9;                  %emmisivity

                % GYPSUM BOARD PROPERTIES = REGULAR GYPSUM BOARD

k=0.1683;               %thermal conductivity at room temperature
p=645.7;                % density at room temperature
cp=950;                 %specific heat at room temperature

%grid properties
N = 72;                 % number of divisions (N+1 = total number of nodes)
dx = L/N;               % thickness of each division

dtime=p*cp*dx^2/(2*hc*dx+2*k+2*em*St*dx*(Tini+273.15)^3); % stability
criterion (max. time)
dt=dtime/7;     % setting up for stability and timestep

tspace = (0:dt:10)'; % time increaement and duration of test
[sp,sy] = size(tspace);


T = zeros(sp,sy);       %Initialize temperature matrix

for j=2:1:sp;
    n=N+1;  % total number of nodes including surface temperatures
            T(1,1)=0;
    for ny=1:n;
```

```
     T(1,ny)=Tini;
end


    for x=1:1:n

     if x<=1;   % FIRST NODE
        % THERMAL CONDUCTIVITY
        Tm1=(T(j-1,x+1)+T(j-1,x))/2;

     if Tm1<=90;
     k1=0.1683;
     elseif Tm1<=200;
     k1=-0.00057*(Tm1-90)+0.1683;
     elseif Tm1<=300;
     k1=0.000055*(Tm1-200)+0.1056;
     elseif Tm1<=600;
     k1=0.0001283*(Tm1-300)+0.1111;
     elseif Tm1<=700;
     k1=0.000352*(Tm1-600)+0.1496;
      elseif Tm1<=800;
     k1=-0.000121*(Tm1-700)+0.1848;
      elseif Tm1>800;
     k1=0.000495*(Tm1-800)+0.1727;

     end

     % DENSITY
     if T(j-1,x)<=140;
      p1=645.7;
     elseif T(j-1,x)<=250;          %Regular
     p1=-1.02725*T(j-1,x)+789.515;
     elseif T(j-1,x)<=720;
     p1=-0.0137*T(j-1,x)+536.13;
     elseif T(j-1,x)<=800;
     p1=-0.3632*T(j-1,x)+787.75;
     elseif T(j-1,x)>800;
     p1=497.189;
     end

     %  SPECIFIC HEAT
     if T(j-1,x)<=90;
     cp1=950;
     elseif T(j-1,x)<=130;
     cp1=388.75*(T(j-1,x)-90)+950;
     elseif T(j-1,x)<=160;
     cp1=-350*(T(j-1,x)-130)+16500;
     elseif T(j-1,x)<=190;
     cp1=33.333*(T(j-1,x)-160)+6000;
     elseif T(j-1,x)<=220;
     cp1=-201.67*(T(j-1,x)-190)+7000;
     elseif T(j-1,x)<=600;
     cp1=950;
     elseif T(j-1,x)<=680;
     cp1=38.125*(T(j-1,x)-600)+950;
     elseif T(j-1,x)<=740;
     cp1=-50.833*(T(j-1,x)-680)+4000;
```

```
        elseif T(j-1,x)>740;
        cp1=950;
        end


    syms T1

        EQ1= hc*(T(j-1,x)-Tamb)+F*em*St*((Tcone+273)^4-(T(j-1,x)+273)^4)-(1-
F)*em*St*((T(j-1,x)+273)^4-(Tamb+273)^4)+k1*(T(j-1,x+1)-T(j-1,x))/dx-
p1*cp1*(dx/2)*(T1-T(j-1,x))/(dt);
        [T1]=solve(EQ1);
        T(j,x)= T1;
        clear T1
        clear EQ1
        clear k1
        clear p1
        clear cp1

        % INTERIOR NODES OF FIRST LAYER
        elseif x<9;

        T2l=(T(j-1,x-1)+T(j-1,x))/2;

        %conductivity
         if T2l<=90;
        k2l=0.1683;
        elseif T2l<=200;
        k2l=-0.00057*(T2l-90)+0.1683;
        elseif T2l<=300;
        k2l=0.000055*(T2l-200)+0.1056;
        elseif T2l<=600;
        k2l=0.0001283*(T2l-300)+0.1111;
        elseif T2l<=700;
        k2l=0.000352*(T2l-600)+0.1496;
        elseif T2l<=800;
        k2l=-0.000121*(T2l-700)+0.1848;
        elseif T2l>800;
        k2l=0.000495*(T2l-800)+0.1727;

        end

        T2r=(T(j-1,x+1)+T(j-1,x))/2;

        %conductivity
        if T2r<=90;
        k2r=0.1683;
        elseif T2r<=200;
        k2r=-0.00057*(T2r-90)+0.1683;
        elseif T2r<=300;
        k2r=0.000055*(T2r-200)+0.1056;
        elseif T2r<=600;
        k2r=0.0001283*(T2r-300)+0.1111;
        elseif T2r<=700;
        k2r=0.000352*(T2r-600)+0.1496;
        elseif T2r<=800;
        k2r=-0.000121*(T2r-700)+0.1848;
        elseif T2r>800;
```

```
k2r=0.000495*(T2r-800)+0.1727;

end


% density
if T(j-1,x)<=140;
 p2=645.7;
elseif T(j-1,x)<=250;          %Regular
p2=-1.02725*T(j-1,x)+789.515;
elseif T(j-1,x)<=720;
p2=-0.0137*T(j-1,x)+536.13;
elseif T(j-1,x)<=800;
p2=-0.3632*T(j-1,x)+787.75;
elseif T(j-1,x)>800;
p2=497.189;
end

%  specific heat
if T(j-1,x)<=90;
cp2=950;
elseif T(j-1,x)<=130;
cp2=388.75*(T(j-1,x)-90)+950;
elseif T(j-1,x)<=160;
cp2=-350*(T(j-1,x)-130)+16500;
elseif T(j-1,x)<=190;
cp2=33.333*(T(j-1,x)-160)+6000;
elseif T(j-1,x)<=220;
cp2=-201.67*(T(j-1,x)-190)+7000;
elseif T(j-1,x)<=600;
cp2=950;
elseif T(j-1,x)<=680;
cp2=38.125*(T(j-1,x)-600)+950;
elseif T(j-1,x)<=740;
cp2=-50.833*(T(j-1,x)-680)+4000;
elseif T(j-1,x)>740;
cp2=950;
end


syms T2
EQ2=k2l*(T(j-1,x-1)-T(j-1,x))/dx+k2r*(T(j-1,x+1)-T(j-1,x))/dx-
p2*cp2*(dx)*(T2-T(j-1,x))/(dt);
[T2]=solve(EQ2);
T(j,x)=T2;
clear T2
clear EQ2
clear k2l
clear k2r
clear cp2
clear p2

%FIRST IINTERFACE (GYPSUM-INSULATION)

elseif x==9;
%GYPSUM
   TI1=(T(j-1,x-1)+T(j-1,x))/2;
```

```
if TI1<=90;
kI1g=0.1683;
elseif TI1<=200;
kI1g=-0.00057*(TI1-90)+0.1683;
elseif TI1<=300;
kI1g=0.000055*(TI1-200)+0.1056;
elseif TI1<=600;
kI1g=0.0001283*(TI1-300)+0.1111;
elseif TI1<=700;
kI1g=0.000352*(TI1-600)+0.1496;
elseif TI1<=800;
kI1g=-0.000121*(TI1-700)+0.1848;
elseif TI1>800;
kI1g=0.000495*(TI1-800)+0.1727;

end


% density
if T(j-1,x)<=140;
 pI1g=645.7;
elseif T(j-1,x)<=250;          %Regular
pI1g=-1.02725*T(j-1,x)+789.515;
elseif T(j-1,x)<=720;
pI1g=-0.0137*T(j-1,x)+536.13;
elseif T(j-1,x)<=800;
pI1g=-0.3632*T(j-1,x)+787.75;
elseif T(j-1,x)>800;
pI1g=497.189;
end

%  specific heat
if T(j-1,x)<=90;
cpI1g=950;
elseif T(j-1,x)<=130;
cpI1g=388.75*(T(j-1,x)-90)+950;
elseif T(j-1,x)<=160;
cpI1g=-350*(T(j-1,x)-130)+16500;
elseif T(j-1,x)<=190;
cpI1g=33.333*(T(j-1,x)-160)+6000;
elseif T(j-1,x)<=220;
cpI1g=-201.67*(T(j-1,x)-190)+7000;
elseif T(j-1,x)<=600;
cpI1g=950;
elseif T(j-1,x)<=680;
cpI1g=38.125*(T(j-1,x)-600)+950;
elseif T(j-1,x)<=740;
cpI1g=-50.833*(T(j-1,x)-680)+4000;
elseif T(j-1,x)>740;
cpI1g=950;
end

 % STONE WOOL INSULATION
if TI1<=101;
kI1i=0.036;
elseif TI1<=194;
 kI1i=0.000194*(TI1-101)+0.036;
```

```
          elseif TI1<=297;
           kI1i=0.0002135*(TI1-194)+0.054;
          elseif TI1<=396;
           kI1i=0.0004343*(TI1-297)+0.076;
          elseif TI1<=501;
           kI1i=0.000447*(TI1-396)+0.119;
          elseif TI1<=602;
           kI1i=0.0007525*(TI1-501)+0.166;
          elseif TI1>724;
          kI1i=-0.0002869*(TI1-602)+0.242;
          elseif TI1<=856;
           kI1i=0.0001667*(TI1-724)+0.207;
          elseif TI1>856;
           kI1i=0.0004757*(TI1-856)+0.229;

          end

         % density
           pI1i=31.32;

          %  specific heat of INSULATION
           cpI1i=700;

          syms T3
          EQ3=dx^2*(cpI1g*pI1g + cpI1i*pI1i)/((kI1g+kI1i)*dt)*(T3-T(j-1,x)) +
2*T(j-1,x) - 2*(kI1g*T(j-1,x-1)+(kI1i*T(j-1,x+1)))/(kI1g+kI1i);
          [T3]=solve(EQ3);
          T(j,x)=T3;
          clear T3
          clear EQ3
          clear cpI1g
          clear kI1g
          clear kI1i
          clear cpI1i
          clear pI1g
          clear pI1i


           % INTERIOR NODES OF SECOND LAYER

          elseif  x<65;

          %CONDUCTIVITY OF INSULATION        T

          T4l=(T(j-1,x-1)+T(j-1,x))/2;
           if T4l<=101;
          k4l=0.036;
           elseif T4l<=194;
           k4l=0.000194*(T4l-101)+0.036;
            elseif T4l<=297;
           k4l=0.0002135*(T4l-194)+0.054;
            elseif T4l<=396;
           k4l=0.0004343*(T4l-297)+0.076;
          elseif T4l<=501;
           k4l=0.000447*(T4l-396)+0.119;
          elseif T4l<=602;
           k4l=0.0007525*(T4l-501)+0.166;
```

```
          elseif T4l>724;
          k4l=-0.0002869*(T4l-602)+0.242;
          elseif T4l<=856;
           k4l=0.0001667*(T4l-724)+0.207;
           elseif T4l>856;
           k4l=0.0004757*(T4l-856)+0.229;

          end

          T4r=(T(j-1,x+1)+T(j-1,x))/2;
           if T4r<=101;
          k4r=0.036;
           elseif T4r<=194;
           k4r=0.000194*(T4r-101)+0.036;
            elseif T4r<=297;
           k4r=0.0002135*(T4r-194)+0.054;
            elseif T4r<=396;
           k4r=0.0004343*(T4r-297)+0.076;
          elseif T4r<=501;
           k4r=0.000447*(T4r-396)+0.119;
          elseif T4r<=602;
           k4r=0.0007525*(T4r-501)+0.166;
          elseif T4r>724;
          k4r=-0.0002869*(T4r-602)+0.242;
          elseif T4r<=856;
           k4r=0.0001667*(T4r-724)+0.207;
           elseif T4r>856;
           k4r=0.0004757*(T4r-856)+0.229;

          end
         % density
           p4i=31.32;

          %  specific heat of INSULATION
           cp4i=700;

         %CHECKING FOR STABILITY
          dat4 = (cp4i*p4i*(dx)^2)/(k4l+k4r);
          dt4 = dat4;

          syms T4

          EQ4=k4l*(T(j-1,x-1)-T(j-1,x))/dx+k4r*(T(j-1,x+1)-T(j-1,x))/dx-
p4i*cp4i*(dx)*(T4-T(j-1,x))/(dt4);
          [T4]=solve(EQ4);
          T(j,x)=T4;
          clear T4
          clear EQ4
          clear k4l
          clear k4r
          clear cp4i
          clear p4i

         %SECOND INTERFACE (INSULATION-GYPSUM)

          elseif x==65;
```

```
TI2=(T(j-1,x-1)+T(j-1,x))/2;
 %  insulation.................................

if TI2<=101;
kI2i=0.036;
 elseif TI2<=194;
 kI2i=0.000194*(TI2-101)+0.036;
  elseif TI2<=297;
 kI2i=0.0002135*(TI2-194)+0.054;
  elseif TI2<=396;
 kI2i=0.0004343*(TI2-297)+0.076;
elseif TI2<=501;
 kI2i=0.000447*(TI2-396)+0.119;
elseif TI2<=602;
 kI2i=0.0007525*(TI2-501)+0.166;
elseif TI2>724;
kI2i=-0.0002869*(TI2-602)+0.242;
elseif TI2<=856;
 kI2i=0.0001667*(TI2-724)+0.207;
 elseif TI2>856;
 kI2i=0.0004757*(TI2-856)+0.229;

end

% density
  pI2i=31.32;
 %  specific heat of INSULATION
  cpI2i=700;

  %GYPSUM

if TI2<=90;
kI2g=0.1683;
elseif TI2<=200;
kI2g=-0.00057*(TI2-90)+0.1683;
elseif TI2<=300;
kI2g=0.000055*(TI2-200)+0.1056;
elseif TI2<=600;
kI2g=0.0001283*(TI2-300)+0.1111;
elseif TI2<=700;
kI2g=0.000352*(TI2-600)+0.1496;
elseif TI2<=800;
kI2g=-0.000121*(TI2-700)+0.1848;
elseif TI2>800;
kI2g=0.000495*(TI2-800)+0.1727;

end

% density
if T(j-1,x)<=140;
  pI2g=645.7;
elseif T(j-1,x)<=250;
pI2g=-1.02725*T(j-1,x)+789.515;
elseif T(j-1,x)<=720;
pI2g=-0.0137*T(j-1,x)+536.13;
elseif T(j-1,x)<=800;
pI2g=-0.3632*T(j-1,x)+787.75;
```

```
        elseif T(j-1,x)>800;
        pI2g=497.189;
        end

        %  specific heat
        if T(j-1,x)<=90;
        cpI2g=950;
        elseif T(j-1,x)<=130;
        cpI2g=388.75*(T(j-1,x)-90)+950;
        elseif T(j-1,x)<=160;
        cpI2g=-350*(T(j-1,x)-130)+16500;
        elseif T(j-1,x)<=190;
        cpI2g=33.333*(T(j-1,x)-160)+6000;
        elseif T(j-1,x)<=220;
        cpI2g=-201.67*(T(j-1,x)-190)+7000;
        elseif T(j-1,x)<=600;
        cpI2g=950;
        elseif T(j-1,x)<=680;
        cpI2g=38.125*(T(j-1,x)-600)+950;
        elseif T(j-1,x)<=740;
        cpI2g=-50.833*(T(j-1,x)-680)+4000;
        elseif T(j-1,x)>740;
        cpI2g=950;
        end

        syms T5
        EQ5=dx^2*(cpI2g*pI2g + cpI2i*pI2i)/((kI2g+kI2i)*dt)*(T5-T(j-1,x)) +
2*T(j-1,x) - 2*(kI2i*T(j-1,x-1)+(kI2g*T(j-1,x+1)))/(kI2g+kI2i);
        [T5]=solve(EQ5);
        T(j,x)=T5;
        clear T5
        clear EQ5
        clear cpI2g
        clear kI2g
        clear kI2i
        clear cpI2i
        clear pI2g
        clear pI2i


        %INTERIOR NODES OF THE THIRD LAYER

        elseif  x<n;
         %CONDUCTIVITY OF GYPSUM
        T6l=(T(j-1,x-1)+T(j-1,x))/2;

       %conductivity
        if T6l<=90;
        k6l=0.1683;
        elseif T6l<=200;
        k6l=-0.00057*(T6l-90)+0.1683;
        elseif T6l<=300;
        k6l=0.000055*(T6l-200)+0.1056;
        elseif T6l<=600;
        k6l=0.0001283*(T6l-300)+0.1111;
        elseif T6l<=700;
        k6l=0.000352*(T6l-600)+0.1496;
```

```
elseif T6l<=800;
k6l=-0.000121*(T6l-700)+0.1848;
elseif T6l>800;
k6l=0.000495*(T6l-800)+0.1727;

end

T6r=(T(j-1,x+1)+T(j-1,x))/2;

%conductivity
 if T6r<=90;
k6r=0.1683;
elseif T6r<=200;
k6r=-0.00057*(T6r-90)+0.1683;
elseif T6r<=300;
k6r=0.000055*(T6r-200)+0.1056;
elseif T6r<=600;
k6r=0.0001283*(T6r-300)+0.1111;
elseif T6r<=700;
k6r=0.000352*(T6r-600)+0.1496;
elseif T6r<=800;
k6r=-0.000121*(T6r-700)+0.1848;
elseif T6r>800;
k6r=0.000495*(T6r-800)+0.1727;

end

if T(j-1,x)<=140;
 p6=645.7;
elseif T(j-1,x)<=250;          %Regular
p6=-1.02725*T(j-1,x)+789.515;
elseif T(j-1,x)<=720;
p6=-0.0137*T(j-1,x)+536.13;
elseif T(j-1,x)<=800;
p6=-0.3632*T(j-1,x)+787.75;
elseif T(j-1,x)>800;
p6=497.189;
end

%  specific heat
if T(j-1,x)<=90;
cp6=950;
elseif T(j-1,x)<=130;
cp6=388.75*(T(j-1,x)-90)+950;
elseif T(j-1,x)<=160;
cp6=-350*(T(j-1,x)-130)+16500;
elseif T(j-1,x)<=190;
cp6=33.333*(T(j-1,x)-160)+6000;
elseif T(j-1,x)<=220;
cp6=-201.67*(T(j-1,x)-190)+7000;
elseif T(j-1,x)<=600;
cp6=950;
elseif T(j-1,x)<=680;
cp6=38.125*(T(j-1,x)-600)+950;
elseif T(j-1,x)<=740;
cp6=-50.833*(T(j-1,x)-680)+4000;
elseif T(j-1,x)>740;
```

```
        cp6=950;
        end

        det6 = (cp6*p6*(dx)^2)/(k6l+k6r);
        dt6 = det6/4;

        syms T6
        EQ6=k6l*(T(j-1,x-1)-T(j-1,x))/dx+k6r*(T(j-1,x+1)-T(j-1,x))/dx-
p6*cp6*(dx)*(T6-T(j-1,x))/(dt6);
        [T6]=solve(EQ6);
        T(j,x)=T6;
        clear T6
        clear EQ6
        clear k6l
        clear k6r
        clear cp6
        clear p6

        %LAST BOUNDARY NODE

        elseif x>=n;
        T7l=(T(j-1,x-1)+T(j-1,x))/2;

        %conductivity
        if T7l<=90;
        k7=0.1683;
        elseif T7l<=200;
        k7=-0.00057*(T7l-90)+0.1683;
        elseif T7l<=300;
        k7=0.000055*(T7l-200)+0.1056;
        elseif T7l<=600;
        k7=0.0001283*(T7l-300)+0.1111;
        elseif T7l<=700;
        k7=0.000352*(T7l-600)+0.1496;
        elseif T7l<=800;
        k7=-0.000121*(T7l-700)+0.1848;
        elseif T7l>800;
        k7=0.000495*(T7l-800)+0.1727;

        end

        % density
        if T(j-1,x)<=140;
         p7=645.7;
        elseif T(j-1,x)<=250;          %Regular
        p7=-1.02725*T(j-1,x)+789.515;
        elseif T(j-1,x)<=720;
        p7=-0.0137*T(j-1,x)+536.13;
        elseif T(j-1,x)<=800;
        p7=-0.3632*T(j-1,x)+787.75;
        elseif T(j-1,x)>800;
        p7=497.189;
        end

        %  specific heat
        if T(j-1,x)<=90;
        cp7=950;
```

```
        elseif T(j-1,x)<=130;
        cp7=388.75*(T(j-1,x)-90)+950;
        elseif T(j-1,x)<=160;
        cp7=-350*(T(j-1,x)-130)+16500;
        elseif T(j-1,x)<=190;
        cp7=33.333*(T(j-1,x)-160)+6000;
        elseif T(j-1,x)<=220;
        cp7=-201.67*(T(j-1,x)-190)+7000;
        elseif T(j-1,x)<=600;
        cp7=950;
        elseif T(j-1,x)<=680;
        cp7=38.125*(T(j-1,x)-600)+950;
        elseif T(j-1,x)<=740;
        cp7=-50.833*(T(j-1,x)-680)+4000;
        elseif T(j-1,x)>740;
        cp7=950;
        end

        % STABILITY...

        dtimel=p7*cp7*dx^2/(2*hco*dx+2*k7+2*emo*St*dx*(Tout+273.15)^3); %
maximum time for instablity
         dtl=dtimel/2;

        syms T7

        EQ7=k7*(T(j-1,x-1)-T(j-1,x))/dx-hco*(T(j-1,x)-Tout)-emo*St*((T(j-
1,x)+273.15)^4-(Tout+273.15)^4)-p7*cp7*(dx/2)*(T7-T(j-1,x))/(dtl);
        [T7]=solve(EQ7);
        T(j,x)=T7;
        clear T7
        clear EQ7
        clear T7l
        clear k7
        clear cp7
        clear p7

       end
       end



end
% OBTAIN RESULTS FROM MATLAB WORKSPACE (T).
plot (tspace,T(:,n),'-b','LineWidth',2)
```